Polymer complexes. LXXV. Characterization of quinoline polymer complexes as potential bio-active and anti-corrosion agents

M.I. Abou-Dobara[a], N.F. Omar[a], M.A. Diab[b], A.Z. El-Sonbati[b,*], Sh.M. Morgan[c], O.L. Salem[d], A.M. Eldesoky[e,f]

[a] Botany and Microbiology Department, Faculty of Science, Damietta University, Damietta, Egypt
[b] Chemistry Department, Faculty of Science, Damietta University, Damietta, Egypt
[c] Environmental Monitoring Laboratory, Ministry of Health, Port Said, Egypt
[d] Ministry of Health, Damietta Laboratory, Damietta, Egypt
[e] Engineering Chemistry Department, High Institute of Engineering &Technology, New Damietta, Egypt
[f] Al-Qunfudah Center for Scientific Research (QCSR), Chemistry Department, Al-Qunfudah University College, Umm Al-Qura University, Saudi Arabia

ARTICLE INFO

ABSTRACT

The Cu^{2+}, Co^{2+}, Ni^{2+} and UO_2^{2+} polymer complexes of 5-(2,3-dimethyl−1-phenylpyrazol-5-one azo)-8-hydroxyquinoline (**HL**) ligand were prepared and characterized. Elemental analyses, IR spectra, X-ray diffraction analysis and thermal analysis studies have been used to confirm the structure of the prepared polymer complexes. The chemical structure of metal chelates commensurate that the ligand acts as a neutral bis(bidentate) by through four sites of coordination (azo dye nitrogen, carbonyl oxygen, phenolic oxygen and hetero nitrogen from pyridine ring). The molecular and electronic structures of the hydrogen bond conformers of **HL** ligand were optimized theoretically and the quantum chemical parameters were calculated. Elemental analysis data suggested that the polymer complexes have composition of octahedral geometry for all the polymer complexes. Molecular docking of the binding between **HL** and the receptors of prostate cancer (PDB code 2Q7L Hormone) and the breast cancer (PDB code 1JNX Gene regulation) was studied. The interaction between **HL** and its polymer complexes with the calf thymus DNA (CT-DNA) was determined by absorption spectra. The antimicrobial activity of **HL** and its Cu^{2+}, Co^{2+}, Ni^{2+} and UO_2^{2+} polymer complexes were investigated; only Cu(II) polymer complex **(1)** was specifically active against *Aspergillus niger*. It inhibited the fungal sporulation and distorted the fungal mycelia, which became squashed at a concentration of 150 μg/ml; transmission electron microscope (TEM) also showed a deactivation of autophagy in the treated *A. niger* cells *via* accumulation of autophagic bodies in vacuoles. The inhibition process of the prepared ligand (**HL**) against the corrosion of carbon steel in 2 M HCl solution was determined by various methods (weight loss, potentiodynamic polarization, electrochemical impedance spectroscopy (EIS) and electrochemical frequency modulation (EFM) techniques) are found to be in reasonable agreement. The mechanism of inhibition in presence of **HL** in carbon steel corrosion obeys Friendlish adsorption isotherm.

1. Introduction

Quinolines compounds are considered as the major class of heterocyclics that are found in many biologically active natural products and synthetic molecules and quinoline derivative compounds are known to be the best chelating agents. They have pharmacological properties which include wide applications in medical chemistry [1,2]. They form very stable chelate rings with metal centers, and very stable complexes with a number of metal ions. The deprotonated oxygen atom and the ring nitrogen atom are involved in the metal chelation. The transition metal complexes with nitrogen donors are applied in various activities such as anticancer, antibiotic, antimicrobial and antifungal agents [3]. Many of the metals such as Cu^{2+}, Co^{2+} and Ni^{2+} have found widespread application in organic synthesis and biology [4].

Literature surveys indicate that quinoline derivatives possess diverse pharmacological activities, including antimicrobial, antimalarial, antiviral, antitumor [5–8] and anti-inflammatory activities [9]. As well as quinoline derivatives have been used for the preparation of nano and mesostructures with enhanced electronic and photonic properties [10]. Accordingly, they have been used in chromatography and for the

---

detection of metal ions, biological effect and antioxidant activities [11–13]. The chemistry of transition metal complexes of 8-hydroxyquinoline has received much attention as their rational design and synthesis in coordination chemistry, also because of their potential applications as functional materials and in bioinorganic chemistry. The immune response of the 8-hydroxyquinoline polymer complexes with Bovine respiratory syncytial (BRS) vaccine in cattle was studied using serum neutralizations test (SNT). It was found that the isolated polymer complexes with BRS vaccine caused a significant increase in the antibody titer against BRS virus in SNT compared to BRS vaccine alone [14].

The inhibition action of certain organic compounds on metallic corrosion processes has been extensively studied in recent years [3,15]. The exact nature of the interaction between the inhibitors and the metallic surface is, however, far from being explained and general conclusions are more difficult to draw. There is agreement of some stages participating in the overall inhibition process, particularly with respect to the mechanism in which inhibition occurs. Some heterocyclic compounds were found to be good corrosion inhibitors in different environments. 8-Hydroxyquinolines derivatives proved to be a good corrosion inhibitor of mild steel in acid media [15]. Also, it was found that some 8-hydroxyquinolines derivatives are excellent inhibitors for carbon steel in acidic solutions [16,17].

The present study deals with the preparation of polymer complexes of Cu^{2+}, Co^{2+}, Ni^{2+} and UO_2^2 with 5-(2,3-dimethyl-1-phenylpyrazol-5-one azo)-8-hydroxyquinoline (**HL**) ligand. The chemical structur of the polymer complexes of **HL** was characterized by elemental analyses, IR spectra, X-ray diffraction analysis and thermal studies. The molecular and electronic structure of **HL** was optimized theoretically and the quantum chemical parameters were calculated. A study of the molecular docking binding between **HL** and the receptors of prostate cancer and the breast cancer was reported. The interaction of calf thymus DNA (CT-DNA) with the ligand and its polymer complexes has been studied. Investigation of antibacterial and antifungal activities of **HL** and its Cu^{2+}, Co^{2+}, Ni^{2+} and UO_2^{2+} polymer complexes and ultrastructural changes of the inhibited microorganisms was examined and discussed. A study of the inhibition process of the prepared ligand (**HL**) against the corrosion of carbon steel in 2 M HCl solution was determined by various methods such as weight loss, potentiodynamic polarization, electrochemical impedance spectroscopy (EIS) and electrochemical frequency modulation (EFM) techniques.

2. Experimental details

All the used compounds and solvents were purchased from Aldrich and Sigma and used as received without further purification.
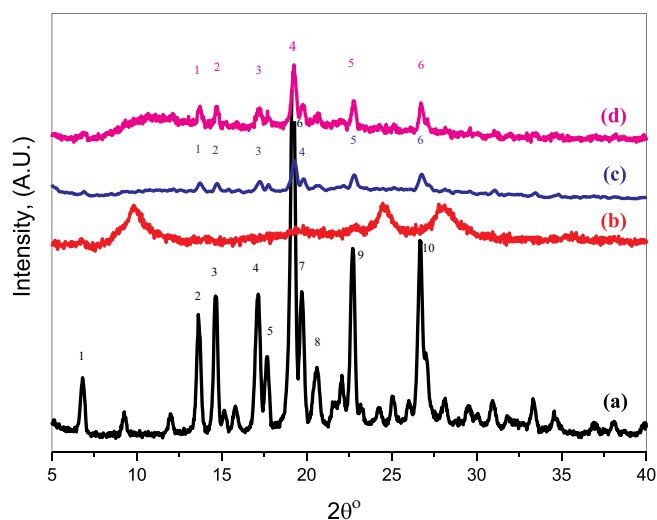
2.1. Synthesis of the polymer complexes

The **HL** ligand was prepared as described previously [18,19] by coupling an equimolar amount of the 4-aminoantipyrene and 8-hydroxyquinoline. To a warm and clear solution of **HL** (30 mL) a solution of each metal salt (30 mL) was added with constant stirring. The resulting mixture was refluxed for ~ 4 h and allowed to cool whereupon the polymer complexes precipitated at room temperature (Fig. S1). They were collected by filtration and purified by washing with hot water followed by acetone, ethanol and diethyl ether. They were dried in air at room temperature and all the formed polymer complexes were almost quantitative.

2.2. Analytical and computational measurements

Microanalyses of carbon, hydrogen and nitrogen were carried out using a CHNS-932 (LECO) Vario elemental analyzer at the Microanalytical Center, Cairo University, Egypt. The weight percentages of metals were determined by the dissolution of the solid polymer

Table 1
Elemental analysis of **HL** and its polymer complexes.

Compound	Exp. (Calcd.) (%)			
	C	H	N	M
HL	66.69	4.70	19.54	–
	(66.85)	(4.74)	(19.50)	
{[Cu (**HL**) (Cl)$_2$] H$_2$O}$_n$	46.73	3.15	13.52	12.45
(1)	(46.92)	(3.32)	(13.68)	(12.42)
{[Co (**HL**) (H$_2$O)$_2$]Cl$_2$. H$_2$O}$_n$	43.98	3.68	12.67	10.26
(2)	(44.20)	(3.87)	(12.89)	(10.85)
{[Ni (**HL**) (H$_2$O)$_2$]Cl$_2$. 4H$_2$O}$_n$	39.91	3.44	11.52	9.85
(3)	(40.22)	(3.52)	(11.73)	(9.84)
{[(UO$_2$) (**HL**) (NO$_3$)$_2$] H$_2$O}$_n$	30.88	2.06	12.51	31.04
(4)	(31.13)	(2.20)	(12.71)	(30.87)

Fig. 1. X-ray diffraction pattern of (a) **HL**, (b) **1**, (c) **2** and (d) **4** in the powder form.

complexes in concentrated HNO_3, neutralizing the diluted aqueous solutions with ammonia and titrating the metal solutions with EDTA. ^{1}H NMR spectra of **HL** and polymer complexes in DMSO-d_6 solvent were recorded with a 330 MHz Varian-Oxford Mercury at room temperature using tetramethylsilane (TMS) (as an internal standard). The molecular structures of the ligand were optimized using the Hartree-Fock method with 3-21G basis set and the molecules were built with Perkin Elmer ChemBio3D software [20,21]. Infrared spectra were recorded as KBr discs using a Perkin-Elmer 1340 spectrophotometer. Simultaneous Thermal Analyzer (STA) 6000 system was used in computing the thermal studies by thermogravimetric analysis (TGA) method. Thermal properties were studied from 50 °C to 800 °C at the heating rate of 15 °C/min under dynamic nitrogen atmosphere. X-ray diffractometer was used in X-ray diffraction measurement (XRD) at diffraction angle range 2θ° = 5–80°. This analysis is carried out using $CuK_{\alpha 1}$ radiation (λ = 1.540598 Å) with 40 KV as applied voltage and 30 mA as the tube current. CRYSFIRE computer program [22] was used in indexing the diffraction peaks and determining the lattice parameters.

2.3. Biological activity and DNA binding measurements

The UV–Vis absorption spectra technique (300–900 nm) has been used in studying the binding between compounds under investigation (**HL**, **1**, **2**, **3** and **4**) and calf thymus DNA (CT-DNA). A solution of HCl/NaCl (5:50 mM) at pH = 7.2–7.4 has been used as a buffer solution in all CT-DNA experiments. The CT-DNA solution free of protein must give absorption beaks at 260 and 280 nm with ratio 1.8–1.9 [19] and the

Table 2
Crystallographic data of **HL**, (**2**) and (**4**).

Peak no.	Compound[a]								
	HL			**(2)**			**(4)**		
	$2\theta_{Obs.}$ (°)	$d_{Obs.}$ (Å)	(hkl)	$2\theta_{Obs.}$ (°)	$d_{Obs.}$ (Å)	(hkl)	$2\theta_{Obs.}$ (°)	$d_{Obs.}$ (Å)	(hkl)
1	6.8057	12.968	1 0 0	13.6430	6.473101	−1 −1 2	13.7024	6.473101	2 0 0
2	13.6388	6.473101	1 1 1	14.7270	6.017961	0 1 2	14.7031	6.017961	−1 2 0
3	14.6412	6.065346	−1 2 0	17.2140	5.135327	−1 −3 2	17.1985	5.169792	1 1 1
4	17.1355	5.169792	2 0 1	1,901,910	4.668479	−1 −2 3	19.2509	4.612569	−1 0 2
5	17.6654	5.001942	1 2 1	22.7630	3.910147	−2 −3 0	22.7700	3.910147	2 1 1
6	19.1942	4.612569	−1 0 2	26.7810	3.320254	−2 −4 3	26.7518	3.334628	−4 2 1
7	19.7066	4.504673	0 1 2						
8	20.6045	4.303346	−1 3 0						
9	22.7073	3.910147	0 2 2						

[a] Numbers are given in Table 1.
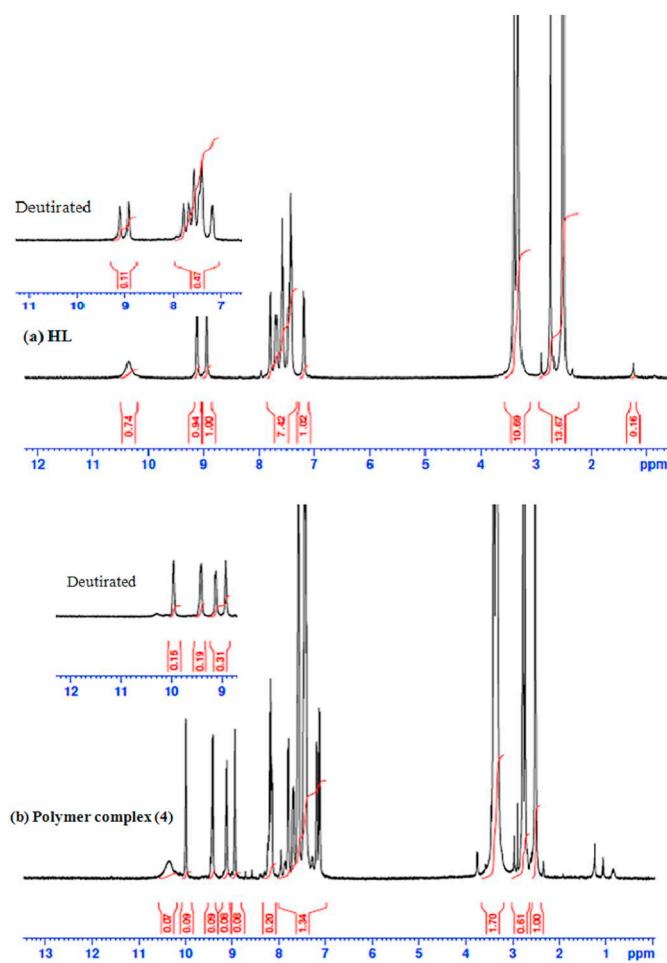
Fig. 2. ^{1}H NMR spectra of (a) **HL** and (b) polymer complex (**4**).

concentration of CT-DNA was determined by absorption spectroscopy [23].

All experiments included prepared stock solutions of **HL** ligand and its polymer complexes dissolved in DMSO then diluted in the corresponding buffer till the required concentrations. In the final concentrations, the percentage of DMSO must not be > 0.1% in the tested solutions for preventing any effect on DNA conformation from DMSO.

The absorption titration measurements were carried out at room temperature by fixing compound and increasing CT-DNA concentration gradually. For eliminating CT-DNA absorbance, an amount of CT-DNA was added to the compound solution and the reference during measuring the absorption spectra. The binding constant (K_b) can be calculated by [18,23]:

$$[DNA]/(\varepsilon_a − \varepsilon_f) = [DNA]/(\varepsilon_b − \varepsilon_f) + 1/K_b[(\varepsilon_a − \varepsilon_f)] \qquad (1)$$

where [DNA] is CT-DNA concentration of in base pairs, the apparent absorption coefficient, ε_a, ε_f, and ε_b correspond to A_{obsd}/[compound], the extinction coefficient of the free compounds and the extinction coefficient of the compound when fully bind to DNA, respectively. By plotting a relation between [DNA]/($\varepsilon_a − \varepsilon_f$) versus [DNA], K_b is calculated by the ratio of slope to the intercept.

2.4. Molecular docking measurements

Molecular docking measurements were carried out on prostate cancer (PDB code 2Q7L Hormone) and the breast cancer (PDB code 1JNX Gene regulation) proteins model. AutoDock tools [24–27] was used in adding essential hydrogen atoms, Kollman united atom type charges, and solvation parameters.

2.5. Antimicrobial activity assay

Agar well diffusion technique [28] was used to compare the antimicrobial activities of different concentrations (50, 100 and 150 μg/ml) of the **HL** ligand and its polymer complexes with those of the antimicrobial standards (penicillin and miconazole), all dissolved in dimethyl sulfoxide (DMSO). The antibacterial activities were tested, on nutrient agar medium; against local isolates of gram-positive and gram-negative bacteria: (*Bacillus cereus* and *Staphylococcus aureus*) and (*Escherichia coli* and *Klebsiella pneumoniae*), respectively. The antifungal activities were also tested against two local isolates of fungi (*Aspergillus niger* and *Fusarium oxysporium*), on DOX agar medium. Wells (10 mm) were made by a sterile cork-borer in the inoculated agar medium. Each well was loaded with 200 μl of the tested compound. The agar plates were put at 4 °C until the complete diffusion of the tested compound; then incubated at 37 °C or 30 °C for bacteria and fungi, respectively. After 24 h and 7 days for bacteria and fungi, respectively, the inhibition zone diameters around the wells were measured and those of the DMSO control were omitted.

2.5.1. Transmission and Scanning electron microscopy (TEM and SEM) examinations

The harvested mycelia (treated, normal, and control DMSO treated mycelia) after the antifungal activity test were fixed by paraformaldehyde-glutaraldehyde in 0.1 M phosphate buffer pH 7.4; then washed and post-fixed in 2% osmium tetra oxide (in 0.1 M phosphate buffer pH 7.4) for 90 min. These cells were dehydrated through ethanol gradients then acetone-methanol solutions were added.

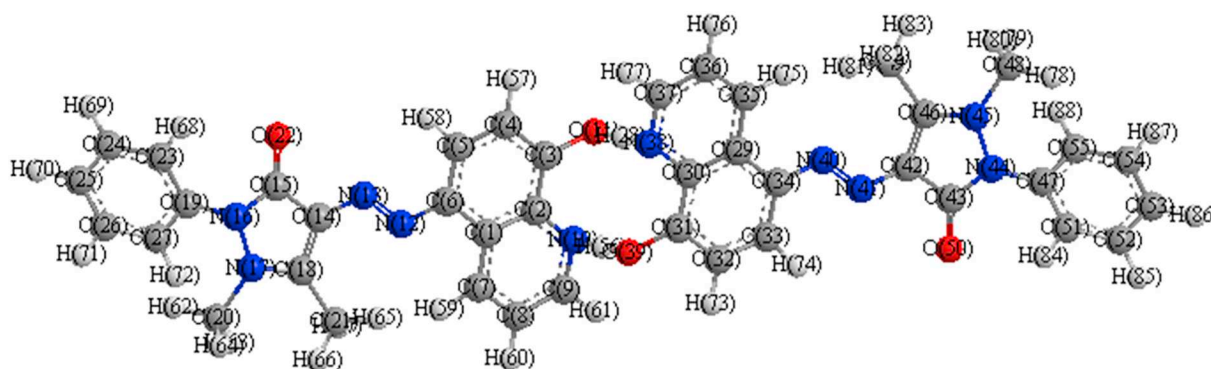Transmission electron microscopy (TEM; JEOL JEM-2100 TEM, Unit

Fig. 3. The optimized structures of dimmer form **(E)** of **HL** ligand.

of Electron Microscopy, Mansoura University, Egypt) was used to examine sections of the mycelia. Scanning electron microscopy (SEM; JEOL JSM-6510 L.*V* SEM, Unit of Electron Microscopy, Mansoura University, Egypt) was used to examine the morphology of the mycelia. For TEM, the dehydrated fungi were embedded for 1 h in Epon-Araldite (1:1) mixture, which was polymerized at 65 °C for 24 h. Ultra-sections (50 μm) were cut by ultratome on copper grids; then double stained with uranyl acetate and lead citrate. For SEM, the dehydrated fungi were dried at critical drying point under a vacuum; then coated with gold using a sputter coater at 20 mA.

2.6. Corrosion measurements

2.6.1. Weight loss

Square specimens of carbon steel (2 cm × 2 cm × 0.2 cm) were used in weight loss experiments. The inhibition efficiency (% IE) and the degree of surface coverage (θ) of the investigated inhibitors on the corrosion of carbon steel were calculated by the following equation [3,29]:

$$\theta = [(W_o - W)/W_o] \times 100 \tag{2}$$

$$\%IE = \theta \times 100 \tag{3}$$

where W_o and W are the values of the average weight losses in the absence and presence of the inhibitor, respectively.

2.6.2. Electrochemical measurements

Gamry instrument PCI300/4 Potentiostat/Galvanostat/Zra analyzer, EIS300 electrochemical impedance, DC105 corrosion software, spectroscopy software, EFM140 electrochemical frequency modulation software and Echem Analyst 5.5 for plotting results, graphing, data fitting and calculating were used for all electrochemical experiments.

(i) Electrochemical frequency modulation technique (EFM)

EFM measurements were carried out using potential perturbation signal (10 mV amplitude and 2 and 5 Hz sine waves). These two frequencies were chosen because of three arguments. i_{corr}, corrosion current density, β_c and β_a, Tafel slopes, and CF-2 and CF-3, the causality factors, were calculated using the larger peaks [29].

(ii) Electrochemical impedance spectroscopy (EIS)

EIS measurements were performed using AC signals of 5 mV peak to peak amplitude at the open circuit potential in the frequency range of 100 kHz to 0.1 Hz. The inhibition efficiency (% IE) was calculated by the following equation:

$$\%IE = \theta \times 100 = [1 - (R°_{ct}/R_{ct})] \tag{4}$$

where, $R°_{ct}$ and R_{ct} are the charge transfer resistance in the absence and

presence of inhibitor, respectively.

(iii) Potentiodynamic polarization measurements

Potentiodynamic polarization measurements were recorded in using a typical three-compartment glass cell consisted of:

1- Carbon steel specimen (1 cm^2) welded from one side to copper wire for electric connection as working electrode.
2- Saturated Calomel electrode (SCE) as a reference electrode.
3- A platinum foil (1 cm^2) as a counter electrode.

By applying different electrode potential ranging from −800 to 500 mV vs. SCE, Tafel polarization curves were obtained. The determination of corrosion current is performed by extrapolation of the anodic and cathodic of Tafel lines by using Stern-Geary method [30,31]. i_{corr} was used to calculate the inhibition efficiency (% IE) and surface coverage (θ) using the following relation:

$$\%IE = \theta \times 100 = [1 - (i_{corr(inh)}/i_{corr(Free)})] \times 100 \tag{5}$$

where $i_{corr.(Free)}$ is the corrosion current density in the absence of inhibitor and $i_{corr(inh)}$ is the corrosion current density in the presence of inhibitor.

2.7. Statistical analysis

The antimicrobial activity results were recorded as mean ± SE. It was analysed for significant differences at *p*-value < 0.05; using one-way analysis of variance (ANOVA) with SPSS software version 17.

3. Results and discussion

3.1. Structure identification of azo dye and its polymer complexes

The ligand is soluble partially in some common organic solvents on hot and completely soluble in hot DMF and cold DMSO, its melting temperature is ~250 °C, air-stable and colored. The polymer complexes are stable in air, colored and soluble only in hot DMSO. Polymer complexes (**1**–**4**) have been deduced from their elemental analyses (Table 1). The experimental data of elemental analyses are in agreement with the calculated values of % (carbon, hydrogen, nitrogen and metal) which indicates that they are polymeric in nature.

The two hydroxyquinoline units of the dimmer are in one plane and intramolecular (I) hydrogen bonding occurs between the hydroxyl group and the quinoline nitrogen atom (Fig. S2(G)). The intermolecular hydrogen bond distance II = 2.16 Å is shorter than the intramolecular distance *I* = 2.32 Å (Fig. S2). This observation was also made for other 8-hydroxyquinoline dimmers and might be due to an unflavored small O-H…N angle of 113.7° (observed for G) for the intramolecular interaction [32–34]. The corresponding intermolecular O-H…N angle of (G) is 135.5° [35] (Fig. S2).

The transfer of two equivalent protons within a doubly hydrogen

Table 3

Table 3 The selected geometrical bond lengths and bond angles of dimmer form (E) of HL ligand.

Bond lengths (Å)		Bond angles (°)		Bond angles (°)	
C(55)-H(88)	1.103	H(87)-C(54)-C(55)	120.166	C(15)-N(16)-C(19)	130.291
C(54)-H(87)	1.103	H(87)-C(54)-C(53)	119.779	N(17)-N(16)-C(19)	123.12
C(53)-H(86)	1.103	C(55)-C(54)-C(53)	120.052	H(67)-C(21)-H(66)	108.316
C(52)-H(85)	1.103	H(86)-C(53)-C(54)	120.501	H(67)-C(21)-H(65)	109.937
C(51)-H(84)	1.102	H(86)-C(53)-C(52)	120.506	H(67)-C(21)-C(18)	110.509
C(49)-H(83)	1.112	C(54)-C(53)-C(52)	118.992	H(66)-C(21)-H(65)	104.022
C(49)-H(82)	1.113	H(85)-C(52)-C(53)	119.581	H(66)-C(21)-C(18)	112.297
C(49)-H(81)	1.112	H(85)-C(52)-C(51)	120.113	H(65)-C(21)-C(18)	111.535
C(48)-H(80)	1.113	C(53)-C(52)-C(51)	120.306	C(18)-N(17)-N(16)	114.15
C(48)-H(79)	1.114	H(88)-C(55)-C(47)	120.87	C(18)-N(17)-C(20)	115.925
C(48)-H(78)	1.112	H(88)-C(55)-C(54)	116.848	N(16)-N(17)-C(20)	129.375
C(37)-H(77)	1.105	C(47)-C(55)-C(54)	122.253	N(17)-C(18)-C(14)	104.502
C(36)-H(76)	1.102	H(84)-C(51)-C(52)	116.071	N(17)-C(18)-C(21)	128.823
C(35)-H(75)	1.101	H(84)-C(51)-C(47)	121.932	C(14)-C(18)-C(21)	126.53
C(33)-H(74)	1.103	C(52)-C(51)-C(47)	121.964	C(14)-C(15)-N(16)	111.229
C(32)-H(73)	1.104	H(80)-C(48)-H(79)	108.925	C(14)-C(15)-O(22)	123.585
C(27)-H(72)	1.103	H(80)-C(48)-H(78)	103.779	N(16)-C(15)-O(22)	125.043
C(26)-H(71)	1.103	H(80)-C(48)-N(45)	112.716	C(18)-C(14)-C(15)	106.569
C(25)-H(70)	1.102	H(79)-C(48)-H(78)	109.43	C(18)-C(14)-N(13)	132.157
C(24)-H(69)	1.103	H(79)-C(48)-N(45)	110.636	C(15)-C(14)-N(13)	121.275
C(23)-H(68)	1.101	H(78)-C(48)-N(45)	111.111	C(14)-N(13)-N(12)	120.737
C(21)-H(67)	1.113	C(55)-C(47)-C(51)	116.424	N(10)-H(56)-O(39)	177.891
C(21)-H(66)	1.112	C(55)-C(47)-N(44)	119.622	H(61)-C(9)-N(10)	117.733
C(21)-H(65)	1.112	C(51)-C(47)-N(44)	123.938	H(61)-C(9)-C(8)	119.345
C(20)-H(64)	1.114	C(43)-N(44)-N(45)	102.52	N(10)-C(9)-C(8)	122.897
C(20)-H(63)	1.113	C(43)-N(44)-C(47)	130.096	H(60)-C(8)-C(9)	121.092
C(20)-H(62)	1.112	N(45)-N(44)-C(47)	123.077	H(60)-C(8)-C(7)	121.395
C(9)-H(61)	1.106	H(83)-C(49)-H(82)	108.398	C(9)-C(8)-C(7)	117.505
C(8)-H(60)	1.102	H(83)-C(49)-H(81)	103.982	N(13)-N(12)-C(6)	120.399
C(7)-H(59)	1.101	H(83)-C(49)-C(46)	112.138	H(59)-C(7)-C(8)	116.787
C(5)-H(58)	1.103	H(82)-C(49)-H(81)	109.886	H(59)-C(7)-C(1)	123.128
C(4)-H(57)	1.104	H(82)-C(49)-C(46)	110.512	C(8)-C(7)-C(1)	119.887
C(47)-C(55)	1.349	H(81)-C(49)-C(46)	111.698	N(12)-C(6)-C(1)	119.448
C(54)-C(55)	1.342	C(46)-N(45)-N(44)	114.172	N(12)-C(6)-C(5)	123.12
C(53)-C(54)	1.34	C(46)-N(45)-C(48)	115.912	C(1)-C(6)-C(5)	117.43
C(52)-C(53)	1.34	N(44)-N(45)-C(48)	129.358	H(58)-C(5)-C(6)	122.537
C(51)-C(52)	1.343	N(45)-C(46)-C(42)	104.54	H(58)-C(5)-C(4)	116.097
C(47)-C(51)	1.349	N(45)-C(46)-C(49)	128.794	C(6)-C(5)-C(4)	121.366
C(19)-C(27)	1.349	C(42)-C(46)-C(49)	126.52	H(28)-O(11)-C(3)	109.118
C(26)-C(27)	1.342	C(42)-C(43)-N(44)	111.281	H(57)-C(4)-C(5)	119.217
C(25)-C(26)	1.34	C(42)-C(43)-O(50)	123.616	H(57)-C(4)-C(3)	118.979
C(24)-C(25)	1.34	N(44)-C(43)-O(50)	124.98	C(5)-C(4)-C(3)	121.796
C(23)-C(24)	1.343	C(46)-C(42)-C(43)	106.566	H(56)-N(10)-C(2)	104.605
C(19)-C(23)	1.349	C(46)-C(42)-N(41)	132.148	H(56)-N(10)-C(9)	101.858
N(45)-C(46)	1.276	C(43)-C(42)-N(41)	121.284	C(2)-N(10)-C(9)	119.304
C(42)-C(46)	1.346	C(42)-N(41)-N(40)	120.606	O(11)-C(3)-C(4)	119.956
C(43)-C(42)	1.364	H(76)-C(36)-C(37)	121.084	O(11)-C(3)-C(2)	122.508
N(44)-C(43)	1.274	H(76)-C(36)-C(35)	121.416	C(4)-C(3)-C(2)	117.495
N(45)-N(44)	1.362	C(37)-C(36)-C(35)	117.492	N(10)-C(2)-C(3)	117.047
N(17)-C(18)	1.276	N(41)-N(40)-C(34)	120.418	N(10)-C(2)-C(1)	122.104
C(14)-C(18)	1.346	H(75)-C(35)-C(36)	116.794	C(3)-C(2)-C(1)	120.849
C(15)-C(14)	1.364	H(75)-C(35)-C(29)	123.131	C(7)-C(1)-C(6)	121.886
N(16)-C(15)	1.274	C(36)-C(35)-C(29)	119.884	C(7)-C(1)-C(2)	117.059
N(17)-N(16)	1.362	N(40)-C(34)-C(29)	119.42	C(6)-C(1)-C(2)	121.026
N(38)-H(28)	1.041	N(40)-C(34)-C(33)	123.133		
H(56)-N(10)	1.042	C(29)-C(34)-C(33)	117.442		
O(39)-H(56)	1	H(74)-C(33)-C(34)	122.524		
C(43)-O(50)	1.215	H(74)-C(33)-C(32)	116.113		
C(46)-C(49)	1.508	C(34)-C(33)-C(32)	121.363		
N(45)-C(48)	1.485	H(56)-O(39)-C(31)	109.34		
N(44)-C(47)	1.279	H(73)-C(32)-C(33)	119.234		
N(41)-C(42)	1.266	H(73)-C(32)-C(31)	118.988		
N(40)-N(41)	1.25	C(33)-C(32)-C(31)	121.775		
C(34)-N(40)	1.271	O(39)-C(31)-C(32)	119.901		
C(31)-O(39)	1.374	O(39)-C(31)-C(30)	122.575		
C(30)-N(38)	1.277	C(32)-C(31)-C(30)	117.49		
C(37)-N(38)	1.271	C(35)-C(29)-C(34)	121.912		
C(36)-C(37)	1.339	C(35)-C(29)-C(30)	117.075		
C(35)-C(36)	1.34	C(34)-C(29)-C(30)	120.976		
C(29)-C(35)	1.349	H(77)-C(37)-N(38)	117.435		
C(29)-C(34)	1.354	H(77)-C(37)-C(36)	119.651		
C(33)-C(34)	1.347	N(38)-C(37)-C(36)	122.88		
C(32)-C(33)	1.339	N(38)-C(30)-C(31)	117.005		
C(31)-C(32)	1.343	N(38)-C(30)-C(29)	122.07		

Table 3 (*continued*)

Bond lengths (Å)		Bond angles (°)		Bond angles (°)	
C(30)-C(31)	1.353	C(31)-C(30)-C(29)	120.925		
C(29)-C(30)	1.354	H(28)-N(38)-C(30)	104.812		
O(11)-H(28)	1.001	H(28)-N(38)-C(37)	101.566		
C(15)-O(22)	1.215	C(30)-N(38)-C(37)	119.412		
C(18)-C(21)	1.508	N(38)-H(28)-O(11)	177.355		
N(17)-C(20)	1.485	H(71)-C(26)-C(27)	120.171		
N(16)-C(19)	1.279	H(71)-C(26)-C(25)	119.781		
N(13)-C(14)	1.266	C(27)-C(26)-C(25)	120.044		
N(12)-N(13)	1.25	H(70)-C(25)-C(26)	120.491		
C(6)-N(12)	1.271	H(70)-C(25)-C(24)	120.52		
C(3)-O(11)	1.375	C(26)-C(25)-C(24)	118.988		
C(2)-O(10)	1.278	H(69)-C(24)-C(25)	119.575		
C(9)-N(10)	1.271	H(69)-C(24)-C(23)	120.111		
C(8)-C(9)	1.339	C(25)-C(24)-C(23)	120.313		
C(7)-C(8)	1.34	H(72)-C(27)-C(19)	120.886		
C(1)-C(7)	1.349	H(72)-C(27)-C(26)	116.81		
C(1)-C(6)	1.354	C(19)-C(27)-C(26)	122.273		
C(5)-C(6)	1.347	H(68)-C(23)-C(24)	116.055		
C(4)-C(5)	1.339	H(68)-C(23)-C(19)	121.945		
C(3)-C(4)	1.343	C(24)-C(23)-C(19)	121.968		
C(2)-C(3)	1.354	H(64)-C(20)-H(63)	108.965		
C(1)-C(2)	1.355	H(64)-C(20)-H(62)	109.4		
		H(64)-C(20)-N(17)	110.677		
		H(63)-C(20)-H(62)	103.824		
		H(63)-C(20)-N(17)	112.621		
		H(62)-C(20)-N(17)	111.11		
		C(27)-C(19)-C(23)	116.404		
		C(27)-C(19)-N(16)	119.564		
		C(23)-C(19)-N(16)	124.014		
		C(15)-N(16)-N(17)	102.478		

Table 4

The calculated quantum chemical parameters for conformers of **HL** ligand.

Conformer[a]	E_{HOMO} (eV)	E_{LUMO} (eV)	ΔE^* (eV)	χ (eV)	η (eV)	σ (eV)$^{-1}$	Pi (eV)	S (eV)$^{-1}$	ω (eV)	ΔN_{max}
(A)	−3.034	−1.774	1.260	2.404	0.630	1.587	−2.404	0.794	4.587	3.816
(B)	−7.490	−2.515	4.975	5.003	2.488	0.402	−5.003	0.201	5.030	2.011
(C)	−2.598	−1.398	1.200	1.998	0.600	1.667	−1.998	0.833	3.327	3.330
(D)	−3.102	−1.770	1.332	2.436	0.666	1.502	−2.436	0.751	4.455	3.658
(E)	−2.352	−1.762	0.590	2.057	0.295	3.390	−2.057	1.695	7.172	6.973

[a] Symbols are given in Fig. S2.

bonded dimmer is an important type of excited state proton transfer. It is a little, known about the excited state proton transfer in 8-hydroxyquinoline, but Bardez and coworkers [36] have characterized the steady state spectroscopy. 8-Hydroxyquinoline forms a very stable hydrogen bonded dimmer, whose structure is given in the lower part of Fig. S2 along with that for the tautomer.

The IR spectra provide valuable information regarding the coordinating sites of the ligand. The infrared spectrum of **HL** reveals that a broad medium intensity band of phenolic hydroxyl stretching is observed at ~3200–3450 cm^{-1} with peak centered at 3350 cm^{-1} [37]. This low value of υ(OH) reflects the existence of strong hydrogen bonding both intramolecular [N-H…O (Fig. S2(B)), OH-N (Fig. S2(C(I)))] and intermolecular hydrogen bonding of the O-…H…O type between O-H of one molecule and OH group of another one [Fig. S2(D (II))] and O-H…N type between C=N of one molecule and OH group of another one [Fig. S2(E, dimmer (II))] or N-H…O type between NH of one molecule and C=O group of another one [Fig. S2(F, tautomer (II))], This band is shifted to lower frequency at 3150, 3160, 3180, 3090 and 3175 cm^{-1}, respectively, in the Cu(II), Co(II), Ni(II) and UO$_2$(II) polymer complexes, indicating that the ligand function as a neutral ligand. The spectrum of the free ligand shows the peak of azomethine group (CN$_{py}$) at ~1570 cm^{-1} has been found to experience a negative shift of 10 ± 5 cm^{-1} pointing to the probable participation of the nitrogen of the quinoline moiety, of the ligand polymer

complexes formation with M(II). Coordination of the ligand to the metal chloride through the nitrogen atom is expected to reduce the electron density in the azomethine link and lowest the stretching vibration motion of υ(C=N). The vibrational band at 1460 cm^{-1} assigned to υ(N=N) is shifted to lower frequency by ~18 cm^{-1} in the spectra of the polymer complexes confirming the coordination through one of the azo nitrogen atom [38–40]. This lowering of frequency can be explained by the transfer of electrons from the nitrogen atom to the metal ion due to coordination. The infrared spectra of all the polymer complexes show a considerable shift to lower frequency in the carbonyl (pyrazolone) (1670 cm^{-1}) absorption by 20–32 cm^{-1}, indicating a decrease in stretching force constant of CO as a consequence of coordination through the oxygen atom of the free ligand. It is well known that as a result of coordination through the carbonyl oxygen the double bond character between the carbon and the oxygen is reduced [41]. The decrease in the bond character causes a bathochromic shift in the carbonyl stretching frequency. This exceptionally high shift to lower frequency of the carbonyl frequency may be attributed to the greater flow of electrons from the carbonyl group to the divalent transition atom due to greater delocalization of the positive charge on the nitrogen atom. IR bands due to quinoline system appearing at ~ 1545 cm^{-1}, υ(C-C) and 1585 cm^{-1}, υ(C-N) [42] in the free ligand have been found to experience shifts in the higher energy side ($\Delta\upsilon$ ~ 13 ± 5 cm^{-1}) in the metal polymer complexes indicating thereby, the expected involvement of the
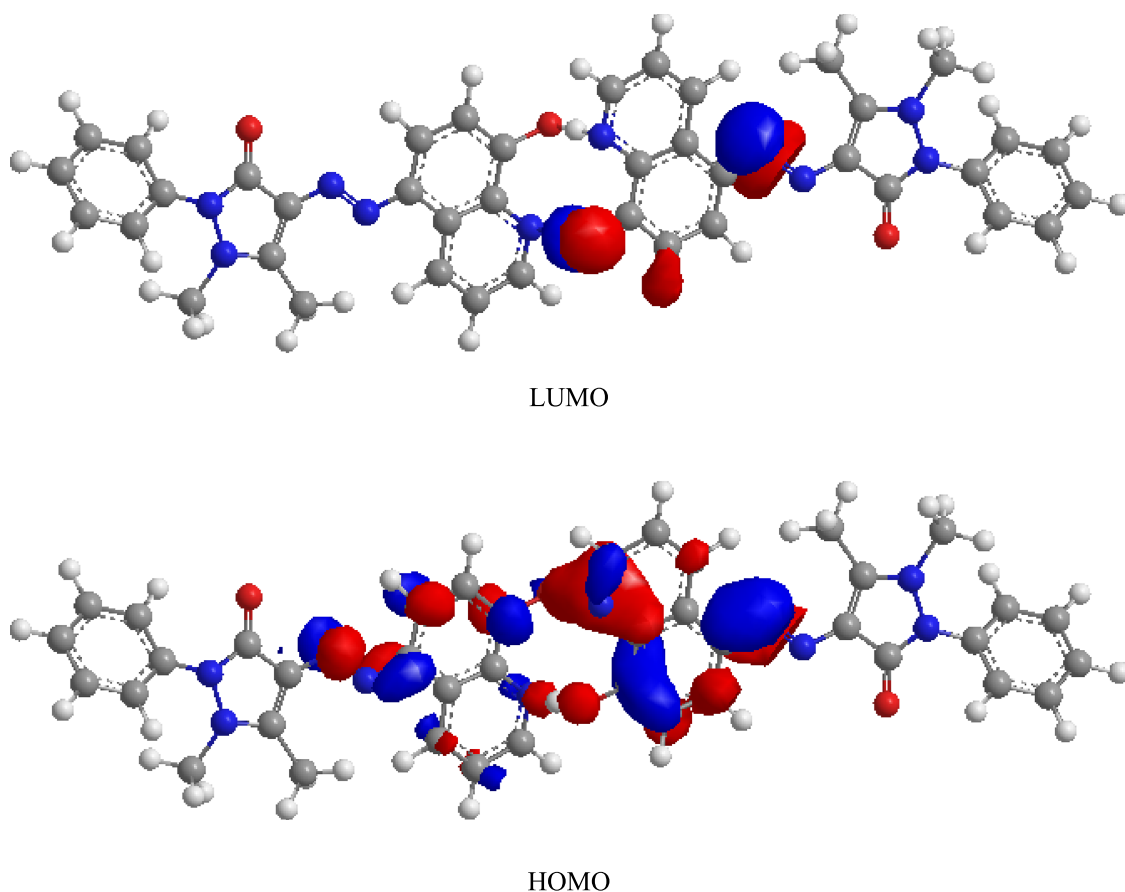
LUMO

HOMO

Fig. 4. HOMO and LUMO molecular orbital of dimmer form **(E)** of **HL** ligand.
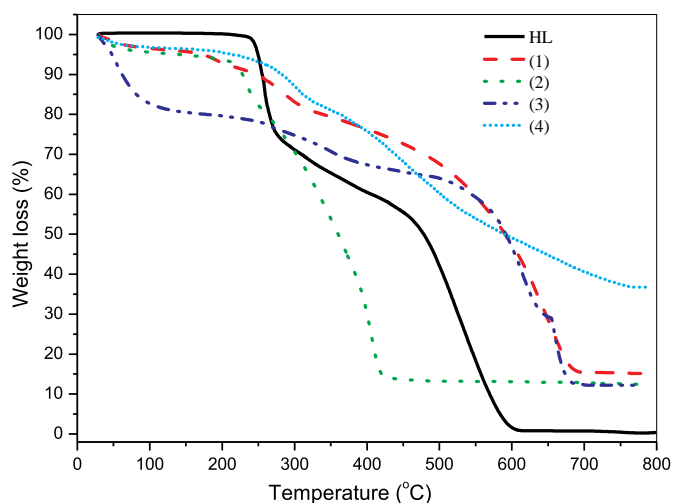

Fig. 5. TGA curves of **HL** and its polymer complexes **(1–4)**.

quinoline ring nitrogen in complexation. The phenolic C-O stretching frequencies appeared at $1215\,cm^{-1}$ in the ligand shift towards lower vibration (20–45 cm^{-1}) in the polymer complexes. This shift confirms the participation of oxygen in the C-O-M bond [19,43].

The presence of rocking band indicates the coordination nature of the water molecule [18]. The relation of the IR spectral of ligand (**HL**) and polymer complexes **(1–4)** showed some differences [44]. One of the expected significant differences was the presence of a more broadened band in the range from 2750 to $3450\,cm^{-1}$ for the chelates as the oxygen of the OH group of the ligand forms a coordination bond with

metal ions. IR spectra of the polymer complexes show new bands at 422–$478\,cm^{-1}$ and 501–$561\,cm^{-1}$ assigned to υ(M-N) and υ(M-O), respectively, [37,45].

IR bands due to the uranyl group of uranyl nitrate polymer complex **(4)** appear at $903\,cm^{-1}$ [υ_{asym}(U-O) and $832\,cm^{-1}$ [υ_{sym}(M-O)] [37]. The force constant (F_{UO}) was calculated by the method of McGlynn et al. [46] as $6.729\ 10^{-8}\,N/\text{Å}$, which agree well with the force constant values of similar dioxouranium(VI) complexes. The U-O bond distance is in the usual range (1.60–$1.92 \cdot 10^{-8}\,N/\text{Å}$) observed for dioxouranium (VI) complexes [37]. The uranyl polymeric complex display, the unidentate NO_3 group exhibits three NO stretching bands at $1418\,cm^{-1}(\upsilon_5)(NO_2)$, $1303\,cm^{-1}(\upsilon_1)(NO_2)$ and $1006\,cm^{-1}(\upsilon_2)(NO)$. Polymer complex **(4)** show IR bands at ~ $1428\,cm^{-1}$ (υ_1), $1374\,cm^{-1}$ (υ_3), $1310\,cm^{-1}$ (υ_5), $1011\,cm^{-1}$ (υ_2) and $840\,cm^{-1}$ (υ_6). The separation between υ_1 and υ_5 of polymer complex **(4)** was ~$118\,cm^{-1}$ indicates that both nitrate groups are unidentate [47].

The IR spectra of the polymer complexes were compared with that of the free ligand to determine the changes that might have taken place during the complexation. A comparative study of the IR spectra of ligand and polymer complexes reveals that certain peaks are common and therefore, only important peaks, which have been either shifted or newly appeared, are discussed. The ligand exhibits bands at $3350\,cm^{-1}$ (υ(OH)), $1670\,cm^{-1}$ (υ(C=O)), $1570\,cm^{-1}$ (υ(C=N$_{py}$)) and $1460\,cm^{-1}$ (υ(N=N)) [18,19,25,26]. In the spectra of the polymer complexes, these bands are shifted to lower wavenumber. This indicate the coordination of (C=N$_{py}$), keto (C=O), azo dye nitrogen and OH groups to the metal atom in polymer complexes, indicating thereby that the ligand function as a neutral bis(bidentate) ligand (Fig. S1).

The resulted data suggest that the ligand **(HL)** behaves as a neutral bis(bidentate) ligand by through four sites of coordination (azo dye nitrogen, carbonyl oxygen, phenolic oxygen and hetero nitrogen from

Table 5
The thermal analysis data of ligand (**HL**) and polymer complexes.

Compound[a]	Temp. range (K)	Found mass loss (calc.) %	Assignment
HL	485–713	43.24 (43.18)	Decomposition of a part of the ligand ($C_5H_7N_4O_2$)
	713–873	56.76 (56.82)	Decomposition of a part of the ligand ($C_{15}H_{10}N$)
(1)	310–393	3.52 (3.51)	Loss of one uncoordinated H_2O molecule
	393–633	16.65 (16.62)	Evaluation of Cl_2 and ½N_2 gases
	633–983	64.24 (64.31)	Evaluation of 2N_2 gas and decomposition the last part of the ligand ($C_{20}H_{17}O$)
	> 983	15.59 (15.55)	Metal oxide residue (CuO)
(2)	313–353	3.33 (3.31)	Loss of one uncoordinated H_2O molecule
	353–543	13.60 (13.08)	Evaluation of Cl_2 gas
	543–923	69.77 (69.8)	Loss of coordinated 2H_2O molecules, evaluation of 2N_2 gas and decomposition the last part of the ligand ($C_{20}H_{17}NO$)
	> 923	13.05 (13.8)	Metal oxide residue (CoO)
(3)	310–353	12.02(12.07)	Loss of uncoordinated 4H_2O molecules
	353–578	11.9 (11.9)	Evaluation of Cl_2 gas
	578–978	63.61 (63.52)	Loss of coordinated 2H_2O molecules, evaluation of 2N_2 gas and decomposition the last part of the ligand ($C_{20}H_{17}NO$)
	> 978	12.53 (12.50)	Metal oxide residue (NiO)

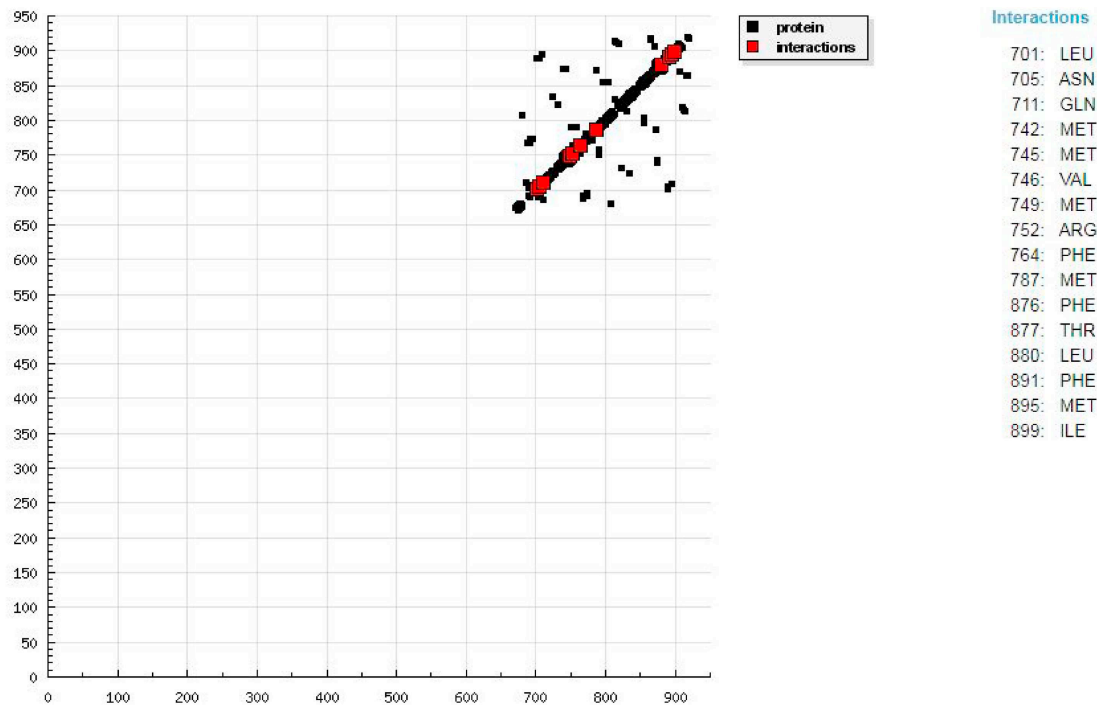[a] Numbers are given in Table 1.

(a)

(b)

(a)

(b)
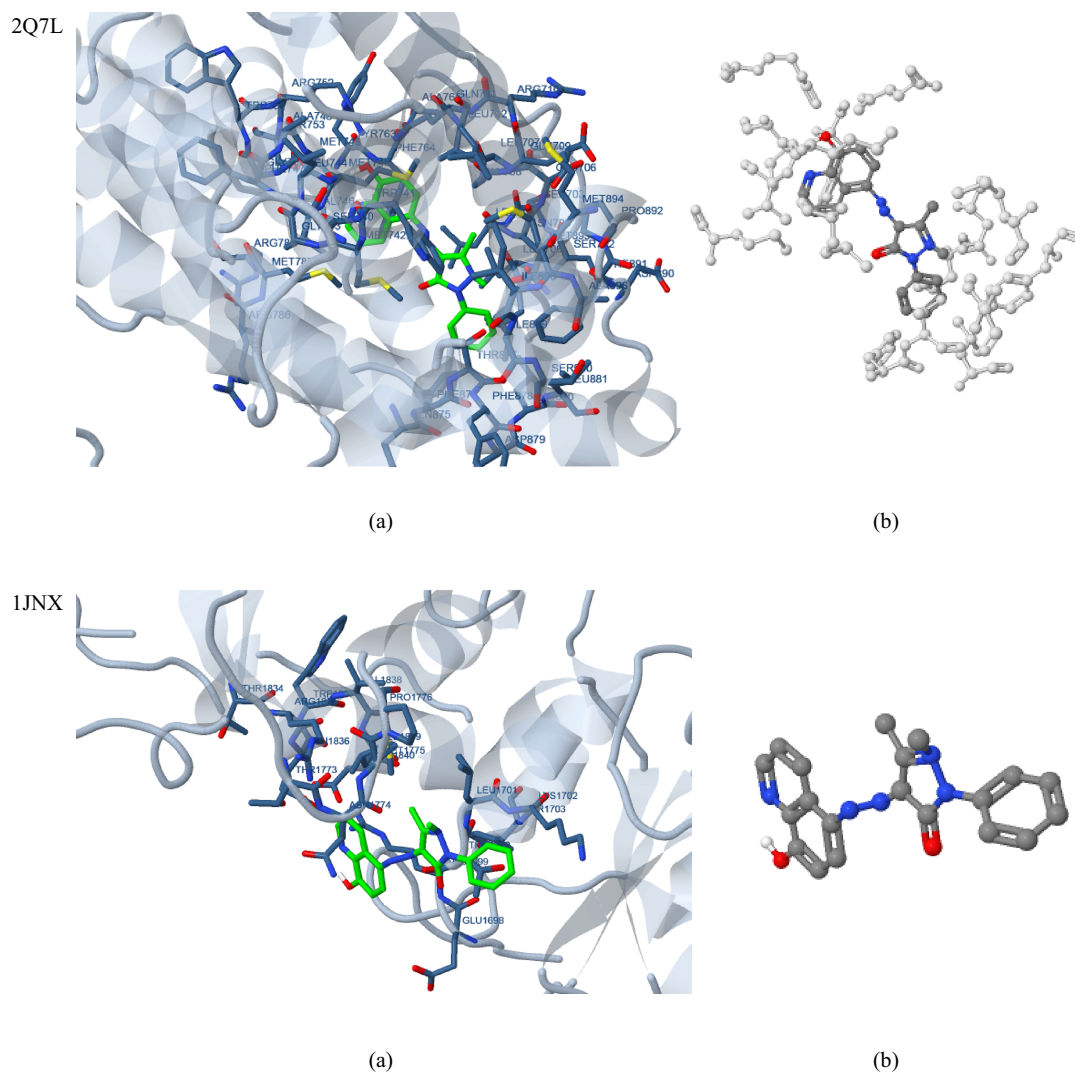
Fig. 6. HL ligand (green in (a) and gray in (b)) in interaction with receptors of prostate cancer (PDB code 2Q7L Hormone) and the breast cancer (PDB code 1JNX Gene regulation). (For interpretation of the references to colour in this figure legend, the reader is referred to the web version of this article.)
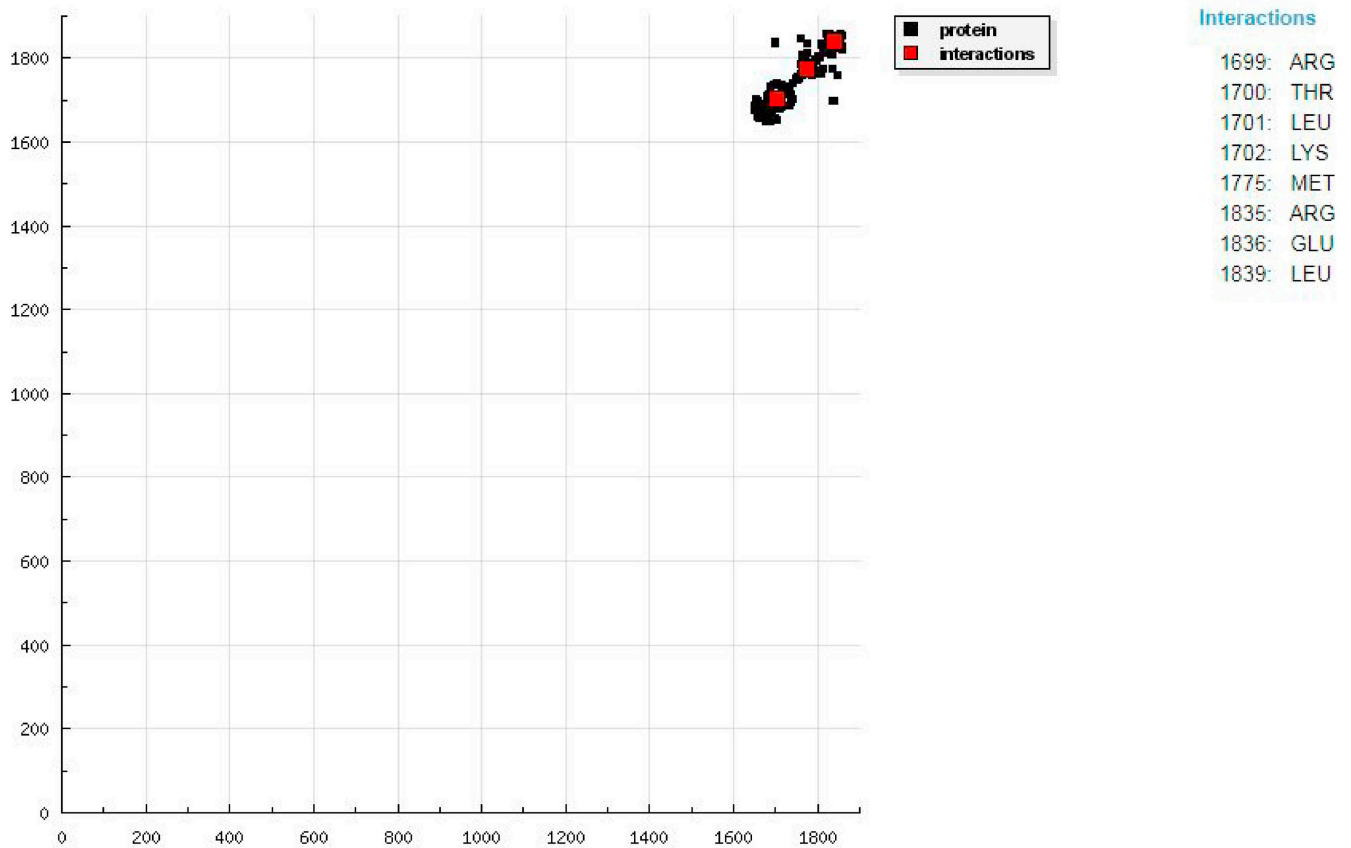
pyridine ring) [(OH, N_{Py}) and (O, N_{azo})] with respect to the evidence above, the structures of the polymer complexes are shown in Fig. S1. The data suggested that the polymer complexes have composition of octahedral geometry for all the polymer complexes.

The azo dye ligand (**HL**) prepared in this work may exist in tautomeric forms as shown in Fig. S2, characteristic for a tautomeric azo-hydrazone mixture form, both in solution and in solid state and this has been confirmed by El-Sonbati et al. [18,41].The electronic spectrum of
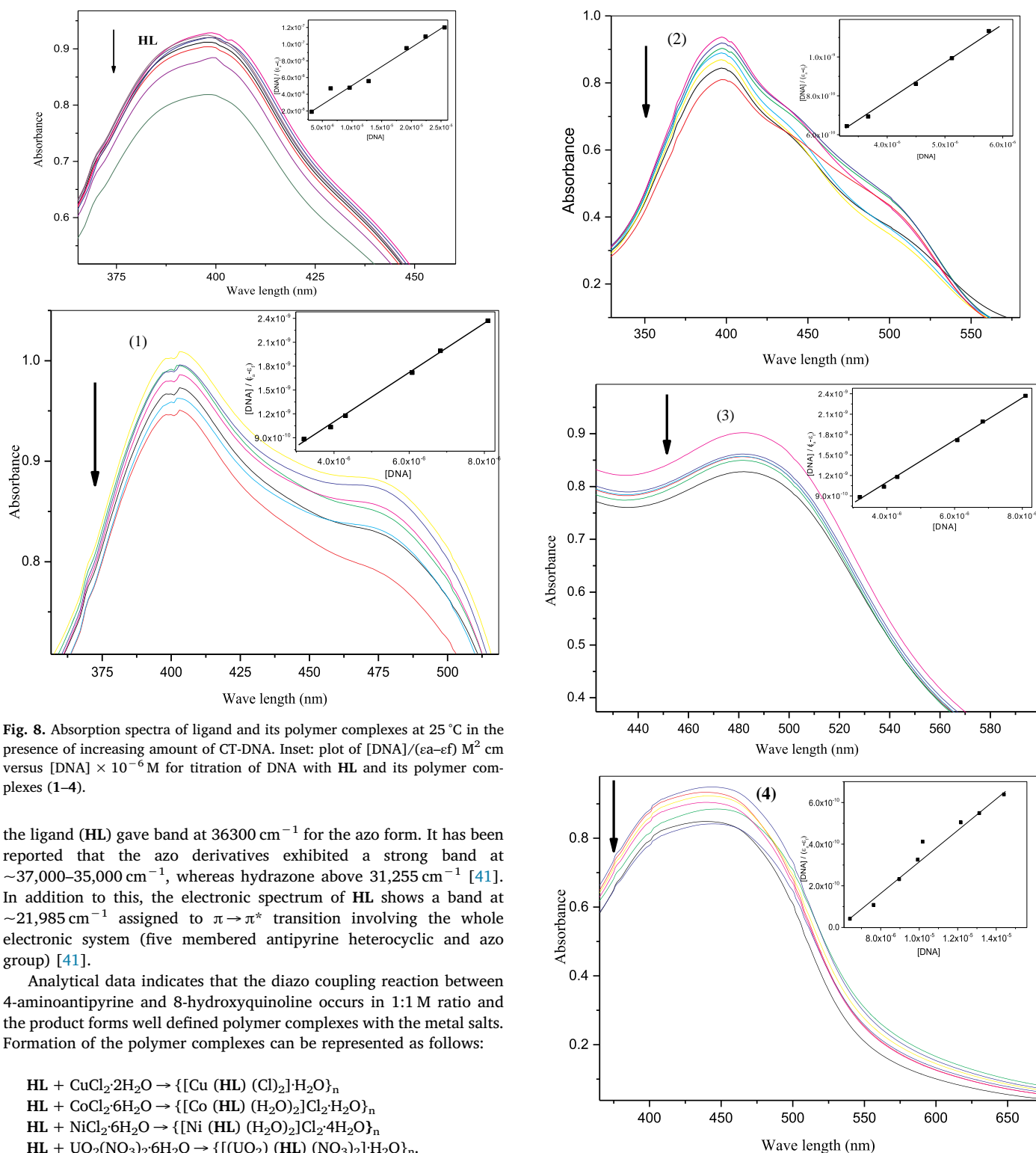
Interactions

701:	LEU
705:	ASN
711:	GLN
742:	MET
745:	MET
746:	VAL
749:	MET
752:	ARG
764:	PHE
787:	MET
876:	PHE
877:	THR
880:	LEU
891:	PHE
895:	MET
899:	ILE

(a)

Interactions

1699:	ARG
1700:	THR
1701:	LEU
1702:	LYS
1775:	MET
1835:	ARG
1836:	GLU
1839:	LEU

(b)

Fig. 7. HB plot of interaction between **HL** and receptors of (a) prostate cancer (PDB code 2Q7L Hormone) and (b) breast cancer (PDB code 1JNX Gene regulation).

Table 6

Energy values obtained in docking calculations of **HL** with receptors of prostate cancer (PDB code 2Q7L Hormone) and the breast cancer (PDB code 1JNX Gene regulation).

Receptors	Est. free energy of binding (kcal/mol)	Est. inhibition constant (K_i) (μM)	vdW + bond + desolv energy (kcal/mol)	Electrostatic energy (kcal/mol)	Total intercooled energy (kcal/mol)	Interact surface
2Q7L	−7.07	6.57	−6.05	−0.23	−6.28	623.32
1JNX	−5.16	164.01	−5.60	−0.03	−5.63	650.267

Fig. 8. Absorption spectra of ligand and its polymer complexes at 25 °C in the presence of increasing amount of CT-DNA. Inset: plot of [DNA]/(εa–εf) M^2 cm versus [DNA] × 10^{-6} M for titration of DNA with **HL** and its polymer complexes (**1–4**).

the ligand (**HL**) gave band at 36300 cm^{-1} for the azo form. It has been reported that the azo derivatives exhibited a strong band at ~37,000–35,000 cm^{-1}, whereas hydrazone above 31,255 cm^{-1} [41]. In addition to this, the electronic spectrum of **HL** shows a band at ~21,985 cm^{-1} assigned to $\pi \rightarrow \pi^*$ transition involving the whole electronic system (five membered antipyrine heterocyclic and azo group) [41].

Analytical data indicates that the diazo coupling reaction between 4-aminoantipyrine and 8-hydroxyquinoline occurs in 1:1 M ratio and the product forms well defined polymer complexes with the metal salts. Formation of the polymer complexes can be represented as follows:

HL + $CuCl_2 \cdot 2H_2O \rightarrow \{[Cu\ (\textbf{HL})\ (Cl)_2] \cdot H_2O\}_n$

HL + $CoCl_2 \cdot 6H_2O \rightarrow \{[Co\ (\textbf{HL})\ (H_2O)_2]Cl_2 \cdot H_2O\}_n$

HL + $NiCl_2 \cdot 6H_2O \rightarrow \{[Ni\ (\textbf{HL})\ (H_2O)_2]Cl_2 \cdot 4H_2O\}_n$

HL + $UO_2(NO_3)_2 \cdot 6H_2O \rightarrow \{[(UO_2)\ (\textbf{HL})\ (NO_3)_2] \cdot H_2O\}_n$.

Fig. 8. (*continued*)

Fig. 9. The relation between binding constants (K_b) vs. ionic radii of metal polymer complexes.

Table 7

Antifungal activity of Cu(II) polymer complex (**1**) against *Aspergillus niger* in comparison to miconazole as a standard drug. The results were recorded as the average diameter of inhibition zone (mm) ± standard errors.

Compound	Concentration (µg/mL)	Diameter of inhibition zone (mm)
Cu(II) polymer complex (**1**)	50	10 ± 0*
	100	10 ± 0*
	150	14 ± 0.58*
Miconazole (Standard drug)	50	1 ± 0
	100	3 ± 0.14
	150	4 ± 0

* Indicate significant different value from that of miconazole at probability (p) value = 0.05.

On the basis of the proposed structure is shown in Fig. S1, the molecular formula of the HL ligand is $C_{20}H_{17}N_5O_2$ which upon chelation coordinates with one central metal atom at four coordination sites and with two water or Cl_2 or $(NO_3)_2$ molecules. There is an evidence of the existing of chlorine ions in Cu(II) complex (**1**) which has been confirmed by the addition of $AgNO_3$ solution. The data of elemental analyses reported in Table 1 are in agreement with the calculated percentage values of carbon, hydrogen and nitrogen based on the above mentioned molecular formula of parent ligand as well as coordination polymers.

3.2. X-ray analysis

The X-ray powder diffraction is used for determining the structure of the azo ligand (**HL**) and its polymer complexes (**1**, **2** and **4**). The XRD patterns show that **HL** ligand and its polymer complexes (**2** and **4**) have a polycrystalline nature while polymer complex (**1**) has completely amorphous nature as shown in Fig. 1. The crystallographic data of **HL** and polymer complexes (**2** and **4**) are tabulated in Table 2. The calculated crystal system of **HL** and polymer complex **4** is found to be monoclinic with spacing group P21 for each compound. Polymer complex **2** has triclinic crystal system with spacing group P1. The lattice parameters are found to be 13.08 Å, 13.70 Å, 9.57 Å, 90°, 95.24° and 90° for a, b, c, α, β and γ, respectively for **HL** azo ligand. The estimated lattice parameters of polymer complex (**2**) are 10.16 Å, 19.62 Å, 14.81 Å, 106.56°, 101.26° and 86.09° for a, b, c, α, β and γ, respectively, while they are 15.38 Å, 13.63 Å, 9.56 Å, 90°, 122.84° and 90° for a, b, c, α, β and γ, respectively for polymer complex (**4**). Table 2 shows the Miller indices (hkl) and inter-planar spacing (d) estimated by CRYSFIRE [22].

From the XRD pattern and according to Debye–Scherrer equation
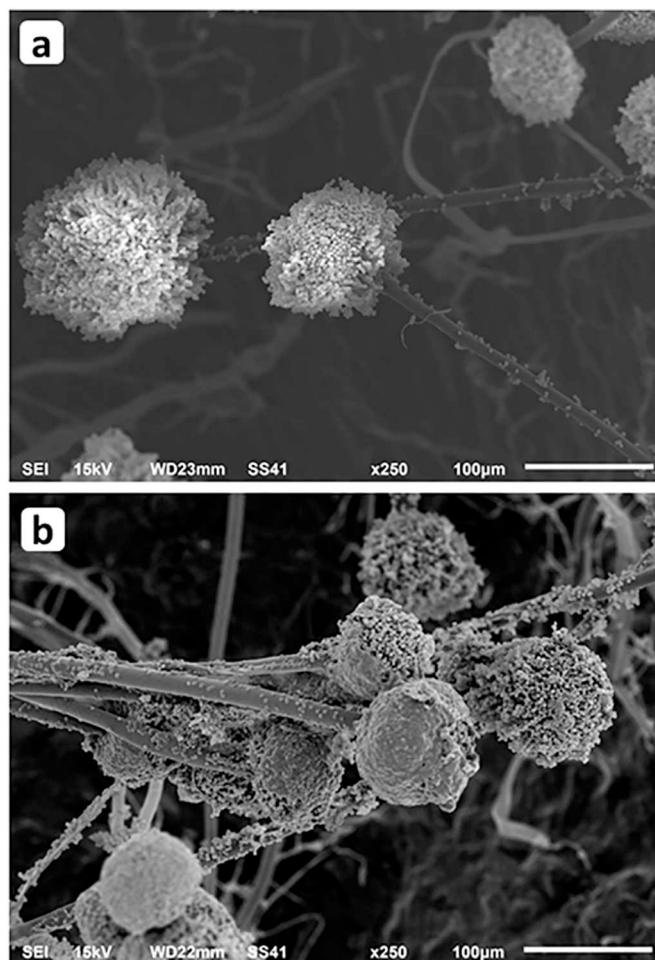
Fig. 10. Scanning Electron Micrograph of normal *A. niger* mycelia (a) and control DMSO-treated mycelia (b) show smooth and plump mycelia with normal conidial heads on conidiophores.

[3,48], the average crystallite size (*V*) can be calculated:

$$V = \frac{K\lambda}{\Psi \cos\theta} \tag{6}$$

The equation uses the reference peak width at angle (θ), where K is the constant taken as 0.95 for organic compounds [3,48], k is the wavelength of X-ray radiation (1.540598 A) and ψ is the width at half maximum of the reference diffraction peak measured in radians. The dislocation density, δ_*, is the number of dislocation lines per unit area of the crystal. The value of δ_* is related to the average particle diameter (V) by the relation [3,48]:

$$\delta_* = \frac{1}{V^2} \tag{7}$$

The values of (V) are calculated and found to be 45.3, 55.1 and 135.98 nm for **HL** ligand and its polymer complexes (**2** and **4**), respectively. δ_* values are 4.87×10^{-4}, 3.29×10^{-4} and $5.41 * 10^{-5} \, nm^{-2}$ for **HL**, polymer complex (**2**) and polymer complex (**4**), respectively.

3.3. ^1H and ^{13}C NMR spectral studies

Further evidence for the coordinating mode of the ligand was obtained by ^1H NMR spectral study. The ^1H NMR spectral (Fig. 2a) of **HL** and its UO_2(II) polymer complex (Fig. 2b) were recorded in DMSO-d_6 solution. The signals assigned to the aryl protons in the aromatic system appear as overlapped doublets/multiplets at the region 7.18–8.95 ppm.
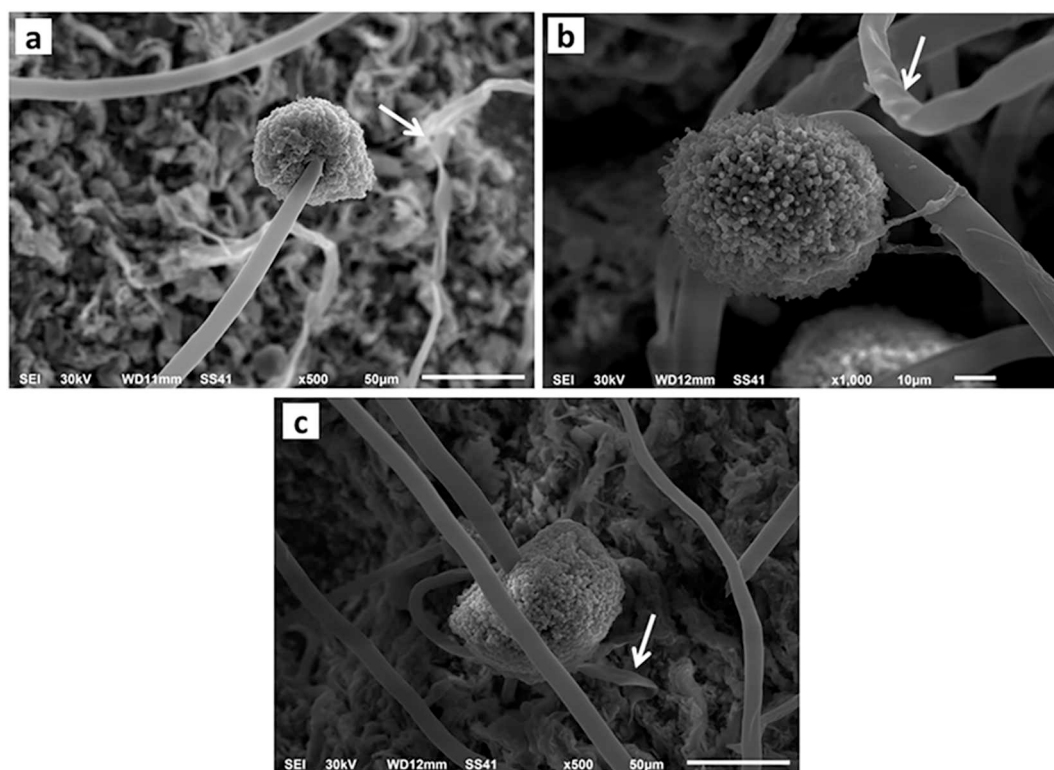
Fig. 11. Scanning Electron Micrograph of *A. niger* treated-mycelia by different concentrations of miconazole: 50 μg/ml (a), 100 μg/ml (b), and 150 μg/ml (c). Arrows indicate distorted *A. niger* mycelia.

The formed signal at δ 8.94 ppm is due to the proton of azomethine quinoline group (C=N$_{py}$) group. Broad and weak signal peak shows at δ 10.350 ppm, not affected by dilution but disappears when a D$_2$O exchange experiment was carried out. This signal appears without any other fragments which meant that **HL** ligand has only one tautomeric structure in the solution under the experimental conditions. The weakness and broadness of this type of proton signal might be caused by dimmer formation between two hydroxyl quinoline groups of two different molecules [49].

Fig. 2b shows the ^{1}H NMR spectrum of the uranyl polymer complex (**4**). The resonance resulting from –OH proton is shifted to δ 10.327 ppm which attributed to the involvement of the phenolic group in the coordination as neutral group. The shift in the C=N$_{py}$ group signal assigned to the participation of this group in the complexation reaction. The aromatic protons observed in the ligand, show small shifts in polymer complex (**4**), due to variation in electron density and steric constraints because of chelation A new singlet appeared at 3.85 ppm in the spectrum of UO$_2$(II) complex indicates the presence of coordinated water molecule in the polymer complex [50].

The ^{13}C NMR spectrum of **HL** displays the signals at 12 and 36 ppm which were due to carbon atoms of two methyl groups attached to the pyrazolone ring. The carbon atoms of N=N, –OH and C=O groups appear at 124, 153 and 157 ppm, respectively. The disappearance of the signal for the N—H proton in the hydrazone form (Fig. S2(B)) indicated that **HL** is found in solution as azo-keto form (Fig. S2(A)). Some azo quinolines structures were found in the azo form in the crystal form [37].

3.4. Theoretical studies of tautomerisation

The synthesized azo ligand (**HL**) is found to have tautomeric structures (**A-F**) as shown in Fig. S2. The geometrical studies of the **HL** conformers have been optimizes by the theoretical studies using HF method with 3-21G basis set. The geometrical structure of the

conformer dimmer (**E**) (Fig. 3) has been done using Perkin Elmer ChemBio Draw and optimized by Perkin Elmer ChemBio3D software. Selected bond lengths and bond angles for each conformer are tabulated in Table 3. The highest occupied molecular orbital energy (E$_{HOMO}$), the lowest unoccupied molecular orbital energy (E$_{LUMO}$) and the energy gab between them values are listed in Table 4. Fig. 4 shows the HOMO and LUMO orbital's for dimmer form (**E**). It is known that the lest energy gab values, the most reactive and stable molecule [51–54]. The values of the energy gab point to that the dimmer form (**E**) is more stable and reactive than the other conformers. Quantum chemical parameters have been calculated [53] and tabulated in Table 4.

3.5. Thermal studies

The TGA analysis of **HL** and all polymer complexes (**1–4**) are measured from 30 °C to 800 °C with heat flow 15 °C/min as shown in Fig. 5 and listed in Table 5. The TGA curve of **HL** shows two degradation stages, the first stage in the range 212–440 °C with 43.24% (calc. 43.18%) mass loss which assigned to loss C$_5$H$_7$N$_4$O$_2$. The second stage is found from 440 °C to 600 °C and mass loss percentage equals 56.76% (calc. 56.82%) due to C$_{15}$H$_{10}$N loss.

TGA measurements and spectroscopic analyses studies can elucidate the structure of the polymer complexes. TGA studies of the polymer complexes (**1–4**) under investigation can be used in determining the thermal stability of these new compounds, as well as to determining the nature of the coordinated (water and/or solvent and/or anions) molecules to the central metal ion and its coordination nature (outside and/or inside) in the coordination sphere. All investigated polymer complexes have three degradation stages, the first degradation starts at ~40 °C indicating the loss of uncoordinated water molecules. The second degradation stage assigns to the loss of coordinated chlorine atoms in polymer complex (**1**), while polymer complexes (**2 and 3**) lost the outer Cl$_2$ molecule and polymer complex (**4**) lost a part of the ligand (Table 5). The final stage is due to the removal of the coordinated water
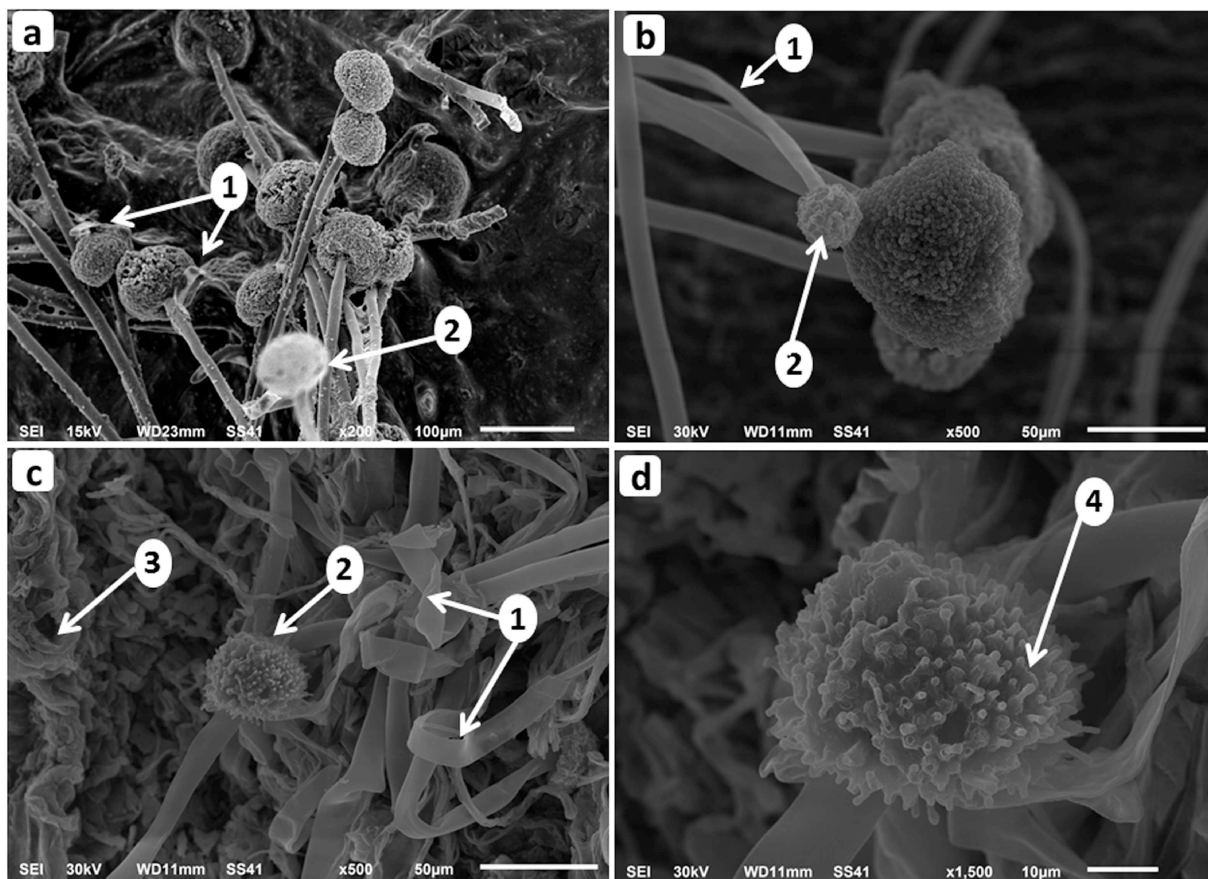
Fig. 12. Scanning Electron Micrograph of *A. niger* treated-mycelia by different concentrations of Cu(II) polymer complex **(1)**: 50 µg/ml (a), 100 µg/ml (b), and 150 µg/ml (c and d). Arrows indicate flattened distorted mycelia and conidiophores (1) bearing reduced conidial heads (2), some squashed mycelia (3), and sterigmata of a reduced conidial head without any conidia (4).
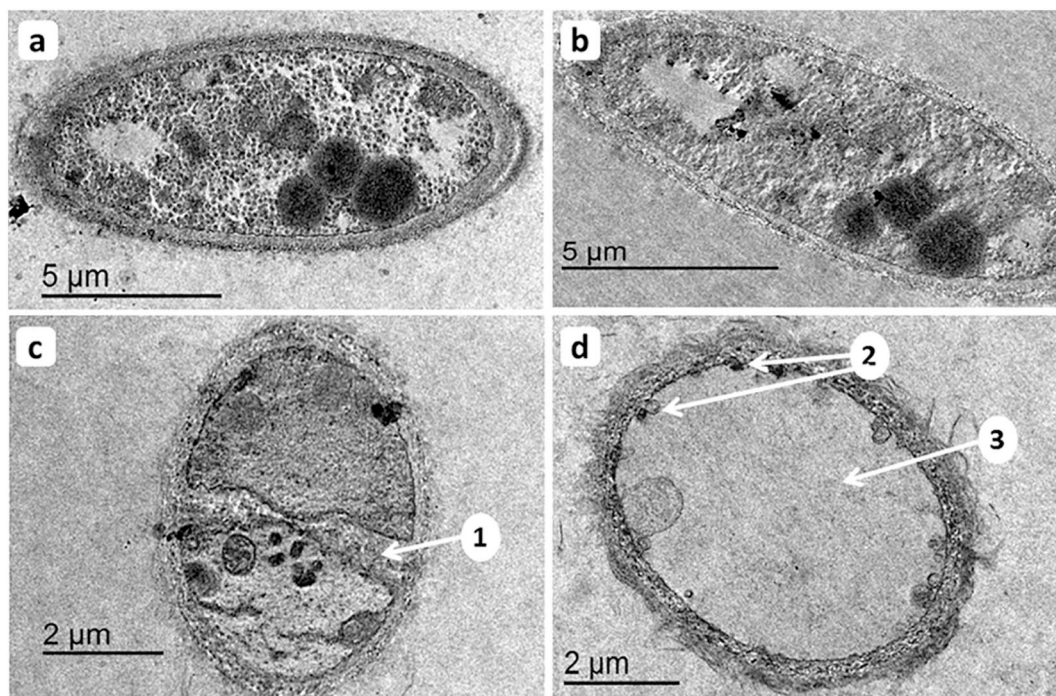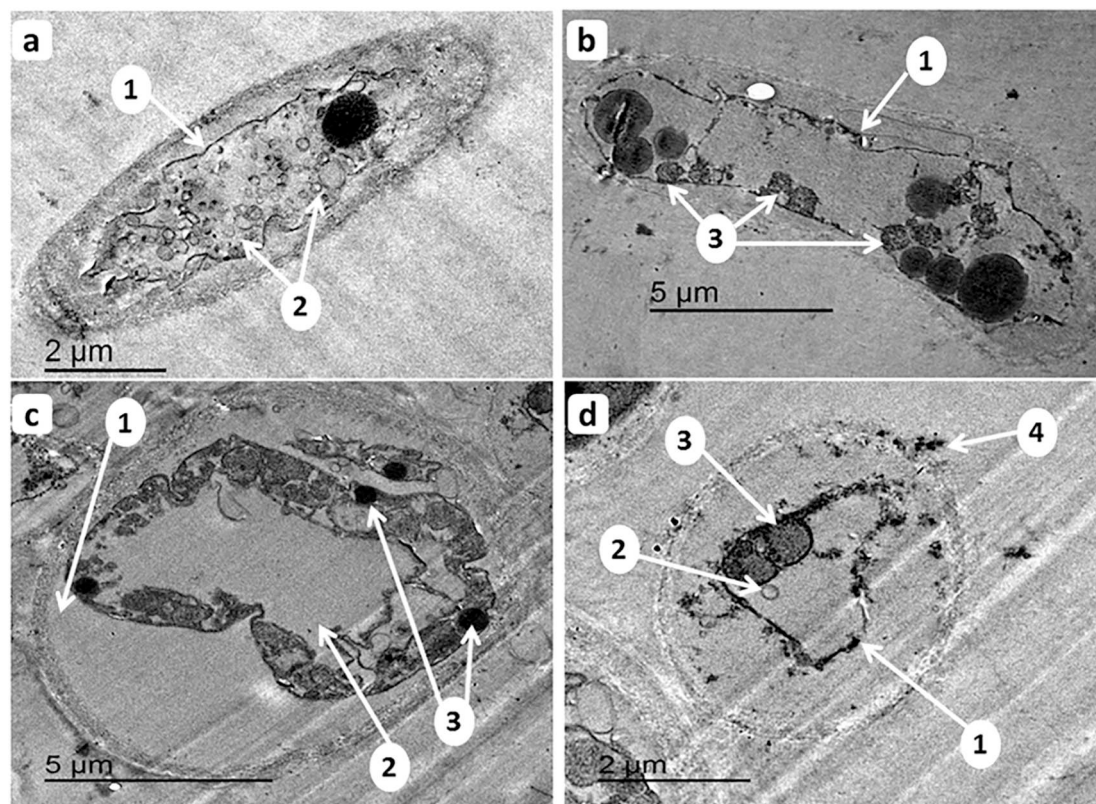

Fig. 13. Transmission Electron Micrograph of sections in normal *A. niger* mycelium (a) shows normal organelles in a homogeneous cytoplasm enclosed by a regular cell wall with a tight plasma membrane; and control DMSO-treated mycelia (b–d) show a normal mycelial cell (b), a normal proliferated mycelial cell (c), and an empty mycelial cell (d). Arrows indicate a septum in the proliferated cell (1), autophagosomes engulfed by a vacuole (2) and an expanded vacuole covering the entire cell (3).

Fig. 14. Transmission Electron Micrograph of sections in *A. niger* treated-mycelia by different concentrations of miconazole: 50 μg/ml (a), 100 μg/ml (b), and 150 μg/ml (c and d) show cells containing vacuoles with ruptured cell walls that detached from cell membranes. Arrows indicate detachment of cell wall which increased electron lucent region between the cell wall and cell membrane (1), vacuoles (2), autophagosomes (3), and lysed cell wall with leakage of cytoplasmic contents (4).

molecules if found leaving metal oxides as a residue.

3.6. Molecular docking studies

The molecular docking is to simulate the molecular recognition process by achieving an optimized conformation for the protein and drug with relative orientation between them such that the free energy of the overall system is minimized. Molecular docking has been studied between azo **HL** ligand and two types of proteins which are receptors of prostate cancer (PDB code 2Q7L Hormone) and the breast cancer (PDB code 1JNX Gene regulation). The docking studies show an acceptable interaction between **HL** and the receptor of each protein as cleared in Fig. 6. Fig. 7 shows HB plot curves due to the binding of ligand **HL** to the proteins by hydrogen bonding interactions. The calculated binding energy values are tabulated in Table 6.

The **HL** is lower free energy of binding, the higher inhibition constant affinity and stronger inhibitory activity against receptor target. According to the results showed in Table 6, the receptor of prostate cancer (PDB code 2Q7L Hormone) shows the best interaction with **HL**.

3.7. DNA binding studies

The binding mode and binding extent of **HL** and its polymer complexes (**1–4**) with Calf Thymus (CT) DNA have been investigated by UV absorption spectra of fixed concentration (40 μM) of each compound in the absence and presence of gradually increasing concentration of DNA at room temperature.

By studying the absorption intensity changes of the charge transfer spectral bands, the intrinsic binding constant (K_b) can be determined near 399, 405, 412, 480 and 427 nm for **HL** ligand, Cu^{2+}, Co^{2+}, Ni^{2+} and UO_2^{2+} polymer complexes, respectively. The absorption spectra of these compounds with increasing concentration of calf thymus DNA

(CT-DNA) in the range 300–700 nm are shown in Fig. 8.

Increasing CT-DNA concentration leads to a red shift and hypochromism behavior, due to the non-covalently intercalative binding between compound and DNA helix. This because of the strong stacking interaction of the aromatic chromophore of the compound and base pairs of DNA [55,56]. In hypochromism behavior, the π* orbital of the interacting compound couples with the π orbitals of the base pairs and decreasing the $\pi \rightarrow \pi^*$ transition energies after interacting the compound to the base pairs of DNA [57].

In order to quantitative comparing between the binding strengths of the azo ligand and its polymer complexes, the intrinsic binding constant (K_b) has been determined by observing the changes in absorbance of the compounds with increasing concentration of DNA. Calculated K_b values are 5.36×10^5, 1.65×10^6, 1.29×10^6, 2.39×10^6 and $1.85 \times 10^6 \, M^{-1}$ for **HL**, **1**, **2**, **3** and **4** polymer complexes, respectively. From resulted K_b values, it is clear that the binding ability of the polymer complexes (**1–4**) to the CT-DNA is stronger that the binding of their corresponding ligand (**HL**), that is due to existing intermolecular containing π-π stacking and hydrogen-bonding interactions. It was found that the K_b value increase with decreasing the ionic radii of metal polymer complexes and the polymer complex (**3**) is higher compared to the other polymer complexes (Fig. 9), due to the lower ionic radius.

3.8. Antimicrobial activities of the HL and polymer complexes

HL ligand did not showed any antimicrobial activity; among its Cu^{2+}, Co^{2+}, Ni^{2+} and UO_2^{2+} polymer complexes. Only Cu(II) polymer complex (**1**) showed a significant specific antimicrobial activity only against the fungus *Aspergillus niger* (Table 7). This effect was higher than that of miconazole by at least three times; it also increased with increasing the concentration (Table 7). This represents a promising finding; since the antifungal-resistant strains of *Aspergillus* are becoming
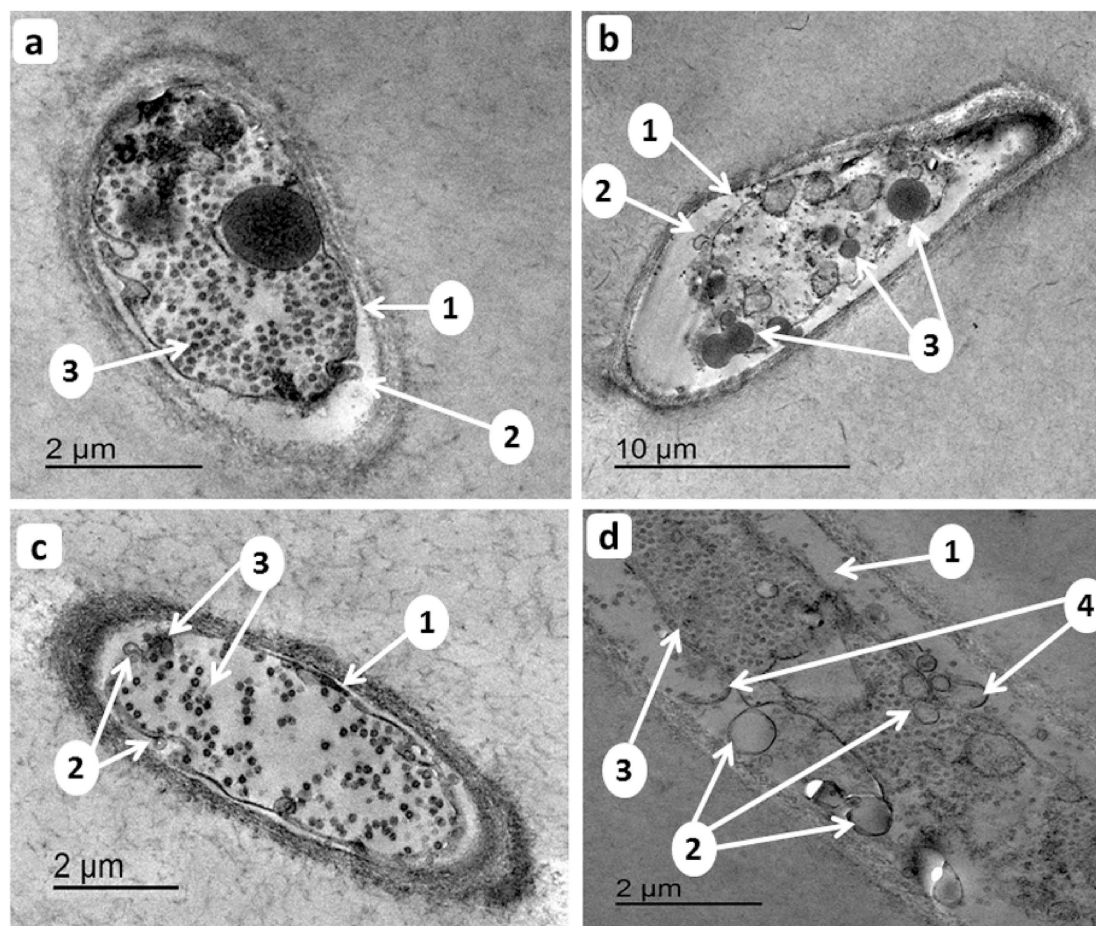
Fig. 15. Transmission Electron Micrograph of sections in *A. niger* treated-mycelia by different concentrations of Cu(II) polymer complex **(1)**: 50 μg/ml (a), 100 μg/ml (b), and 150 μg/ml (c and d) show cells containing vacuoles and several autophagosomes with detached cell walls from cell membranes. Arrows indicate detachment of cell wall which increased electron lucent region between the cell wall and cell membrane (1), autophagosomes engulfed by vacuoles (2), accumulated intact autophagic bodies within vacuoles (3), and some phagophores (4).

Table 8
Surface coverage (θ) and inhibition efficiency (%IE) of **HL** with their molar concentrations at different temperatures from weight loss measurements at 60 min immersion in 2 M HCl.

Compound	Concentration (M)	30 ± 0.1 °C		40 ± 0.1 °C		50 ± 0.1 °C		60 ± 0.1 °C	
		Surface coverage (θ)	Inhibition efficiency (%IE)	Surface coverage (θ)	Inhibition efficiency (%IE)	Surface coverage (θ)	Inhibition efficiency (%IE)	Surface coverage (θ)	Inhibition efficiency (%IE)
HL	1×10^{-6}	0.55	54.59	0.46	45.67	0.40	40.44	0.28	28.94
	3×10^{-6}	0.60	59.85	0.53	52.55	0.51	50.95	0.39	39.04
	5×10^{-6}	0.64	64.20	0.60	59.84	0.57	56.75	0.44	44.42
	7×10^{-6}	0.70	69.84	0.66	66.15	0.62	62.23	0.50	49.71
	9×10^{-6}	0.76	75.75	0.74	73.8	0.68	67.51	0.55	54.90
	11×10^{-6}	0.82	82.16	0.81	81.01	0.71	71.27	0.60	60.19

more common and the mechanisms of their resistance are evolving [58]. *A. niger* is a saprophytic mold which can grow upon different organic substrates causing deterioration of food [59], archives [60], and museum collections [61]. It also implicates in mycotoxins production [58], nosocomial infections [62], and aspergillosis diseases [63].

HL and its polymer complexes, as 8-hydroxyquinoline derivatives, were expected to have fungicidal property since the activity of quinoline derivatives are attributed to the C-4 and/or C-8 substitution on the quinolone ring [64]. However, only Cu(II) polymer complex **(1)** showed a significant activity. The presence of chlorine atoms would enhance the antifungal activity of a compound depending on their positions (*para* is the most effective position) and numbers (more groups are the

more effective) [64]. In addition, copper complexes usually have antifungal activities [65] beside the fact that copper itself damages fungal cell membrane [66,67]; and also increases liposolubility of the complexes [68].

3.9. Morphological changes in Cu(II) polymer complex (1) treated A. niger

Both untreated and DMSO-treated mycelia showed the typical characteristic morphology of *A. niger*; smooth plump hyphae and large radiated conidial heads with sterigmata bearing chains of conidia appear in Fig. 10. Upon treating *A. niger* with either miconazole or Cu(II) polymer complex **(1)**, distorted mycelia represented the prominent morphological changes (Figs. 11 and 12). The mycelial distortion
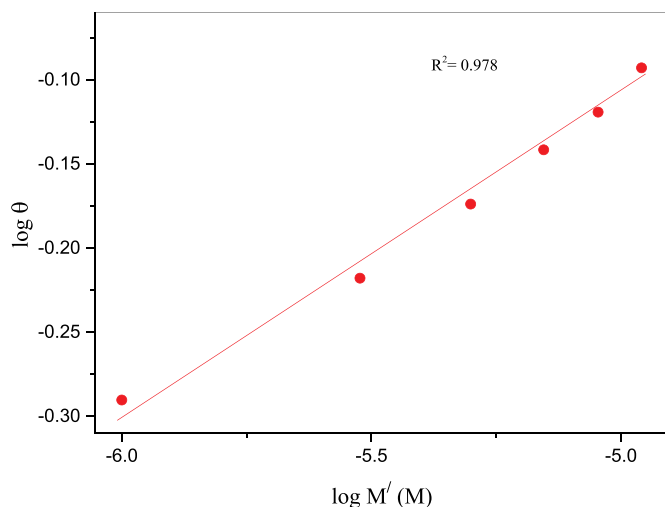
Fig. 16. Friendlish adsorption isotherm plotted as θ vs. log M′ of **HL** for corrosion of carbon steel in 2 M HCl solution from weight loss method at 30 ± 0.1 °C.

increased with increasing the concentration of the treatments; at 150 μg/ml of Cu(II) polymer complex **(1)**, the mycelia became squashed. This indicates some modifications in the cell walls, which is expected upon miconazole treatment; miconazole inhibits the biosynthesis of ergosterol (the major fungal cell wall component) [69]. This morphological malformation is usually associated with altered cell walls due to stress of antimicrobial chemicals [28].

In addition to the altered hyphae, Cu(II) polymer complex **(1)**-treated *A. niger* formed reduced conidial heads (Fig. 12); which contained only sterigmata without any conidia at 150 μg/ml (Fig. 12d). This response was observed under stress of other antimicrobials by *A. niger* [70,71]. This defect in sporulation reflects some physiological changes that may be attributed to cytological changes.

3.10. Cytological changes in Cu(II) polymer complex (1) treated A. niger

Control untreated *A. niger* cells showed normal organelles in a homogeneous cytoplasm enclosed by a regular cell wall with a tight plasma membrane (Fig. 13a); while control DMSO-treated mycelia became heterogeneous showing some normal cells (Fig. 13b), some proliferated cells (Fig. 13c), and little empty cells (Fig. 13d). By comparing with controls, Cu(II) polymer complex **(1)**-treated *A. niger* cells showed a characteristic accumulation of autophagic bodies within expanded vacuoles in addition to other autophagic markers and disruption of cell membranes (Figs. 14 and 15). But, those treated with miconazole only showed disrupted plasma membrane and some autophagic markers (vacuoles and autophagosomes) (Figs. 14 and 15).

Although Cu(II) polymer complex **(1)** more inhibited *A. niger* than miconazole, the plasma membrane in the Cu(II) polymer complex **(1)** treated mycelia was less disrupted than that in miconazole treated ones; where it was more detached from the cell wall increasing electron-lucent region between them (Figs. 14 and 15); and where cell walls were also sometimes ruptured and cytoplasmic contents were leaked (Fig. 14d). This indicates that miconazole rather Cu(II) polymer complex **(1)** targets the cell membrane and cell wall; miconazole represents an antifungal targeting cell walls through the ergosterol biosynthesis pathway [69].

Autophagy was observed by TEM in treated mycelia with DMSO, miconazole and Cu(II) polymer complex **(1)**. Autophagy involves a catabolic mechanism to recycle defective cell constituents (cytoplasmic proteins and organelles), within vacuoles, under stress conditions [72] or during normal developmental transitions [73]. DMSO-treated mycelial cells included little empty cells with autophagosomes fused with

an expanded vacuole (Fig. 13d); it might have adapted to DMSO stress through autophagy; hence, showed normal morphology in SEM. Vacuoles and autophagosomes also appeared in both miconazole and Cu(II) polymer complex **(1)** treated mycelia (Figs. 14 and 15); autophagosome is usually observed by TEM as two parallel membrane bilayers separated by an electron-lucent region [74]. In Cu(II) polymer complex-treated mycelial cells (Fig. 15d), stages of a non-selective autophagy-as described by Voigt and Pöggeler [72] was observed (a phagophore non-selectively engulfs cytoplasm containing proteins and organelles to form a double-membrane autophagosome; whose outer membrane fuses with a vacuole; an autophagic body surrounding by the inner autophagosomal membrane released into the vacuole), but the released autophagic bodies were accumulated in the vacuoles rather than degraded by hydrolytic enzymes for re-use. Thus, Cu(II) polymer complex **(1)** appeared to deactivate autophagy in *A. niger*. Impairment of autophagy in *A. niger* reduced conidiation considerably [75]; that was observed by SEM in the morphology of Cu(II) polymer complex **(1)**-treated mycelial cells.

3.11. Corrosion studies

One of the most effective methods in metals and alloys protection from corrosion is the inhibition process. Organic corrosion inhibitors are better than inorganic salt corrosion inhibitors as they are inexpensive and less pollution in reducing metals or alloys degradation in many fields of applications, and which has been extensively investigated during the last decade [76–78].

3.11.1. Weight loss measurements and adsorption isotherm

Fig. S3 shows the relation between percentage of weight loss and time during corrosion reaction for carbon steel immersed in 2 M HCl in presence and absence of **HL** at concentrations $(1 \times 10^{-6}$–11×10^{-6} M) at 30 ± 0.1 °C after 60 min. of immersion. The resulted surface coverage (θ) and the inhibition efficiency (% IE) values (using Eqs. (2) and (3)) are tabulated in Table 8. From values of θ and % IE, we concluded that by increasing the **HL** concentration the surface coverage (θ) and the inhibition efficiency (% IE) are increased. It seems that the **HL** molecule may form monomolecular layers adsorbing on the surface of the metal thereby protecting corrosion of carbon steel in 2 M HCl [79]. By increasing the temperature, the calculated values of θ and %IE are decreased as shown in Table 8.

Testing several adsorption isotherms leads to the most suitable one which is found to be Friendlish isotherm. It can be described by:

$$\log \theta = \log K_{ads} + a \log M' \qquad (8)$$

where K_{ads} is the constant of the adsorption equilibrium, a is the interaction parameter and M' is **HL** concentration. By plotting a relation between θ versus log M' as shown in Fig. 16, K_{ads} can be calculated from the resulted linear relation. $\Delta G°_{ads}$ can be calculated from:

$$\text{Log } K_{ads} = -\log 55.5 - \Delta G°_{ads}/2.303 \, RT \qquad (9)$$

The value of $\Delta G°_{ads}$ equals -14.906 kJ mol^{-1}, the negative value of $\Delta G°_{ads}$ is due to the spontaneity of the adsorption process and the stability of the adsorbed layer on the carbon steel surface [76]. The values of K_{ads} and a equal to 6.683593 M^{-1} and 0.18715, respectively. The value of ΔG_{ads} is -14.906 kJ mol^{-1} which indicates that the adsorption mechanism is physisorption, as it is known that ΔG_{ads} values up to -20 kJ mol^{-1}.

3.11.2. Electrochemical Frequency Modulation technique (EFM)

Fig. 17 shows the EFM intermodulation spectra of carbon steel in 2 M HCl solution containing different concentrations solution in presence of different concentrations of **HL** at 30 ± 0.1 °C. The causality factors (CF-2 and CF-3) are the great strength of the EFM as they serve as an internal check on the validity of EFM measurement. They are calculated from the frequency spectrum of the current responses. The
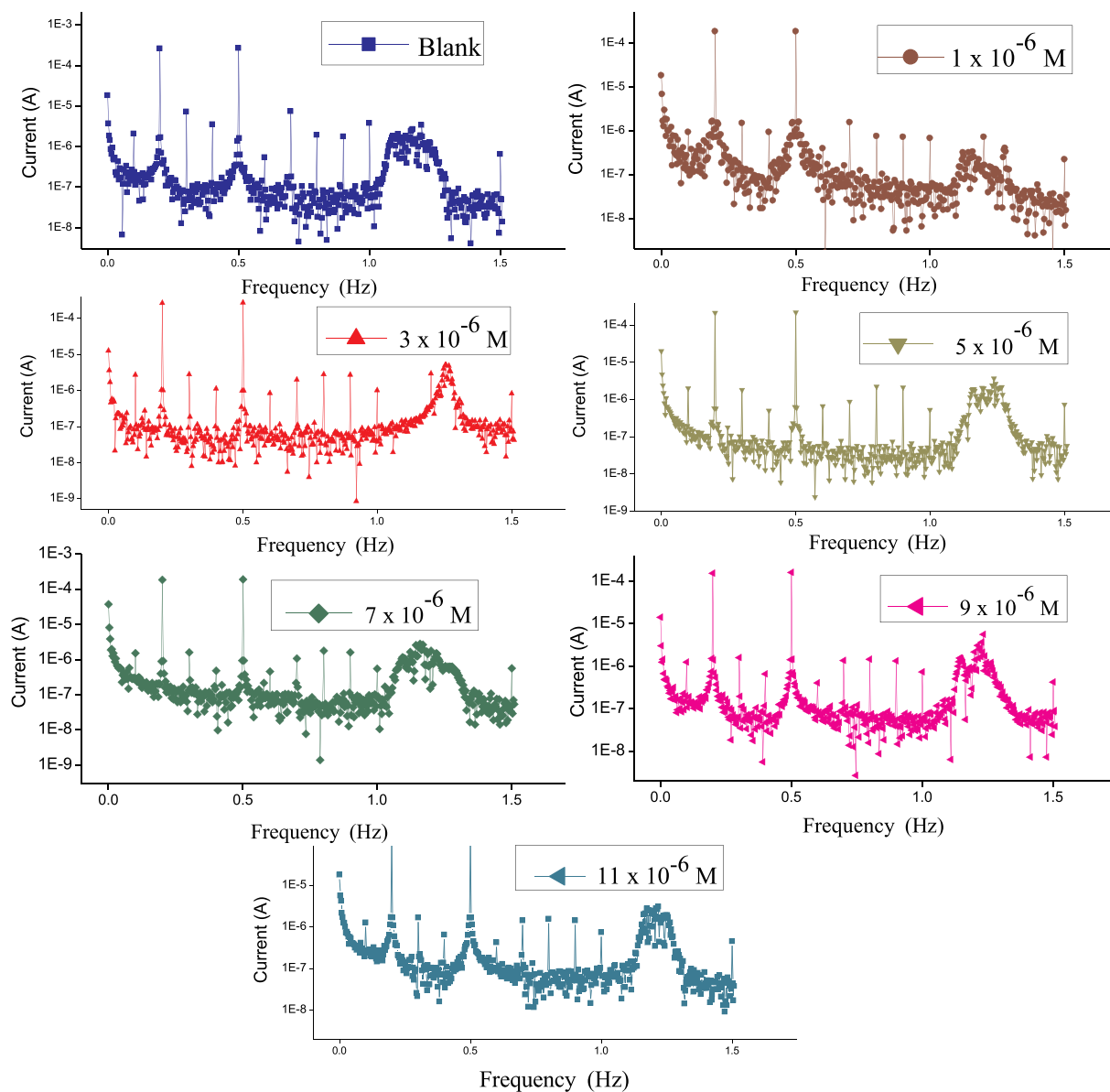
Fig. 17. EFM spectra for the corrosion of carbon steel in 2 M hydrochloric acid in the absence and presence of various concentrations of **HL** ligand at 30 $\pm$ 1 °C.

Table 9
Electrochemical kinetic parameters obtained by EFM technique for carbon steel in 2 M HCl without and with various concentrations of **HL** at 30 $\pm$ 0.1 °C.

Compound	Concentration (M)	i_{corr}, μA cm^2	$\beta a \times 10^{-3}$, mV dec^{-1}	$\beta c \times 10^{-3}$, mV dec^{-1}	CF-2	CF-3	θ	%IE
Blank		508.9	170.1	186.1	1.8	2.9	–	–
HL	1×10^{-6}	294	120.3	117.3	2.0	3.1	0.481	48.1
	3×10^{-6}	291.7	118.2	123.2	2.0	2.9	0.482	48.2
	5×10^{-6}	283.3	121.0	110.1	3.1	2.1	0.508	50.8
	7×10^{-6}	282.2	108.5	116.9	1.9	2.2	0.562	56.2
	9×10^{-6}	273.3	122.8	119.3	3.1	2.3	0.593	59.3
	11×10^{-6}	248.6	125.3	119.0	3.2	1.9	0.611	61.1

intermodulation and harmonic peaks are visible and much larger than the background noise. The two large peaks at 200 μA amplitude are the response to the 40 and 100 mHz (2 and 5 Hz) excitation frequencies. Between the peaks there is nearly no current response (< 100 nA). The experimental EFM data have been treated using two different models:

1. Complete diffusion control of the cathodic reaction.
2. The "activation" model.

For activation model a set of three non-linear equations have been solved, assuming that the corrosion potential does not change due to the polarization of the working electrode. The corrosion current density (i_{corr}), the Tafel slopes (β_c and β_a), the causality factors (CF-2 and CF-3) and the inhibition efficiency (%IE) (Table 9) are calculated from the larger beaks. Table 9 shows that the corrosion current densities decrease and the inhibition efficiencies increase by increasing the concentration of **HL** indicating that this compound inhibit the corrosion of

Table 10

Electrochemical impedance spectroscopy technique (EIS) for carbon steel in 2 M HCl without and with various concentrations of **HL** at 30 $\pm$ 0.1 °C.

Compound	Conc., M	R_S, Ωcm^2	Y, $\times 10^{-6}$ $\mu\Omega^{-1} s^n cm^{-2}$	$n \times 10^{-3}$	R_{CT}, Ωcm^2	C_{dl}, $\times 10^{-4}$ μFcm^{-2}	θ	IE%
Blank		1.1	115.7	796.6	53.77	1.80	–	–
HL	1×10^{-6}	1.174	443.8	774.8	96.60	1.56	0.443	44.3
	3×10^{-6}	1.141	445	773.9	97.64	1.55	0.449	44.9
	5×10^{-6}	1.344	468.3	761.9	111.30	1.49	0.516	51.6
	7×10^{-6}	1.331	456.8	770.1	130.8	1.44	0.588	58.8
	9×10^{-6}	1.190	447.5	771.1	147.0	1.43	0.634	63.4
	11×10^{-6}	1.362	446.7	778.1	193.0	0.48	0.721	72.1
	11×10^{-6}	2.453	111.9	868.4	267.7	0.6575	0.94	94.58
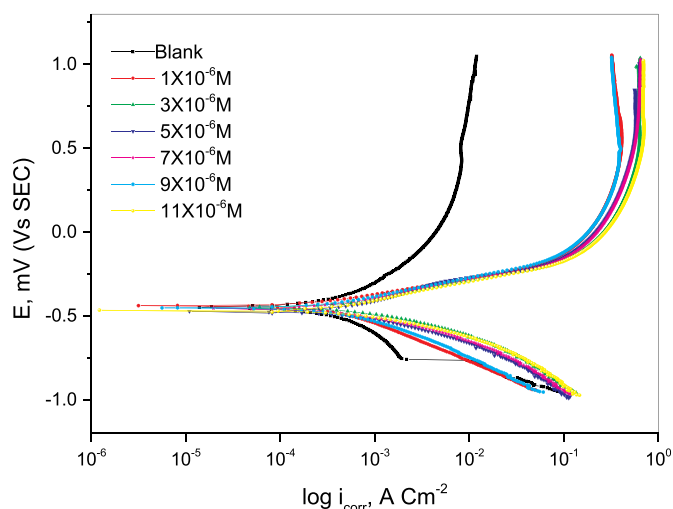
Fig. 18. Potentiodynamic polarization curves for the corrosion of carbon steel in 2 M HCl in the absence and presence of various concentrations of **HL** at 30 $\pm$ 0.1 °C.

carbon steel in 2 M HCl through adsorption. Increasing the inhibitor concentrations leads to increasing the inhibition efficiencies % IE$_{EFM}$ and which is calculated from the following equation:

$$\%IE_{EFM} = [1 - (i_{corr}/i^o_{corr})] \times 100 \qquad (10)$$

where i_{corr}^o and i_{corr} are corrosion current densities in the absence and presence of inhibitor, respectively.

3.11.3. Electrochemical impedance spectroscopy technique (EIS)

Electrochemical impedance spectroscopy technique curves give valuable information about the kinetics of the electrode processes as well as the surface properties of the studied system [29]. The Nyquist curves (Fig. S4(a)) and Bode (Fig. S4(b)) give mechanistic information about the effect of **HL** concentration on the impedance behavior of carbon steel immersed in 2 M HCl at 30 $\pm$ 0.1 °C. Fig. S4(C) shows the open-circuit potentials that was used in all the impedance spectra measurements. R_s, R_{ct} and CPE are solution resistance, charge transfer

resistance and constant phase element, respectively. The impedance diagrams show a semi-circular appearance which means that the corrosion of carbon steel in 2 M HCl is controlled by a charge transfer resistance process. Small distortion was observed in some diagrams may be due to frequency dispersion as a result of surface roughness, dislocation, impurities, adsorption of inhibitors, grain boundaries, formation of porous layers and in homogenates of the electrode surface. The data reveal that each impedance diagram consists of a large capacitive loop with one capacitive time constant in the Bode –phase plots (Fig. S4(b)). By increasing the concentration of the compound, the diameter of the capacitive loop increases which was indicative of the degree of inhibition of the corrosion process (Fig. S4(a)). The observed high frequency capacitive loop, the semi-circles rolled over and extended to the fourth quadrant, and a pseudo-inductive loop at low frequency end indicated that Faradic process is occurred on the free electrode sites. The inductive loop is attributed to the adsorption of species resulting from the carbon steel dissolution and the adsorption of hydrogen [29].

The inhibition efficiency (% IE) was calculated using eq. (4). The extracted impedance parameters from EIS plots are listed in Table 10. Increasing the inhibitor concentration leads to increasing the R$_{ct}$ values and decreasing the C$_{dl}$ values due to water molecules replacement by the adsorbed inhibitor molecules on the metal surface so, decreases the extent of dissolution reaction. The high R$_{ct}$ values are associated with slower corroding system [3,29]. Decreasing the local dielectric constant and/or from the increase of thickness of the electrical double layer leads to decreasing the C$_{dl}$ values, indicated that the inhibitor molecules function by adsorption at the metal/solution interface.

3.11.4. Potentiometric polarization technique

The polarization studies of the carbon steel/2 M HCl in absence and presence different concentrations of **HL** at 30 $\pm$ 0.1 °C is shown in Fig. 18. It is found that the Tafel-tybe is the dominant behavior. Fig. 18 showed that the existence of various concentrations of **HL** affected on the cathodic and anodic reactions of the corrosion process. Some electrochemical parameters resulted from the polarization curves are listed in Table 11, including the corrosion current densities (i$_{corr}$), corrosion potential (E$_{corr}$), the cathodic Tafel slope (β$_c$), anodic Tafel slope (β$_a$) surface coverage (θ) and inhibition efficiency (% IE) that calculated from the curves of Fig. 18. From Table 11, we can infer that

Table 11

Effect of concentrations of **HL** on the free corrosion potential (E$_{corr}$.), corrosion current density (i$_{corr}$.), Tafel slopes (βa & βc), degree of surface coverage (θ) and inhibition efficiency (% IE) for carbon steel in 2 M HCl at 30 $\pm$ 0.1 °C.

Compound	Conc, M	$i_{corr}. \times 10^{-4}$ mA cm^{-2}	$-E_{corr}.$ mV vs·SEC	$\beta_a \times 10^{-3}$, mV dec^{-1}	$\beta_c \times 10^{-3}$ mV dec^{-1}	θ	% IE
Blank		8.12	494	135.0	131.5	–	–
HL	1×10^{-6}	3.14	466	115.4	106.4	0.613	61.3
	3×10^{-6}	2.80	438	73.1	106.8	0.655	65.5
	5×10^{-6}	2.11	459	102.0	101.3	0.740	74.0
	7×10^{-6}	1.95	453	491.1	105.9	0.759	75.9
	9×10^{-6}	1.92	469	94.7	85.5	0.763	76.3
	11×10^{-6}	1.79	452	39.6	40.6	0.779	77.9

by increasing the concentration of **HL** the corrosion current density decreases. This indicates that **HL** acts as inhibitor compound retards the compound retards the dissolution of C-steel in 2 M HCl solution and the inhibition efficiency depends on the type of the inhibitor and its concentration. The presence of **HL** inhibitor retards anodic and cathodic reactions indicating that this inhibitor acts as mixed inhibitor. Increasing the inhibitor concentration leads to increasing the inhibition efficiency.

4. Conclusions

5-(2,3-Dimethyl-1-phenylpyrazol-5-one　azo)-8-hydroxyquinoline (**HL**) ligand and Cu^{2+}, Co^{2+}, Ni^{2+} and UO_2^{2+} polymer complexes are synthesized and characterized. Coordination polymers were structurally characterized by thermal analysis and spectroscopic studies. The ligand behaves as a neutral bis(bidentate) ligand when reacting with Cu^{2+}, Co^{2+}, Ni^{2+} and UO_2^{2+} ions and undergo coordination through four sites of coordination (azo dye nitrogen, carbonyl oxygen, phenolic oxygen and hetero nitrogen from pyridine ring). The XRD patterns show that **HL** ligand and its polymer complexes (**2** and **4**) have a polycrystalline nature while polymer complex (**1**) has completely amorphous nature. The calculated geometric parameters and vibrational frequencies are in good agreement for some of the bands. The molecular docking studies show that the binding between **HL** and receptor of prostate cancer (PDB code 2Q7L Hormone) is better than its interaction with receptor of breast cancer (PDB code 1JNX Gene regulation). The binding between **HL** and its polymer complexes with CT-DNA has been studied. All the polymer complexes bind to CT-DNA better than their corresponding ligand (**HL**). Cu(II) polymer complex (**1**) is an effective antifungal against *A. niger* even more than the miconazole standard drug; that finding may open a new way to combat resistant *A. niger* strains.

Appendix A. Supplementary data

Supplementary data to this article can be found online at https://doi.org/10.1016/j.msec.2019.05.012.

References

[1] Y.L. Chen, K.C. Fang, J.Y. Sheu, L.S. Hsu, C.C. Tzeng, J. Med. Chem. 44 (2001) 2374.
[2] A.Z. El-Sonbati, M.A. Diab, M.S. El-Shehawy, M. Moqbal, Spectrochim. Acta A 75 (2010) 394.
[3] A.Z. El-Sonbati, M.A. Diab, A.M. Eldesoky, Sh.M. Morgan, O.L. Salem, Appl. Organometal. Chem. 33 (2019) e4839.
[4] M.N. Hughes, The Inorganic Chemistry of Biological Processes, 2nd Ed, John Wiley and Sons, 1988.
[5] S.G. Abdel-Moty, M.H. Abdel-Rahman, H.A. Elsherief, A.H.N. Kafafy, Bull. Pharm. Sci. (Assiut University) 28 (2005) 79.
[6] R. Vlahov, St. Parushev, J. Vlahov, P. Nickel, G. Snatzke, Pure Appl. Chem. 62 (1990) 1303.
[7] M. Normand-Bayle, C. Bénard, V. Zouhiri, J. Mouscadet, H. Leh, C. Thomas, G. Mbemba, D. Desmaële, J. d'Angelo, Bioorg. Med. Chem. Lett. 15 (2005) 4019.
[8] S.T. Hazeldine, L. Polin, J. Kushner, K. White, T.H. Corbett, J. Biehl, J.P. Horwitz, Bioorg. Med. Chem. 13 (2005) 1069.
[9] L. Savini, L. Chiasserini, C. Pellerano, W. Filippelli, G. Falcone, Farmaco 56 (2001) 939.
[10] S.A. Jenekhe, L. Lu, M.M. Alam, Macromolecules 34 (2001) 7315.
[11] G. De Armas, M. Miró, A. Cladera, J.M. Estela, V. Cerdà, Anal. Chim. Acta 455 (2002) 149.
[12] R.T. Bronson, M. Montalti, L. Prodi, N. Zaccheroni, R.D. Lamb, N.K. Dalley, R.M. Izatt, J.S. Bradshaw, P.B. Savage, Tetrahedron 60 (2004) 11139.
[13] K.B. Patel, G.J. Kharadi, K.S. Nimavat, J. Chem. Pharm. Res. 4 (2012) 2422.
[14] A.Z. El-Sonbati, M.A. Diab, G.G. Mohamed, M.A. Saad, Sh.M. Morgan, S.E.A. El-Sawy, Appl. Organometal. Chem. 33 (2019) e4973.
[15] M. Rbaa, M. Galai, M. El Faydy, Y. Lakhrissi, M. EbnTouhami, A. Zarrouk, B. Lakhrissi, J. Mater. Environ. Sci. 9 (2018) 172.
[16] M. Rbaa, M. Galai, M.E.L. Faydy, Y. El Kacimi, M. Ebn Touhami, A. Zarrouk, B. Lakhrissi, J. Mater. Environ. Sci. 8 (10) (2017) 3203.
[17] M. El Faydy, M. Galai, R. Touir, A. El Assyry, M. Ebn Touhami, B. Benali, B. Lakhrissi, A. Zarrouk, J. Mater. Environ. Sci. 7 (4) (2016) 1406.
[18] A.Z. El-Sonbati, M.A. Diab, Sh.M. Morgan, J. Mol. Liq. 225 (2017) 195.
[19] Sh.M. Morgan, A.Z. El-Sonbati, M.A. El-Mogazy, Appl. Organometal. Chem. 32 (2018) e4264.
[20] G.G. Mohamed, A.A. El-Sherif, M.A. Saad, S.E.A. El-Sawy, Sh.M. Morgan, J. Mol. Liq. 223 (2016) 1311.
[21] H.M. Refaat, H.A. El-Badway, Sh.M. Morgan, J. Mol. Liq. 220 (2016) 802.
[22] R. Shirley, The CRYSFIRE System for Automatic Powder Indexing: User's Manual, the Lattice Press, Guildford, Surrey GU2 7NL, England, 2000.
[23] Sh.M. Morgan, A.Z. El-Sonbati, H.R. Eissa, J. Mol. Liq. 240 (2017) 752.
[24] Sh.M. Morgan, M.A. Diab, A.Z. El-Sonbati, Appl. Organometal. Chem. 32 (2018) e4504.
[25] A.Z. El-Sonbati, M.A. Diab, Sh.M. Morgan, M.A. El-Mogazy, Appl. Organometal. Chem. 32 (2018) e4530.
[26] M.A. Diab, A.Z. El-Sonbati, Sh.M. Morgan, M.A. El-Mogazy, Appl. Organometal. Chem. 32 (2018) e4378.
[27] M.A. Diab, G.G. Mohamed, W.H. Mahmoud, A.Z. El-Sonbati, Sh.M. Morgan, S.Y. Abbas, Appl. Organometal. Chem. 33 (2019) e4945.
[28] M.I. Abou-Dobara, N.F. Omar, M.A. Diab, A.Z. El-Sonbati, Sh.M. Morgan, M.A. El-Mogazy, J. Cell. Biochem. 120 (2019) 1667.
[29] A.S. Fouda, A.M. Eldesoky, A.Z. El-Sonbati, S.F. Salam, Int. J. Electrochem. Sci. 9 (2014) 1867.
[30] R.G. Parr, D.A. Donnelly, M. Levy, M. Palke, J.Chem. Phys. 68 (1978) 3801.
[31] R.G. Parr, R.G. Pearson, J. Am. Chem. Soc. 105 (1983) 7512.
[32] P. Roychowdhury, P.N. Das, B.S. Basak, Acta Crystallgr., Sect. B 34 (1978) 1047.
[33] T. Banerjce, N.N. Saha, Acta Crystallogr., Sect. C 43 (1986) 1408.
[34] M. Albrecht, O. Blau, E. Wegehas, K. Risssanen, New J. Chem. 23 (1999) 667.
[35] M. Albrecht, K. Wit, E. Wegelius, K. Rissamen, Tetrahedron 56 (2000) 591.
[36] E. Bardez, I. Devol, B. Larry, B. Valeur, J. Phys. Chem. B 101 (1997) 7786.
[37] N.A. El-Ghamaz, M.A. Diab, A.Z. El-Sonbati, O.L. Salem, Spectrochim. Acta 83 (2011) 61.
[38] M.I. Abou-Dobara, A.Z. El-Sonbati, Sh.M. Morgan, World J. Microbiol. Biotechnol. 29 (2013) 119.
[39] A.Z. El-Sonbati, M.A. Diab, A.A.M. Belal, Sh.M. Morgan, Spectrochim. Acta A 99 (2012) 353.
[40] N.A. El-Ghamaz, A.Z. El-Sonbati, Sh.M. Morgan, J. Mol. Struc. 1027 (2012) 92.
[41] A.Z. El-Sonbati, M.A. Diab, A.A. El-Bindary, A.M. Eldesoky, Sh.M. Morgan, Spectrochim. Acta A 135 (2015) 774.
[42] V. Sadasivam, M. Alaudeen, Ind. J. Chem. 46A (2007) 1959.
[43] A.Z. El-Sonbati, A.A.M. Belal, M.S. El-Gharib, Sh.M. Morgan, Spectrochim. Acta A 95 (2012) 627.
[44] K. Nakamoto, "Infrared Spectra of Inorganic and Coordination Compounds", part B, 5th ed, Wiley, Interscience, New York, 1997.
[45] A.Z. El-Sonbati, M.A. Diab, A.A. El-Bindary, G.G. Mohamed, Sh.M. Morgan, M.I. Abou-Dobara, S.G. Nozha, J. Mol. Liq. 215 (2016) 423.
[46] S.P. McGlynn, J.K. Smith, W.C. Neely, J. Chem. Phys. 35 (1961) 105.
[47] K. Nakamoto, Infrared Spectra of Inorganic and Coordination Compounds, Wiley Interscience, New York, 1970.
[48] N.A. El-Ghamaz, A.Z. El-Sonbati, M.A. Diab, A.A. El-Bindary, G.G. Mohamed, Sh.M. Morgan, Spectrochim. Acta A 147 (2015) 200.
[49] M. Albrecht, K. Witte, R. Frohlich, O. Kataeva, Tetrahedron 58 (2002) 561.
[50] M. Sabsstian, V. Arun, P.P. Robinson, A.A. Varghese, R. Abraham, E. Suresh, K.K.M. Yusff, Polyhedron 29 (2010) 3014.
[51] M.A. Diab, A.Z. El-Sonbati, N.A. El-Ghamaz, Sh.M. Morgan, O. El-Shahat, Eur. Polym. J. 115 (2019) 268.
[52] Sh.M. Morgan, M.A. Diab, A.Z. El-Sonbati, Appl. Organometal. Chem. 32 (2018) e4305.
[53] Sh.M. Morgan, M.A. Diab, A.Z. El-Sonbati, Appl. Organometal. Chem. 32 (2018) e4281.
[54] A.Z. El-Sonbati, M.A. Diab, Sh.M. Morgan, H.A. Seyam, J. Mole. Struct. 1154 (2018) 354.
[55] A.Z. El-Sonbati, M.A. Diab, Sh.M. Morgan, M.Z. Balboula, Appl. Organometal. Chem. 32 (2018) e4059.
[56] A.Z. El-Sonbati, M.A. Diab, Sh.M. Morgan, A.M. Eldesoky, M.Z. Balboula, Appl. Organometal. Chem. 32 (2018) e4207.
[57] D.S. Raja, N.S.P. Bhuvanesh, K. Natarajan, Inorg. Chim. Acta 385 (2012) 81.
[58] M.A. Pfaller, Am. J. Med. 125 (2012) S3.
[59] C.Z. Blumenthal, Regul. Toxicol. Pharmacol. 39 (2004) 214.
[60] S. Borrego, P. Lavin, I. Perdomo, S. Gómez de Saravia, P. Guiamet, ISRN Microbiology 2012 (2012) 680598, , https://doi.org/10.5402/2012/680598.
[61] N. Valentín, R. Garcia, O. De Luis, S. Maekawa, Restaurator 19 (1998) 85.
[62] S. Walmsley, S. Devi, S. King, R. Schneider, S. Richardson, L. Ford-Jones, Pediatr. Infect. Dis. J. 12 (1993) 673.
[63] E.J. Anaissie, S.F. Costa, Clin. Infect. Dis. 33 (2001) 1546.
[64] M.K. Kathiravan, A.B. Salake, A.S. Chothe, P.B. Dudhe, R.P. Watode, M.S. Mukta, S. Gadhwe, Bioorg. Med. Chem. 20 (2012) 5678.
[65] M. Mosaad, S. Awad, N. Ahmed, Acta Pharma. 61 (2011) 171.
[66] L.M. Gaetke, S.C. Hannah, K.C. Ching, Arch. Toxicol. 88 (2014) 1929.
[67] S. García-Santamarina, J.T. Dennis, J. Biol. Chem. 290 (2015) 18945.
[68] G.S. Dantas, A. Almeida-Apolonio, R. Araújo, L.R.V. Favarin, P. Castilho, F. Galvão, T.E. Svidzinski, G.A. Casagrande, K. Oliveira, Molecules 23 (2018) 1856.
[69] S. Campoy, J.L. Adrio, Biochem. Pharmacol. 133 (2017) 86.
[70] N. Sharma, A. Tripathi, Microbiol. Res. 163 (2008) 337.
[71] M. Tolouee, S. Alinezhad, R. Saberi, A. Eslamifar, S.J. Zad, K. Jaimand, J. Taeb, M.-B. Rezaee, M. Kawachi, M. Shams-Ghahfarokhi, Int. J. Food Microbiol. 139 (2010) 127.
[72] O. Voigt, S. Pöggeler, Appl. Microbiol. Biotechnol. 97 (21) (2013) 9277.
[73] H. Nakatogawa, K. Suzuki, Y. Kamada, Y. Ohsumi, Nat. Rev. Mol. Cell Biol. 10 (2009) 458.
[74] E.-L. Eskelinen, A.L. Kovács, Autophagy 7 (2011) 931.
[75] B.M. Nitsche, A.-M. Burggraaf-van Welzen, G. Lamers, V. Meyer, A.F. Ram, Appl. Microbiol. Biotechnol. 97 (2013) 8205.
[76] K.F. Khaled, Electrochim. Acta 53 (2008) 3484.
[77] I. Ahamad, M.A. Quraishi, Corros. Sci. 51 (2009) 2006.
[78] A. Amin, K.F. Khaled, Q. Mohsen, H.A. Arida, Corros. Sci. 52 (2010) 1684.
[79] M. Benabdellah, R. Touzani, A. Aouniti, Mat. Chem. Phys. 105 (2007) 373.

Experimental and theoretical investigations for some spiropyrazoles derivatives as corrosion inhibitors for copper in 2 M HNO₃ solutions

H.S. Gadow [a,*], Thoraya A. Farghaly [b,c], A.M. Eldesoky [d]

[a] Engineering Chemistry Department, High Institute of Engineering &Technology, New Damietta, Egypt
[b] Department of Chemistry, Faculty of Science, Cairo University, Giza 12613, Egypt
[c] Department of Chemistry, Faculty of Applied Science, Umm Al-Qura University, Makkah Almukkarramah, Saudi Arabia
[d] Engineering Chemistry Department, High Institute of Engineering &Technology (New Damietta), Egypt and Al-Qunfudah Center for Scientific Research (QCSR), Chemistry Department, Al-Qunfudah University College, Umm Al-Qura University, Saudi Arabia

ARTICLE INFO

ABSTRACT

Rates of corrosion for copper were monitored in aerated stagnant 2 M HNO₃ solutions at different temperatures (25-55 °C) using Tafel extrapolation method, electrochemical impedance spectroscopy technique, non-destructive electrochemical frequency modulation (EFM) technique and weight-loss method, accompanied by EDX examinations, molecular docking, molecular dynamics, and quantum chemical calculations. Some spiropyrazoles derivatives were introduced as corrosion-safe inhibitors. Compound (1) has the best inhibition activity (89.9% at 11×10^{-6}M). Tafel plots indicated that these compounds acted mainly as mixed-type inhibitors. The inhibition process was ascribed to the formation of an adsorbed film on the copper surface that protects the metal against corrosive agents. EDX examinations of the electrode surface confirmed the existence of such adsorbed film. The inhibition efficiency increased by increasing the concentration of spiropyrazoles compounds, while it decreased by increasing the temperature, this expresses on the physical adsorption. Activation energy has been calculated in the existence and nonexistence of a number of concentrations from spiropyrazoles derivatives by measuring the corrosion rate obtained from the weight loss method at different temperatures. It was found that the activation energy in the presence of spiropyrazoles derivatives is higher than that in 2 M HNO₃ solution alone. The adsorptive behavior of spiropyrazoles compounds followed Freundlich -type isotherm.

© 2019 Elsevier B.V. All rights reserved.

1. Introduction

Copper is used in electronic productions as conductors, heat exchangers, pipelines for water production, and as a conductor in electrical solid lines to receive their higher conductivities in thermal and electrical mode. Therefore, Cu corrosion and its inhibition in many solutions have been significant in many researches [1–10]. Nitric acid is the most important corrosive mediums based that focused on corrosion of copper [11–16]. There is inversely proportional relationship between the movement of heat and the corrosion yield. Consequently, the increase of the corrosion product gives the bad efficiency of the equipment. The periodic cleaning of the equipment is a significant step, it happens by acids, through contact by copper metal, hence the corrosion occur [17]. Nitric acid is important acids, which use in cleaning on a large scale [18]. Therefore, the study of corrosion inhibition of copper in nitric acid is very important. There is a need for novel inhibitors for copper corrosion in acidic media. A thinkable solution to this problem is to find new ecologically, friendly green corrosion inhibitors [19–23]. Many organic compounds used as inhibitors for copper corrosion were toxic compounds that must be substituted by the novel ecofriendly inhibitors. Azole and pyrazole compounds and their derivatives are one of the most important inhibitors, which attract the interest of researchers [24–33]. The corrosion inhibition by these compounds happens from the precipitation of organometallic complexes into the metal surface, which is a barrier to the corrosive environment [34–38]. The composition of the inhibitor is one of the main factors that determine the interaction between metal and inhibitor [39]. Copper gives many-bonds with the molecules of inhibitors, which contain N and S atoms and heterocyclic structure. These bonds are used to hindrance the corrosion of copper in the aqueous solutions [40]. Heterocyclic compounds are used as inhibitors for corrosion of copper in different productions processes [41]. Spiropyrazoles derivatives contain nitrogen atoms that may react with Cu by the lone pair of electrons to give complexes [42]. These complexes are polymeric form and as a film (natural hindrance) which are adhesive on the Cu metal. The

* Corresponding author.
E-mail addresses: hsgado73@gmail.com (H.S. Gadow), amahmed@uqu.sa (T.A. Farghaly), a.m.eldesoky79@hotmail.com (A.M. Eldesoky).

Spiropyrazoles derivatives offer important possibilities for corrosion hindrance due to the existence of the heteroatoms in their molecules. The use of derivatives is important due to the size of molecules [43–49].

The aim of the current work is to study the impact of some spiropyrazoles compounds as new compounds on the inhibition of copper corrosion in 2 MHNO$_3$ solutions. In our investigation, we used the chemical method (gravimetric method), electrochemical practices (potentiodynamic polarization, electrochemical frequency modulation, and electrochemical impedance spectroscopy) based on the theoretical study.

2. Experimental

2.1. Materials

Gravimetric method and electrochemical investigations in this manuscript were carried out on copper coupons having a composition (wt %): 0.019 Al, 0.001 Ni, 0.116 Si, 0.004 Mn and rest Cu. The copper samples have dimensions 2.0 cm × 2.0 cm × 0.1 cm for gravimetric method and 1.0 cm × 1.0 cm × 0.1 cm for electrochemical investigation. These

coupons were automatically cut and scraped with various kinds from emery papers (300, 500, 800, 1200 grade). The samples were washed with distilled water, degreased in acetone, dried, and stored in vacuum desiccator according to the standard tests [50].

2.2. Test solution

The aggressive solutions used were made from HNO$_3$ (6 M) and the preparation was by dilution of analytical-grade 37% HNO$_3$ (Ramkem) and its concentration was checked using standardized NaOH. Suitable concentration (2 M) of acid was prepared by means of dilution utilizing bi-distilled water. The concentrations of the two compounds ranged from 1×10^{-6} to 11×10^{-6} M, and the volume of the test solution used for weigh-loss method and electrochemical studies was 100 mL.

2.3. Synthesis of Spiropyrazoles derivatives

Table 1 demonstrates the chemical structure of spiropyrazoles derivatives used for this manuscript [51].

Table 1
Chemical composition of some spiropyrazoles derivatives.

Cpd. no.	Name	Structure	Chemical Formula & Molecular Weight
(1)	3′-(3,4-Dichlorophenyl)-2′,3′,6,7,8,9-hexahydro-2′-phenyl-5′styrylspiro [benzocyclo-heptene-6(5H),4′(4H-pyrazol)]-5-one		C$_{33}$H$_{26}$Cl$_2$N$_2$O (536.14)
(2)	3′-(3,4-Dichlorophenyl)-2′,5′-diphenyl-2′,3′,6,7,8,9-hexahydrospiro [benzocycloheptene-6(5H),4′(4H-pyrazol)]-5-one		C$_{31}$H$_{24}$Cl$_2$N$_2$O (510.13)

2.4. Methods

2.4.1. Weight loss technique

Our investigations in gravimetric experiments were applied according to the standard methods [52]. All measurements of weight loss method (inhibition efficiency (IE%),corrosion rate (CR), and surface coverage (θ))were completed through the next equations:

$$((C.R) = \Delta m/At \tag{1}$$

where T = time (min.), A = objective area (cm^2) and Δ m = the loss mass. The hindrance yield (% IE) and (θ) were calculated from (2):

$$\%IE = [(R^* - R)/R^*] \times 100 = \theta \times 100 \tag{2}$$

where R and R* are the quantities of Cu corrosion in nonexistence and the existence of our investigated compounds respectively.

These investigations were repeated at different temperatures of (25–55 °C) via water circulation Ultra thermostat to control the inhibition efficiency temperature.

2.4.2. Electrochemical tests

The study conducted in traditional three electrodes by using Gamry potentiostat/galvanostat/ZRA (model PCI300/4). Foil from platinum was used as a counter electrode and (SCE) as a reference. The copper electrode was joined from the first side to copper wire to connect each other electrically. The potential of an electrode was obtained for half an hour to stabilize earlier first method. The spiropyrazoles compounds Tafel polarization bends were got by adding the potential of an electrode beginning from −600 to +200 mV vs. OCP used of a scan rate of 1mVS^{-1}.

The techniques of EFM and EIS were accomplished by using similar means by a Gamry framework based on ESA400. The gamry device include EFM140 software for EFM checking and EIS300 for EIS process, the computer was used as a collector for the data. Echem Analyst 5.5 Software was applied to draw and fit the data.

2.4.3. EDX - SEM test

The surface of copper was recognized by placing the specimen for (3 h.) immersing in 2.0 M HNO$_3$ in the presence and lack of higher dose of spiropyrazoles compounds, before that: different emery papers up to1200 size grit was used for polishing mechanically. The sheets of Cu were examined by utilizing diffractometer X-ray Philips (pw-1390) by means of Cu-pipes, ("SEM, JSM-T20, JOEL, Japan").

2.4.3.1. Quantum chemical calculations.
By PM3 semi-empirical way, optimizations of the molecular structures were performed. Also, molecules were examined by using the DMol3 module in Materials Studio version 7.0. A basic set of double number polarization (DNP), the exchange- relationship functions of Becke One Parameter (BOP), and popularized gradient approximation (GGA) were completed inside the DMol3 module. The solvent effects were treated through COSMO controls. From the two techniques, the different chemical parameters (electronegativity **χ,** chemical potential **Pi,** global hardness η and softness**σ**) were determined [53,54] as demonstrated in the next equations:

$$P_i = -\chi \tag{3}$$

$$P_i = (E_{LUMO} + E_{HOMO})/2 \tag{4}$$

$$\eta = \Delta E/2 = (E_{LUMO} - E_{HOMO})/2 \tag{5}$$

By the global hardness the softness is designated σ:

$$\sigma = 1/\eta \tag{6}$$

The electronegativity and global hardness were utilized to calculate the fraction of electrons transferred(ΔN) as shown from the next equation:

$$\Delta N = (\chi_{Cu} - \chi_{inh})/2(\eta_{Cu} - \eta_{inh}) \tag{7}$$

where χ$_{Cu}$ and χ$_{in}$ giving the absolute electronegativity of copper and molecules of inhibitors, respectively.

According to Pearsons electronegativity scale, the electronegativity of copper is 4.48 and its hardness is 0 eV/mol [55].

2.4.3.2. Molecular dynamics simulation.
In our study, the simulations of molecular dynamics (MD) were accomplished by means of Materials Studio version 7.0 using adsorption Locator module [56]. In the adsorption process for the molecules of our derivatives compounds on the Cu surface, the adsorption Locator module is a simulation module. Simulated box (32.27 Å × 32.27 Å × 50.18 Å) was used to proceed Cu (111) with periodic boundary situations to simulate a typical part of the interface bypass any arbitrary boundary effects. To optimize the energy of molecules of our compounds, we used the forcite classical simulation engine. Firstly, the surface of Cu (111) was constructed, after Cu (111) surface area was increment and by creating a supercell, its periodicity was modified, and a vacuum block with a density of 20 Å was constructed on the surface of Cu (1 1 1) at that point [57]. After reducing the surface of Cu (1 1 1), and the molecules of the investigated compounds, the system of corrosion was shaped by layer builder. This is the molecules of studied compounds on the surface of Cu (111), and the condensed phase optimized molecular potentials for atomistic simulation studies force field (COMPASS) that was used to imitate the attitude of the molecules of investigated compounds adsorption on the surface of Cu (1 1 1). Adsorption detector determines the possibility of adsorption configurations of the investigated compounds molecules on Cu (111) surface by applying Monte Carlo examinations. Thus, the adsorption conformation and its influences on inhibition efficiencies of our investigated compounds was obtained [58].

2.4.3.3. Molecular docking calculation.
In our research, we carried out the Docking calculations using DockingServer [59]. In this technique, we used the MMFF94 force field (2) to minimize the energy of the ligand molecule (1). we added Gasteiger partial charges to the ligand atoms.

Table 2
Weight loss data for copper in 2MHNO$_3$ solution for numerous concentrations from compound (1) after 90 min., at (25, 35) °C.

Conc., ppm	25 °C				35 °C			
	Δm mg/cm^2	θ	% IE	C.R., mg/cm^2 min	Δm mg/cm^2	θ	% IE	C.R., mg/cm^2 min
Blank	3.880	–	–	0.0430	3.926	–		0.0436
0.1 × 10^{-5}	0.640	0.835	83.5	0.0070	1.056	0.730	73.0	0.0117
0.3 × 10^{-5}	0.607	0.843	84.3	0.0067	1.014	0.741	74.1	0.0113
0.5 × 10^{-5}	0.543	0.860	86.0	0.0060	0.966	0.754	75.1	0.0107
0.7 × 10^{-5}	0.479	0.877	87.7	0.0053	0.909	0.769	76.9	0.0101
0.9 × 10^{-5}	0.406	0.895	89.5	0.0045	0.860	0.781	78.1	0.0096
1.1 × 10^{-5}	0.392	0.899	89.9	0.0044	0.812	0.793	79.3	0.0090

Table 3
Values of weight loss experiments of carbon steel in a 2MHNO$_3$ solution for several concentrations of compound (1) after 90 min., at (45, 55) °C.

Conc., ppm	45 °C				55 °C			
	Δm mg/cm^2	θ	% IE	C.R., mg/cm^2 min	Δm mg/cm^2	θ	% IE	C.R., mg/cm^{2}min
Blank	4.592	–	–	0.0510	5.190	–	–	0.0588
0.1×10^{-5}	1.802	0.607	60.7	0.0200	2.879	0.449	44.9	0.0320
0.3×10^{-5}	1.786	0.611	61.1	0.0198	2.851	0.451	45.1	0.0317
0.5×10^{-5}	1.736	0.621	62.1	0.0193	2.806	0.459	45.9	0.0312
0.7×10^{-5}	1.705	0.629	62.9	0.0190	2.768	0.467	46.7	0.0308
0.9×10^{-5}	1.677	0.635	63.5	0.0186	2.729	0.474	47.4	0.0303
1.1×10^{-5}	1.635	0.644	64.4	0.0182	2.682	0.483	48.3	0.0298

Non-polar hydrogen atoms were combined, and rotatable bonds were definite. Docking calculations were applied on 3hb5 - OXIDOREDUCTASE protein model.The vital hydrogen atoms, Kollman united atom type charges and solvation parameters were added by the aid of AutoDock tools [60]. Affinity (grid) maps of $20 \times 20 \times 20$ Å grid points and 0.375 Å spacing were established using the Autogrid program [61]. In the calculations of van der Waals and the electrostatic terms, we used AutoDock parameter and distance based dielectric functions.

Docking simulations were completed by using the Lamarckian genetic algorithm (LGA) and the Solis & Wets local search method [62]. Randomly, initial position, orientation, and torsion of the ligand molecules were determined. Each docking experiment was resultant from 10 different runs that were set to terminate after a maximum of 250,000 energy evaluations. The population size was 150. During our research, a translational step of 0.2 Å, and quaternion and torsion steps of 5 were applied.

3. Results and discussion

3.1. Results of weight loss

3.1.1. The effect of temperature and inhibitor concentration

The corrosion parameters [the efficacy of inhibition (%IE), corrosion rate (CR) and surface coverage (θ)] in 2 M nitric acid solutions in the existence and non-existence of different concentrations (1×10^{-6}–11 $\times 10^{-6}$ M) of spiropyrazoles derivatives at varies temperatures (25–55 °C) obtained from weight loss technique shown in Tables 2 and 3. Tables 2 and 3 and Fig. 2 show that inhibition efficiency improved by increasing the concentrations of the spiropyrazoles derivatives. The efficacy of inhibition for these compounds at11 $\times 10^{-6}$ M was 89.9 for

compound 1 and was 80.9% for compound 2 (the results not shown) at 25 °C. By increasing the concentration of our investigated compounds, the coverage on the metal surface by inhibitor molecules increases that gives increasing in the inhibition efficiencies [63]. It is also clear from (Tables 2 & 3 and Figs. 1 & 2) that, the inhibition efficiency lessens, and the corrosion rate increase by increasing the temperature from 25 to 55 °C. These actions were explained on the base that the increase in the temperature gives equilibrium constant shift to desorption of the inhibitors molecules from the surface of copper [64]. The inhibition efficiency of compound1 is greater than compound2 in all cases (change in temperature or change in concentration).

3.1.2. The effect of temperature on activation parameters

The corrosion is considered as Arrhenius process, that means, the corrosion rate can be used to calculate the apparent activation energy, *Ea*, by Arrhenius equation:

$$Log\ C.R = \ log\ A - (Ea./2.303RT) \tag{8}$$

where C.R. is the corrosion rate, A refers to Arrhenius constant, R stems for constant for molar gas and T refers to the absolute temperature.

Arrhenius plots were demonstrated in Fig. 3 [log (C.R) versus 1/T] which gave straight lines with slopes [$-E_a/2.303R$], so the values of E_a can be determined. The enthalpy change (ΔH^*) and entropy (ΔS^*) of activation can be calculated from the transition state theory [65].

C.R. $= (RT/Nh)\exp.(\Delta S^*/R)\exp.(-\Delta H^*/RT(9)$ where the character gives Planck's constant and symbol N gives number of Avogadro.

Straight lines were obtained for two compounds by plotting log (C.R/T) versus 1000/T. where Fig. 4 presents the transition state plots of two compounds. The slopes of the lines ($-\Delta H^*/2.303R$) were used to calculate ΔH^*, and the entr/opy of activation (ΔS^*) is calculated by using
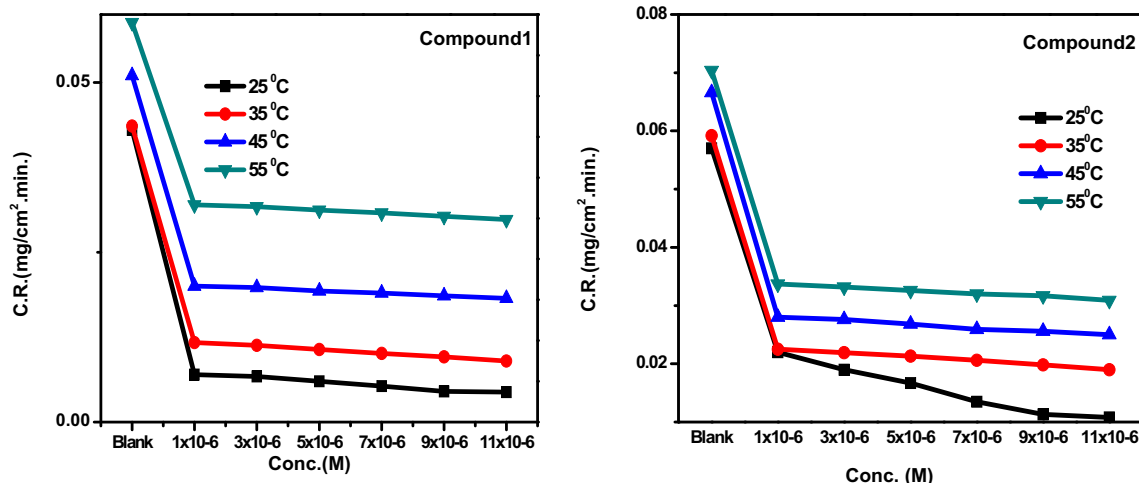

Fig. 1. The corrosion rate of various concentrations from compounds (1 & 2) on the copper surface in 2 M HNO$_3$ at 25–55 °C.
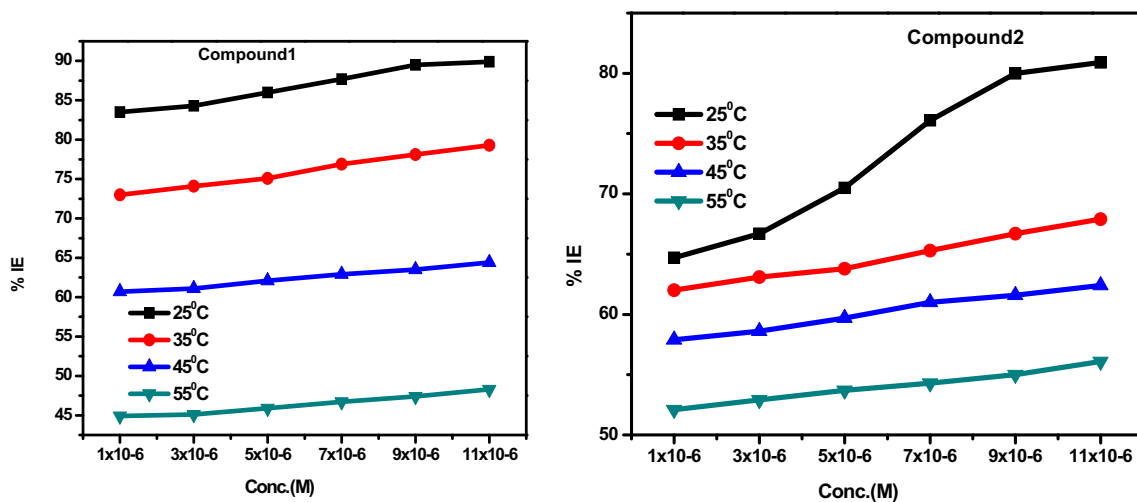
Fig. 2. Variation of the inhibition efficiency with different concentrations from compounds (1 & 2) on the copper surface in 2 M HNO$_3$ solution at 25–55 °C.

the intercepts of these lines [log(R/Nh) + ΔS*/2.303R]. The obtained data listed in Table 4 show that the E$_a$ for blank solution =19.62 KJ/ mol and this activation energy of the corrosion of Cu in 2.0 M HNO$_3$ is

in good correspondence with other work [66]. The activation energy increases in the existence of spiropyrazoles derivatives as inhibitors. The higher value of E$_a$ in the presence of two compounds is attributed to
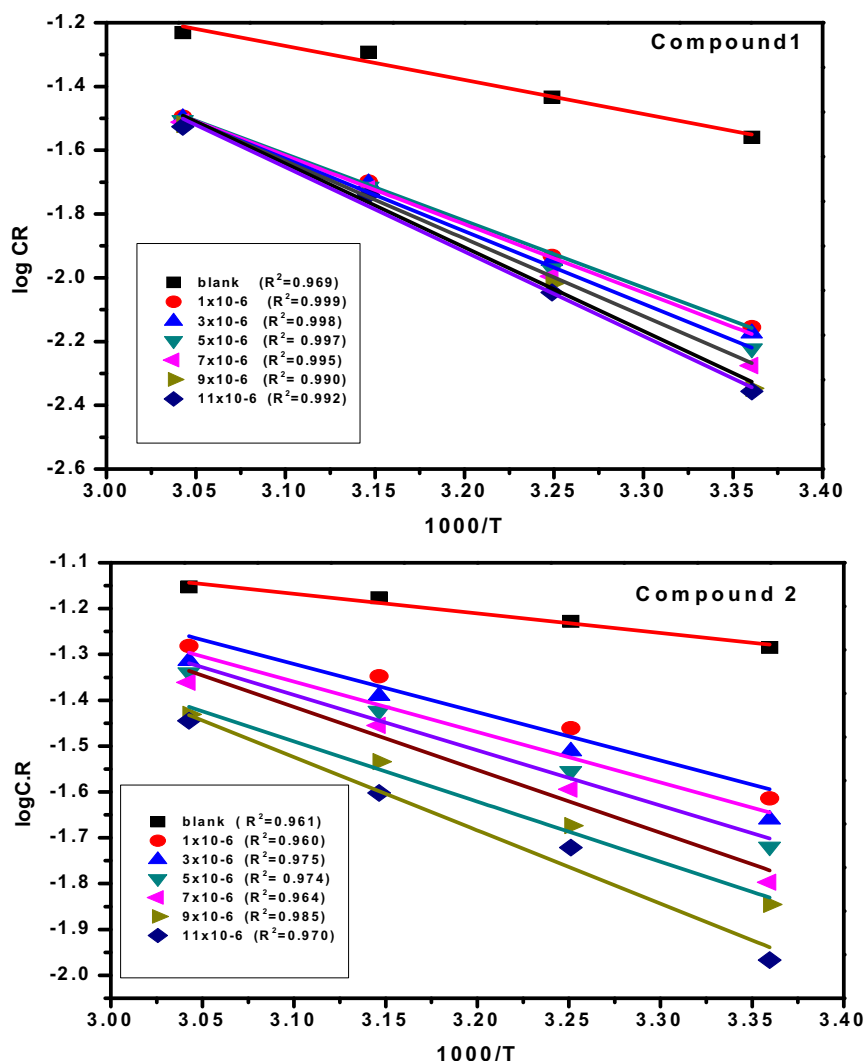
Fig. 3. log C.R. vs. 1/T (Arrhenius relation) for the copper surface in 2 M HNO$_3$ with adding and without adding several concentrations from compounds (1&2).
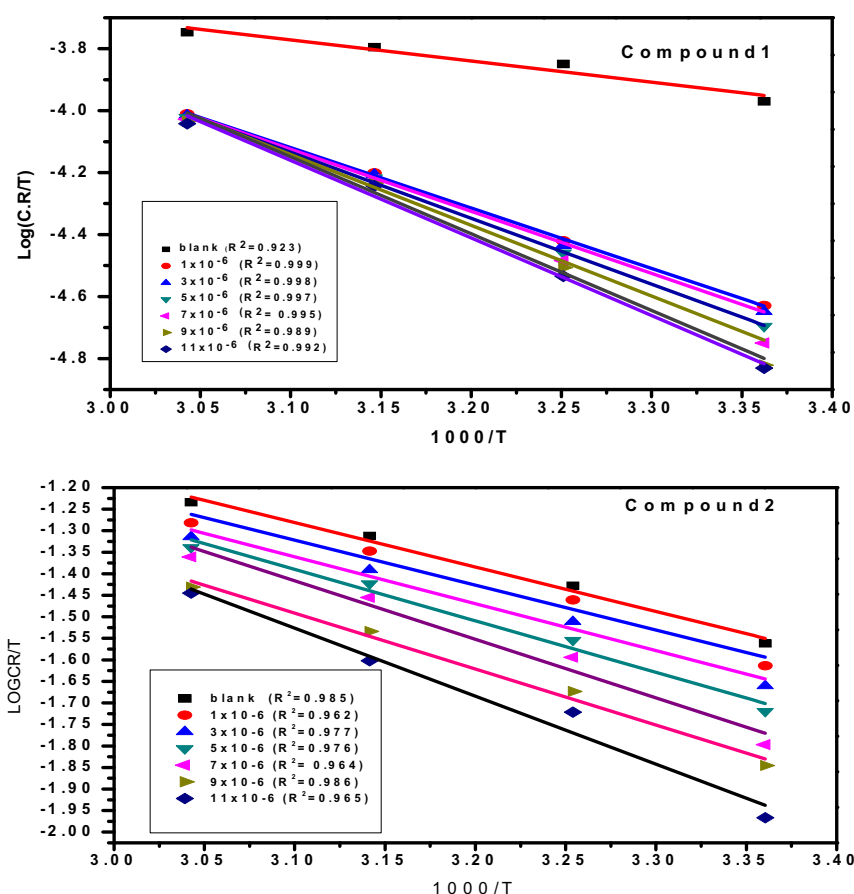
Fig. 4. The relation between log C.R./T vs. 1000/T for the copper surface in 2 M HNO$_3$ without adding and adding several concentrations from compounds(1&2).

their adsorption nature on the copper surface [67–70]. Increasing the concentration of inhibitors is combined with increasing in the activation energy. This refers to typical physical adsorption mechanism [71]. The results also revealed that Δ H* has positive value reflecting the endothermic nature of the corrosion process. The entropy values (ΔS*) in the existence of spiropyrazoles derivatives were negative indicating the activated complex in the attribution determining step that give an association rather from the dissociation step. This illustrates that the preliminary state was lower order than that at the activated molecules [72,73].

3.1.2.1. Adsorption isotherm. It is clear that the anticorrosion action of examined derivatives is due to their tendency to interact and adsorb at the copper/solution interface. The adsorption mode is dependent on the

molecular structure, solution chemical composition, nature of corroding copper surface and electrochemical potential at copper/solution interface, one or more of the three main types of adsorption: π-bond, electrostatic adsorption (physical adsorption) and chemisorption [75]. The attitude of the adsorption of spiropyrazoles derivatives on the copper surface can be discovered by finding a suitable isotherm. The weight loss experiments data at different temperatures were used, and fitted with different mathematical adsorption isotherm expressions. The adsorption of the spiropyrazoles derivatives was the best designated by Freundlich isotherm according to the following equation [76]:

$$\log \theta = n \ \log C + \ \log K_{ads} \qquad (10)$$

The Freundlich isotherm describes the relationship between adsorbed compounds molecules, their intermolecular reaction, and effect on the mechanism of adsorption [68] constant that reveal the number of adsorbed compounds molecules, K$_{ads}$ is the adsorption-desorption equilibrium constant illustrating the intermolecular

Table 4
Activation parameters for copper corrosion in 2MHNO$_3$ without and with inhibitors.

	Conc.(M)	E$^*_a$ Kjmol^{-1}	ΔH* Kjmol^{-1}	-ΔS*Jmol^{-1} K^{-1}	logA
Compound 1	Blank	19.62	12.96	229.57	2.03874
	0.1 × 10^{-5}	35.48	37.50	160.35	4.88313
	0.3 × 10^{-5}	41.13	38.5	157.20	5.04058
	0.5 × 10^{-5}	43.60	40.97	149.75	5.43133
	0.7 × 10^{-5}	46.57	43.93	140.70	5.90528
	0.9 × 10^{-5}	50.32	47.65	129.30	6.50384
	1.1 × 10^{-5}	50.76	48.11	128.11	6.56562
Compound 2	0.1 × 10^{-5}	20.61	19.99	160.97	1.94394
	0.3 × 10^{-5}	21.05	20.85	159.023	2.04714
	0.5 × 10^{-5}	23.10	22.89	153.24	2.35251
	0.7 × 10^{-5}	26.30	26.05	143.98	2.84254
	0.9 × 10^{-5}	27.43	26.81	149.00	2.77865
	1.1 × 10^{-5}	30.58	30.24	133.11	3.42765

Table 5
Adsorption parameters on copper corrosion inhibition by compounds (1 & 2) obtained from Freundlich adsorption isotherms.

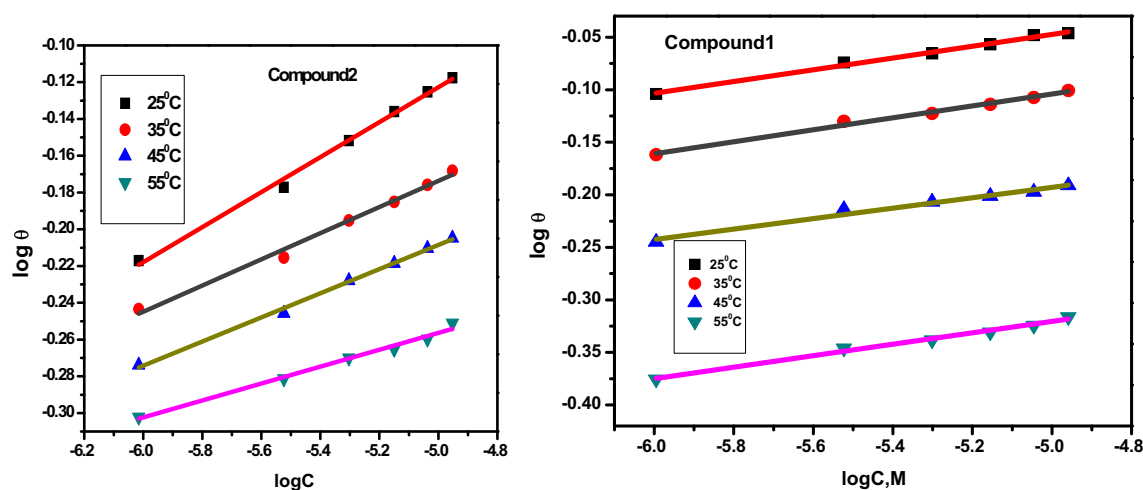|	Temperature °C	R^2	n	logK	−ΔG^0 (Kj/mol)
Compound (1)	25	0.99227	0.0951	0.3528	11.28
	35	0.98986	0.0711	0.1819	11.35
	45	0.97502	0.0657	0.1198	10.96
	55	0.98773	0.0459	−0.0271	10.33
Compound 2	25	0.99604	0.0560	0.2333	11.97
	35	0.99476	0.0568	0.1800	11.36
	45	0.98991	0.0497	0.0555	11.36
	55	0.98648	0.0544	−0.0484	10.78

Fig. 5. Freundlich adsorption isotherm of compounds (1 & 2) on copper in 2NHNO$_3$ at different temperatures.

strength of the adsorbed layer. By increasing the temperature, and decreasing the adsorption equilibrium constant (K_{ads}) value, the adsorption on the copper surface for the two inhibitors is at a lower temperature. Thus, by increasing the temperature, the adsorbed inhibitors tended to desorb from the copper surface [77,78].

In our study, we used the free energy of adsorption $\Delta G°_{ads}$ to characterize the interaction of adsorbed molecules and copper surface (Eq. (11)):

$$\Delta G°_{ads} = -RT\ln(55.5 \times k_{ads}) \qquad (11)$$

Symbol (R) is the gas constant (8.314 J/K. mol), symbol T is the absolute temperature in Kelvin and the value 55.5 reveal the concentration of water in the solution, where was given by mol/L [79]. The parameters of adsorption for the two compounds in 2MHNO$_3$ are given in Table 5. The negative value of $\Delta G°_{ads}$ confirms the process of adsorption and constancy of the adsorbing layer on the copper surface. By increasing the temperature, the stability of the adsorbed layer decreases. The values of ΔG_{ads} show the kind of adsorption, because it is physically when the negative values less than −20 KJ/mol, and when the negative values are higher than −40 KJ/mol, it includes sharing or transfer of electrons from the inhibitors to the copper surface to form a coordinate type of bond (Chemisorption) [80]. According to the experimental data in Table 5, the calculated values of $\Delta G°_{ads}$ were negative and less than -20KJ/mol. The values of $\Delta G°_{ads}$ for two compounds in the range from10.33 KJ/mol to 11.97 KJ/mol indicate that the molecules of two compounds are adsorbed on the copper surface by a strong physical

adsorption process. The negative free energy value reveals a strong and spontaneous adsorption of the two investigated compounds on the surface of copper, which gives the reason for the increasing inhibition efficiency. Thus, the proposed mechanism for the two inhibitors system is based on the physical adsorption. In general, the adsorption may be improved by the existence of hetero - atoms like O/N/S atoms, which give lone pair of electrons, in the molecules of compounds, make the adsorbed electrostatically on the copper surface forming insoluble stable films and thus decreasing copper dissolution (Fig. 5).

3.2. PP study

The important information about the kinetic of anodic and cathodic reaction can be provided by potentiodynamic polarization measurements (pp study) [81]. From Tafel polarization curves for copper was immersed in 2 M HNO$_3$ in the absence and presence of different concentrations from spiropyrazoles derivatives, the electrochemical corrosion parameters were derived [the corrosion potential (E_{corr}), corrosion current density (i_{corr}), and the anodic and cathodic Tafel constants (βa and βc)]. Table 6 and Fig. 6, show that the values of corrosion currents decrease with the increase in the concentrations of two compounds. Nitric acid is a strong copper oxidizer and capable of fast attacking copper. Furthermore, the potentiodynamic polarization curves in Fig. 6 show no steep slope in the anodic range, revealing that no passive films are formed on copper surface. Then, copper may directly dissolve in 2 M nitric acid. From Pourbaix diagram for copper-water system [82,83], the copper is corrode to Cu^{+2} in nitric acid solutions, and no oxide film is

Table 6
The effect of concentration of the of spiropyrazoles derivatives on the free corrosion potential (Ecorr), Tafel slopes (βa & βc), corrosion current density (i_{corr}), inhibition efficiency (% IE$_p$) and degree of surface coverage for the corrosion of copper in 2 M HNO$_3$ at 25 ± 1 °C.

| Comp.	Conc., M.	- E$_{corr}$ (mV vs. SCE)	R$_P$ ohm	i$_{corr}$ (μA/cm^2)	β_a (mV/dec)	β_c - (mV/dec)	θ	% IE$_p$
	Blank	9.47	2.93	156.50	54.0	156.0	–	–
(1)	0.1 × 10^{-5}	8.90	10.92	31.50	56.7	155.3	0.798	79.8
	0.3 × 10^{-5}	9.92	11.30	26.90	47.7	150.0	0.828	82.8
	0.5 × 10^{-5}	6.17	11.50	24.70	51.2	153.7	0.842	84.2
	0.7 × 10^{-5}	14.50	12.07	20.50	60.4	154.1	0.869	86.9
	0.9 × 10^{-5}	8.96	14.61	19.60	52.2	148.0	0.874	87.4
	1.1 × 10^{-5}	12.70	14.98	17.12	46.5	159.5	0.891	89.1
(2)	0.1 × 10^{-5}	6.83	6.83	46.50	48.2	139.7	0.703	70.3
	0.3 × 10^{-5}	6.29	7.80	36.20	53.6	148.3	0.767	76.7
	0.5 × 10^{-5}	12.20	8.35	28.20	56.2	156.0	0.820	82.0
	0.7 × 10^{-5}	13.30	9.18	24.30	56.0	145.0	0.845	84.5
	0.9 × 10^{-5}	9.34	9.34	20.50	53.2	137.0	0.869	86.9
	1.1 × 10^{-5}	8.55	9.81	19.2	61.1	145.0	0.875	87.5
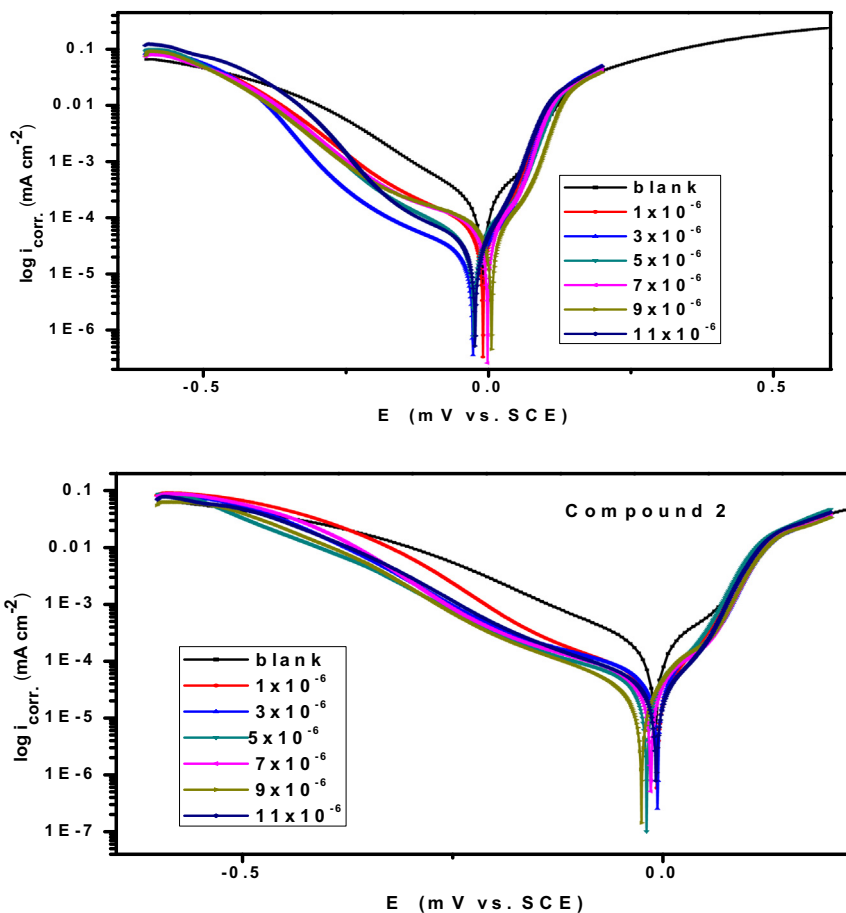
Fig. 6. The curves of Potentiodynamic polarization for the corrosion of copper in 2 M HNO$_3$ in the existence and nonexistence of numerous concentrations from compounds (1&2) at 25 ± 1 °C.

formed to give protection for the surface from corrosion [84]. Copper dissolution is expected to be the controlling reaction in nitric acid solutions. If the displacement values of E$_{corr}$ in the presence of two inhibitors $> \pm 85$ mV related to E$_{corr}$ of the blank solution, the inhibitors are classified as cathodic or anodic - type inhibitors and the inhibitors can be classified as a mixed type inhibitor if the displacement in E$_{corr}$ $< \pm$ 85 mV [85–87]. Table 6 data explained slightly change in anodic and cathodic Tafel slopes by increasing the concentrations of Spiropyrazoles derivatives. This recommended that the mechanism of inhibition in the existence and nonexistence of our investigating derivatives not

affect both the anodic and cathodic reactions [88–90].The dissimilarity in the values of E$_{corr}$ is small, this demonstrated that the investigated derivatives act as a mixed-type inhibitor [91–93]. From this technique, Table 6 shows i$_{corr}$ reduction with attending our investigated compounds and increases % IE with improving the dosage. The %IEp designed was applied as the next:

$$\%IEp = 100 \times \left[(i^{o}_{corr} - i_{corr}) / i^{o}_{corr} \right] \qquad (12)$$

where; i$^{o}_{corr}$ and i$_{corr}$ are the currents of corrosion in the presence and an absence of investigated compounds correspondingly. Fig. 7 demonstrated that the increase in the polarization resistance by increasing the doses of our examined compounds cause the adsorption of these compounds on the copper surface [94]. The %IE$_p$ of spiropyrazoles derivatives follow the arrangement: (1) > (2).

3.3. EIS tests

EIS is a rigorous examination in the manuscript of corrosion [95–98]. The equivalent circuit (Fig. 8) measured the values from impedance for a copper electrode in the existence of various concentrations from spiropyrazoles derivatives. Such circuit consists of constant phase

Fig. 7. Polarization resistance for the Cu corrosion existence and nonexistence of altered doses of examined compounds (1,2) at 25 ± 1.0 °C.

Fig. 8. Equivalent circuit used to fit the result of EIS.

Table 7
Electrochemical kinetic parameters obtained from the EIS technique for copper in 2 M HNO_3 in the absence and presence of different concentrations of spiropyrazoles derivatives at 25 ± 1 °C.

Comp.	Conc., M.	R_S (Ω cm^2)	$Y_{o \times 10}^6$ ($\mu\Omega^{-1}s^n$)	$n_{\times 10}^3$	R_{ct} (Ω cm^2)	C_{dl} (μF/cm^2)	θ	%IE
	Blank	1.886 ± 0.016	955.3 ± 16.53	679.4 ± 2.70	200.7 ± 2.135	4.38	–	–
(1)	0.1×10^{-5}	1.941 ± 0.009	341.1 ± 3.91	764.3 ± 1.72	1007.0 ± 11.75	2.60	0.800	80.0
	0.3×10^{-5}	1.993 ± 0.009	366.4 ± 4.03	780.5 ± 1.73	1142.0 ± 14.12	2.56	0.824	82.4
	0.5×10^{-5}	1.043 ± 0.009	366.2 ± 4.01	765.5 ± 1.74	1245.0 ± 16.10	2.45	0.838	83.8
	0.7×10^{-5}	1.054 ± 0.009	302.3 ± 3.36	779.1 ± 1.76	1263.0 ± 15.13	2.30	0.841	84.1
	0.9×10^{-5}	1.175 ± 0.010	351.0 ± 3.86	778.7 ± 1.75	1290.0 ± 16.22	2.00	0.844	84.4
	1.1×10^{-5}	1.015 ± 0.009	250.0 ± 2.78	$784.l \pm 1.68$	1389.0 ± 16.04	1.86	0.855	85.5
(2)	0.1×10^{-5}	1.953 ± 0.008	416.0 ± 5.6	788.8 ± 2.05	432.2 ± 4.16	3.08	0.535	53.5
	0.3×10^{-5}	1.963 ± 0.008	388.4 ± 4.77	764.5 ± 1.86	702.6 ± 7.65	2.96	0.714	71.4
	0.5×10^{-5}	1.954 ± 0.008	291.0 ± 3.58	800.3 ± 1.85	770.5 ± 7.77	2.87	0.739	73.9
	0.7×10^{-5}	1.989 ± 0.009	429.9 ± 5.06	763.4 ± 1.83	798.0 ± 9.36	2.86	0.748	74.8
	0.9×10^{-5}	1.016 ± 0.009	404.1 ± 4.72	776.9 ± 1.84	837.2 ± 9.75	2.78	0.760	76.0
	1.1×10^{-5}	1.975 ± 0.009	361.0 ± 4.23	768.7 ± 1.80	888.2 ± 10.07	2.62	0.774	77.4

elements (CPE) instead capacitors for giving numerous kinds of non-homogeneities perfect of corroding electrodes such as; grain boundaries, deficient polishing, impurities of the surface and the roughness of the surface [99]. The two parameters (Υ_0 and n) were used in our examination to express mathematically on frequency, where the impedance of copper reliant on it [100].

$$Z_{CPE} = \Upsilon_0^{-1}(j\omega)^{n-1} \tag{13}$$

The CPE coefficient appointed by symbol Υ_0, imaginary number and sine wave angular frequency particular by symbols $j^2 = -1$ and ω respectively. Character ω equal $2\pi f$, where f is the AC frequency. In actual experimental conditions, the values of n are between 0 and 1, because of numerous reasons, as dielectric constant, the roughness of the electrode and surface heterogeneity. In our investigation, the n values for $2MHNO_3$ are a blank compared to the system of inhibition where the copper surface is comparatively more homogeneous, that is because of the uniform adsorption for molecules of spiropyrazoles derivatives on the copper surface [101]. The subsequent equation confirmed how the double layer capacitance calculated (C_{dl}) [102]:

$$C_{dl} = \Upsilon_0\omega^{n-1}/\sin[n(\pi/2)] \tag{14}$$

In the present investigation, we considered the stage of surface coverage (θ) and the efficiency of inhibition (%IE) through the subsequent equation [103]:

$$\%IE = \theta \times 100 = \left[1 - \left(R_{ct}^0/R_{ct}\right)\right] \times 100 \tag{15}$$

The resistance of charge transfer is with and without adding the investigated compounds articulated by R_{ct}^0 and R_{ct} respectively. Additionally, it has film formation or coating on the surface. C_{dl} (the electrical double layer), Rs (solution resistance), R_{ct} (charge transfer resistance), and diffusion of ions give capacitance. Numerous of impedances happen as the result of locomotion of charges on or far from the copper surface; several impedances are because of anions and cations adsorption. The information, which obtainable from Table 7, exemplify impedance parameters for copper in $2MHNO_3$ with and without adding different concentrations from examined compounds. The got diagrams [Nyquist and Bode plots] for copper in the existence of several concentrations from compound 1 are depicted in Figs. 9, 10 (the other compound not shown). As demonstrated in the Bode plots in Fig. 10, at the low frequency region, the values of impedance increase in the presence of our compounds by two-fold compared to their absence, which show the remarked corrosion inhibition of the studied our compounds. Furthermore, increasing in the concentration of our compounds leads to the increase of the frequency range and the maximum phase angle representing the efficient adsorption of our compounds molecules on the surface of copper. The Nyquist figure showed that the diameter of the semicircle growths by increasing the concentration of the studied compound. Consequently, the charge transfer resistance of corrosion reaction increases. This leads to high resistance that is confirmed by the
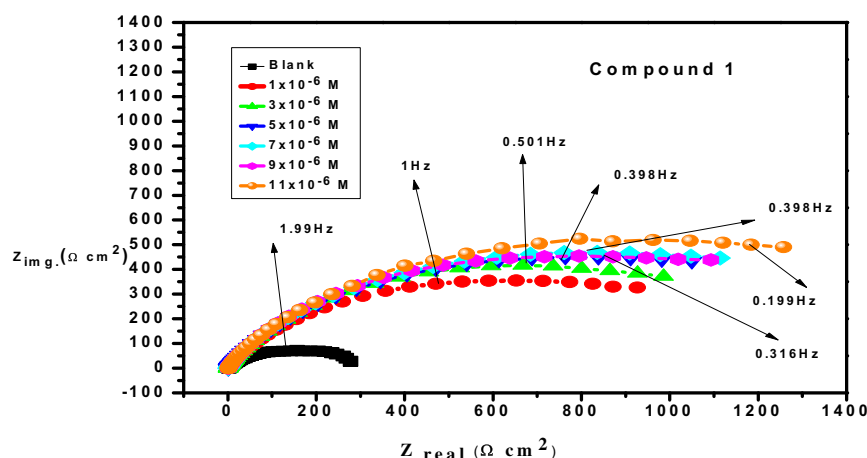
Fig. 9. EIS Nyquist bends for Cu surface without and with of altered doses of composite (**1**) at 25 ± 1 °C.
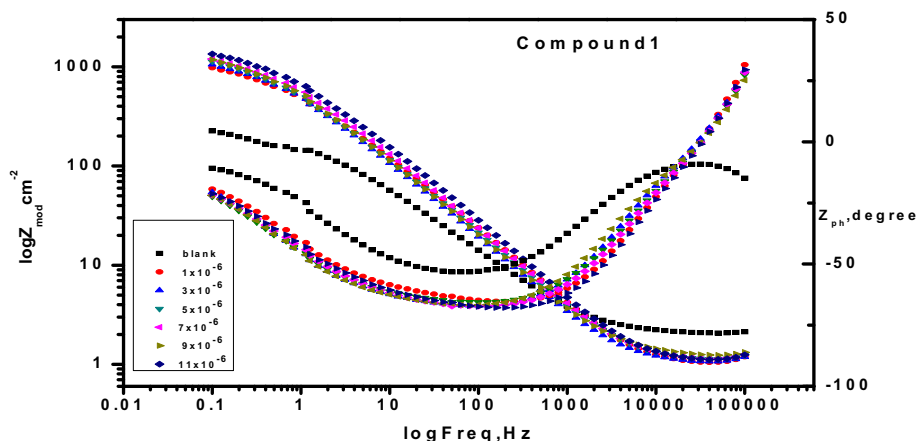
Fig. 10. EIS Bode bends for Cu surface without and with of altered doses of composite (**1**) at 25 ± 1 °C.

adsorbed molecules of examined compounds at the copper -solution interface [104]. The Nyquist plots presented the deviation from the theory of EIS, and it does not closed as expected. The nonconformity from ideal semicircle was because of the frequency dispersion and the inhomogeneity of the copper surface [105]. The decreasing of local dielectric constant and/or the increasing in the thickness of the electrical double layer are the result from adding different concentrations from examined compounds that give decreasing in C_{dl} compared to the blank solution. This, as a result, the adsorption of spiropyrazoles derivatives molecules at the copper/interface of solution [106–108]. The presented impedance charts with very nearly semicircular presence, proving the process of charge transfer and this process principally controls the corrosion of copper [109,110]. This technique was examined at corrosion potential, E_{corr}, and through a frequency range of 10^5Hz to 0.1 Hz and a signal capacity perturbation of 10 mV. The order of % IE: (1) > (2).

3.4. EFM tests

In the present study, we used the EFM technique because it is no damaging corrosion investigation method, which can assume and rapidly assesses the current corrosion value without previous information from Tafel slopes [111]. The causality factors appear as an internal scanning on the accuracy of EFM tests [112]. From the frequency spectra current, CF-2 and CF-3 were obtained. The signal in this technicality is a small AC signal alike EIS system, but the two techniques have a discrepancy, for the cause that, EFM has two sine waves (at differs frequencies) which are used to the cell with each other. Because of the current is a nonlinear function for potential, the system responds in a nonlinear way to the potential excitation. The current response has the input

frequencies, and frequency components (variance, sum, and manifold of the two input frequencies). For determination the length of the experiment, the frequencies have to tiny, integer multiples of the base of frequency. Table 8 demonstrated the corrosion parameters. Table 8 proves that good quality for examined values of causality factors. The steady data 2 for CF-2 and 3 for CF-3. The values deviancy of causality factors from the standard values happen because of noise. The deviance of values for causality factors from the standard values happen because of noise. Found a causal connection between the response signal and the perturbation signal when happening matching between the experimental values and theoretical values for causality factors, the data are supposed to authoritative [113]. From our search, we found that by increasing the doses of our investigated derivatives, the densities of corrosion current decrease (Fig. 11). At the same moment, the inhibition efficiencies for studied derivatives increase. Depending on the subsequent equation, the inhibition efficiencies for this technique were calculated:

$$\%IE_{EFM} = \theta x 100 = 100 \ x \left[1 - \left(i_{corr}/i^0_{corr}\right)\right] \tag{16}$$

Symbols i_{corr} and i^0_{corr} are equivalent to the densities of corrosion current in the existence and nonexistence of different concentration from examined derivatives. The dissimilarities between the individual methods and the numerous models, which used for the interpretations, make changes in the inhibition efficiency (%IE_{EFM}) [114,115]. By putting a potential perturbation, signal amplitude 10 mV using two sine waves from 2 to 5 Hz, EFM technique was used. There are three factors which

Table 8
Electrochemical kinetic parameters obtained by EFM technique for copper in 2 M HNO₃ without and with various concentrations of spiropyrazoles derivatives. at 25 ± 1 °C.

| Comp.	Conc., M.	i_{corr} (μA/cm²)	β_a (mV/dec)	$-\beta_c$ (mV/dec)	CF-2	CF-3	C.R	θ	%IE_{EFM}
	Blank	102.20	54.55	133.20	1.96	2.98	60.27	–	–
(1)	0.1×10^{-5}	21.19	68.96	124.00	1.93	2.92	9.70	0.792	79.2
	0.3×10^{-5}	21.09	52.99	135.00	1.84	2.96	9.66	0.793	79.3
	0.5×10^{-5}	20.47	73.83	129.10	1.79	2.81	9.37	0.799	79.9
	0.7×10^{-5}	18.26	65.57	133.50	2.01	3.06	8.36	0.821	82.1
	0.9×10^{-5}	17.97	65.42	123.80	1.75	3.11	8.23	0.824	82.4
	1.1×10^{-5}	13.55	64.02	136.20	2.20	3.05	6.20	0.867	86.7
(2)	0.1×10^{-5}	24.92	62.91	143.20	1.81	2.84	11.42	0.756	75.6
	0.3×10^{-5}	24.46	51.57	135.01	1.85	3.23	11.21	0.760	76.0
	0.5×10^{-5}	24.26	55.68	139.90	1.90	2.85	11.06	0.762	76.2
	0.7×10^{-5}	24.02	64.50	134.00	1.78	3.13	11.01	0.764	76.4
	0.9×10^{-5}	21.77	77.95	127.70	1.73	2.81	9.97	0.786	78.6
	1.1×10^{-5}	21.71	66.83	128.50	1.84	3.23	9.94	0.787	78.7
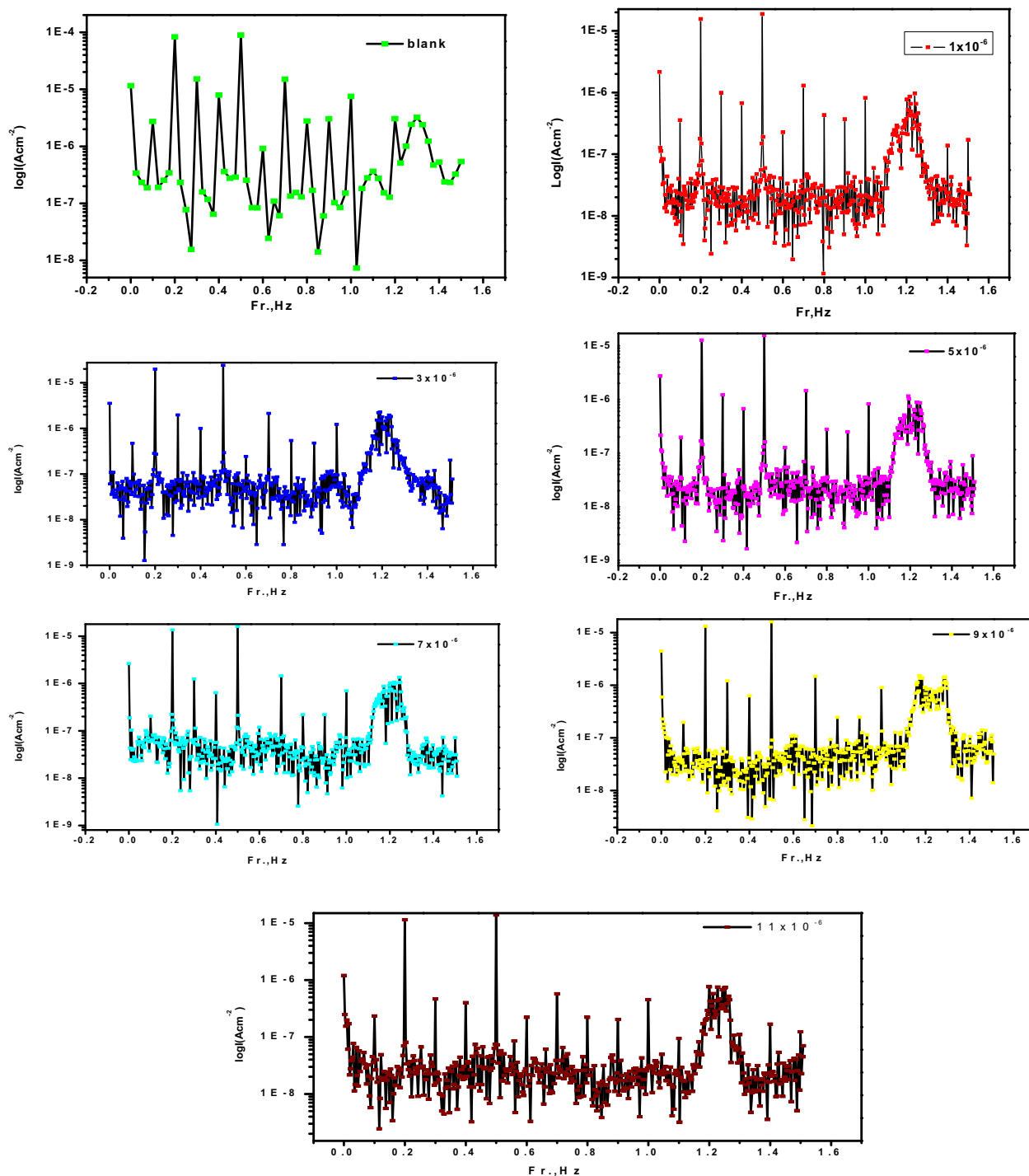
Fig. 11. EFM plots for corrosion of copper in 2 M HNO₃ in the existence and nonexistence of several concentrations from investigated compound (1) at 25 ± 1 °C.

control the choice of frequencies [116]. The order of %IE_EFM obtains from experiments are (1) > (2).

3.5. EDX and SEM examinations of the electrode surface

In our study, we used EDX survey spectra to set the elements, which existed on the surface of copper before and after contact by the solution of inhibitor. Fig. 12 gives spectra for exposed copper samples for 3 h in 2MHNO₃ with and without added 11 × 10⁻⁶ M spiropyrazoles

derivatives. Fig. 12 depicts the EDX tests of Cu and the existence of 11 × 10⁻⁶ M of spiropyrazoles compounds. These values show that the O and C atoms increase on the surface of copper in the presence of the inhibitors because of the adsorption of these inhibitors on the surface of copper [117]. The elemental distribution has achieved in Table 9.

Fig. 13 presented the micrograph because of Cu specimen absence and presence 11 × 10⁻⁶ M of spiropyrazoles compounds after contact for 3 h dipping. The surface of copper offers the corrosion destructive in the coins put in the blank. We noticed the formation of a film,

(Pure sample)   (Blank)

Compound1   Compound2
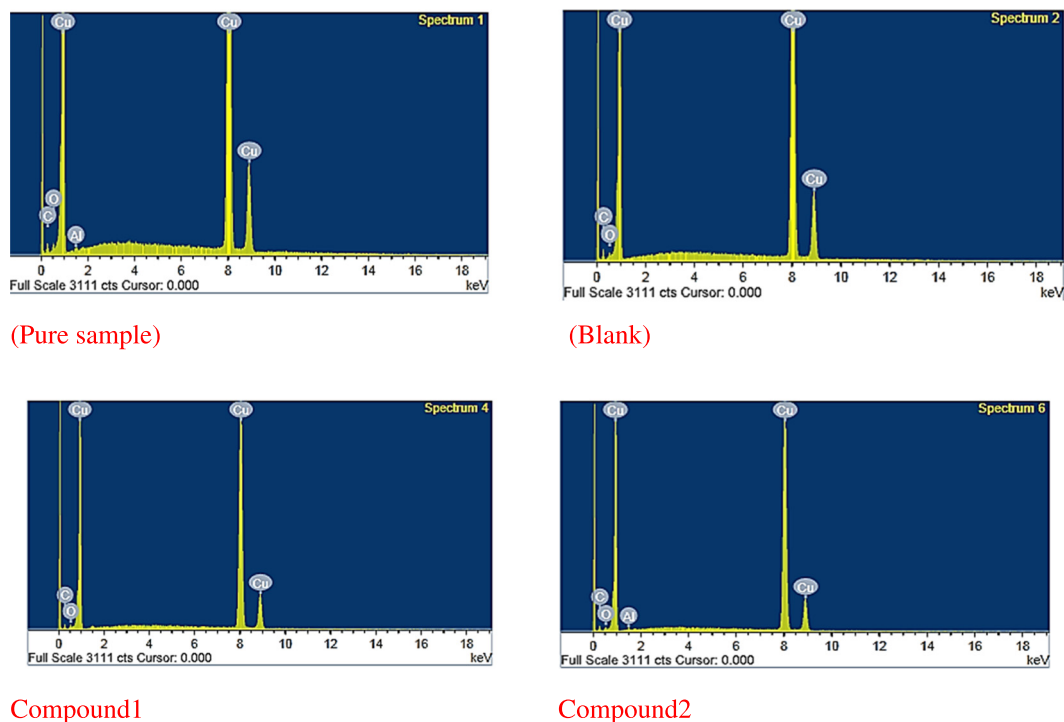
Fig. 12. EDS analysis of Copper in 2 M HNO$_3$ solution after immersion for 3 h without and in presence of 11×10^{-6} M of spiropyrazoles derivatives.

Table 9
Surface composition (weight %) of Copper in 2 M HNO$_3$ solution after immersion for 3 h without and in presence of 11×10^{-6} M of spiropyrazoles derivatives.

(Mass %)	C	O	Al	Cu
Pure sample	9.28	1.90	0.47	88.36
Blank	11.99	1.52	–	86.49
Compound (1)	13.03	1.88	–	85.09
Compound (2)	11.87	1.92	0.95	85.25

which spreads in a random overall Cu surface, owing to absorved spiropyrazoles derivatives on the Cu surface to give the passive coat to block the active sites, which found on the surface of Cu [118,119].

3.6. Quantum chemical calculations

In our study, we presented the relationship between the inhibitive action of investigated compounds and their molecular structures using quantum chemical calculations. Table 10 shows the intended quantum chemical parameters for the examined compounds, especially E$_{HOMO}$, E$_{LUMO}$, the hole of energy ΔE, molecular surface area, and dipole

(Pure sample)   (Blank)

(compound1)   (compound2)
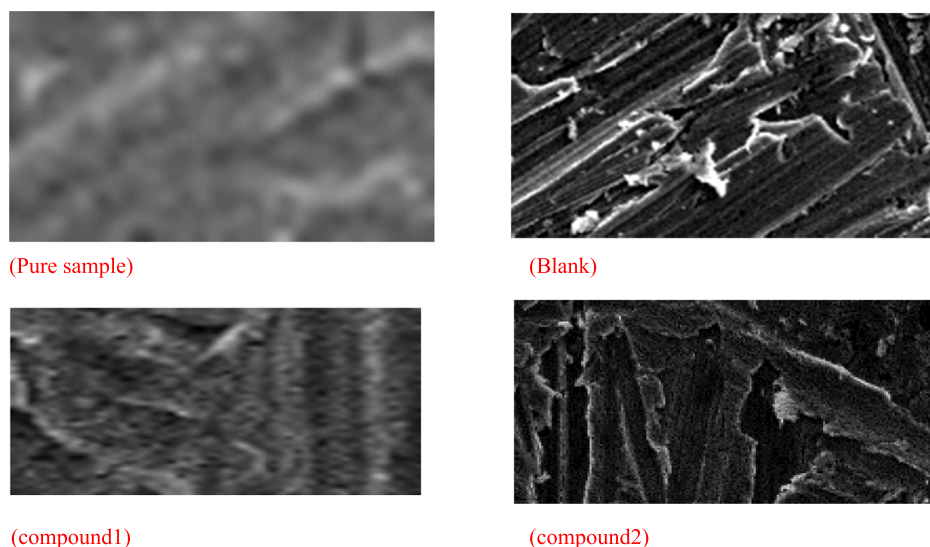
Fig. 13. SEM images of Copper in 2 M HNO$_3$ solution after immersion for 3 h without and in presence of 11×10^{-6} M of spiropyrazoles derivatives.

Table 10
The quantum measurements for investigated spiropyrazoles derivatives.

	Factors	Comp. (1)	Comp. (2)
PM3	$-E_{HOMO}$ (eV)	8.99	9.288
	$-E_{LUMO}$ (eV)	1.153	0.65
	ΔE (eV)	7.837	8.638
	η (eV)	3.92	4.32
	σ (eV)$^{-1}$	0.255	0.232
	-Pi (e.V)	5.072	4.969
	χ (eV)	5.072	4.969
	dipole moment μ (debyes)	5.248	4.898
	Molecular area (A° ^{2})	534.83	502.308
	ΔN_{max} (e)	0.0755	0.0566
DMol3	$-E_{HOMO}$ (eV)	4.599	4.472
	$-E_{LUMO}$ (eV)	2.525	2.139
	ΔE (eV)	2.074	2.333
	η (eV)	1.037	1.167
	σ (eV)-1	0.964	0.857
	-Pi (e)	3.56	3.31
	χ(eV)	3.56	3.31
	dipole moment μ (debyes)	6.894	6.275
	Molecular area (A° ^{2})	498.61	454.51
	$\Delta Nmax$(e)	−0.444	−0.501

moment μ. The improved structure, LUMO and HOMO orbitals for the molecules of our compounds were shown in Figs. 14, 15. The data of E_{HOMO} focused on the facility of the molecules to give electrons to a suitable acceptor owing vacant molecular orbitals. The E_{LUMO} values express the strength of these molecules to receive electrons. The more capacity the molecules to accept electrons at few values of E_{LUMO}, the higher values of E_{HOMO} for the compound, the more ability of the compound to give electrons to the unoccupied d-orbital of the copper surface, and give more protection [120,121]. Table 10 shows that compound 1 presents the maximum values of energy E_{HOMO} by two used methods which are PM3and DMol3. Thus, it may give the maximum corrosion protection. When the values of energy gap are low, the reactivity of the molecules increases and the small energy gap values gives good corrosion inhibitors. This is due to the reduction of ionization energy that are necessary to eliminate an electron from the outer shell orbital [123]. From the previous data, the soft molecules have a small energy gap, and they are more polarizable and associated with great stability, so these molecules provide more protection. Table 10 describes that compound (1) has the lowest ΔE by PM3 semi-empirical method and DMol3 module. This shows that compound (1) has more reactivity than compound 2, and more facility to adsorb on the Cu surface. Thus, it has better presentation of corrosion protection, which is in good agreement with the investigational data. ΔE suggests that the

COMP.	1	2
Optimized Structure		
HOMO		
LUMO		
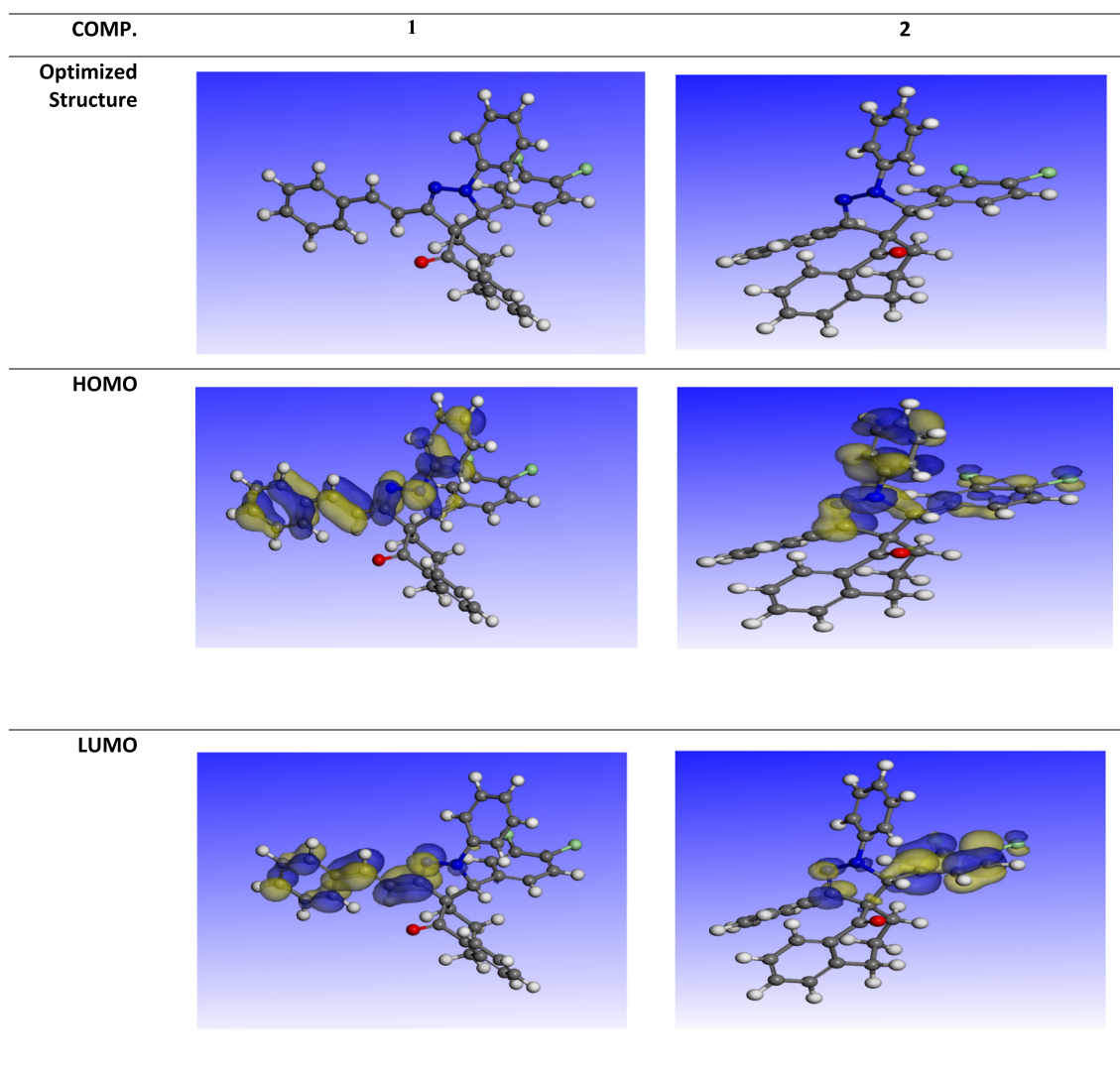
Fig. 14. The molecular structures optimization, LUMO and HOMO of the protonated inhibitor molecules using PM3 module.

	1	2
Optimized Structure		
HOMO		
LUMO		
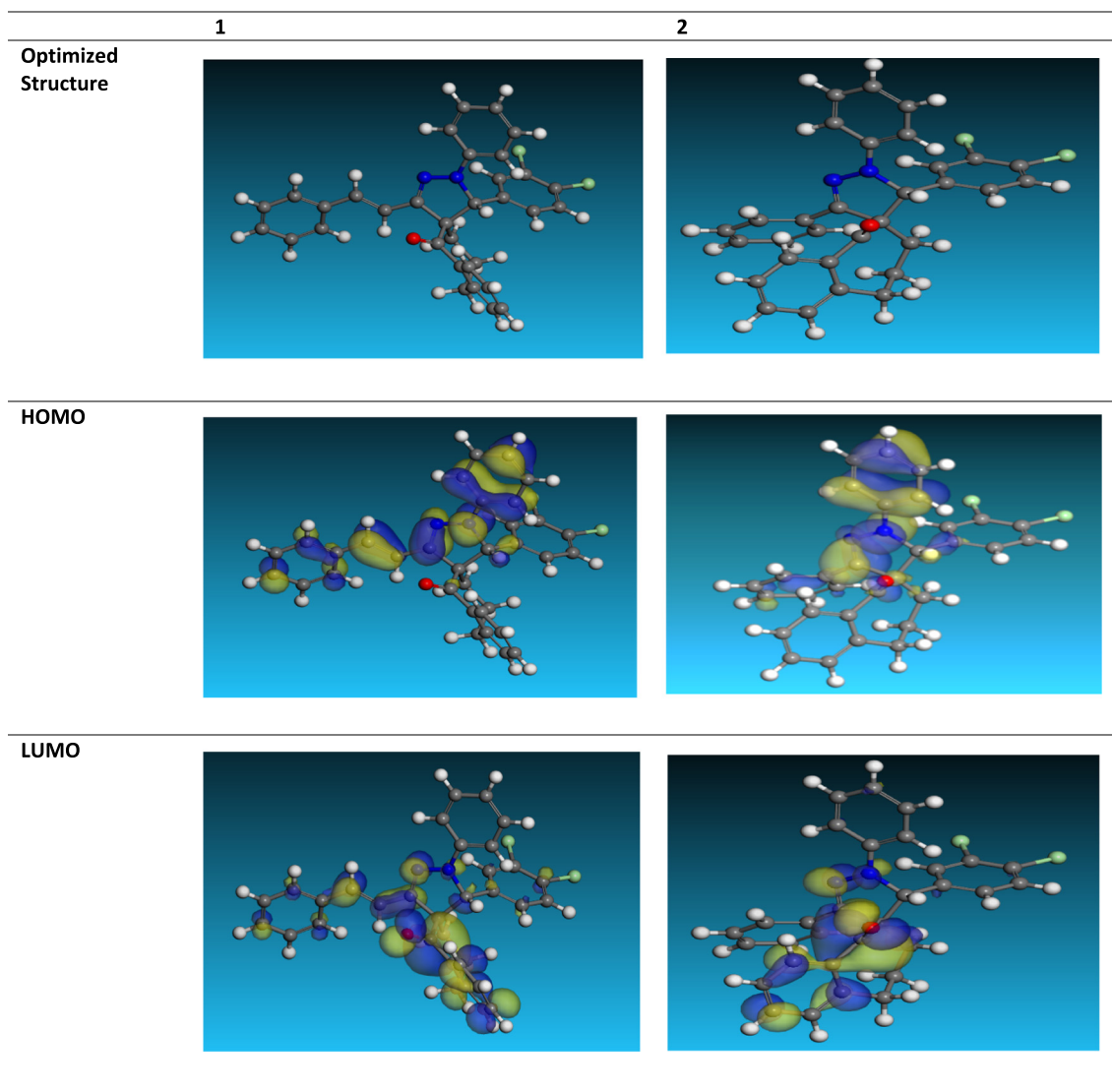
Fig. 15. The molecular structures optimization, LUMO and HOMO for the protonated inhibitor molecules utilizing DMol3 module.

arrangement of inhibitors efficiency is 1 ˃ 2 as the same order occasioned from experimental methods. The dipole moment also is used to justify the structure [124]. The powerful dipole-dipole interactions between the surface of copper and investigated compounds are as a result of high values of μ for these compounds. Thus, the adsorption on the copper surface becomes durable and thence resulting in better IE % [125]. Softness σ, absolute hardness η and reactivity of molecules are among other properties and are used to exam the stabilization. The molecules, with larger energy gap, are harder than molecules, with less energy gap. The molecules, that are soft, considered more reactive than hard ones because they give electrons to an acceptor. For the simple transfer of electrons, adsorption may occur at the part of the inhibitor molecule where σ is a native property and has the maximum value [126]. In the classification of corrosion, the molecules of our compounds become a Lewis base but the metal becomes a Lewis acid. The soft base inhibitors are more effective than bulk metals that is consider soft acids in acidic corrosion for our metal.

Table 10 shows the comparatively best agreement of Pi and ΔN with the inhibition efficiency according to the factors. This means that the reasons improve in Pi, and ΔN and reinforce the electronic releasing power of the inhibitor molecule. The confirmed value of ΔN of inhibition effect is resulted from electrons donation [127–129], if ΔN is <3.6, the capability of electrons donation and the inhibition efficiency increase on the metal surface [130].The used two methods presented a correlation between the molecular area of the molecule and the efficiency of protection. By increasing the area of the molecules for the investigated compounds and the efficacy of inhibition. This is due to increasing the interaction area between the molecule and the copper surface.

Table 11
Data and descriptors calculated by the Monte Carlo simulation for adsorption of inhibitors on Cu (1 1 1).

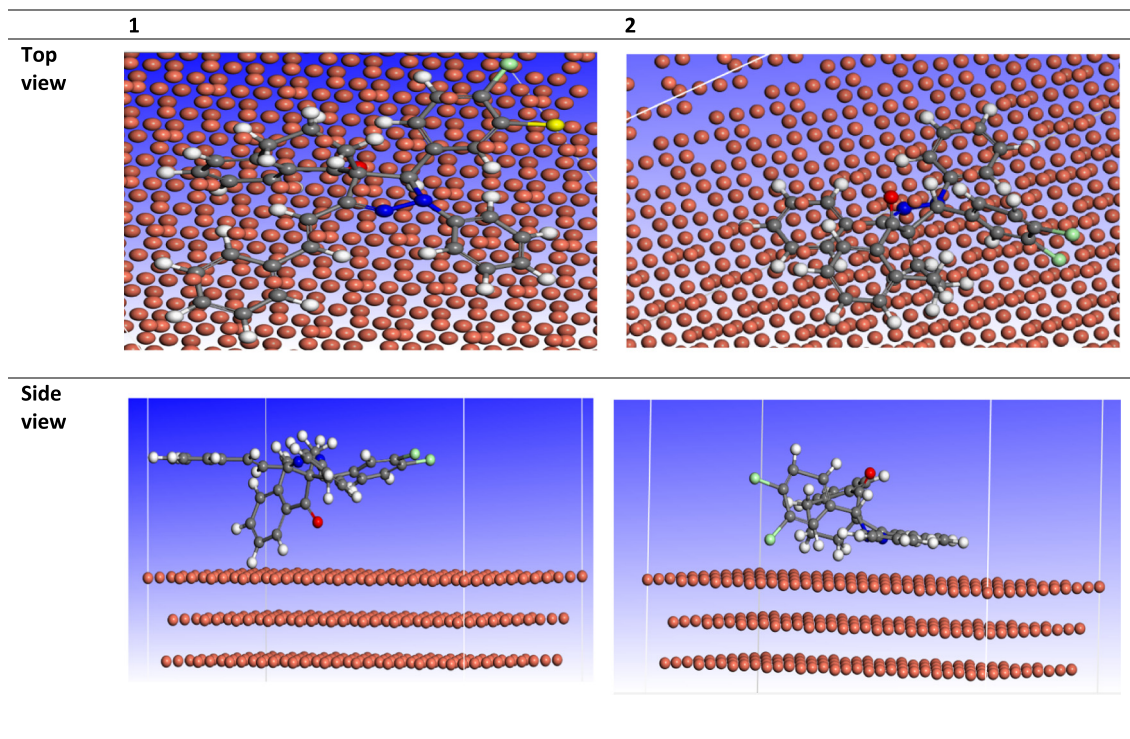| Structures Cu (1 1 1)	Total energy k (cal mol^{-1})	Adsorption energy k (cal mol^{-1})	Rigid adsorption energy k (cal mol^{-1})	Deformation energy k (cal mol^{-1})	: dEad/dNi k (cal mol^{-1})
cpd 1	−2814.47	−2855.02	−3188.64	333.62	−63.02
cpd 2	−2618.04	−2683.56	−2952.36	268.80	−38.29
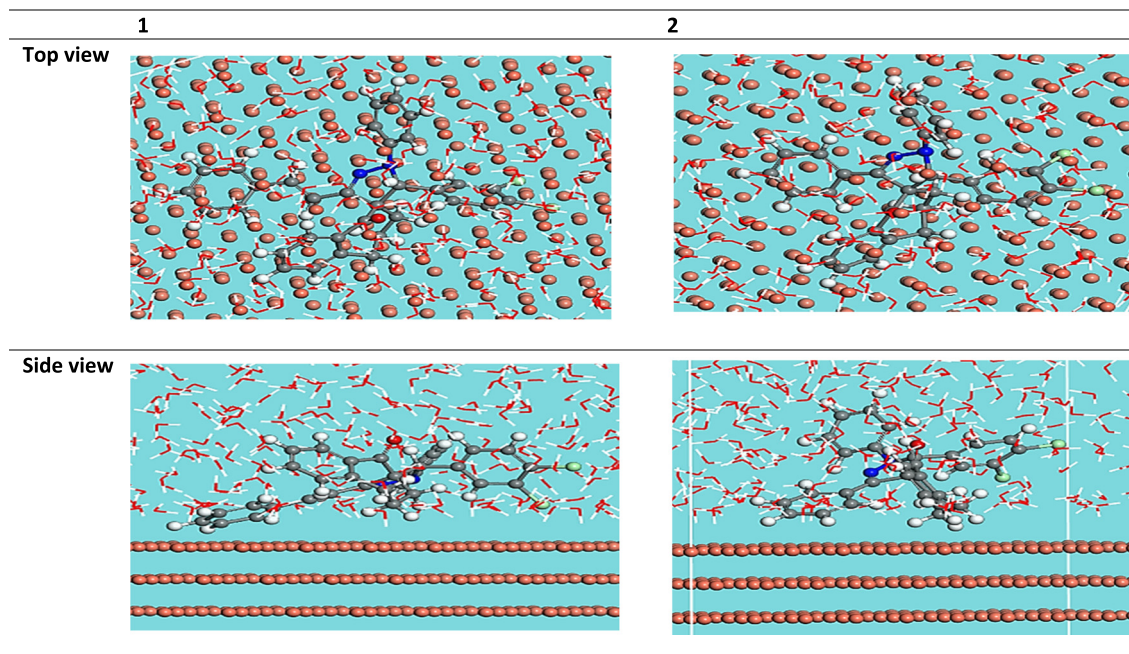
Fig. 16. The most appropriate formation for adsorption of the spiropyrazoles derivatives molecules on Cu (1 1 1) substrate got by adsorption locator module.

3.7. Simulation of molecular dynamics

In our study, we selected the appropriate arrangement for adsorption of our investigated molecules on Cu (1 1 1) substrate accomplished by adsorption locator module shown in Fig. 15. Table 11 shows the output of Monte Carlo simulation; the total energy, rigid adsorption, and deformation energies. The overall energy (kcal/ mol) for configuring the substrate - adsorbate is identified as the summation of the energies of the rigid adsorption energy, molecules, and the deformation energy. In our research, the energy of the copper (111) surface is considered zero. The energy of adsorption (kcal mol^{-1}) is the released energy when the relaxing adsorbate molecules (compounds (1 & 2)) are adsorbed on the substrate surface. The sum of the deformation energy and the rigid adsorption energy give the adsorption energy to the adsorbate molecules. Firm adsorption energy (kcal/ mol) is the released energy when the disturbed adsorbate molecules are adsorbed on the substrate and this before the step of geometry optimization. The energy produced when the adsorbed adsorbate components are relaxed on the substrate surface that is called the deformation energy, by kcal mol^{-1} [131]. In addition, one of the adsorbate molecules have been removed in the formation of substrate-adsorbate that obtained by dE$_{ads}$/dN$_i$, which registers the energy by kcal mol^{-1}. Table 11 showed that compound 1 is the most effective inhibitor; because of the adsorption energy of Compound 1 is higher than the adsorption energy of Compound 2 for the duration of the simulation process [132]. Consequently, the molecules of compound 1 are surely adsorbed on the copper surface for forming stable adsorbed layers more than compound 2 that gives corrosion protection for copper surface from nitric acid assured by both investigational and theoretical studies. In our study, we compared between the adsorption of molecule in acid medium and in

vacuum. It shows that in the presence of aqueous solution, the energies of adsorption become high, comparison to in the vacuum, so the adsorption of molecules in the protonated case is more effective on the copper surface (Fig. 16, Table 12).

3.7.1.1. Molecular docking. In our investigation, the docking research presented a favorable interaction amend spiropyrazoles derivatives and the 3hb- OXIDOREDUCTASE protein model. The calculated energy is registered in Table 12, and shown in Figs. 18–21. Supportive to these results in this manuscript, HB bends lead to spiropyrazoles derivatives that binds to the bond of proteins hydrogen and disintegrated contacts energies in kcal/mol amid the spiropyrazoles derivatives with 3hb-OXIDOREDUCTASE protein receptor as displayed in Fig. 17. The measured efficiency is hopeful where Ki data calculated by Auto Dock were paralleled with data Ki, with the ΔG^o is negative [133–135], and with 2D bends of docking with spiropyrazoles derivatives are revealed in Fig. 20 (Table 13).

3.7.1.2. Inhibition mechanism. In aggressive acidic media, the first step in the corrosion inhibition of metal by organic compounds happen through their adsorption at the metal/solution interface. Different types of adsorption may yield through inhibition of organic compounds: 1) the interaction of π-electrons with the metal, 2) electrostatic attraction between charged molecules, 3) interaction of unshared electron pairs in the molecule 4) and may occur combination of the above situations [136]. Spiropyrazoles derivatives have centers for π electron as rings of benzene and the presence of heteroatoms (nitrogen and oxygen). Consequently, their existence raises the adsorption of the spiropyrazoles derivatives molecules on the surface of copper [137].

Table 12
Data and descriptors calculated by the Monte Carlo simulation for adsorption of inhibitors on Cu (1 1 1) in vacuum.

Structures Cu (1 1 1)	Total energy k (cal mol^{-1})	Adsorption energy k (cal mol^{-1})	Rigid adsorption energy k (cal mol^{-1})	Deformation energy k (cal mol^{-1})	: dEad/dNi k (cal mol^{-1})
cpd 1	−61.73	−932.70	−113.70	−819.7	−932.78
cpd 2	−29.53	−724.90	−100.53	−624.8	−724.9

Fig. 17. The most appropriate formation for adsorption of the spiropyrazoles derivatives molecules on Cu (1 1 1) substrate got by adsorption locator module without aqueous solution.

Dissolution of copper in nitric acid is given by the next two continuous steps [138]:

$$Cu - e^- = Cu\ (I)_{ads}\ (fast\ step)$$

$$Cu\ (I)_{ads} - e^- = Cu(II)\ (slow\ step)$$
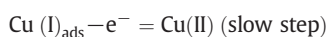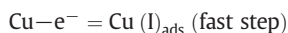
where is Cu(I) is an adsorbed species at the surface of copper and it does not diffuse into the bulk solution [139]. The dissolution of copper is controlled by the diffusion of soluble Cu (II) species from the outer Helmholtz plane to the bulk solution. NO_3^- ions are attracted by the charges on the copper surface, which has a tendency to be charged negatively. The obtained results are based on the supposition that the negatively charged NO_3^- would attach to the positively charged surface. This may be a synergism between NO_3^- and the protonated spiropyrazoles derivatives adjacent the interface, and the concentrations of NO_3^- and that of the neutral forms from spiropyrazole derivatives and the protonated forms from them thta were probably much higher than those in the bulk solution. These protonated forms attach electrostatically to the negative charges at the copper surface [140]. When the neutral forms and the protonated forms of the inhibitors adsorb on the copper surface, coordinate bonds are formed by partial transference of electrons from the unprotonated nitrogen and oxygen atoms, delocalized π electrons in the spiropyrazole derivatives rings to the metal surface via vacant d orbitals of Cu^{2+} ions. Therefore, in the

process of adsorption, both physical and chemical adsorptions might take place.

Another mechanism depends on the dissolution of copper as Cu^{+2} [141] and on chelating effect of Cu^{+2} ions close to the surface of copper. That is because no oxide film formed to protect the surface from corrosion [82,83]. The organic compounds can be also adsorbed through the interactions between the lone pairs of electrons of nitrogen, or oxygen atoms with surface of copper. These procedures are eased by the existence of d vacant orbitals of low energy in the ions of copper, as detected in metals of transition group. The difference between two compounds (1 & 2) that styryle group which found in compound 1 replaced by phenyl group in compound 2. Compound 1 exhibited high inhibition effect than compound 2 and this may be attributed to increasing electron density in it than compound 2 and that enhance anticorrosive effect.

4. Conclusions

In this research, our two derivatives compounds investigated for their corrosion inhibitory properties on copper 2 M HNO₃. Chemical and electrochemical techniques based on theoretical study (quantum calculations, molecular docking, and molecular dynamics simulations) were used. Both investigated compounds are good mixed type inhibitors for copper corrosion in 2 M HNO₃ solution. Chemical and electrochemical measurements show that the inhibition efficiency increases with increasing our investigated compounds concentrations and decreases with increasing temperature. Furthermore, double layer capacitances decrease by increasing the concentrations of our investigated compounds. This fact approves the adsorption of the molecules of

Table 13
Energy values obtained in docking calculations of compounds (1 & 2) with breast cancer (3hb5) receptor.

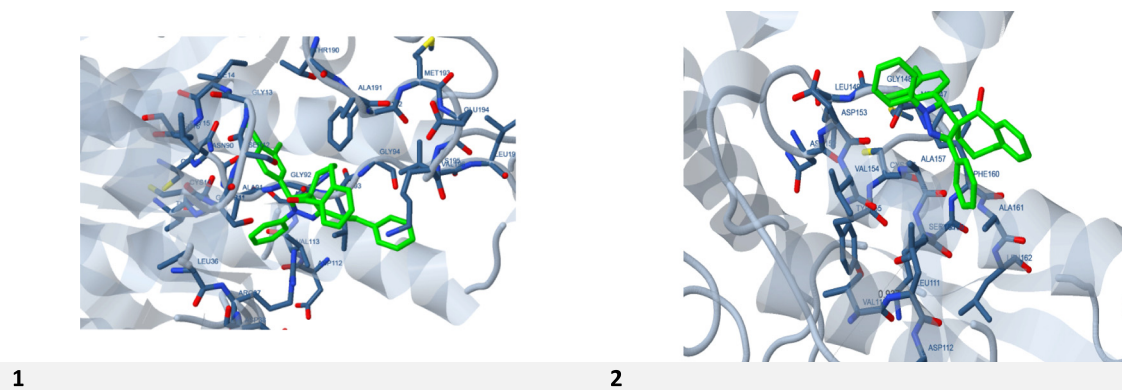| Compound	Est. free binding energy (kcal/mol)	Est. inhibition constant (K_i) (μM)	vdW+ bond + desolve energy (kcal/mol)	Electrostatic energy (kcal/mol)	Total intercooled energy (kcal/mol)	Interact surface
1	−9.02	244.90	−10.13	−0.01	−10.14	1147.817
2	−5.71	64.79	−6.56	−0.01	−6.57	606.552

Fig. 18. Top-ranked docking poses of compounds (1 & 2) in green with selected anti-cancer protein receptors in gray.
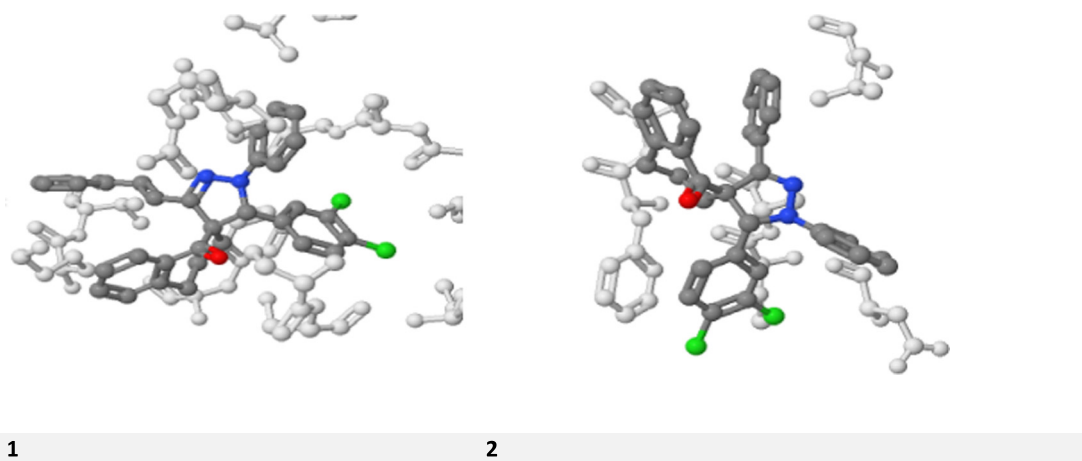

Fig. 19. The interaction between breast cancer active sites with the targeted compounds 1 & 2.
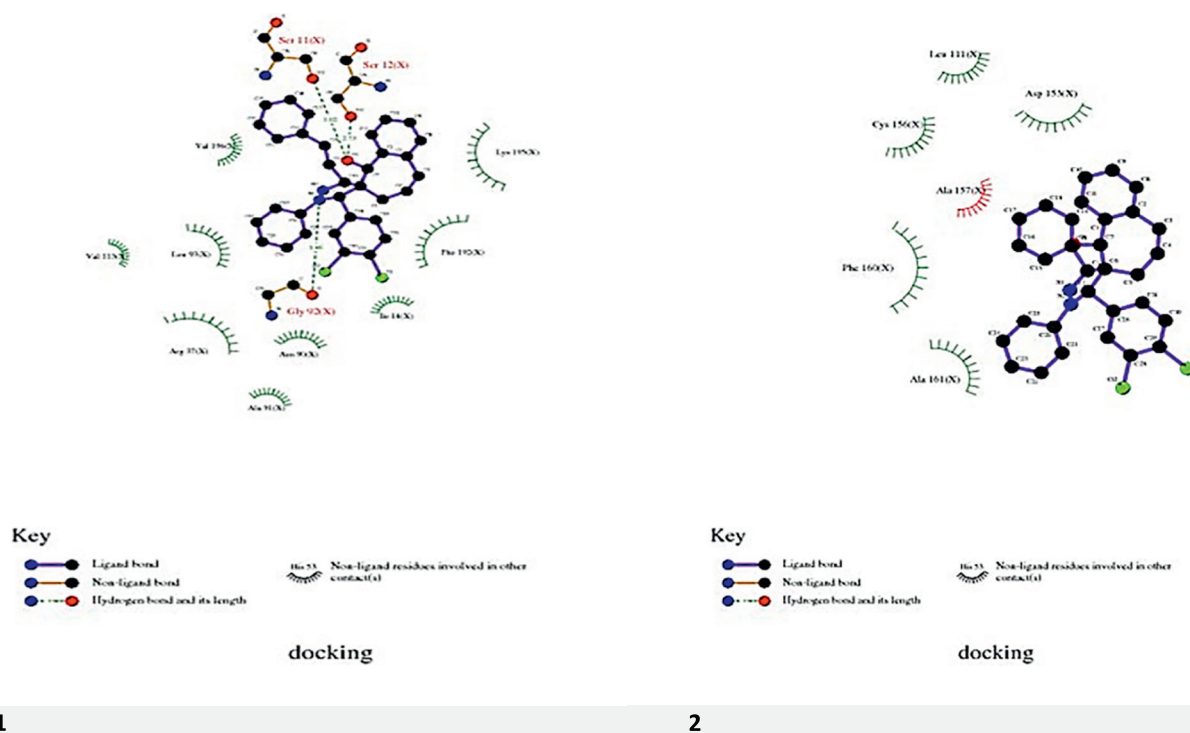

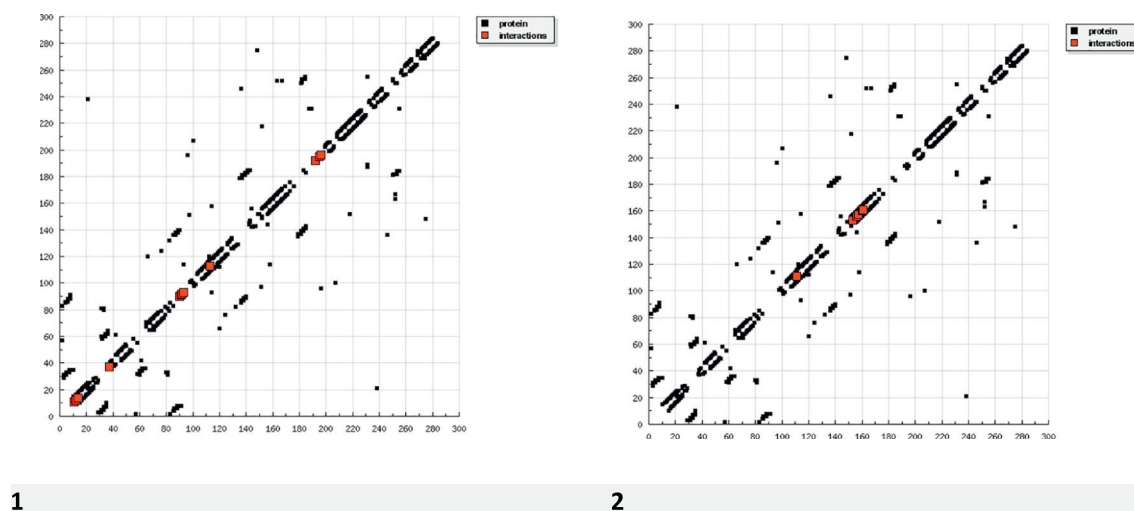**Fig. 20.** The 2D plot of interaction between compounds (1 & 2) with anti-cancer active sites.

1   **2**

Fig. 21. HB plot of interaction between compounds (1 & 2) with anti-cancer active sites.

these compounds on the copper surface. As predictable, the adsorption of compounds (1&2) on the copper surface, at a different temperature, submits the Freundlich adsorption isotherm and this adsorption refers to physisorption. Interestingly, experimental and theoretical study results supported the notion where compounds (1&2) are good corrosion inhibitors, and the order of inhibition efficiency for the studied compounds is 1 > 2.

References

[1] K.F. Khaled, Corrosion control of copper in nitric acid solutions using some amino acids, a combined experimental and theoretical study, Corro. Sci. 52 (2010) 3225–3234, https://doi.org/10.1016/j.corsci.2010.05.039.

[2] A.S. Foud, H.A. Abdul Wahid, Corrosion inhibition of copper in HNO3 solution using thiophene and its derivatives, Arab. J. Chem. 9 (2016) S91–S99, https://doi.org/10.1016/j.arabjc.2011.02.014.

[3] H.T. Rahal, A.M. Abdel-Gaber, G.O. Younes, Inhibition of steel corrosion in nitric acid by sulfur-containing compounds, Chem. Eng. Commun. 203 (2016) 435–445, https://doi.org/10.1080/00986445.2015.1017636.

[4] G. Karthik, M. Sundaravadivelu, P. Rajkumar, M. Manikandan, Diaza-adamantane derivatives as corrosion inhibitor for copper in nitric acid medium, Res. Chem. Intermed. 41 (2015) 7593–7615, https://doi.org/10.1007/s11164-014-1846-8.

[5] G. Tansuğ, T. Tüken, E.S. Giray, G. Fındıkkıran, G. Sığırcık, O. Demirkol, M. Erbilb, A new corrosion inhibitor for copper protection, Corr. Sci. 84 (2014) 21–29, https://doi.org/10.1016/j.corsci.2014.03.004.

[6] P. FerozKhan, V. Shanthi, R.K. Babu, Srinivasan Muralidharan, R. Chandra Banik, Effect of benzotriazole on corrosion inhibition of copper under flow conditions, Journal of Environmental Chemical Engineering 3 (1) (2015) 10–19, https://doi.org/10.1016/j.jece.2014.11.005.

[7] L. Vrsalović, S. Gudić, D. Gracić, I. Smoljko, I. Ivanić, M. Kliškić Emeka, E. Oguzie, Corrosion protection of copper in sodium chloride solution using propolis, Int. J. Electrochem. Sci. 13 (2018) 2102–2117, https://doi.org/10.20964/2018.02.71.

[8] A.S. Fouda, F.I. El-Dossoki, I.A. Shady, Adsorption and corrosion inhibition behavior of polyethylene glycol on α-brass alloy in nitric acid solution, Journal Green Chemistry Letters and Reviews 11 (2018) 67–77, https://doi.org/10.1080/17518253.2018.1438525.

[9] L. Feng, S. Zhang, Y. Qiang, Y. Xu, L. Guo, L.H. Madkour, S. Chen, Experimental and Theoretical Investigation of Thiazolyl Blue as a Corrosion Inhibitor for Copper in Neutral Sodium Chloride Solution, vol. 11(6), 2018 1042–1059, https://doi.org/10.3390/ma11061042.

[10] A.S. Fouda, M.A. Ismael, R.M. Abo Shahba, L.A. Kamel, A.A. El-Naggar, Corrosion inhibition of copper and α-Brass in 1 M HNO3 solution using new arylpyrimido [5, 4-c] quinoline-2,4-dione derivative, Int. J. Electrochem. Sci. 12 (2017) 3361–3384, https://doi.org/10.20964/2017.04.57.

[11] A.S. Fouda, S. El-din, H. Etaiw, D.M. Abd El-Aziz, O.A. Elbaz, Int. J. Electrochem. Sci. 12 (2017) 5934–5950, https://doi.org/10.20964/2017.07.08.

[12] N. Coulibaly, Y. Serge Brou, S. Akpa, J. Creus, A. Trokourey, Corrosion inhibition of copper in 2M nitric acid solution by 2-(thiobenzyl)-5-nitro-1H-benzimidazole, International Journal of Applied Pharmaceutical Sciences and Research 3 (2018) 54–63, https://doi.org/10.21477/ijapsr.3.4.2.

[13] Zarrouk, B. Hammouti, H. Zarrok, M. Bouachrine, K.F. Khaled, S.S. Al-Deyab, Corrosion inhibition of copper in nitric acid solutions using a new triazole derivative, Int. J. Electrochem. Sci., 7 (2012) 89 - 105.

[14] K.F. Khaled, Mohammed A. Amin, Dry and wet lab studies for some benzotriazole derivatives as possible corrosion inhibitors for copper in 1.0 M HNO3, Corros. Sci. 51 (2009) 2098–2106, https://doi.org/10.1016/j.corsci.2009.05.038.

[15] A.S. Fouda, F.I. El-Dossoki, I.A. Shady, Adsorption and corrosion inhibition behavior of polyethylene glycol on α-brass alloy in nitric acid solution, GREEN CHEMISTRY LETTERS AND REVIEWS 11 (2018) 67–77, https://doi.org/10.1080/17518253.2018.1438525.

[16] A. Fiala, A. Chibani, A. Darchen, A. Boulkamh, K. Djebbar, Investigations of the inhibition of copper corrosion in nitric acid solutions by ketene dithioacetal derivatives, Appl. Surf. Sci. 253 (2007) 9347–9356, https://doi.org/10.1016/j.apsusc.2007.05.066.

[17] A.S. Fouda, H.A. Wahed, Corrosion inhibition of copper in HNO3 solution using thiophene and its derivatives, Arab. J. Chem. 9 (2016) S91, https://doi.org/10.1016/j.arabjc.2011.02.014.

[18] A. Howida, M. Fetouh, Tarek and Abdel-Fattah, Int. J. Electrochem. Sci. 9 (2014) 1565–1582.

[19] O.K. Abiolaa, A.O. Jamesb, The effects of Aloe vera extract on corrosion and kinetics of corrosion process of zinc in HCl solution, Corros. Sci. 52 (2010) 661–664, https://doi.org/10.1016/j.corsci.2009.10.026.

[20] M.M. Solomon, S.A. Umoren, I.I. Udosoro, A.P. Udoh, Inhibitive and adsorption behavior of carboxymethyl cellulose on mild steel corrosion in sulphuric acid solution, Corros. Sci. 52 (2010) 1317–1325, https://doi.org/10.1016/j.corsci.2009.11.041.

[21] A.K. Satapathy, G. Gunasekaran, Kumar Amit, P.V. Rodrigues, Corrosion inhibition by Justicia gendarussa plant extract in hydrochloric acid solution, Corros. Sci. 51 (2009) 2848–2856, https://doi.org/10.1016/j.corsci.2009.08.016.

[22] O.K. Abiola, J.O.E. Otaigbe, The Effects of Phyllanthus amarus Extract on Corrosion and Kinetics of Corrosion Process of Aluminum in Alkaline Solution, vol. 51, 2009 2790–2793, https://doi.org/10.1016/j.corsci.2009.07.006.

[23] E.E. Oguzie, Evaluation of the inhibitive effect of some plant extracts on the acid corrosion of mild steel, 50 (2008) 2993–2998, https://doi.org/10.1016/j.corsci.2008.08.004.

[24] E.M. Sherif, Su-Moon Park, 2-Amino-5-ethyl-1,3,4-thiadiazole as a corrosion inhibitor for copper in 3.0% NaCl solutions, Corros. Sci. 48 (2006) 4065–4079, https://doi.org/10.1016/j.corsci.2006.03.011.

[25] El-Sayed M. Sherif, A.M. Shamy, Mostafa M. Ramla, Ahmed O.H.El Nazhawy, 5-(Phenyl)-4H-1,2,4-triazole-3-thiol as a corrosion inhibitor for copper in 3.5% NaCl solutions, Mater. Chem. Phys. 102 (2007) 231–239, https://doi.org/10.1016/j.matchemphys.2006.12.009.

[26] Stanley Udochukwu Ofoegbu, Tiago L. P. Galvãʔo,a Jose R. B. Gomes, Joaʔo Tedim, Helena I. S. Nogueira, M. G. S. Ferreiraa and M. L. Zheludkevich, Phys. Chem. Chem. Phys., Corrosion inhibition of copper in aqueous chloride solution by 1H-1,2,3-triazole and 1,2,4-triazole and their combinations: electrochemical, Raman and theoretical studies 19(2017) 6113—6129. DOI: https://doi.org/10.1039/c7cp00241f.

[27] Dunja Gustinʔciʔc, Anton Kokalj, DFT study of azole corrosion inhibitors on Cu2O model of oxidized copper Surfaces: I. molecule–surface and Cl–surface bonding, Metals 8 (2018) 310, https://doi.org/10.3390/met8050310.

[28] Yu.I. Kuznetsov, Triazoles as a class of multifunctional corrosion inhibitors. A review. Part I. 1,2,3-Benzotriazole and its derivatives. Copper, zinc and their alloys, Int. J. Corros. Scale Inhib. 7 (3) (2018) 271–307, https://doi.org/10.17675/2305-6894-2018-7-3-1.

[29] Y.E. Louadi, F. Abrigach,a A. Bouyanzer, R. Touzani, A. El Assyry, A. Zarrouk, B. Hammoutia, Theoretical and experimental studies on the corrosion inhibition potentials of two Tetrakis Pyrazole derivatives for mild steel in 1.0 M HCl, Port. Electrochim. Acta 2017, 35(3), 159–178. DOI: https://doi.org/10.4152/pea.201703159.

[30] Hassane Lgaz, Rachid Salghi, Abdelkarim Chaouiki, Shehdeh Jodeh Shubhalaxmi, K. Subrahmanya Bhat, Pyrazoline derivatives as possible corrosion inhibitors for mild steel in acidic media: a combined experimental and theoretical approach, Cogent Engineering 5 (2018), 1441585. https://doi.org/10.1080/23311916.2018.1441585.

[31] A. El-Faham, S.M. Osman, H.A. Al-Lohedan, G.A. El-Mahdy, Hydrazino-methoxy-1,3,5-triazine Derivatives' excellent corrosion organic inhibitors of steel in acidic chloride solution, Molecules 21 (2016) 714, https://doi.org/10.3390/molecules21060714.

[32] M.N. El-Haddad, K.M. Elattar, Synthesis, characterization and inhibition effect of new antipyrinyl derivatives on mild steel corrosion in acidic solution, Int J Ind Chem 6 (2015) 105–117, https://doi.org/10.1007/s40090-015-0037-9.

[33] M. Yadav, S. Kumar, R. Ranjan Sinha, D. Behera, Experimental and quantum chemical studies on the corrosion inhibition performance of benzimidazole derivatives for mild steel in HCl, Ind. Eng. Chem. Res. 52 (19) (2013) 6318–6328, https://doi.org/10.1021/ie400099q.

[34] F.M. Al Kharafi, N.A. Al-Awadi, I.M. Ghayad, R.M. Abdullah, M.R. Ibrahim, Novel technique for the application of azole corrosion inhibitors on copper surface, Mater. Trans. 51 (9) (2010) 1671–1676.

[35] A. Fateh, M. Aliofkhazraei, A.R. Rezvanian, Review of corrosive environments for copper and its corrosion inhibitors, Arab. J. Chem., doi:https://doi.org/10.1016/j.arabjc.2017.05.021.

[36] L. Alamiparvin, E.G. Kalhor, S.R. Nabavi, Sh. Ebrahimi, A. Farzamnia, Studies on corrosion inhibitor activity of azoles for copper, Adv. Sci. Lett. 23 (11) (2017) 11293–11297.

[37] A.S. Fouda, A. Abd El-Aa, A.B. Kandil, The effect of some phthalimide derivatives on corrosion behavior of copper in nitric acid, Desalination 201 (2006)https://doi.org/10.1016/j.desal.2005.11.030.

[38] N. Zulfareen, T. Venugopal, K. Kannan, Experimental and theoretical studies on the corrosion inhibition of brass in hydrochloric acid by N-(4-((4-benzhydryl piperazin-1-yl) methyl carbamoyl) phenyl) Furan-2 carboxamide, International Journal of Corrosion 2018 (2018) 9372804, https://doi.org/10.1155/2018/9372804.

[39] J.H. Ahn, J.A. Kim, H.M. Kim, H.M. Kwon, S.C. Huh, S.D. Rhee, K.R. Kim, S.D. Yang, S.D. Park, J.M. Lee, S.S. Kim, H.G. Cheon, Synthesis and evaluation of pyrazolidine derivatives as dipeptidyl peptidase IV (DP-IV) inhibitors, Bioorg. Med. Chem. Lett. 15 (2005) 1337–1340, https://doi.org/10.1016/j.bmcl.2005.01.020.

[40] P. Prasanna, K. Balamurugan, S. Perumal, P. Yogeeswari, D. Sriram, A regio- and stereoselective 1,3-dipolar cycloaddition for the synthesis of novel spiro-pyrrolothiazolyloxindoles and their antitubercular evaluation, Eur. J. Med. Chem. 45 (2010) 5653–5661, https://doi.org/10.1016/j.ejmech.2010.09.019.

[41] A.A. Raj, R. Raghunathan, M.R.S. Kumari, N. Raman, Synthesis, antimicrobial and antifungal activity of a new class of Spiro pyrrolidines, Bioorg. Med. Chem. 11 (2003) 407–419, https://doi.org/10.1016/S0968-0896 (02)00439-X.

[42] A.S. Girgis, N.S.M. Ismail, H. Farag, W.I. El-Eraky, D.O. Saleh, S.R. Tala, A.R. Katritzky, Regioselective synthesis and molecular modeling study of vasorelaxant active 7,9-dioxa-1,2-diaza-spiro[4.5]dec-2-ene-6,10-diones, Eur. J. Med. Chem. 45 (2010) 4229–4238, https://doi.org/10.1016/j.ejmech.2010.06.018.

[43] G. Mariappan, B.P. Saha, L. Sutharson, A. Haldar, Synthesis and bioactivity evaluation of pyrazolone derivatives, Indian J. Chem. 49B (2010) 1671–1674http://hdl.handle.net/123456789/10738.

[44] N. Uramaru, H. Shigematsu, A. Toda, R. Eyanagi, S. Kitamura, S. Ohta, Design, synthesis, and pharmacological activity of nonallergenic pyrazolone-type antipyretic analgesics, J. Med. Chem. 53 (2010) 8727–8733, https://doi.org/10.1021/jm101208x.

[45] J. Choi, Y. Park, H.S. Lee, Y. Yang, S. Yoon, 1,3-Diphenyl-1H-pyrazole derivatives as a new series of potent PPARγ partial agonists, Bioorg MedChem 18 (2010) 8315–8323, https://doi.org/10.1016/j.bmc.2010.09.068.

[46] C. Congiu, V. Onnis, L. Vesci, M. Castorina, C. Pisano, Synthesis and in the vitro antitumor activity of new 4,5-dihydropyrazole derivatives, Bioorg. Med. Chem. 18 (2010) 6238–6248, https://doi.org/10.1016/j.bmc.2010.07.037.

[47] F. Caruso, C. Pettinari, F. Marchetti, Mannti Rossi, C. Opazo, S. Kumar, S. Balwani, B. Ghosh, Inhibitory effect of β-diketones and their metal complexes on TNF-α induced expression of ICAM-1 on human endothelial cells, Bioorg. Med. Chem. 17 (2009) 6166, https://doi.org/10.1016/j.bmc.2009.07.064.

[48] E.-S.M.N. Abdel-Hafez, G.E.-D.A.A. Abuo-Rahma, M. Abdel-Aziz, M.F. Radwan, H.H. Farag, Design, synthesis and biological investigation of certain pyrazole-3-carboxylic acid derivatives as novel carriers for nitric oxide, Bioorg. Med. Chem. 17 (2009) 3829–3837, https://doi.org/10.1016/j.bmc.2009.04.037.

[49] G. Ouyang, Z. Chen, X.-J. Cai, B.-A. Song, P.S. Bhadury, S. Yang, L.-H. Jin, W. Xue, D.-Y. Hu, S. Zeng, Synthesis and antiviral activity of novel pyrazole derivatives containing oxime esters group, Bioorg. Med. Chem. 16 (2008) 9699–9707, https://doi.org/10.1016/j.bmc.2008.09.070.

[50] ASTM, AST G 31–72, Standard Recommended Practice for the Laboratory Immersion Corrosion Testing of Metals, American Society for Testing and Materials, Philadelphia, PA, USA, 1990.

[51] Sayed M. Riyadh, Thoraya A. Farghaly, Effect of solvent on the regioselective synthesis of spiropyrazoles, Tetrahedron 68 (2012) 9056–9060, https://doi.org/10.1016/j.tet.2012.08.064.

[52] L. Zhou, Y.-L. Lv, Y.-X. Hu, J.-H. Zhao, X. Xia, X. Li, Experimental and theoretical investigations of 1,3,5 tris(4-aminophenoxy)benzene as an effective corrosion inhibitor for mild steel in 1 M HCl, J. Mol. Liq. 249 (2018) 179–187, https://doi.org/10.1016/j.molliq.2017.10.129.

[53] H.M. Abd El-Lateef, M.A. Abo-Riya, A.H. Tantawy, Empirical and quantum chemical studies on the corrosion inhibition performance of some novel synthesized cationic Gemini surfactants on carbon steel pipelines in acid pickling processes, Corros. Sci. 108 (2016) 94–110, https://doi.org/10.1016/j.corsci.2016.03.004.

[54] R.G. Pearson, Absolute electronegativity and hardness: application to inorganic chemistry, Inorg. Chem. 27 (1988) 734–740, https://doi.org/10.1021/ic00277a030.

[55] Y.M. Abdallah, K. Shalabi, Nesma M. Bayoumy, Eco-friendly synthesis, biological activity and evaluation of some new pyridopyrimidinone derivatives as corrosion inhibitors for API 5L X52 carbon steel in 5% sulfamic acid medium, J. Mol. Struct. 1171 (2018) 658–671, https://doi.org/10.1016/j.molstruc.2018.06.045.

[56] Zhe Zhang, Xiaodong Huang, Ningchen Tian, Fusong Ni, Le Ruan1, Yuzeng Lv, Ling Wu, Corrosion inhibition effect of histidine and its derivatives self-assembled films formed of 304 stainless steel, Int. J. Electrochem. Sci. 11 (2016) 9175–9191, https://doi.org/10.20964/2016.11.73.

[57] A.S. Fouda, G.Y. Elewady, K. Shalabi, H.K. Abdel-Aziz, Alcamines as corrosion inhibitors for reinforced steel and their effect on cement-based materials and mortar performance, RSC Adv. 5 (2015) 36957–36968, https://doi.org/10.1039/c5ra00717h.

[58] Z. Bikadi, E. Hazai, Application of the PM6 semi-empirical method to modeling proteins enhance docking accuracy of AutoDock, J Cheminform 1 (2009) 1–15, https://doi.org/10.1186/1758-2946-1-15.

[59] J.L. Banks, G.A. Kaminski, R. Zhou, D.T. Mainz, B.J. Berne, Parametrizing a polarizable force field from ab initio data. I. the fluctuating point charge model, J. Chem. Phys. 110 (2) (1999) 741–754, https://doi.org/10.1063/1.478043.

[60] G.M. Morris, D.S. Goodsell, Automated docking using a Lamarckian genetic algorithm and an empirical binding free energy function, J. Comput. Chem. 19 (1998) 1639–1662, https://doi.org/10.1002/(SICI)1096-987X(19981115)19:14.

[61] F.J. Solis, R.J.B. Wets, Minimization by random search techniques, Math. Oper. Res. 6 (1) (1981) 19–30, https://doi.org/10.1287/moor.6.1.19.

[62] Mahendra Yadav, Rajesh Ranjan Sinha, Tarun Kanti Sarkar, Nidhi Tiwari, Corrosion inhibition effect of pyrazole derivatives on mild steel in hydrochloric acid solution, J. Adhes. Sci. Technol. (2015)https://doi.org/10.1080/01694243.2015.1040979.

[63] L. Fragoza-Mar, O. Olivares-Xometl, M.A. Domínguez-Aguilar, E.A. Flores, P. Arellanes-Lozada, F. Jiménez-Cruz, Corrosion inhibitor activity of 1,3-diketone malonates for mild steel in aqueous hydrochloric acid solution, Corros. Sci. 61 (2012) 171–184, https://doi.org/10.1016/j.corsci.2012.04.031.

[64] A. Kumar, M. Trivedi, R.K. Sharma, G. Singh, Synthetic, spectral and structural studies of a Schiff base and its anticorrosive activity on mild steel in H_2SO_4, New J. Chem. 41 (2017) 8459–8468, https://doi.org/10.1039/c7nj00896a.

[65] A.S. Fouda, R.R. Fouad, New azonitrile derivatives as corrosion inhibitors for copper in nitric acid solution, Cogent Chemistry 2 (2016), 1221174. https://doi.org/10.1080/23312009.2016.1221174.

[66] Savita, Namrata Chaubey, Punita Mourya, V.K. Singh, M.M. Singh, Fruit extract as a green inhibitor for copper corrosion in nitric acid solution, International Journal of Innovative Research in Science, Engineering and Technology 4 (2015) 4545–4553, https://doi.org/10.15680/IJIRSET.2015.0406067.

[67] A. Zarrouk, B. Hammouti, A. Dafali, F. Bentiss, Inhibitive properties and adsorption of purpald as a corrosion inhibitor for copper in nitric acid medium, Ind. Eng. Chem. Res. 52 (2013) 2560–2568, https://doi.org/10.1021/ie301465k.

[68] A.S. Fouda, A.A. Badawy, Adsorption and corrosion inhibition of cu in nitric acid by expired simvastatin drug, Protection of metals and physical chemistry of surfaces 55 (2019) 572–582, https://doi.org/10.1134/S2070205119030146.

[69] H.S. Gadow, M.M. Motaweab, Investigation of the corrosion inhibition of carbon steel in hydrochloric acid solution by using ginger roots extract, RSC Adv. 7 (2017) 24576–24588, https://doi.org/10.1039/c6ra28636d.

[70] H. Bourazmi, M. Tabyaoui, L.E.L. Hattabi, Y. El Aoufir, E.E. Ebenso, A. Ansari, Camphor as an effective corrosion inhibitor for carbon steel in 1M HCl solution: electrochemical and quantum chemical investigation, J. Mater. Environ. Sci. 9 (3) (2018) 1058–1074, https://doi.org/10.26872/jmes.2017.9.3.118.

[71] M. Yadav, D. Behera, U. Sharma, Nontoxic corrosion inhibitors for N80 steel in hydrochloric acid, Arab. J. Chem. 9 (2016) S1487–S1495, https://doi.org/10.1016/j.arabjc.2012.03.011.

[72] Q.B. Zhang, Y.X. Hua, Corrosion inhibition of mild steel by alkyl imidazolium ionic liquids in hydrochloric acid, Electrochim. Acta 54 (2009) 1881–1887, https://doi.org/10.1016/j.electacta.2008.10.025.

[73] F. Krid, E. Zouaoui, M. Salah Medjram, Aqueous extracts of Opuntia ficus-indica as a green corrosion inhibitor of A283C carbon steel in sulfuric acid solution, Chem. Chem. Technol. 12 (3) (2018) 405–409https://doi.org/10.23939/chcht12.03.405.

[75] Roland Tolulope Loto, Richard Leramo, Babatunde Oyebade, Synergistic combination effect of Salvia officinalis and Lavandula officinalis on the corrosion inhibition of low-carbon steel in the presence of SO_4^{-2} and Cl^--containing aqueous environment, J Fail. Anal. and Preven. (2018) 1429–1438, https://doi.org/10.1007/s11668-018-0535-0.

[76] K.S. Ashish, M.A. Quraishi, Investigation of the effect of disulfiram on corrosion of mild steel in hydrochloric acid solution, Corrosion Sci 53 (4) (2011) 1288–1297, https://doi.org/10.1016/j.corsci.2011.01.002.

[77] Q. Qu, Z. Hao, L. Li, W. Bai, Y. Liu, Z. Ding, Synthesis and evaluation of Tris-hydroxymethyl-(2-hydroxybenzylidenamino)-methane as a corrosion inhibitor for cold rolled steel in hydrochloric acid, Corros. Sci. 51 (2009) 569–574, https://doi.org/10.1016/j.corsci.2008.12.010.

[78] M.A. Hegazy, H.M. Ahmed, A.S. El-Tabei, Investigation of the inhibitive effect of p-substituted 4-(N,N,N-dimethyl dodecyl ammonium bromide)benzylidene-benzene-2-yl-amine on corrosion of carbon steel pipelines in acidic medium, Corros. Sci. 53 (2011) 671, https://doi.org/10.1016/j.corsci.2010.10.004.

[79] R. Idouhli, A. N'Ait Ousidi, Y. Koumya, A. Abouelfida, A. Benyaich, A. Auhmani, and Moulay Youssef Ait Itto, Electrochemical studies of monoterpene thiosemicarbazones as corrosion inhibitor for steel in 1MHCl, International Journal of Corrosion 2018(2018), 9212705, doi:https://doi.org/10.1155/2018/9212705.

[80] F. El-Taib Heakal, M. A. Deyab, b M. M. Osman,b M. I. Nessimb and A. E. Elkholyb, Synthesis and assessment of new cationic gemini surfactants as inhibitors for

carbon steel corrosion in oilfield water, RSC Adv.,7(2017) 47335–47352, DOI: https://doi.org/10.1039/c7ra07176k.

[81] H.M. Abd El-Lateef, M.A. Abo-Riya, A.H. Tantawy, Empirical and quantum chemical studies on the corrosion inhibition performance of some novel synthesized cationic gemini surfactants on carbon steel pipelines in acid pickling processes, Corros. Sci. 108 (2016) 94–110, https://doi.org/10.1016/j.corsci.2016.03.004.

[82] M. Pourbaix, Atlas of Electrochemical Equilibria in Aqueous Solutions, NACE, Houstron, TX, 1975.

[83] H.E. Johnson, J. Leja, J. Electrochem. Soc. 112 (1956) 638.

[84] A.S. Foudaa, A.A. Badawya, Adsorption and corrosion inhibition of cu in nitric acid by expired simvastatin drug, Protection of Metals and Physical Chemistry of Surfaces 55 (2019) 572–582, https://doi.org/10.1134/S2070205119030146.

[85] F. Krid, E. Zouaoui, M. Salah Medjram, Aqueous extracts of Opuntia ficus-indica as a green corrosion inhibitor of A283C carbon steel in sulfuric acid solution, Chem. Chem. Technol. 12 (3) (2018) 405–409, https://doi.org/10.23939/chcht12.03.405.

[86] C. Kamal, M.G. Sethuraman, Caulerpin—a bis-indole alkaloid as a green inhibitor for the corrosion of mild steel in 1 M HCl solution from the marine alga Caulerpa racemose, Ind. Eng. Chem. Res. 51 (2012) 10399–10407, https://doi.org/10.1021/ie3010371.

[87] M.A. Amin, M.A. Ahmed, H.A. Arida, F. Kandemirli, M. Saracoglu, T. Arslan, M.A. Basaran, Monitoring corrosion and corrosion control of iron in HCl by non-ionic surfactants of the TRITON-X series – part III. Immersion time effects and theoretical studies, Corros. Sci. 53 (2011) 1895–1909, https://doi.org/10.1016/j.corsci.2011.02.007.

[88] G. Moretti, F. Guidi, F. Fabris, Corrosion inhibition of the mild steel in 0.5 M HCl by 2-butyl-hexahydropyrrolo[1,2-b][1,2]oxazole, Corros. Sci. 76 (2013) 206–218, https://doi.org/10.1016/j.corsci.2013.06.044.

[89] H. Hamani, T. Douadi, D. Daoud, M. Al-Noaimi, R.A. Rikkouh, S. Chafaa, 1-(4-Nitrophenyl-imino)-1-(phenylhydrazone)-propane-2-one as a corrosion inhibitor for mild steel in 1 M HCl solution: weight loss, electrochemical, thermodynamic and quantum chemical studies, J. Electroanal. Chem. 801 (2017) 425–438, https://doi.org/10.1016/j.jelechem.2017.08.031.

[90] Ismat H. Ali, Mohamed H.A. Suleiman, Effect of acid extract of leaves of Juniperus procera on corrosion inhibition of carbon steel in HCl solutions, Int. J. Electrochem. Sci. 13 (2018) 3910–3922, https://doi.org/10.20964/2018.04.01.

[91] A.M. Eldesoky, M.A. Diab, A.Z. El-Sonbati, S.F. Salam, Anti-corrosive properties of new eco-friendly dimethylamino compounds on C- steel corrosion in 2 M HCl, Int. J. Electrochem. Sci. 12 (2017) 4215–4237, https://doi.org/10.20964/2017.05.73.

[92] H.S. Gadow, M.M. Motawea, Investigation of the corrosion inhibition of carbon steel in hydrochloric acid solution by using ginger roots extract, RSC Adv. 7 (2017) 24576–24588, https://doi.org/10.1039/c6ra28636d.

[93] A.Y. Musa, A.A.H. Kadhum, A.B. Mohamad, M.S. Takriff, A.R. Daud, S.K. Kamarudin, Adsorption isotherm mechanism of amino organic compounds as mild steel corrosion inhibitors by electrochemical measurement method, J. Cent. S. Univ. Technol. 17 (2010) 34–39, https://doi.org/10.1007/s11771−010−0007−5.

[94] Y. Yan, W. Li, L. Cai, B. Hou, Electrochemical and quantum chemical study of purines as corrosion inhibitors for mild steel in 1 M HCl solution, Electrochim. Acta 53 (2008) 5953–5960, https://doi.org/10.1016/j.electacta.2008.03.065.

[95] Jie Chen, Yujie Qiang, Shini Peng, Zhili Gong, Shengtao Zhang, Lanzhou Gao, Bochuan Tan, Shijin Chen, Lei Guo, Experimental and computational investigations of 2-amino-6-bromobenzothiazole as a corrosion inhibitor for copper in sulfuric acid, J. Adhes. Sci. Technol. 32 (19) (2018) 2083–2098doi.org/10.1080/01694243.2018.1460948.

[96] D.D. Macdonald, M.C.H. Mckubre, Impedance measurements in electrochemical systems, in: J.O'M. Bockris, B.E. Conway, R.E. White (Eds.), Modern Aspects of Electrochemistry, vol. 14, Plenum Press, New York 1982, p. 61.

[97] S.M. Ali, H.A. Al Lehaibi, Control of zinc corrosion in acidic media: green fenugreek inhibitor, Trans. Nonferrous Met. Soc. China 26 (2016) 3034–3045, https://doi.org/10.1016/S1003-6326(16)64434-5.

[98] M. Galai, H. Benqlilou, M. Ebn Touhami, T. Belhaj, K. Berrami, H.El Kafssaoui, Comparative analysis for the corrosion susceptibility of copper alloys in sandy soil, Environ. Eng. Res. 23 (2) (2018) 164–174, https://doi.org/10.4491/eer.2017.077.

[99] M. Outirite, M. Lagrenee, M. Lebrini, M. Traisnel, C. Jama, H. Vezin, F. Bentiss, ac impedance, X-ray photoelectron spectroscopy and density functional theory studies of 3,5-bis(n-pyridyl)-1,2,4-oxadiazoles as efficient corrosion inhibitors for carbon steel surface in hydrochloric acid solution, Electrochim. Acta 55 (2010) 1670–1681, https://doi.org/10.1016/j.electacta.2009.10.048.

[100] P. Muthukrishnan, P. Prakash, B. Jeyaprabha, K. Shankar, Stigmasterol extracted from Ficus hispida leaves as a green inhibitor for the mild steel corrosion in 1M HCl solution, Arab. J. Chem. (2015)https://doi.org/10.1016/j.arabjc.2015.09.005.

[101] S. Mo, T. Ting Qin, H. Qun Luo, N.B. Li, Insights into the corrosion inhibition of copper in hydrochloric acid solution by self-assembled films of 4-octylphenol, RSC Adv. 5 (2015) 90542–90549, https://doi.org/10.1039/C5RA13074C.

[102] W. Chen, S. Hong, B. Xiang, H. Luo, M. Li, N. Li, Corrosion inhibition of copper in hydrochloric acid by coverage with trithiocyanuric acid self-assembled, monolayers, Corros. Eng. Sci. Technol. 48 (2) (2013) 98–107, https://doi.org/10.1179/1743278212Y.0000000053.

[103] H. Jwad Habeeb, H. Mohammed Luaibi, R. Mohammed Dakhil, H. Abdul Amir Kadhum, A. Ahmed Al-Amiery, T. Sumer Gaaz, Development of new corrosion inhibitor tested on mild steel supported by the electrochemical study, Results in Physics 8 (2018) 1260–1267, https://doi.org/10.1016/j.rinp.2018.02.015.

[104] P. Preethi Kumari, Prakash Shetty Suma A. Rao, Electrochemical measurements for the corrosion inhibition of mild steel in 1 M hydrochloric acid by using an aromatic hydrazide derivative, Arab. J. Chem. 10 (2017) 653–663, https://doi.org/10.1016/j.arabjc.2014.09.005.

[105] H.S. Gadow, M.M. Motawea, Investigation of the corrosion inhibition of carbon steel in hydrochloric acid solution by using ginger roots extract, RSC Adv. 7 (2017) 24576–24588, https://doi.org/10.1039/c6ra28636d.

[106] Enrico Volpi, Cristian Foiadelli, Stefano Trasatti, Dessi Koleva, Development of smart corrosion inhibitors for reinforced concrete structures exposed to a microbial environment, Ind. Eng. Chem. Res. 56 (20) (2017) 5778–5794, https://doi.org/10.1021/acs.iecr.7b00127.

[107] Ismat H. Ali, Mohamed H.A. Suleiman, Effect of acid extract of leaves of Juniperus procera on corrosion inhibition of carbon steel in HCl solutions, Int. J. Electrochem. Sci. 13 (2018) 3910–3922, https://doi.org/10.20964/2018.04.01.

[108] N. Idusuyi, O.O. Ajide, O.O. Oluwole, O.A. Arotiba, Electrochemical impedance study of an Al6063-12%SiC-Cr composite immersed in 3 wt. % sodium chloride, Procedia Manufacturing 7 (2017) 413–419, https://doi.org/10.1016/j.promfg.2016.12.019.

[109] R. Mohan, A. Joseph, Corrosion protection of mild steel in hydrochloric acid up to 313 K using propyl benzimidazole: electroanalytical, adsorption and quantum chemical studies, Egypt. J. Pet. 27 (1) (2018) 11–20, https://doi.org/10.1016/j.ejpe.2016.12.003.

[110] M. Benabdellah, A. Tounsi, K.F. Khaled, B. Hammouti, Thermodynamic, chemical and electrochemical investigations of 2-mercapto benzimidazole as a corrosion inhibitor for mild steel in hydrochloric acid solutions, Arab. J. Chem. 4 (2011) 17–24, https://doi.org/10.1016/j.arabjc.2010.06.010.

[111] Guo Wenjuan, Chen Shenhao, Ma Houyi, A study of the inhibition of copper corrosion by triethyl phosphate and triphenyl phosphate self-assembled monolayers, Serb. Chem. Soc. 71 (2) (2006) 167–175, https://doi.org/10.2298/JSC0602167G.

[112] M.A. Amin, G.A.M. Mersal, Q. Mohsen, Monitoring corrosion and corrosion control of low alloy ASTM A213 grade T22 boiler steel in HCl solutions, Arab. J. Chem. 4 (2) (2011) 223–229, https://doi.org/10.1016/j.arabjc.2010.06.040.

[113] K. Shalabi, Y.M. Abdallah, A.S. Fouda, Corrosion inhibition of aluminum in 0.5 M HCl solutions containing phenyl sulfonylacetophenoneazo derivatives, Res. Chem. Intermed. 41 (2015) 4687–4711, https://doi.org/10.1007/s11164-014-1561-5.

[114] A.S. Fouda, A.A. Nazeer, A. Saber, Electrochemical adsorption properties and inhibition of zinc corrosion by two chromones in sulfuric acid solutions, J. Korean Chem. Soc. 58 (2014) 160–168, https://doi.org/10.5012/jkcs.2014.58.2.160.

[115] M.N. El-Haddad, Inhibitive action and adsorption behavior of cefotaxime drug at the copper/hydrochloric acid interface: electrochemical, surface and quantum chemical studies, RSC Adv. 6 (2016) 57844–57853, https://doi.org/10.1039/c6ra03316d.

[116] M.N. EL-Haddad, A.S. Fouda, Corrosion inhibition and adsorption behavior of some azo dye derivatives on carbon steel in acidic medium: synergistic effect of halide, Chem. Eng. Commun. 200 (2013) 1366–1393, https://doi.org/10.1080/00986445.2012.746675.

[117] R.W. Bosch, W.F. Bogaerts, B. Syrett, Proc. 8th International Symposium on Electrochemical Methods in Corrosion Research Modulation (EFM) Technique, Nieuwpoort, Belgium, 4–9 May 2003.

[118] A.S. Fouda, K. Shalabi, A.A. Idress, Ceratonia siliqua extract as a green corrosion inhibitor for copper and brass in nitric acid solutions, Green Chemistry Letters and Reviews 8 (2015) 17–29, https://doi.org/10.1080/17518253.2015.1073797.

[119] M.N. El-Haddad, Inhibitive action and adsorption behavior of cefotaxime drug at the copper/hydrochloric acid interface: electrochemical, surface and quantum chemical studies, RSC Adv. 6 (2016) 57844–57853, https://doi.org/10.1039/C6RA13117D.

[120] A.de Mendonça Santos, T. Felix de Almeida, F. Cutting, Idalina V. Aoki, H. Gomes de Melo, V. Rosa Capelossi, Evaluation of castor bark powder as a corrosion inhibitor for carbon steel in acidic media, Mater. Res. 20 (2017) 492–505, https://doi.org/10.1590/1980-5373-MR-2016-0963 Suppl. 2.

[121] R. Idouhli, A. N'Ait Outside, Y. Koumya, A. Abouelfida, A. Benyaich, A. Auhmani, Moulay Youssef Ait Itto, Electrochemical studies of monoterpenic thiosemicarbazones as corrosion inhibitor for steel in 1MHCl, International Journal of Corrosion 2018 (2018)https://doi.org/10.1155/2018/9212705.

[123] A.K. Satapathy, G. Gunasekaran, S.C. Sahoo Kumar, A.P.V. Rodrigues, Corrosion inhibition by Justicia gendarussa plant extract in hydrochloric acid solution, Corros. Sci. 51 (2009) 2848–2856, https://doi.org/10.1016/j.corsci.2009.08.016.

[124] E.E. Ebenso, T. Arslan, F. Kandemirli, N. Caner, I. Love, Int. J. Quant. Chem. 110 (2010) 1003–1018, https://doi.org/10.1002/qua.22249.

[125] M. Ozcan, I. Dehri, M. Erbil, Organic sulfur-containing compounds as corrosion inhibitors for mild steel in acidic media: correlation between inhibition efficiency and chemical structure, Appl. Surf. Sci. 236 (2004) 155–164, https://doi.org/10.1016/j.apsusc.2004.04.017.

[126] B.D. Mert, M.E. Mert, M.E. Kardas, G. Yazici, Experimental and theoretical investigation of 3-amino-1, 2, 4-triazole-5-thiol as a corrosion inhibitor for carbon steel in HCl medium, Corros. Sci. 53 (2011) 4265–4272, https://doi.org/10.1016/j.corsci.2011.08.038.

[127] J.M. Roque, T. Pandiyan, J. Cruz, E. Garcl0a-Ochoa, DFT and electrochemical studies of tris (benzimidazole-2-ylmethyl)amine as an effective corrosion inhibitor for carbon steel surface, Corros. Sci. 50 (2008) 614–624, https://doi.org/10.1016/j.corsci.2007.11.012.

[128] G. Gece, The use of quantum chemical methods in corrosion inhibitor studies, Corros. Sci. 50 (2008) 2981, https://doi.org/10.1016/j.corsci.2008.08.043.

[129] A.Y. Musa, A.H. Kadhum, A.B. Mohamad, M.S. Takriff, Experimental and theoretical study on the inhibition performance of triazole compounds for mild steel corrosion, Corros. Sci. 52 (2010) 3331, https://doi.org/10.1016/j.corsci.2010.06.002.

[130] I. Lukovits, E. Lalman, F. Zucchi, Corrosion inhibitors—correlation between electronic structure and efficiency, Corrosion 57 (2001) 3–8, https://doi.org/10.5006/1.3290328.

[131] J.M. Roque, T. Pandiyan, J. Cruz, E. Garcl'a-Ochoa, DFT and electrochemical studies of tris(benzimidazole-2-ylmethyl)amine as an effective corrosion inhibitor for carbon steel surface, Corrosion Sci 50 (2008) 614e624.

[132] V. Cerny, Thermodynamical approach to the traveling salesman problem: an efficient simulation algorithm, J. Optim. Theor. Appl. 45 (1985) 41e51.

[133] A.Z. El-Sonbati, G.G. Mohamed, A.A. El-Bindary, W.M.I. Hassan, M.A. Diab, Sh.M. Morgan, A.K. Elkholy, Supramolecular structure, molecular docking and thermal properties of azo dye complexes, J. Mol. Liq. 212 (2015) 487–502, https://doi.org/10.1016/j.molliq.2015.09.038.

[134] M.A. Diab, A.Z. El-Sonbati, A.A. El-Bindary, Sh.M. Morgan, M.K. Abd El-Kader, Geometrical structures, molecular docking, spectroscopic characterization of mixed ligand and Schiff base metal complexes, J. Mol. Liq. 218 (2016) 571–585, https://doi.org/10.1016/j.molliq.2016.01.102.

[135] A.A. El-Bindary, G.G. Mohamed, A.Z. El-Sonbati, M.A. Diab, W.M.I. Hassan, Sh.M. Morgan, A.K. Elkholy, Geometrical structure, potentiometric, molecular docking and thermodynamic studies of azo dye ligand and its metal complexes, J. Mol. Liq. 218 (2016) 138–149, https://doi.org/10.1016/j.molliq.2016.02.021.

[136] A.S. Fouda, K. Shalabi, A.A. Idress, Ceratonia siliqua extract as a green corrosion inhibitor for copper and brass in nitric acid solutions, Green Chemistry Letters and Reviews 8 (2015) 17–29, https://doi.org/10.1080/17518253.2015.1073797.

[137] H.J. Habeeb, H.M. Luaibi, R.M. Dakhil, A.A.H. Kadhum, A.A. Al-Amiery, T.S. Gaaz, Development of new corrosion inhibitor tested on mild steel supported by the electrochemical study, Results in Physics 8 (2018) 1260–1267, https://doi.org/10.1016/j.rinp.2018.02.015.

[138] Zarrouk, B. Hammouti, H. Zarrok, M. Bouachrine, K.F. Khaled, S.S. Al-Deyab, Corrosion inhibition of copper in nitric acid solutions using a new triazole derivative, Int. J. Electrochem. Sci. 7 (2012) 89–105.

[139] B. Tan, S. Zhang, H. Liu, Y. Qiang, W. Li, L. Guo, S. Chen, Insights into the inhibition mechanism of three 5-phenyltetrazole derivatives for copper corrosion in sulfuric acid medium via experimental and DFT methods, J. Taiwan Inst. Chem. Eng.. doi: https://doi.org/10.1016/j.jtice.2019.06.005.

[140] G. Karthik, M. Sundaravadivelu, Investigations of the inhibition of copper corrosion in nitric acid solutions by levetiracetam drug, Egypt. J. Pet. 25 (2016) 481–493, https://doi.org/10.1016/j.ejpe.2015.10.009.

[141] A.S. Fouda, M.A. Ismael, R.M. Abo Shahba, L.A. Kamel, A.A. El-Nagggar, Corrosion inhibition of copper and α-Brass in 1 M HNO3 solution using new arylpyrimido [5, 4-c] quinoline-2,4-dione derivative, Int. J. Electrochem. Sci. 12 (2017) 3361–3384, https://doi.org/10.20964/2017.04.57.

Further reading [74] Roland Tolulope Loto, Oluwatobilola Olowoyo, Corrosion inhibition properties of the combined admixture of essential oil extracts on mild steel in the presence of SO42− anions, South African Journal of Chemical Engineering 26 (2018) 35–41, https://doi.org/10.1016/j.sajce.2018.09.002.

[122] D.A. Lopez, S.N. Simison, S.R. de Sanchez, Inhibitors performance in CO2 corrosion EIS studies on the interaction between their molecular structure and steel microstructure, Corros. Sci. 47 (2005) 735–755, https://doi.org/10.1016/j.corsci.2004.07.010.

Evaluation of petroleum hydrocarbons and its impact on organic matters of living organisms in the northwestern Gulf of Suez, Egypt

Omayma E. Ahmed, Ahmed M. Eldesoky & Mohamed M. El Nady

Taylor & Francis
Taylor & Francis Group

Check for updates

Evaluation of petroleum hydrocarbons and its impact on organic matters of living organisms in the northwestern Gulf of Suez, Egypt

Omayma E. Ahmed[a], Ahmed M. Eldesoky[b], and Mohamed M. El Nady[a]

[a]Egyptian Petroleum Research Institute, Nasr City, Egypt; [b]Engineering Chemistry Department, High Institute of Engineering &Technology (New Damietta), Egypt and Al-Qunfudah Center for Scientific Research (QCSR), Chemistry Department, Al-Qunfudah University College, Umm Al-Qura University, Mecca, Saudi Arabia

ABSTRACT

The levels of Total Petroleum Hydrocarbons (TPH) have been reported for ten commercially important fish species from the northwestern Gulf of Suez, Egypt. Target compounds were analytically determined with gas chromatography–flame ionization detector and High-performance liquid chromatography analysis. Results showed that total petroleum hydrocarbon varied from 21700 to 1503100 ng/g wet wt., *Argyrops Spinifer* showed the highest level of TPH in the muscle tissue followed by *Euthynnus affinis* 1459800 ng/g wet wt. These data are very important for coming pollution monitoring program to the Suez Gulf. Polycyclic aromatic hydrocarbons (16 PAHs) varied between 81.499 and 5895.608 ng/g wet wt. The diagnostic indices used showed that the hydrocarbons in the area were from both biogenic and anthropogenic sources. Hence, there is need for adequate regulation and control of all activities contributing to the levels of petroleum hydrocarbon in the marine environment for the safety of human, and fish species lives in the area.

1. Introduction

The problem of oil pollution in various marine and estuarine environments has received considerable scientific attention with respect to the effects of petroleum spills, as well as inherent toxicities to specific biological ecosystem components and individual species. Petroleum products are carcinogens and affect a variety of biological processes and potent cell mutagens (Veerasingam et al. 2011).Total Petroleum Hydrocarbon (TPH) is environmental contaminants that are released into the marine environment through oil spills, industrial and domestic activities. The Suez Gulf economy depends heavily on the oil sector where majority of the oil industries are located in the northwestern area. Gulf fishing communities are adversely affected by petroleum production activities. Oil spillage and petroleum products are the major anthropogenic source of total hydrocarbon in the northwestern Gulf of Suez, Egypt. (Renee & Roushdie 2016) declared that oil pollutants related into the marine environment may stimulate adverse effects in man and other organisms. Polycyclic aromatic hydrocarbons (PAHs) a group of compounds consisting of two or more fused aromatic rings, are of special concern because they are widely distributed in the environment and many of them have toxic and carcinogenic properties (Omayma, Sawsan, & El Nady

Table 1. General characteristics and morphometric data of living organisms, Northwestern Gulf of Suez, Egypt.

Sites	Scientific name	Fish species	Feeding habits (Main food)	Habitat type (Environment)
AL- Nasr Oil Company (NPC)	*Sauridaundo squamis*	Brushtooth lizard fish	Carnivore (small fish)	Demersal, (benthic)
Outlet of Suez Oil Petroleum Company (SOPC)	*Euthynnus affinis*	Kawakawa	Feeds on small fish, squids, and sometimes zooplankton (Omnivore)	found in open waters but always close to the shoreline
Old Al-Kabanon	*Rhabdosargus haffara*	Haffara sea bream	Feeds on benthic invertebrates. Consumed fresh. (Predator)	Inhabits shallow waters, mainly around coral reefs, and over sandy bottoms
New Al-Kabanon	*Argyrops spinifer*	Porgies	Feeds on benthic invertebrates, mainly mollusks, important food fish. (Predator)	Young fish occur in very shallow waters of sheltered bays; larger individuals in deeper water
Inlet of Suez Oil Petroleum Company (SOPC)	*Nemipterus japonicus*	Japanese threadfin bream	Carnivore on small fish, invertebrate's polychates. (Predator)	Demersal
Atakah Harbor	*Oreochromis niloticus*	Nile Tilapia	Herbivorous ,feed on phytoplankton (Omnivore)	benthic and pelagic due to air bladder
Adabiya Harbor	*Trachurus indicus*	Horse Mackerel	Carnivore (invertebrates and fish) (Predator)	Pelagic
Suez Beach	*Peneus japonicas*	Red mullets	Prey of small fish and crustaceans. (Predator)	Inhabit the inshore area and coral reefs, found on a range of sea including sand, mud and coarse gravel
El- Sukhna of Loloha Beach	*Scomber japonicus*	Chub mackerel, Pacific mackerel or blue mackerel	feed on copepods and other crustacean, fishes and squids (Predator)	A coastal pelagic species, to a lesser extent epipelagic to mesopelagic over the continental slope
Beach of oil pipeline	*Pomadasys stridens*	Striped piggy	Feeding on a variety of crustaceans, mollusks and small juvenile fishes, called a predator (Predator)	Living in the reef environment and sandy

2017, 2018). The accidental discharge of hazardous materials such as petroleum and chemical solvents to the aquatic environment has become the focus of increasing regulatory and public concern because of the adverse impacts of such materials on human health and the environment (Al-Shawafi 2008). TPH is released to the environment through accidents, as releases from industries, or as by products from commercial or private uses. When TPH is released directly to water through spills or leaks, certain TPH fractions will float in water and form thin surface films. Other heavier fractions will accumulate in the sediment at the bottom of the water which may affect bottom feeding behavior of fish and organisms (Enuneku et al. 2015).

2. Materials and methods

Ten fish species were collected from the coastal waters of the Suez Gulf (Table 1) by using cast or throw fishing net by using cast or throw fishing net. They were first identified, and numbers of individual fish species, total lengths (cm) and the body-wet weights (g) of each fish specimens were measured, labeled, stored in ice at −20 °C length and weight of the fishes were determined and placed immediately in polyethylene bags, put into isolated container of polystyrene ice box and, then, brought to the laboratory.

1. About 20 g of fish sample muscles was treated with 100 ml methanol and 3 g. KOH. The methanolic phase was extracted twice with n-hexane, dried over un-hydrous sodium sulfate. The extract was air dried to constant weight.
2. The oil content was calculated as: ng/g = (A-B) x10^9/Wt g. of sample, where: A& B are the weight of bottle after and before action.
3. Hydrocarbons were extracted by direct saponification via alkaline hydrolysis from fish samples were analyzed according to the standard test method (IP318/75 1993) and subjected to capillary GC, the instrument used was Agilent Technologies 7890 gas chromatograph system, equipped with flame ionization detector (FID). Oven temperature was programed from 100 °C to 300 °C at fixed rate of 3 °C min − 1 and HP-1 fused silica capillary column (60 m × 0.53 mm × 0.5 μm)
4. PAH identification and quantification in the extracted oil was performed using HPLC technique. The apparatus used was water HPLC 600, Auto Sampler 616 Plus, Dual Absorbance Detector 2487, attached to a computerized system with Millennium 32 Software.

3. Results and discussion

3.1. Total petroleum hydrocarbon

Total Petroleum hydrocarbon concentration (TPHC) residues in ten fish species (Figure 1a) varied between 21700 and 1503100, with mean value 1015860 ng/g wet weight. Among the ten fish species *Argyrops Spinifer* has a high PHC concentration 1503100 ng/g weight, while the lowest concentration found in *Sauridaundo squami*s 21700 ng/g wet weight, the concentration arranged as fellow: *Argyrops Spinifer> Pomadasys Stridens > Euthynnus affinis> Scomber Japonicus > Peneus Japonicas> Nemipterus Japonicu> Oreochromis Niloticus> Trachurus Indicus> Rhabdosargus haffara> Sauridaundo squami*s. This due to different lipid contents, feeding habit, temperature, size, age and sex of fishes (Al-Shawafi 2008). This study suggests that *Argyrops Spinifer* can be used as a good biological indicator for petroleum hydrocarbon pollution in water. Higher TPH concentration in the muscle of the fish may also reflect differences in the marine habitat, feeding habits and the different depths in which they live in the marine environment. This showed strong positive evidence that ability of fish to accumulate hydrocarbons in their tissues is directly related to lipid content and body weight (Veerasingam et al. 2011). *Argyrops Spinifer* fasting when enters Suez Gulf and they feed mainly on feeds on benthic invertebrates, mainly mollusks, important food fish (Omayma, Eldesoky, & El Nady 2019). There are significant correlation between lipid contents, body weight, and body length, which indicate that ability of fish to accumulate hydrocarbons in their tissues is directly related to lipid content and body weight, the same conclusion have been observed by (Jazza, Al-Adhub, & Al-Saad 2015).

3.2. Concentrations of n-alkanes

Concentration of total *n*-alkanes in marine organisms of Suez Gulf, Egypt ranged from 11.391to 96.747, with mean value 60.755 ng/g wet weight (Table 2). High concentration values for nC_{17}, nC_{19}, and nC_{21} and nC_{31} compared with the other alkanes in most of the studied samples. This may be attributed to the selective absorption through the fish tissues. Fish species are affected greatly by waves, tides and winds whereby they may be carried from place to place; as a result these samples probably not reflect the degree of oil pollution in the collected site. Generally the sample may through light on the oil contaminating our shores; in general ten different types of fishes were chosen for such studies in the Suez Gulf. The gas Chromatograms pattern peaks mainly contains *n*-alkanes from nC_{15} to nC_{37}, the striking features of these profiles show the predominance of odd carbon numbers nC_{17}, nC_{19}, and nC_{21} (Omayma et al. 2014). Also, predominance in the higher rang nC_{31} for *Trachurus Indicu*s as example of GC analysis (Figure 1b) consists of *n*- alkanes from nC_{15}
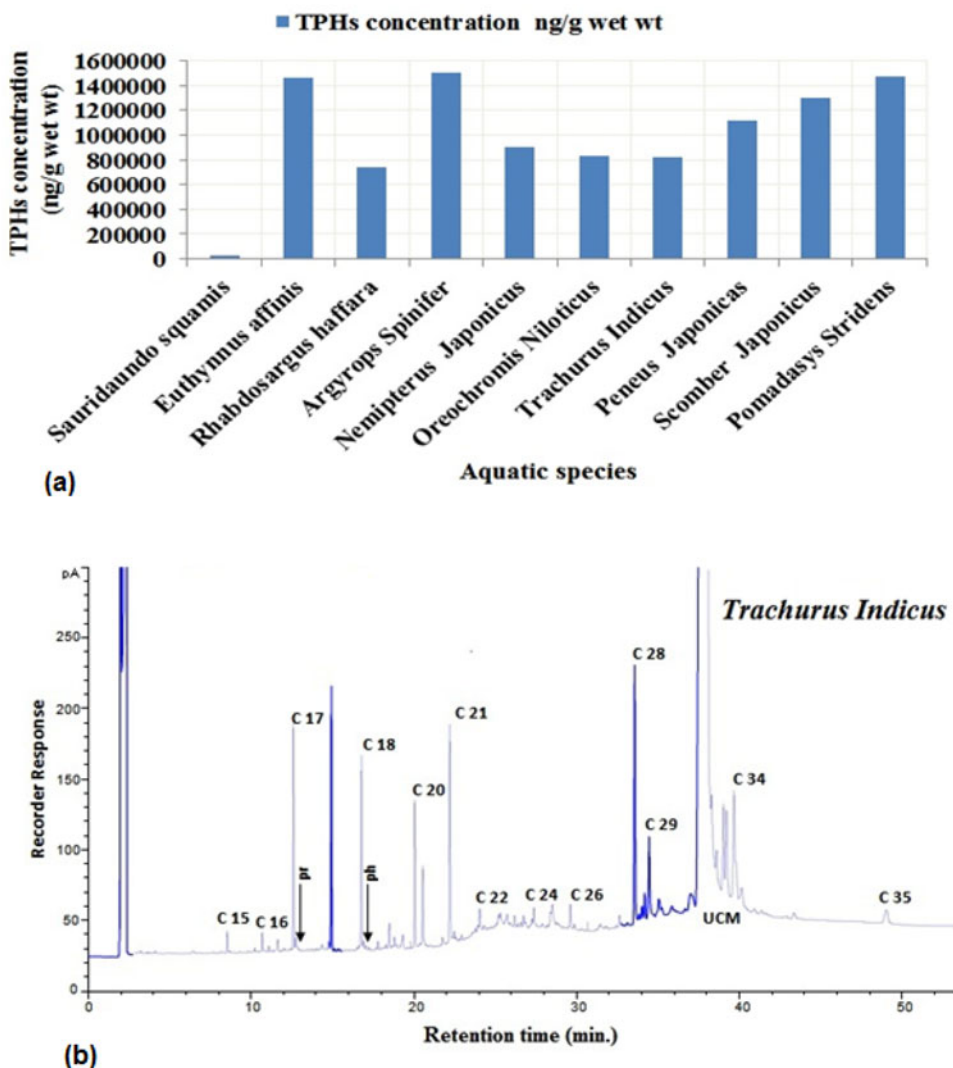
Figure 1. Histogram (a) representing total petroleum hydrocarbon concentration (TPHs) ng/g wet wt., (b) Gas chromatograms for oils extracted from Trachurus Indicus as example of GC analysis in living organisms, Northwestern Gulf of Suez, Egypt.

Table 2. N-alkanes concentrations in the collected living organisms, Northwestern Gulf of Suez, Egypt.

S0 No.	1	2	3	4	5	6	7	8	9	10
Σn-alkanes	29.721	73.513	96.747	11.391	42.253	92.866	35.941	47.051	93.051	85.020
L	1.4894	1.4166	2.3522	1.4078	0.7092	3.4152	3.3321	0.7992	3.28893	1.9815
H	28.267	72.097	94.3944	9.9830	44.6967	89.4506	64.6202	46.2196	89.7618	83.0386
L/H	0.053	0.0196	0.0249	0.1410	0.0159	0.0382	0.0516	0.0173	0.0366	0.0239
UCM	8878.2	805.923	4835.3	1833.153	75040	10095.4	10737	61165.4	46521.1	1215.217
CPI	1.843	5.432	9.725	13.780	20.380	17.644	9.996	16.411	12.159	5.0714
CPI*	0.385	5.065	9.715	13.757	11.936	17.573	9.983	16.252	12.158	4.485
C_{31}/C_{19}	88.969	62.314	328.762	70.742	389.510	762.246	411.450	126.735	700.883	78.060

Σn-alkanes: normal alkanes concentration, L: Low Molecular Weight, H: High Molecular Weight n-Alkane, L/H: Low Molecular Weight/High Molecular Weight n-Alkanes, UCM: un-resolved complexes mixture, CPI: Carbon preference index, CPI*= CPI value without the (n-C25 or n-C23) peak value.

1. AL- Nasr Oil Company (NPC), 2. Outlet of Suez Oil Petroleum Company (SOPC), 3. Old Al-Kabanon, 4. New Al-Kabanon, 5. Inlet of Suez Oil Petroleum Company (SOPC), 6. Atakah Harbor. 7. Adabiya Harbor, 8. Suez Beach, 9. El- Sukhna of Loloha Beach, 10. Beach of oil pipeline.

to $n\mathrm{C}_{36}$. Pristane and phytane may appear as resolved peaks or minor peaks. Generally, all Chromatograms show a mixed biogenic and petrogenic hydrocarbon profiles. Many ratios and indexes, which relate to the hydrocarbon concentration or even UCM, are employed to differentiate between biogenic and anthropogenic sources of hydrocarbons in this area.

3.3.1. Low molecular weight/high molecular weight n-alkanes (L/H)

Ratio of low molecular weight n-alkanes (C_{15}–C_{20}) to high molecular weight n-alkanes (C_{21}–C_{34}) is another marker being used for the determination of n-alkanes sources (Fagbote & Olanipekun 2013). Low molecular weight hydrocarbon usually dominates in a fresh oil release, giving a ratio greater than one. L/H is an indicator of the freshness of the hydrocarbons released into the environments. However, fast degradation of these lower molecules in crude oil can decrease the ratio significantly to a value below unity. The L/H ratio below 1 (unity) reveals natural input from marine and terrestrial biogenic sources, and ratios around and above (1) indicate hydrocarbons from petroleum sources (Wang et al. 2006). The results obtained from fish species showed the L/H ratios lower than one (1) in the all species indicating hydrocarbons from natural sources (Zakaria et al. 2002). However, the results of the L/H ratios greater than one (1), indicating fresh release of petroleum hydrocarbons from agricultural, residential, and/or industrial activities that entered the estuary through rivers and streams in the watershed.

3.3.2. Unresolved complex mixture (UCM)

The UCM is considered a mixture of branched and cyclic hydrocarbon structures, including many of their structurally complex isomers which are un-resolvable by the capillary columns of gas chromatograph (Wang et al. 2006). The aliphatic hydrocarbons are less soluble than the aromatic compounds which are relatively more mobile in water. The branched aliphatics are even less water-soluble than the straight-chained alkanes. Hence, they concentrate more in the sediment compared to the water column (Wang et al. 2006). Although UCMs are mostly present in the higher molecular range of the hydrocarbons, few exist in the lower range as well. Figure 2a revealed the presence of UCM in most of fish species analyzed appearing as a unimodal or sometimes as a bimodal hump in the range of $n\mathrm{C}_{15}$ to $n\mathrm{C}_{17}$ and $n\mathrm{C}_{22}$ to $n\mathrm{C}_{35}$. The UCM concentrations varied between 4835.3 and 75040 ng/g wet weight. The presence of UCM in the aliphatic fraction is considered as the most important indicator of petrogenic pollution, while the narrow UCM humps for some species of the GC-FID chromatograms indicates that dissolved petroleum oil are adsorbed in the tissues and not due to adhering of oil on the skin or gills (Omayma et al. 2014).

3.3.3. Carbon preference index (CPI)

Petroleum oils are characterized by CPI values around 1.0 (Medeiros & Bícego 2004). Thus CPI data (Table 2) of fish samples range from 1.483 to 61.026, which reveal a biogenic contamination origin. The presence of high concentrations of n-paraffin (n-C_{25} or n-C_{23}) cause confusion given an indication of the biogenic origin. Thus the CPI values were calculated again without taking in consideration the values of (n-C_{23}) peak areas. The results show that the CPI* corrected values are ranging from 1.483 up to 60.865. This indicate that the biogenic origin is mainly predominating while little petrogenic contamination can be detected specially that of (n-C_{23}) (Elfadly, Omayma, & El Nady 2016).

3.3.4. C_{31}/C_{19}

This is another important ratio used to differentiate the sources of n-alkanes in marine organisms. The presence of $n\mathrm{C}_{31}$ is an indication of terrestrial biogenic hydrocarbons, whereas $n\mathrm{C}_{19}$
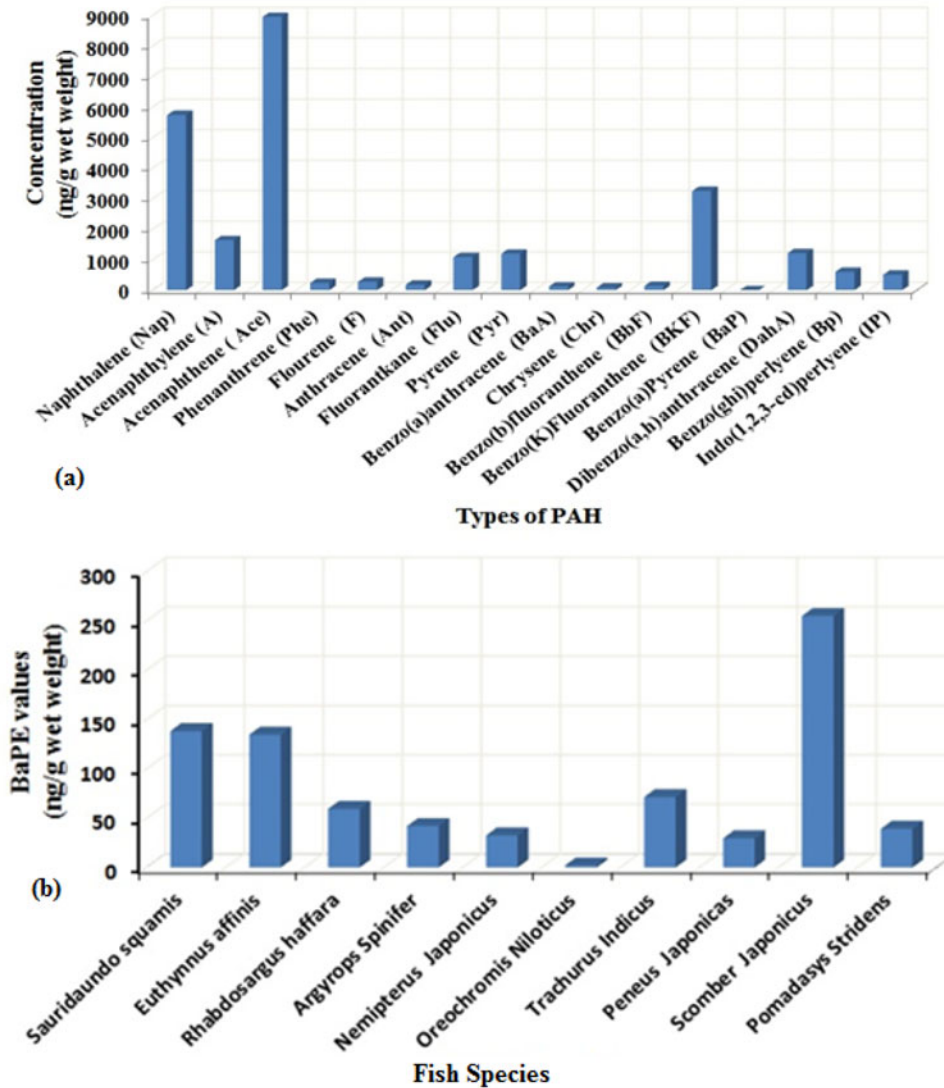
Figure 2. (a)Variation of types of PAH concentrations (ng/g wet weight), (b) BaPE values ng/g wet wt in the collected living organisms, Northwestern Gulf of Suez, Egypt.

suggests marine biogenic inputs. The C_{31}/C_{19} ratio is therefore used to assess the dominance of n-alkanes from either of the two sources. While ratio below 0.4 reveals marines sources, any value above 0.4 is an indication of land derived or non-marine hydrocarbons (Fagbote & Olanipekun 2013). All fish species had nC_{31}; gave higher values than 0.4 (Table 2) which is indicative of hydrocarbons mainly from anthropogenic origins.

4. Distribution pattern of polycyclic aromatic hydrocarbons (PAHs)

PAH distribution patterns in tissue samples (Figure 2b) show variation of types of PAH concentrations (ng/g wet weight) in the marine organisms muscles along the Suez Gulf. Acenaphthene (Ace) is the most abundant PAH in the aquatic species 8948.191 ng/g dry wt., followed by Naphthalene (Nap) 5737.027 ng/g wet weights, Benzo(K) Fluoranthene(BKF) 3245.816 ng/g wet wt. and Pyrene (Pyr) 1195.535 ng/g wet wt. Chrysene concentration is elevated at New Al-

Table 3. Concentration of individual PAHs ng/g wet wt., in the oil extracted from marine organisms muscles along the Suez Gulf.

	1	2	3	4	5	6	7	8	9	10
Naphthalene (Nap).	1493.244	0.0	1045.162	2060.756	10.555	0.0	1127.310	0.0	0.0	0.0
Acenaphthylene (A.)	401.046	279.120	175.435	431.046	352.039	0.0	0.0	0.0	0.0	0.0
Acenaphthene (Ace.)	1589.435	1752.503	2032.565	2084.697	527.6998	0.0	0.0	0.0	0.0	961.293
Phenanthrene (Phe.)	59.443	56.250	43.513	42.777	12.666	13.314	0.0	0.0	11.456	0.0
Flourene (F.)	49.052	3.800	39.631	0.0	60.497	1.701	92.626	3.710	9.632	15.184
Anthracene (Ant).	44.038	16.517	7.586	16.453	93.708	0.0	0.0	0.0	0.0	0.0
Fluorantkane (Flu.)	63.697	77.332	218.595	677.086	49.636	0.0	0.0	0.0	0.0	0.0
Pyrene (Pyr.)	53.081	670.942	137.369	111.297	45.192	38.198	102.970	6.039	30.447	0.0
Benzo (a) anthracene (BaA)	8.001	14.186	0.229	62.425	4.153	4.762	9.287	2.626	1.194	15.478
Chrysene (Chr.)	28.902	6.834	9.238	32.229	4.933	0.0	4.758	0.0	0.0	0.0
Benzo(b) fluoranthene(Bbf)	9.191	20.441	53.459	13.709	25.591	0.0	14.515	0.0	0.0	3.541
Benzo (K) Fluoranthene (Bkf)	1843.138	0.0	0.0	0.0	0.0	0.0	977.388	0.0	0.0	425.290
Benzo (a)Pyrene (Bap)	0.0	0.0	0.0	0.0	0.0	0.0	0.0	0.0	0.0	0.0
Dibenzo (a,h)anthracene(DahA)	0.0	167.467	87.261	56.497	44.031	0.0	0.0	437.512	419.088	0.0
Benzo (ghi) perylene (Bp)	22.430	108.721	25.067	262.979	129.266	0.0	0.0	51.484	0.0	0.0
Indo(1,2,3- cd) perylene (Ip)	101.624	37.485	42.046	43.657	51.055	23.524	17.476	39.762	44.095	103.900
Total PAHs	5766.322	3211.599	3917.156	5895.608	1411.019	81.499	2346.330	541.134	515.910	5766.322
BaPE values (ng/g wet wt.)	138.273	134.668	59.476	42.096	32.544	2.168	71.389	29.589	255.052	39.259
TEQcarc	196.224	174.684	96.844	68.511	52.116	0.711	101.871	441.751	423.975	68.751

BaPE: The BaP equivalent (BaPE) was used to quantitatively assess the PAHs, TEQcarc: Toxic equivalents (TEQs) of seven carcinogenic PAHs.

1. AL- Nasr Oil Company (NPC), 2. Outlet of Suez Oil Petroleum Company (SOPC), 3. Old Al-Kabanon, 4. New Al-Kabanon, 5. Inlet of Suez Oil Petroleum Company (SOPC), 6. Atakah Harbor. 7. Adabiya Harbor, 8. Suez Beach, 9. El- Sukhna of Loloha Beach, 10. Beach of oil pipeline.

Kabanon 32.229 ng/g wet wt, AL- Nasr Oil Company (NPC) (28.902 ng/g wet wt., Old Al-Kabanon 9.238 ng/g wet wt., and Outlet of Suez Oil Petroleum Company (SOPC) 6.834 ng/g wet wt. (Table 3) which may be attributed to small past oil spill near these locations (Stogiannidis & Laane 2015). As reported further degradation of oil spill leads to the enhancement of the chrysene concentration relative to other PAH series, and to a significant decrease in the relative ratios of the sum of naphthalenes, phenanthrenes, dibenzothiophenes, and fluorenes, to chrysenes. Car-PAHs [benzo(a)anthracene, chrysene, benzo (a) pyrene, benzo (b) fluoranthene, benzo (k) fluoranthene, dibenzo (a,h) anthracene, benzo (g,h,i) perylene, and indeno (1,2,3-cd) pyrene] (Table 3) are eight PAHs typically considered as possible carcinogens. Benzo (a) pyrene is the highly carcinogenic PAH (Omayma, Eldesoky, & El Nady 2019). Among factors affecting the uptake of PAHs, bioavailability is important through regulation of the absorption and sequestration of PAHs into the organisms from the surrounding environment. PAH bioavailability is controlled by the partition coefficient (Kow) and the molecular weight (Snyder et al. 2015).

Conclusions

1. Total petroleum hydrocarbon concentration (TPHC) residues in ten fish species varied between 21700 ng/g wet weight, in *Sauridaundo squamis* and reached1459800 ng/g wet weight in *Euthynnus affinis*, while in *Argyrops Spinifer* is 1503100ng/g wet weights.
2. The presence of biogenic hydrocarbons is indicated by the dominances of odd *n*.alkanes in the range of nC $_{17}$, nC $_{19}$, nC $_{21}$ and nC $_{31}$ are presumably synthesized by algae and plankton which are included in fish food.

3. Carbon preference index (CPI) values > 1 for all fish samples in medium and high *n*.alkanes ranges indicates parameter in relation to biogenic hydrocarbon sources.
4. The UCM humps for the GC-FID chromatogram indicates that dissolved petroleum oil are adsorbed in the tissues and not due to adhering of oil on the skin or gills.
5. The BaP-equivalent (BaPE) was high at *Scomber Japonicus* had value 255.052 followed by *Sauridaundo squami*s138.273 and *Euthynnus affinis* 134.668 ng/g wet weights. Since fish metabolize PAH very quickly their detection in these fish indicate continual or recent exposure.
6. The diagnostic indices used showed that the hydrocarbons in the area were from both biogenic and anthropogenic sources. Hence, there is need for adequate regulation and control of all activities contributing to the levels of petroleum hydrocarbon in the marine environment for the safety of human, and fish species lives in the area.

References

Al-Shawafi, N. A. 2008. Total petroleum hydrocarbons carcinogens in commercial fish in the Red Sea and Gulf of Aden – Yemen. *JKAU: Marine Science* 19:15–28.

Elfadly, A. A., E. A. Omayma, and M. M. El Nady. 2016. Significance of GC/FT-IR and GC/MS in recognizing the sources of organic materials from sediments along the Suez Gulf Shoreline, Egypt. *Petroleum Science and Technology* 34(20):1681–960. doi:10.1080/10916466.2016.1217240.

Enuneku, A., M. Ainerua, N. O. Erhunmwunse, and O. E. Osakue. 2015. Total petroleum hydrocarbons in organs of commercially available fish; trachurus trecea (Cadenat, 1949) from Oliha market, Benin City, Nigeria. *Life Journal of Science* 17:383–93.

Fagbote, O. E., and E. O. Olanipekun. 2013. Characterization and sources of aliphatic hydrocarbons of the sediments of River Oluwa at Agbabu Bitumen deposit area, Western Nigeria. *Journal of Scientific Research and Reports* 2013(2):228–48. doi:10.9734/JSRR/2013/3063.

IP Standard Test Methods for analysis and testing of petroleum and related products, and British Standard 2000 Parts, 2019.

Jazza, S. H., A. Y. Al-Adhub, and H. T. Al-Saad. 2015. Polycyclic aromatic hydrocarbons (PAHs) in muscles of two commercial fish species from Al-Kahlaa river in Missan Governorate, Iraq. *ILMU KELAUTAN: Indonesian Journal of Marine Sciences* 20(3):121–6. doi:10.14710/ik.ijms.20.3.121-126.

Medeiros, P. M., and M. C. Bícego. 2004. Investigation of natural and anthropogenic hydrocarbons inputs in sediments using geochemical markers, I, Santos, Sp-Barazil. *Marine Pollution Bulletin* 49(9/10):761–9. doi:10.1016/j.marpolbul.2004.06.001.

Omayma, E. A., A. M. Eldesoky, and M. M. El Nady. 2019. Assessment of poly-aromatic hydrocarbons in the aquatic species along Suez Gulf, Egypt, and their excess cancer risk to human. *Petroleum Science and Technology* 37(5):595–602. doi:10.1080/10916466.2018.1558245.

Omayma, E. A., M. M. El Nady, and A. M. Sawsan. 2018. Assessment of polycyclic aromatic hydrocarbons of organic richness in seawater from some coastal area around Alexandria city, Egypt. *Petroleum Science and Technology* 36(9–10):682–7. doi:10.1080/10916466.2018.1442856.

Omayma, E. A., A. A. Nabila, A. M. Sawsan, and M. D. Mamdouh. 2014. Environmental assessment of contamination by petroleum hydrocarbons in the aquatic species of Suez Gulf. *International Journal of Modern Organic Chemistry* 3(1):1–17.

Omayma, E. A., A. M. Sawsan, and M. M. El Nady. 2017. Organic sources in the Egyptian seawater around Alexandria coastal area as integrated from polycyclic aromatic hydrocarbons (PAHs). *Egyptian Journal of Petroleum* 26(3):819–26. doi:10.1016/j.ejpe.2016.10.016.

Renee, I. A., and M. I. Roushdie. 2016. Monitoring of pollution in sediments of the coasts in Egyptian Red Sea. *Egyptian Journal of Petroleum* 25:133–51.

Snyder, S. M., E. L. Pulster, D. L. Wetzel, and S. A. Murawski. 2015. PAH exposure in Gulf of Mexico demersal fishes, post-deepwater horizon. *Environmental Science & Technology* 49(14):8786–95. doi:10.1021/acs.est.5b01870.

Stogiannidis, E., and R. Laane. 2015. Source characterization of polycyclic aromatic hydrocarbons by using their molecular indices: An overview of possibilities. In *Reviews of environmental contamination and toxicology*, ed. D. M. Whitacre, vol. 234, 49–133.

Veerasingam, S., R. Venkatachalapathy, S. Sudhakar, P. Raja, and V. Rajeswari. 2011. Petroleum hydrocarbon concentrations in eight mollusc species along Tamilnadu coast, Bay of Bengal, India. *Journal of Environmental Sciences* 23(7):1129–34. doi:10.1016/S1001-0742(10)60524-4.

Wang, X., S. Sun, H. Ma, and Y. Liu. 2006. Sources and distribution of aliphatic and polyaromatic hydrocarbons in sediments of Jiaozhou Bay, Qingdao, China. *Marine Pollution Bulletin* 52(2):129–38. doi:10.1016/j.marpolbul.2005.08.010.

Zakaria, M. P., H. Takada, S. Tsutsumi, K. Ohno, J. Yamada, E. Kouno, and H. Kumata. 2002. Distribution of polycyclic aromatic hydrocarbons (PAHs) in rivers and estuaries in Malaysia: widespread input of petrogenic hydrocarbons. *Environmental Science & Technology* 36(9):1907–18. doi:10.1021/es011278+.

Electrochemical and Surface Characterization Studies of 2-amino-6-methyl-5-oxo-4-phenyl-5,6-dihydro-4H-pyrano[3,2-c]quinoline-3-carbonitrile Compound on Copper in 2 M HNO₃

Ahmed M. Eldesoky[1,2], Azza M. Attia[3,4], Omayma E. Ahmed[5], Mohamed A. Abo-Elsoud[6*]

[1]Engineering Chemistry Department, High Institute of Engineering &Technology, New Damietta, Egypt
[2]Chemistry Department, Al-Qunfudah University College, Umm Al-Qura University, Mecca, KSA
[3]Department of Chemistry, Faculty of Science, Mansoura University, Mansoura, Egypt
[4]Faculty of Science and Arts, Chemistry Department, Najran University, Najran, KSA
[5]Evaluation and Analytical Department, Egyptian Petroleum Research Institute, Cairo, Egypt
[6]Physics Department, The University College in Al-Qunfudah, Umm Al-Qura University, Mecca, KSA
Email: *maaboelsoud@uqu.edu.sa

Abstract

The corrosion hindrance of Cu in 2.0 M HNO₃ solution by 2-amino-6-methyl-5-oxo-4-phenyl-5,6-dihydro-4H-pyrano[3,2-c]quinoline-3-carbonitrile compound has been studied, using Potentiodynamic Polarization (PP), AC Impedance (EIS), Electrochemical Frequency Modulation (EFM) techniques. Also, EIS test was utilized to confirm the corrosion protection mechanism. 2-amino-6-methyl-5-oxo-4-phenyl-5,6-dihydro-4H-pyrano[3,2-c]quinoline-3-carbonitrile compound is suggested as a mixed kind inhibitor. SEM and EDX investigations of the Cu in 2.0 M HNO₃ surface revealed that assembles protect Cu from corrosion by adsorption on its surfaces by a forming coating film. Clearly, the assembled mechanisms play a role as a barrier to corrosive solution.

Keywords

Carbonitrile, Cu, SEM, EDX, EIS, EFM

1. Introduction

Copper has varied uses in electronic productions and heat exchangers connection and conductors, pipelines for domestic and production water utilities include water, a conductor in electrical strong lines, gotten its higher conductivi-

ties in thermal and electrical, noble moderately properties and its mechanical workability. Therefore, Cu corrosion and its hindrance in excessive altered solution have been significant in numerous investigators [1]-[10]. The higher information tests for hindrance corrosion are inhibitors utilized to moderate the decrease of beneficial superiority of alloys due to corrosion when they electrochemically attack or chemically by its natural surroundings. The assembly of the inhibitor is one of the main factors that influence the inhibitor/metal interaction [11]. For Cu, which can obtain many-bonds, inhibitor molecules comprise S and N atoms are suggested power. Surrounded by the S, O or N containing organic composite is the heterocyclic structure which has an influence on inhibitors for corrosion of Cu in aqueous solution [12]. Heterocyclic composite counting the group of mercapto has also been introduced as inhibitors for Cu for distinct manufactures uses [13]. Azole assembled contains N atoms, which reply with Cu between the electrons lone pair to obtain complexes (Cu-azole) [14]. These complexes are supposed prevalence to be polymeric in form and nature coating film adherent on the alloy including Cu, which play as a barrier to attraction ions such as Cl. In new papers, numerous thiadiazole investigations [15]-[22] have been noted as excellent inhibitors for Cu and Cu alloys corrosion in distinct aggressive solution. As a result of the toxicity of mostly utilized corrosion hindrance, there is great interest in exchanging harmful inhibitors with helpful non-hazardous [23]. The target of this work is to recognize the 2-amino-6-methyl-5oxo-4-phenyl-5,6-dihydro-4H-pyrano[3,2-2]quinolone-3-carbonitrile assembled as possible corrosion hindrance for Cu in 2.0 M HNO_3. From the data given, we could recognize the examined molecule as possible corrosion hindrance for Cu in our laboratory, which examined experimentally by PP, EIS and EFM tests. The surface morphology of protect Cu was evaluated by SEM and EDX techniques.

2. Experimental

2.1. Composition of Material Samples (See Table 1)

2.2. Chemicals and Solutions

Nitric acid (BDH grade) and organic additive.

The organic inhibitor utilized in this study was organic composite [24] (see Table 2).

2.3. Tests Utilized for Corrosion Calculations
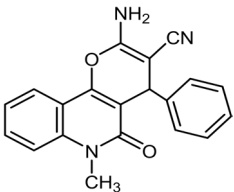
2.3.1. PP Tests

PP tests were accepted in a conformist three-electrode cell with platinum gauze as the auxiliary electrode (1 cm²) and a saturated calomel electrode (SCE) as a reference electrode. The working electrode (WE) was in the form of divided cut

Table 1. Chemical conformation of the Cu in weight %.

Element	Sn	Ag	Fe	Zn	Pb	As	Cu
Weight %	0.001	0.001	0.01	0.05	0.002	0.0002	The rest

Table 2. Chemical structure, name and molecular weight and formula of organic inhibitor.

Structure	Name	Mol. Wt./M. Formula
	2-amino-6-methyl-5-oxo-4-phenyl-5,6-dihydro-4H-pyrano[3,2-c]quinoline-3-carbonitrile	329.35/$C_{20}H_{15}N_3O_2$

from Cu coins of equal arrangement with surface size was 1 cm^2. Before calculation, the electrode was put in solution at potential for half hours, till a steady state was gotten. The started potential was −600 to +400 mV vs. E_{ocp}. All tests were done in freshly ready solutions at 30°C and outcome data were always repetitive at minimum three times to check the reproducibility.

2.3.2. EIS Tests

Impedance tests were occurred utilizing AC signals of 5 mV signal to signal amplitude at the OCP in the frequency variety of 0.1 Hz to 100 kHz. All impedance values were formfitting to a suitable equivalent circuit utilizing the Gamry Echem Analyst software.

2.3.3. EFM Tests

EFM data were achieved with relating potential perturbation signal with amplitude 10 mV with 2 and 5 Hz sine waves [25]. The greater signals were utilized to estimate the current gotten from corrosion density (i_{corr}), the Tafel line slopes (β_C and β_a) and the causality factors CF-2 and CF-3 [26]. All outcome data were obtained utilizing Gamry instrument PCI300/4, DC105 utilize for corrosion software, EIS300 software, EFM140 software and Echem Analyst 5.5 for results drawing, graphing, data correct and measuring.

2.3.4. SEM-EDX Analysis

The Cu surface was ready by observance the coins for 3 days in 2.0 M HNO$_3$ in existence and nonexistence of optimum dose of studied organic composite, after this inundation time, the coins were splashed gently with water bidi-stilled, cautiously dried and mounted into the spectrometer without any extra management. The Cu corroded surfaces were examined utilizing an X-ray diffractometer Philips (pw-1390) with Cu-tube (CuK$_a$, $\lambda = 1.54054$ Å) electron microscope utilize for scanning (SEM, JOEL, JSM-T20, Japan).

3. Results and Discussion

3.1. PP Tests

Theoretically, Cu can hardly be corroded in the deoxygenated acid medium, as Cu cannot relocate hydrogen from acid solutions conferring to the theories of chemical thermodynamics [27] [28] [29]. However, these situations will variation in nitric acid. Oxygen dissolved may be reduced on surface of Cu and this

will agree to corrosion to happen. It is a best estimate to negligible the hydrogen liberate reaction and only deliberates reduction of oxygen in the HNO_3 at potentials adjacent the potentials of corrosion [30].

Figure 1 demonstrates the PP manner of Cu electrode in 2.0M HNO_3 in the existence and nonexistence of unlike dose of 2-amino-6-methyl-5-oxo-4-phenyl-5,6-dihydro-4H-pyrano[3,2-c]quinoline-3-carbonitrile composite. **Figure 1** displays that two anodic reaction and cathodic are influenced by the appending of examined assembled and the protection efficiency improves as the inhibitor dose rise, but the cathodic reaction is more hindrance, significance that the appending of 2-amino-6-methyl-5-oxo-4-phenyl-5,6-dihydro-4H-pyrano[3,2-c]quinoline-3-car-bonitrile composite lower the anodic liquefaction of Cu and also hinders the cathodic reactions. Therefore, studied composite is deliberated as mixed kind inhibitor.

The parameters gotten from electrochemical such as current corrosion densities (i_{corr}), potential gotten from corrosion (E_{corr}), the cathodic Tafel line slope (β_C), anodic Tafel line slope (β_a) and protection efficiency ($\%IE$) were measured from the diagrams (see **Figure 1** and **Table 3**). The outcome data gotten in **Table 3** discovered that the i_{corr} lower clearly after the appending of 2-amino-6-methyl-5-oxo-4-phenyl-5,6-dihydro-4H-pyrano[3,2-c]quinoline-3-carbonitrile composite and $\%IE$ improve with raising the inhibitor dose. In the existence of inhibitor E_{corr}, was improved with no definite trend, demonstrating that 2-amino-6-methyl-5-oxo-4-phenyl-5,6-dihydro-4H-pyrano[3,2-c]quinoline-3-carbonitrile composite play as mixed–kind inhibitor. The $\%IE$ was measured
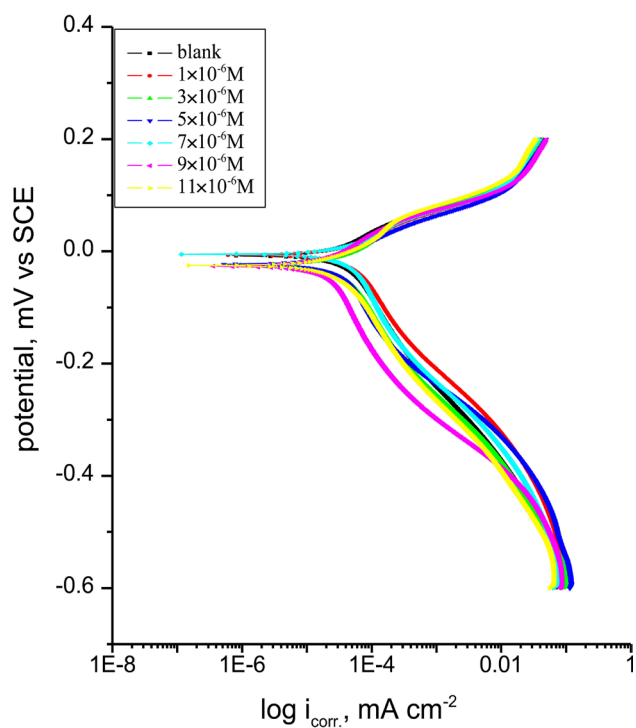
Figure 1. PP plots for the corrosion of Cu in 2.0 M HNO_3 in existence and lack of unlike dose of inhibitor at 30°C ± 0.1°C.

Table 3. Parameters gotten from PP technique for the corrosion of Cu in 2.0 M HNO₃ at 30˚C ± 0.1˚C.

Compound	*Conc.* (M)	E_{Corr} (mV vs. SCE)	$i_{Corr} \times 10^{-5}$ (μA·cm^{-2})	$\beta_a \times 10^{-3}$ (mV·dec^{-1})	$\beta_c \times 10^{-3}$ (mV·dec^{-1})	θ	%IE_p
	Blank	777	92.8	143.4	506.1	----	----
	1×10^{-6}	684	83.2	107.8	332.4	0.103	10.3
	3×10^{-6}	251	58.4	99.8	352.1	0.370	37.0
2-amino-6-methyl-5-oxo-4-phenyl-5,6-dihydro-4H-pyrano[3,2-c]quinoline-3-carbonitrile	5×10^{-6}	232	51.7	97.8	346.0	0.442	44.2
	7×10^{-6}	531	43.6	63.8	160.2	0.530	53.0
	9×10^{-6}	270	38.1	108.4	454.2	0.589	58.9
	11×10^{-6}	257	34.9	83.5	190.1	0.623	62.3

utilizing Equation (1):

$$\%IE_P = \left[i_{Corr}^{\circ} - i_{Corr} / i_{Corr}^{\circ} \right] \times 100 \tag{1}$$

where i_{Corr}° and i_{Corr} are the uninhibited and inhibited corrosion current densities, correspondingly.

Also it is clear from **Table 3** that (β_a) and (β_C) Tafel lines keep almost unmoved upon appending of 2-amino-6-methyl-5-oxo-4-phenyl-5,6-dihydro-4H-pyrano[3,2-c]quinoline-3-carbonitrile composite, mean rise to nearly parallel set of anodic lines slope, and nearly parallel cathodic diagrams data gotten too. Therefore, the inhibitors adsorbed play by simple blocking of the active center for two anodic and cathodic procedures. Meaning no change in mechanism of Cu in solution, and only reasons inactivation of a part of the surface with esteem to the aggressive solution [31] [32].

3.2. EIS Tests

EIS is well-established and commanding tests in the reading of corrosion. Surface characteristic and mechanistic data can be gotten from impedance diagrams [33] [34] [35] [36] [37]. **Figure 2(a)** & **Figure 2(b)** display the Nyquist (a) and Bode (b) diagrams gotten at OCP both in the attendance and lack of improving dose of examined 2-amino-6-methyl-5-oxo-4-phenyl-5,6-dihydro-4H-pyrano[3,2-c]quinoline-3-carbonitrile compound at 30˚C ± 0.1˚C. The improve in the size of the capacitive loop with the appending of 2-amino-6-methyl-5-oxo-4-phenyl-5,6-dihydro-4H-pyrano[3,2-c]quinoline-3-carbonitrile composite at 30˚C ± 0.1˚C displays that a barrier progressively forms on the surface of Cu. Bode schemes (see **Figure 2(b)**), displays the incessant rise in the phase angle shift, clearly correlating with the rise of adsorbed inhibitor on surface of Cu. The Nyquist schemes do not produce perfect semicircles as predictable from the theory of EIS. The abnormality from ideal semicircle was usually credited to the frequency scattering [38] as well as to the in-homogeneities of the surface.

EIS data of the 2-amino-6-methyl-5-oxo-4-phenyl-5,6-dihydro-4H-pyrano[3,2-c]quinoline-3-carbonitrile campsite at 30˚C ± 0.1˚C was examine utilize the equivalent circuit (**Figure 3**), which signifies a single charge transfer reaction and
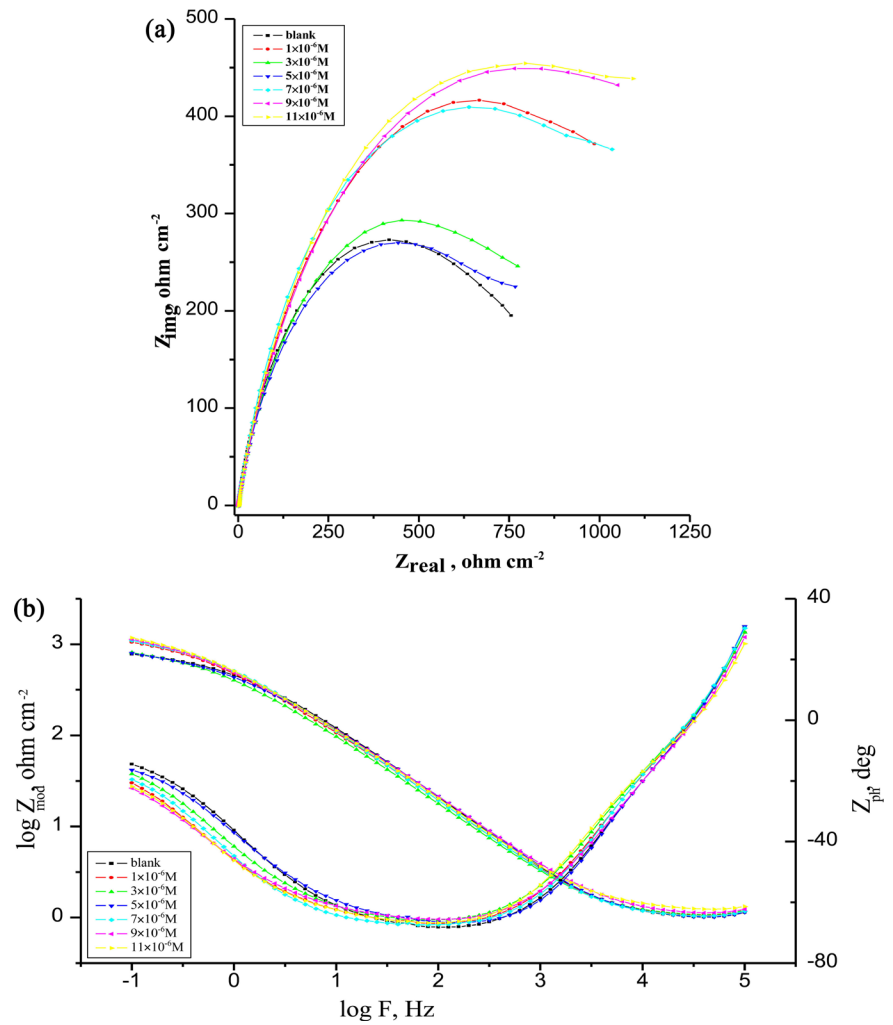
Figure 2. The Nyquist (a) and Bode (b) diagrams for Cu corrosion in nonexistence and existence of unlike dose of 2-amino-6-methyl-5-oxo-4-phenyl-5, 6-dihydro-4H-pyrano [3,2-c]quinoline-3-carbonitrile composite at 30°C± 0.1°C.
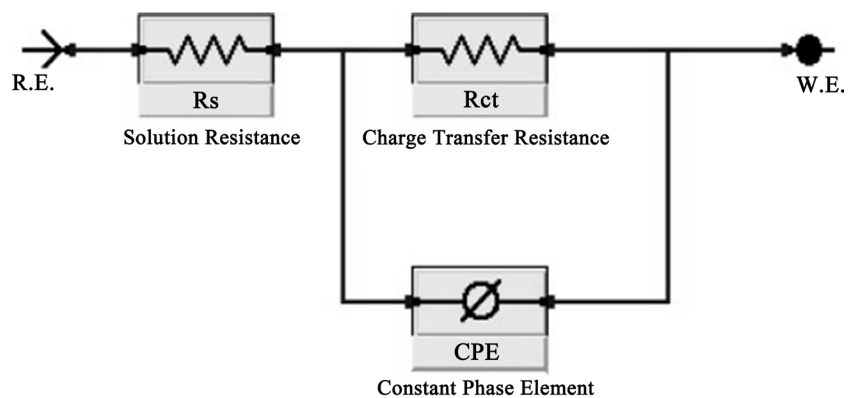
Figure 3. Equivalent circuit model utilized to fit investigational EIS.

fits well with our experimental data. The constant phase element, CPE, is presented in the circuit in its place of a pure double layer capacitor to give a more correct fit [39]. The double layer capacitance, C_{dl}, for a circuit including

$$C_{dl} = Y_o \omega^{n-1} / \sin\left[n\left(\pi/2\right)\right] \qquad (2)$$

where Y_o is the degree of the CPE, $\omega = 2\pi f_{max}$, f_{max} is the frequency at the impedance is maximal and the factor n is an parameter adjustable that regularly lies among 0.50 and 1.0 [40] [41] [42]. The overall figure of the plots is very like for all samples (in existence and nonexistence of inhibitor at unlike immersion times) representing that no exchange in the corrosion mechanism [43]. From the impedance data (see **Table 4**), we achieve that the data of R_{ct} improves with rising the dose of the inhibitor and this designates an improvement in %IE, which in agreement with the data gotten from Potentiodynamic polarization.

In fact, the existence of inhibitor improves the data of R_{ct} in acidic solution. Data of C_{dl} are also brought down to the extreme extent in the existence of inhibitor and the break down in the data of CPE trails the order like to that gotten for i_{Corr} in this study. The lower C_{PE}/C_{dl} data from a break down in local dielectric constant and/or an improvement in the width of the double layer, signify that organic assembles hinder the Cu corrosion by metal/acid adsorbed [44] [45]. The %IE was measured from the charge transfer resistance data from Equation (3) [46]:

$$\%IE_{EIS} = \left[1 - \left(R_{ct}^{\circ} / R_{ct}\right)\right] \times 100 \qquad (3)$$

where R_{ct}° and R_{ct} are the resistance data nonexistence and existence of inhibitor correspondingly.

3.3. EFM Tests

EFM is a no damaging corrosion tests that can straight and quickly measure the corrosion current data without prior information of Tafel slopes, and with only a lesser polarizing signal. These benefits of EFM test make it an ideal applicant for online corrosion observing [47]. The higher strength of the EFM is the causality factors which attend as an inner check on the power of EFM calculation.

Figure 4 displays the EFM of Cu in nitric acid solution inclosing altered dose of 2-amino-6-methyl-5-oxo-4-phenyl-5,6-dihydro-4H-pyrano[3,2-c]quinoline-

Table 4. Outcome data gotten from EIS test for Cu in 2 M HNO₃ in the nonexistence and existence of unlike dose of 2-amino-6-methyl-5-oxo-4-phenyl-5,6-dihydro-4H-pyrano[3,2-c]quinoline-3-carbonitrile compound at 30°C ± 0.1°C.

Compound	*Conc.* (M)	$R_s \times 10^{-3}$ Ω·cm²	$Y_o \times 10^{-6}$ μΩ⁻¹·sⁿ	$n \times 10^{-3}$	R_{ct} Ω·cm²	$C_{dl} \times 10^{-4}$ μF·cm⁻²	θ	%IE_{EIS}
	Blank	0.995	291.0	800.4	751.6	9.0	-----	------
	1×10^{-6}	0.942	320.1	786.3	799.2	7.8	0.059	5.9
	3×10^{-6}	1.017	404.2	776.8	828.2	7.7	0.092	9.2
2-amino-6-methyl-5-oxo-4-phenyl-5,6-dihydro-4H-pyrano[3,2-c]quinoline-3-carbonitrile	5×10^{-6}	0.993	365.7	780.7	1003.7	7.6	0.251	25.1
	7×10^{-6}	0.979	329.3	794.5	1228.3	7.5	0.388	38.8
	9×10^{-6}	1.044	366.0	765.0	1320.2	7.2	0.430	43.0
	11×10^{-6}	1.175	351.0	778.7	1550.2	6.8	0.515	51.1
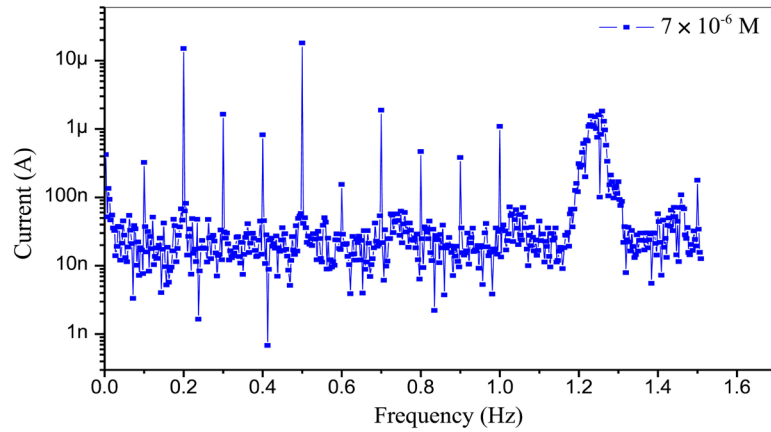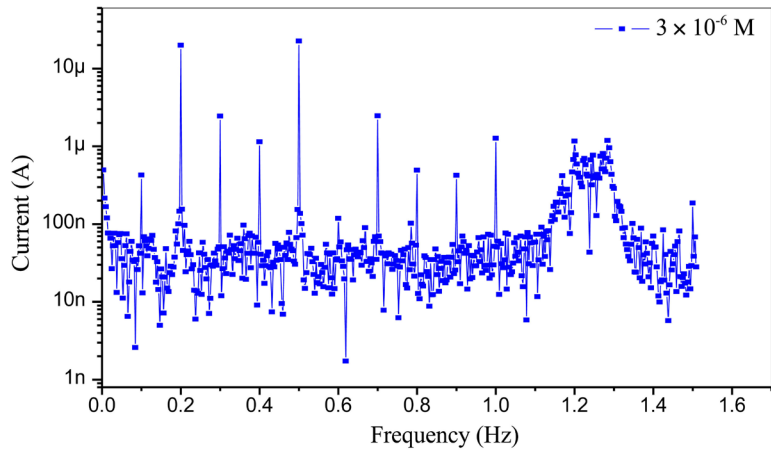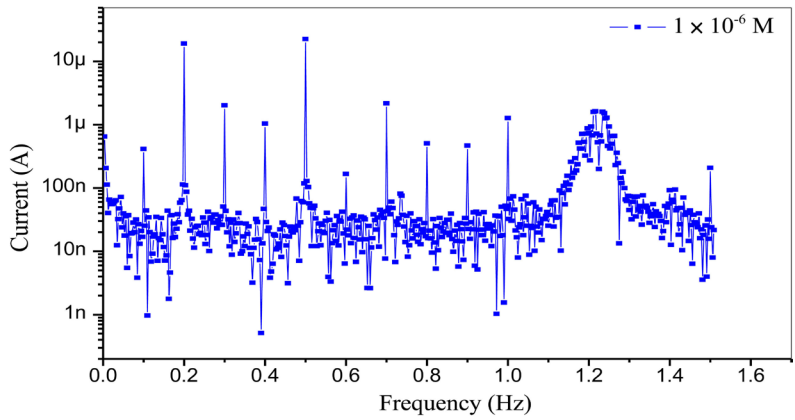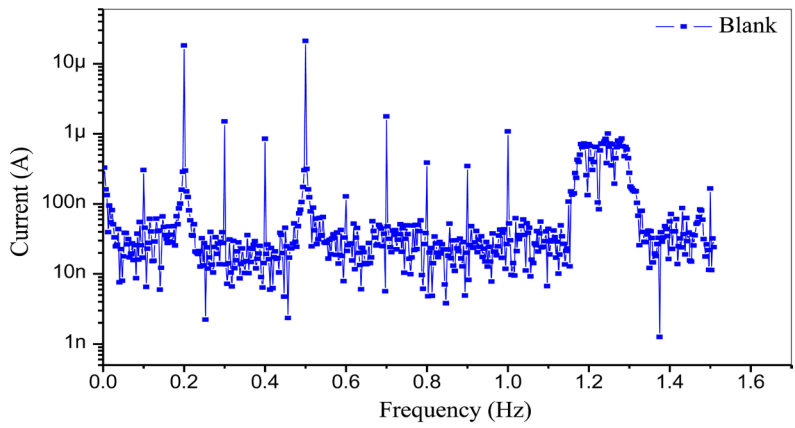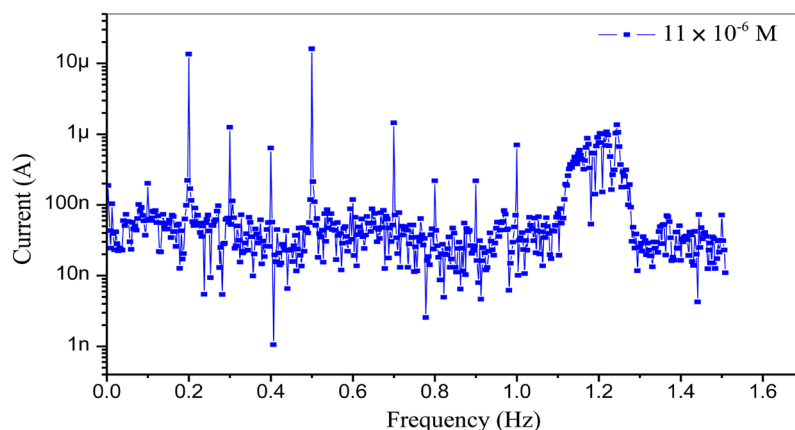
Figure 4. EFM data for Cu nonexistence and existence of different dose of 2-amino-6-methyl-5-oxo-4-phenyl-5,6-dihydro-4H-pyrano[3,2-c]quinoline-3-carbonitrile composite at 30˚C ± 0.1˚C.

3-carbonitrile compound at 30˚C ± 0.1˚C. The harmonic and intermodulation peaks are obviously visible and are much greater than the background noise. The investigational EFM value was preserved utilized two unlike models: complete dispersion control of the cathodic reaction and the "activation" model. For the second, a set of three non-linear equations had been explained, pretentious that the corrosion potential does not exchange due to the polarization of the electrode working [48]. The greater signal was utilized to measure i_{corr}, (β_C and β_a) and (CF-2 and CF-3). These parameters gotten from EFM were recorded in **Table 5**. The data demonstration that, the appending of tested composite at unlike doses to the acidic solution lower i_{corr}, signifying that this composite hinder the corrosion of Cu concluded adsorption. The CF gotten under altered experimental conditions are nearly equal to the values gotten from theoretical Equations (2) and (3) representing that the calculated data are confirmed and best quality. $\%IE_{EFM}$ was improved by improving the inhibitor dose and was measured as from Equation (4):

$$IE_{EFM} = \left[1 - \left(i_{Corr}/i_{Corr}^{\circ}\right)\right] \times 100 \tag{4}$$

where i_{Corr}° and i_{Corr} are current nonexistence and existence of inhibitor, correspondingly.

3.4. SEM Examination and EDX Analysis

The creation of a defending surface film of inhibitor at the electrode surface was further established by SEM clarifications of the Cu surface. Also, in order to see whether the organic additive is adsorbed on the Cu surface or not, both SEM and EDX tests were occurred. **Figure 5** displays the SEM of fresh Cu surface nonexistence any appending of acid or the inhibitor. The images for Cu surface unprotected to 2.0 M HNO$_3$ solution nonexistence and existence the appending of the optimum dose of the 2-amino-6-methyl-5-oxo-4-phenyl-5,6-dihydro-4H-pyrano[3,2-c]quinoline-3-carbonitrile composites are exposed in **Figure 5**. As

Table 5. Outcome data gotten from EFM test for Cu in 2 M HNO$_3$ in the a in nonexistence and existence of unlike dose of 2-amino-6-methyl-5-oxo-4-phenyl-5,6-dihydro-4H-pyrano[3,2-c]quinoline-3-carbonitrile at 30˚C ± 0.1˚C.

Inhibitor	Conc. (M)	i_{Corr} (µA·cm^{-2})	$\beta_a \times 10^{-3}$ (mV·dec^{-1})	$\beta_c \times 10^{-3}$ (mV·dec^{-1})	CF-2	CF-3	θ	%IE_{EFM}
	Blank	39.66	69.0	104.5	1.98	2.94	-----	-----
	1×10^{-6}	23.62	63.9	104.2	1.99	2.94	0.404	40.4
2-amino-6-methyl-5-oxo-4-phenyl-5,6-dihydro-4H-pyrano[3,2-c]quinoline-3-carbonitrile	3×10^{-6}	22.44	58.3	99.7	2.03	3.11	0.434	43.4
	5×10^{-6}	20.21	78.1	118.3	1.96	2.91	0.490	49.0
	7×10^{-6}	19.23	66.9	119.8	1.94	2.85	0.515	51.5
	9×10^{-6}	11.32	73.9	131.2	1.89	2.91	0.714	71.4
	11×10^{-6}	9.54	65.6	104.7	2.01	3.01	0.759	75.9
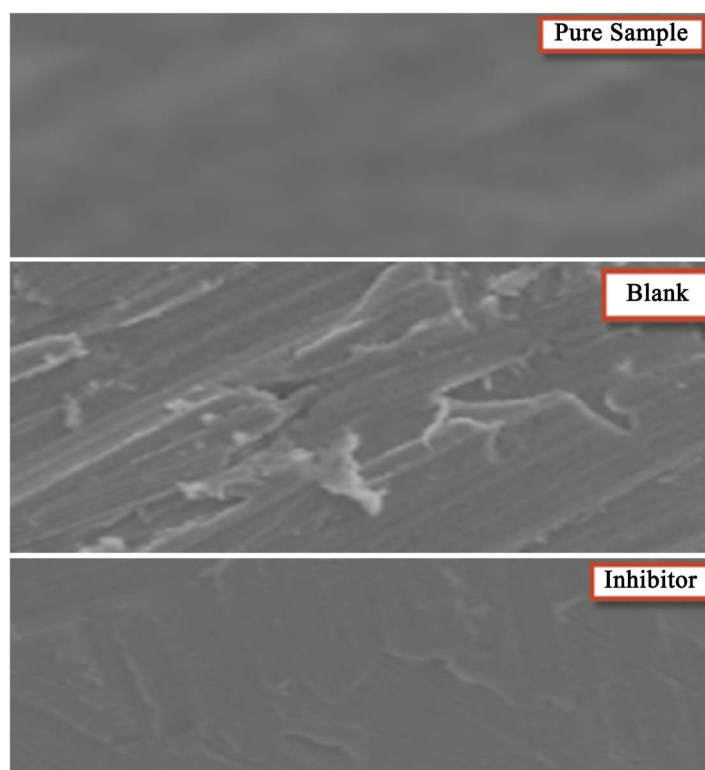
Figure 5. SEM images of Cu in 2.0 M HNO$_3$ solution after inundation for 3 days nonexistence inhibitor and in existence of 11×10^{-6} M of 2-amino-6-methyl-5-oxo-4-phenyl-5,6-dihydro-4H-pyrano[3,2-c]quinoline-3-carbonitrile.

can be gotten, there was a noticeable perfection in the surface image of Cu that was preserved with the inhibitor due to the creation of an adsorbed protecting film of the inhibitor at the Cu surface.

The EDX profile examination exists in **Figure 6**. The EDX review spectra were utilized to measure which elements of inhibitor existed on the electrode surface earlier and later contact to the inhibitor solution. For the coins' nonexistence inhibitor behavior (**Figure 6**), only Cu was noticed. This is established by utilizing XRD, the chief corrosion yields designed on exposed Cu to nitric acid were
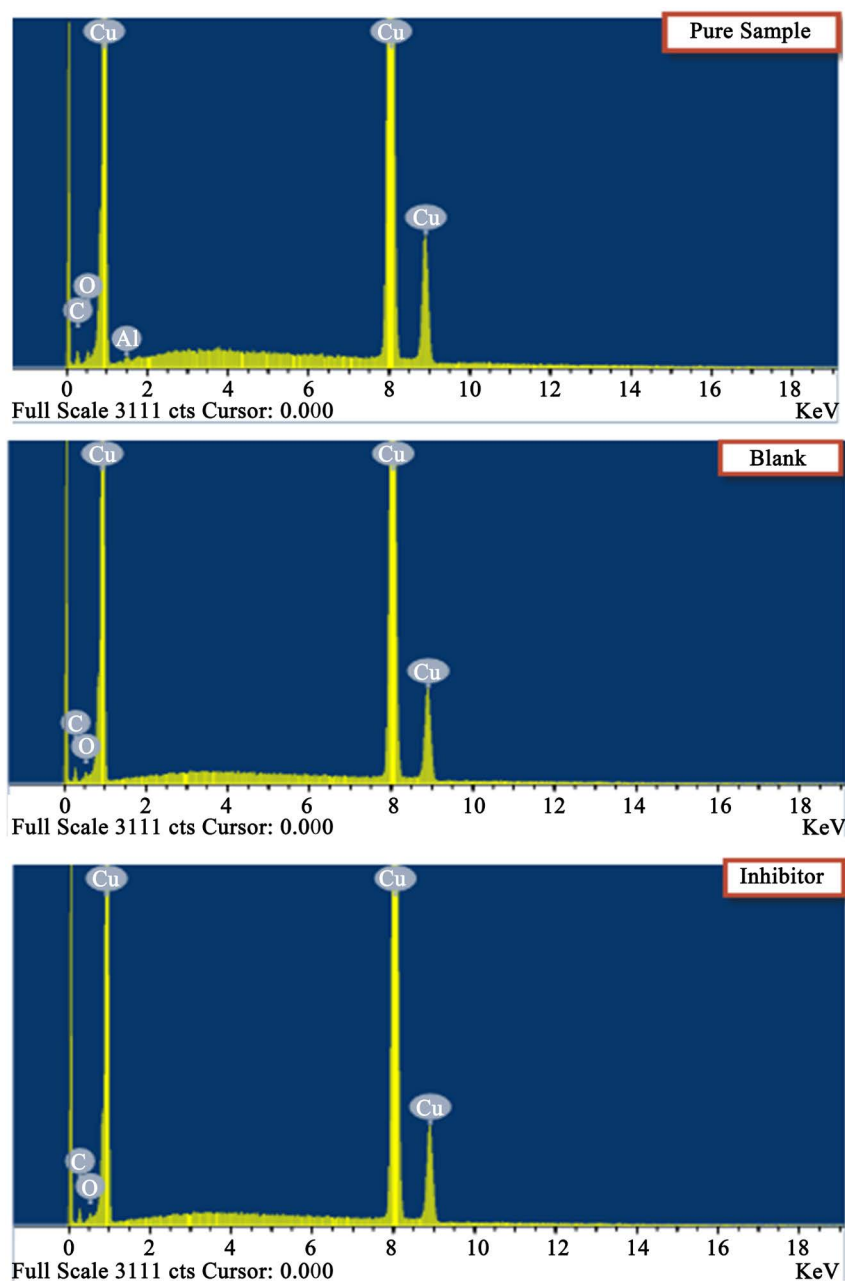
Figure 6. EDS images of Cu in 2.0 M HNO$_3$ solution after inundation for 3 days nonexistence inhibitor and in existence of 11×10^{-6} M of 2-amino-6-methyl-5-oxo-4-phenyl-5,6-dihydro-4H-pyrano[3,2-c]quinoline-3-carbonitrile.

recognized as the basic Cu nitrate, gerhardtite (Cu$_2$(NO$_3$)(OH)$_3$) and to a slighter amount cuprite (Cu$_2$O) [49] [50]. It is observed the existence of the C, O and N signal in the EDX spectra in the example of the coins showing to the inhibitor, could be qualified to the adsorption of organic moiety at the surface of Cu. The rise in quantity of C atom in the item of assembles (15.73%), specified that the liquefaction of Cu is very hinder by composite and thus shows a very high hinder capacity. Also, a strong enrichment with C is renowned in the example of campsite (see **Table 6**). The EDX of **Figure 6** display that the O is significantly

Table 6. Element gotten from EDX of copper in 2.0 M HNO$_3$ solution after inundation for days nonexistence of inhibitor and in existence of 11×10^{-6} M of 2-amino-6-methyl-5-oxo-4-phenyl-5,6-dihydro-4H-pyrano[3,2-c]quinoline-3-carbonitrile.

Weight %	C	O	Al	Cu
Pure Sample	9.24	1.87	0.45	88.44
Blank	12.13	3.52	----	84.35
Inhibitor	15.73	2.45	----	81.82

suppressed relative to the coins ready in 2.0 M HNO$_3$ solution, and definitely this suppression will improve with improve examined dose and engagement time. The destruction of the O occurred due to the overlying inhibitor film. Also it is significant to notification the quantity of Cu peaks of EDX spectra is rise in the existence of inhibitor in a contrast of EDX analysis gotten in the nonexistence of inhibitor might representative that the examined molecule defensive the Cu surface in contradiction of acid corrosion. The configuration of the distinguished elements on the surface of Cu designates that the inhibitor molecule is powerfully adsorbed on the Cu creating a Cu-examined molecule bond, thus hinder the surface against corrosion.

3.5. Mechanism of Inhibition

Protection of the corrosion of Cu in 2.0 M HNO$_3$ solution by examined composite is measured by PP measurements, EIS, EFM and SEM studies; it was obtained that the protection efficiency relies on dose, metal nature, the manner of adsorption of the inhibitors and surface environments.

The corrosion hindrance is due to the inhibitors have adsorbed at the interface of solution/electrode, the amount of adsorption of an inhibitor rely on the type of the metal, the adsorption mode of the inhibitor and the conditions of surface. Adsorption on Cu surface is expected occurred mostly among the active site involved in the inhibitor and would rely on their charge density. The lone pairs of electrons transfer on the N atoms to the Cu surface to procedure a coordinate kind of linkage is favored by the existence of a vacant orbital in Cu atom of little energy.

It was decided that the kind of adsorption rely on the attraction of the Cu to the clouds π-electron of the ring structure. Metals for example Cu, which have a better affinity near aromatic moieties, were gotten to adsorb benzene rings in orientation flat.

2-amino-6-methyl-5-oxo-4-phenyl-5,6-dihydro-4H-pyrano[3,2-c]quinoline-3-carbonitrile assembled displays best hindrance power due to: i) the attendance of CH$_3$ group which is an electron giving group, also this CH$_3$ will improve the electron charge density on the structure, ii) its bigger size of molecular weight (329.25) that may simplify enhanced surface coating, and iii) its adsorption among five active site.

3.6. Conclusions

1) The analysis details of composite reveal that, it is an excellent corrosion hindrance for Cu in 2.0 M HNO₃.

2) C_{dl} breaks down with respect to the blank solution when adding inhibitor. This fact may be decided by inhibitor molecule adsorbed on the surface of Cu.

3) EFM can be utilized for calculation of corrosion in a lack of prior data of Tafel lines slope.

4) The morphology of Cu existence and nonexistence was observed by (SEM) and (EDX).

Conflicts of Interest

The authors declare no conflicts of interest regarding the publication of this paper.

References

[1] Khaled, K.F., Fadl-Allah, A.S. and Hammouti, B. (2009) Some Benzotriazole Derivatives as Corrosion Inhibitors for Copper in Acidic Medium: Experimental and Quantum Chemical Molecular Dynamics Approach. *Materials Chemistry and Physics*, **117**, 148-155. https://doi.org/10.1016/j.matchemphys.2009.05.043

[2] AbdEl-Maksoud, S.A. (2004) Some Phthalazin Derivatives as Non Toxic Corrosion Inhibitors for Copper in Sulphuric Acid. *Electrochimica Acta*, **49**, 4205-4212. https://doi.org/10.1016/j.electacta.2004.04.015

[3] Zarrouk, A., Hammouti, B. and Dafali, A. (2014) A Theoretical Study on the Inhibition Efficiencies of Some Quinoxalines as Corrosion Inhibitors of Copper in Nitric Acid. *Journal of Saudi Chemical Society*, **18**, 450-455. https://doi.org/10.1016/j.jscs.2011.09.011

[4] El-Naggar, M.M. (2000) Is-Aminoazoles Corrosion Inhibitors for Copper in 4.0 M HNO₃ Solutions. *Corrosion Science*, **42**, 773-784. https://doi.org/10.1016/S0010-938X(99)00066-9

[5] Treacy, G.M., Wilcox, G.D. and Richardson, M.O.W. (1999) Behaviour of Molybdate-Passivated Zinc Coated Steel Exposed to Corrosive Chloride Environments. *Journal of Applied Electrochemistry*, **29**, 647-654. https://doi.org/10.1023/A:1026461924663

[6] Elmorsi, M.A. and Hassanein, A.M. (1999) Corrosion Inhibition of Copper by Heterocyclic Science. *Corrosion Science*, **41**, 2337-2352. https://doi.org/10.1016/S0010-938X(99)00061-X

[7] Abd El-Maksoud, S.A. and Hassan, H.H. (2007) Electrochemical Studies on the Effect of (2E)-3-amino-2-phenylazo-but-2-enenitrile and Its Derivative on the Behavior of Copper in Nitric Acid. *Materials and Corrosion*, **58**, 369-375. https://doi.org/10.1002/maco.200604021

[8] Khaled, K.F. (2008) Guanidine Derivative as a New Corrosion Inhibitor for Copper in 3% NaCl Solution. *Materials Chemistry and Physics*, **112**, 104-111. https://doi.org/10.1016/j.matchemphys.2008.05.052

[9] El-Kot, A.M. and AL-Suhybani, A.A. (2013) Organic and Inorganic Corrosion Inhibitors for Copper in HNO₃ Studied by Two Methods. *British Corrosion Journal*, **22**, 29-31. https://doi.org/10.1179/000705987798271848

[10] Assaf, F.H., Krishs, M.A. and Kodari, M. (2003) Studies on Dissolution and Inhibition of Copper in Nitric Acid Using Stripping Voltammetry and Conductance Measurement. *Materials Chemistry and Physics*, **77**, 192-203.
https://doi.org/10.1016/S0254-0584(01)00597-1

[11] Herrag, L., Bourlah, M. and Patel, N.S. (2012) Experimental and Theoretical Study for Corrosion Inhibition of Mild Steel 1 M HCl Solution by Some New Diaminopropanenitrile Compounds. *Research on Chemical Intermediates*, **38**, 1669-1690.
https://doi.org/10.1007/s11164-012-0493-1

[12] Al-Kharafi, F.M., Abdullah, A.M. and Ateya, B.G. (2007) Effect of Sulfide Pollution on the Stability of the Protective Film of Benzotriazole on Copper. *Applied Surface Science*, **253**, 8986-8991. https://doi.org/10.1016/j.apsusc.2007.05.017

[13] Ramji, K., Caims, D.R. and Rajeswari, S. (2008) Synergistic Inhibition Effect of 2-Mercaptobenzothiazole and Tween-80 on the Corrosion of Brass in NaCl Solution. *Applied Surface Science*, **254**, 4483-4493.
https://doi.org/10.1016/j.apsusc.2008.01.031

[14] Altaf, F., Qureshi, R. and Ahmed, S. (2010) Electrochemical Adsorption Studies of Urea on Copper Surface in Alkaline Medium. *Journal of Electroanalytical Chemistry*, **642**, 98-101. https://doi.org/10.1016/j.jelechem.2010.02.011

[15] Varvara, S., Muresan, L.M., Rahmouni, K. and Takenouti, H. (2008) Evaluation of Some Non-Toxic Thiadiazole Derivatives as Bronze Corrosion Inhibitors in Aqueous Solution. *Corrosion Science*, **50**, 2596-2604.
https://doi.org/10.1016/j.corsci.2008.06.046

[16] Lashgari, M., Arshadi, M.R. and Biglar, M. (2010) Experimental and Theoretical Studies of Media Effects on Copper Corrosion in Acidic Environments Containing 2-amino-5-mercapto-1,3,4-thiadiazole. *Journal of the Iranian Chemical Society*, **7**, 478-486. https://doi.org/10.1007/BF03246035

[17] Easton, E. and Pickup, P.G. (2005) An Electrochemical Impedance Spectroscopy Study of Fuel Cell Electrodes. *Electrochimica Acta*, **50**, 2469-2474.
https://doi.org/10.1016/j.electacta.2004.10.074

[18] Krishnaveni, K. and Ravichandran, J. (2014) Influence of Aqueous Extract of Leaves of *Morinda tinctoria* on Copper Corrosion in HCl Medium. *Journal of Electroanalytical Chemistry*, **735**, 24-31. https://doi.org/10.1016/j.jelechem.2014.09.032

[19] Sherif, E.M., Erasmus, R.M. and Comins, G.D. (2010) *In Situ* Raman Spectroscopy and Electrochemical Techniques for Studying Corrosion and Corrosion Inhibition of Iron in Sodium Chloride Solutions. *Electrochimica Acta*, **55**, 3657-3663.
https://doi.org/10.1016/j.electacta.2010.01.117

[20] Fouda, A.S. and Abdul Wahed, H.A. (2016) Corrosion Inhibition of Copper in HNO_3 Solution Using Thiophene and Its Derivatives. *Arabian Journal of Chemistry*, **9**, 91-99. https://doi.org/10.1016/j.arabjc.2011.02.014

[21] Khadom, A.A., Yaro, A.S. and Kadum, A.A.H. (2010) Corrosion Inhibition by Naphthylamine and Phenylenediamine for the Corrosion of Copper-Nickel Alloy in Hydrochloric Acid. *Journal of the Taiwan Institute of Chemical Engineers*, **41**, 122-125. https://doi.org/10.1016/j.jtice.2009.08.001

[22] Tang, Y., Yang, X., Yang, W. and Wan, R. (2010) Experimental and Molecular Dynamics Studies on Corrosion Inhibition of Mild Steel by 2-amino-5-phenyl-1,3,4-thiadzole. *Corrosion Science*, **52**, 242-249.
https://doi.org/10.1016/j.corsci.2009.09.010

[23] Rajeswari, V. and Devarayam, K. (2017) Expired Pharmaceutical Compounds as Potential Inhibitors for Cast Iron Corrosion in Acidic Medium. *Research on Chem-

ical Intermediates, **43**, 3893-3913. https://doi.org/10.1007/s11164-016-2852-9

[24] Maddila, S., Rana, S. and Johalagadda, S.B. (2015) Synthesis of Pyrazole-4-Carbonitrile Derivatives in Aqueous Media with CuO/ZrO_2 as Recyclable Catalyst. *Catalysis Communications*, **61**, 26-30.
https://doi.org/10.1016/j.catcom.2014.12.005

[25] Rauf, A., Bogaerts, W.F. and Mahdi, E. (2012) Implementation of Electrochemical Frequency Modulation to Analyze Stress Corrosion Cracking. *Corrosion Science and Engineering*, **68**, 2-9. https://doi.org/10.5006/1.3691836

[26] Abdel-Rehim, S.S., Khaled, K.F. and Abd-Elshafi, N.S. (2006) Electrochemical Frequency Modulation as a New Technique for Monitoring Corrosion Inhibition of Iron in Acid Media by New Thiourea Derivative. *Electrochimica Acta*, **51**, 3269-3277. https://doi.org/10.1016/j.electacta.2005.09.018

[27] Quartarone, G., Moretti, G., Bellomi, T., Capobianco, G. and Zingales, A. (2003) Inhibition of Copper Corrosion by Isatin in Aerated 0.5 M H_2SO_4. *Corrosion Science*, **45**, 715-733. https://doi.org/10.1016/S0010-938X(02)00134-8

[28] Bjomdahl, W.D. and Nobe, K. (1984) Copper Corrosion in Chloride Media. Effect of Oxygen. *Corrosion Science and Engineering*, **40**, 82-87.
https://doi.org/10.5006/1.3593920

[29] Zelinsky, A.G., Pirogov, B.Y. and Yurjev, O.A. (2004) Open Circuit Potential Transients and Electrochemical Quartz Crystal Microgravimetry Measurements of Dissolution of Copper in Acidic Sulfate Solutions. *Corrosion Science*, **46**, 1083-1093.
https://doi.org/10.1016/j.corsci.2003.09.008

[30] Amin, M.A. (2006) Weight Loss, Polarization, Electrochemical Impedance Spectroscopy, SEM and EDX Studies of the Corrosion Inhibition of Copper in Aerated NaCl Solutions. *Journal of Applied Electrochemistry*, **36**, 215-226.
https://doi.org/10.1007/s10800-005-9055-1

[31] Khaled, K.F. (2008) Adsorption and Inhibitive Properties of a New Synthesized Guanidine Derivative on Corrosion of Copper in 0.5 M H_2SO_4. *Applied Surface Science*, **255**, 1811-1818. https://doi.org/10.1016/j.apsusc.2008.06.030

[32] Gadallah, A.G., Badway, M.W., Rehan, H.H. and Abu-Romia, M.M. (1989) Inhibition of Corrosion of *α*-Brass (Cu-Zn, 67/33) in Acid Chloride Solutions by Some Amino Pyrazole Derivatives. *Journal of Applied Electrochemistry*, **19**, 928-932.
https://doi.org/10.1007/BF01007942

[33] Cheng, T.P. and Tung, J. (1990) Corrosion of Reinforcements in Artificial Sea Water and Concentrated Sulfate Solution. *Cement and Concrete Research*, **20**, 243-252.
https://doi.org/10.1016/0008-8846(90)90077-B

[34] Kendling, M.W., Mansfeld, F. and Lindberg, G. (1983) A Computer Analysis of Electrochemical Impedance Data. *Corrosion Science*, **23**, 1007-1015.
https://doi.org/10.1016/0010-938X(83)90027-6

[35] Milocco, R.H. (1989) An Iterative Least Squares Method for the Identification of Electrochemical Impedances. *Journal of Electroanalytical Chemistry and Interfacial Electrochemistry*, **24**, 243-255. https://doi.org/10.1016/0022-0728(89)87017-2

[36] Debuxck, F., Emaitre, L. and Weyten, L. (1988) Estimating the Barrier Layer Thickness of Porous Aluminium Oxide Films with A.C. Impedance Measurements. *Surface and Coatings Technology*, **34**, 311-318.
https://doi.org/10.1016/0257-8972(88)90121-1

[37] Kapusta, S. and Hackerman, N. (1982) The Electroreduction of Formaldehyde on Tin and Indium. *Journal of Electroanalytical Chemistry and Interfacial Electrochemistry*, **138**, 295-313. https://doi.org/10.1016/0022-0728(82)85084-5

[38] Kuruvilla, M., John, S. and Joseph, A. (2013) Electrochemical Studies on the Interaction of l-cysteine with Metallic Copper in Sulfuric Acid. *Research on Chemical Intermediates*, **39**, 3513-3543. https://doi.org/10.1007/s11164-012-0860-y

[39] Macdonald, J.R., Johanson, W.B. and Macdonald, J.R. (1987) Theory in Impedance Spectroscopy. John Wiley& Sons, New York.

[40] Sorkhabi, A.A. and Jeddi, N.G. (2005) Inhibition Effect of Polyethylene Glycol on the Corrosion of Carbon Steel in Sulphuric Acid. *Materials Chemistry and Physics*, **92**, 480-486. https://doi.org/10.1016/j.matchemphys.2005.01.059

[41] Trabanelli, G., Montecelli, C., Grassi, V. and Frignani, A. (2005) Electrochemical Study on Inhibitors of Rebar Corrosion in Carbonated Concrete. *Cement and Concrete Research*, **35**, 1804-1813. https://doi.org/10.1016/j.cemconres.2004.12.010

[42] Fouda, A.S., Ibrahim, H. and Atef, M. (2017) Adsorption and Inhibitive Properties of Sildenafil (Viagra) for Zinc in Hydrochloric Acid Solution. *Results in Physics*, **7**, 3408-3418. https://doi.org/10.1016/j.rinp.2017.08.012

[43] Rosliza, R. and Senin, H.B. (2008) The Effect of Inhibitor on the Corrosion of Aluminum Alloys in Acidic Solution. *Materials Chemistry and Physics*, **107**, 281-288. https://doi.org/10.1016/j.matchemphys.2007.07.013

[44] Lagrenee, M., Mernari, B., Bouanis, M.T., Traisnel, M. and Bentiss, F. (2002) Study of the Mechanism and Inhibiting Efficiency of 3,5-bis(4-methylthiophenyl)-4H-1,2,4-triazole on Mild Steel Corrosion in Acidic Media. *Corrosion Science*, **44**, 573-588. https://doi.org/10.1016/S0010-938X(01)00075-0

[45] McCafferty, E. (2005) Validation of Corrosion Rates Measured by the Tafel Extrapolation Method. *Corrosion Science*, **47**, 3202-3215. https://doi.org/10.1016/j.corsci.2005.05.046

[46] Wang, C.T., Chen, S.H. and Ma, H.Y. (2003) Protection of Copper Corrosion by Carbazole and N-Vinylcarbazole Self-Assembled Films in NaCl Solution. *Journal of Applied Electrochemistry*, **33**, 179-1862. https://doi.org/10.1023/A:1024097208128

[47] Khaled, K.F. (2008) Application of Electrochemical Frequency Modulation for Monitoring Corrosion and Corrosion Inhibition of Iron by Some Indole Derivatives in Molar Hydrochloric Acid. *Materials Chemistry and Physics*, **112**, 290-300. https://doi.org/10.1016/j.matchemphys.2008.05.056

[48] Eldesoky, A.M., Fouda, A.S. and Nabih, A. (2013) Inhibitive, Adsorption, Synergistic Studies on Copper Corrosion in Nitric Acid Solutions by Some Organic Derivatives. *Advances in Materials and Corrosion*, **2**, 1-15.

[49] Walaa, A.H. and Gaber, G. (2016) Studies of Corrosion and Electrochemical Behavior of Cu-Zn Alloys in H_2SO_4 and HNO_3 Acid Solutions. *Metallurgical Engineering*, **5**, 27-37. https://doi.org/10.14355/me.2016.05.003

[50] Tidblad, J., Kucera, V., Samie, F. and Das, S.N. (2007) Exposure Programme on Atmospheric Corrosion Effects of Acidifying Pollutants in Tropical and Subtropical Climates. *Water, Air, & Soil Pollution: Focus*, **7**, 241-247. https://doi.org/10.1007/s11267-006-9078-6

Water Pipes Corrosion Inhibitors for Q235 Steel in Hydrochloric Acid Medium Using Spiropyrazoles Derivatives

A. M. Eldesoky [1,2,*], Hala. M. Hassan [3,4], Abdu Subaihi [2] , Abeer El Shahawy [5,*] and Thoraya A. Farghaly [6,7]

1   Engineering Chemistry Department, High Institute of Engineering &Technology (New Damietta), New Damietta 34517, Egypt

2   Al-Qunfudah Center for Scientific Research (QCSR), Chemistry Department, Al-Qunfudah University College, Umm Al-Qura University, Al Qunfudhah 21912, Saudi Arabia; aasubaihi@uqu.edu.sa

3   Textile Technology Department, Industrial Education College, Beni-Suef University, Beni Suef 62511, Egypt; dr.halamahfooz@yahoo.com

4   Chemistry Department, Faculty of Science, Jazan University, Jizan 45142, Saudi Arabia

5   Department of Civil Engineering, Faculty of Engineering, Suez Canal University, Ismailia 41522, Egypt

6   Department of Chemistry, Faculty of Science, University of Cairo, Giza 12613, Egypt; thoraya-f@hotmail.com or tamohamed@uqu.edu.sa

7   Department of Chemistry, Faculty of Applied Science, Umm Al-Qura University, Makkah Almukkarramah 21955, Saudi Arabia

*   Correspondence: a.m.eldesoky79@hotmail.com (A.M.E.); abeer_shahawi@eng.suez.edu.eg (A.E.S.)

Abstract: Water pipes and drinking water quality deterioration in distribution systems and sea water desalination impose the use of corrosion inhibitors. The protective effect of spiropyrazole derivatives against Q235 steel and its adsorption performance were examined in solution of 1 M HCl utilizing TP (Tafel polarization), electrochemical frequency modulation (EFM), and electrochemical impedance spectroscopy (EIS) tests. The outcome data from hindrance efficiency rise with the dose of inhibitor. The orders of %IE of spiropyrazole derivatives are given: (1) > (2) > (3).It was noted that the values of E_{HOMO} and E_{LUMO} dropping in order run parallel to the improvement in %IE, which support the preceding order. EIS spectra exhibited one capacitive loop and approve the protective ability. Molecular docking was utilized to get a full picture on the binding mode among spiropyrazoles derivatives and the receptor of 3tt8-hormone of crystal structure examination of Cu human insulin derivative. The morphology of protected Q235 steel was evaluated by checking electron magnifying instrument innovation with energy dispersive X-beam spectroscopy (SEM–EDX).

Keywords: spiropyrazoles; 3tt8-hormone; Q235 steel; SEM–EDX; molecular docking

1. Introduction

Corrosion in distribution systems pipes resulted in not only pipe material destruction, but also deterioration in drinking water quality, i.e., water infection with other wastewater or any other water. Which leads to corrosion of valves or pumps in addition to blockage in pipes as a result of solid corrosion products.Unwanted chemical and biochemical reactions that occur in the distribution systems that release iron into distributed water can accumulate, creating tubers [1]. Corrosion measurements (tubers) consist of reactive types that modify the physical and chemical parameters of water in the distribution system not only by releasing Fe oxyhydroxides, but also by interactions, for example, with by-products of chlorinated disinfection [2], nitrates, or with natural organic substance [3]. Salinity

(chloride) is one of the most aggressive substances in seawater. Oxygen in seawater also affects metal pipes corrosion rate. Moreover, the amount of oxygen affected with the temperature, and consequently influences the rate of corrosion [4].

Salts in the sea water cause corrosion inside the surfaces of pipes that transport saltwater in desalination water treatment plants. Also, the existence of air, salts on the ground, moisture, and other factors lead to outside pipe corrosion in the form of small holes or rough surface.

In any case, corrosion causes a short lifetime of the pipe, hydraulic effects, aesthetic effects, including increasing pumping costs, water leaks, and the buildup of corrosion products. Pipe replacement is not possible due to the high cost, so it is necessary to isolate pipe material from water and any corrosive agents [5].

Corrosion inhibitors are largely utilized as a part of industry, as for instance, corrosive pickling of steel and iron, overflow cleaning and preparing, generation of metal and well oil fermentation [6–8]. Improving the acidic environment needed the progress of altered corrosion control tests among which the implementation of chemical restraints has been the most economical test for the hindrance corrosion of acid [9–14]. Several organic composites, such as heterocyclic assembled, acetylenic alcohol, and quaternary ammonium salts are normally utilized as inhibitors in altered industries. The selected atoms adsorbed on the surface of metal among hetero atoms which include N, S, and O due to its protection for the active centers and to form a physical barrier to lowering the transmit of erosion sample to the metal surface [15–21]. The heterocyclic affluences containing nitrogen atoms, like 4-aminoantipyrine (pyrazole derivative) are excellent corrosion hindrance with corrosive solution because rise hindrance of corrosion and prevent the odor irritating for alloys in altered aggressive environment [22–27]. Therefore, the development of novel adjuster inhibitors consisting of a pyrazol ring and the study of the relations among the inhibitors chemical structure and their inhibition led to the greater significance in theoretical points and industrial application.

In this study, the hindrance effect and electrochemical habit of spiropyrazole products for Q235 steel including 1.0 M HCl are given by the TP, EIS) and EFM tests. A few quantum-chemistry tests and molecular docking have been conducted in order to record the inhibition protection to the molecular properties of the altered kind of assembled [28,29].

2. Experimental

2.1. Measurements

This research mimics the actual docking process in which measuring interaction energies of the ligand–protein pair-wise through Docking Server [30]. Docking computations were carried out on a spiropyrazoles protein model. Kollman united atom kind charges, Essential hydrogen atoms, and solvation parameters were additional with the support of AutoDock tools [31]. Affinity (grid) maps of $20 \times 20 \times 20$ Å grid points and 0.375 Å spacing were generated utilizing the program Autogrid [32].

2.2. Material and Medium

Q235 steel was utilized for the measurements of corrosion. Its % conformation is 0.16 C, 0.30 Si, 0.53 Mn, 0.055 S, 0.045 P, the rest iron. The corrosion dose (HCl 1.0 M) (37% analytical grade). The structure of spiropyrazole derivatives utilized for this paper are given in Table 1 [33].

Table 1. Molecular formulas and structure of spiropyrazoles products.

Cpd. No.	Name	Structure	Molecular Weight &Chemical Formula
(1)	2′,3′,6,7,8,9-Hexahydro-2′-phenyl-5′-styryl-3′-(3,4,5-trimethoxy-phenyl) spiro[benzocyclo–heptane-6(5H), 4′(4H-pyrazol)-5-one		$C_{36}H_{34}N_2O_4$ (558.25)
(2)	3′-(3,4-Dimethoxyphenyl)-2′,3′,6,7,8,9–hexahydro-2′-phenyl-5′-styrylspiro [benzocyclo– heptane–6(5H), 4′(4H-pyrazol)-5-one		$C_{35}H_{32}N_2O_3$ (528.24)
(3)	3′-(4-Chlorophenyl)-2′,3′,6,7,8,9-hexahydro-2′-phenyl-5′-styryl-spiro [benzocycloheptene-6(5H), 4′(4H-pyrazol)-5-one		$C_{33}H_{27}ClN_2O$ (502.18)

2.3. Methods

2.3.1. Electrochemical Tests

Electrochemical tests were performed utilizing three thermostat electrodes cell for the electrode cell using a Gamrypotentiostat/galvanostat/ZRA (model PCI300/4). A saturated platinum and calomel electrode were utilized as auxiliary and reference electrodes. All tests were done at the temperature of 25 ± 1 °C. The measurements of potentiodynamic bends were from −50 to 50 V at a rate scan 1 mV S^{-1} after the steady state is approximated (30 min) and the OCP was detected after the electrode was putted for 15 min in the solution test.

The two tests, EFM and EIS were carried out as before with the system of a Gamry framework rely on ESA400. Echem Analyst 5.5 Software was utilized for graphing, drawing, and fitting value. EIS tests were done in a range of frequency of 100 kHz to 10 mHz with amplitude of 5 mV signal-to-signal ac peaks utilized at respective for corrosion potential. EFM had used 2 frequencies 2 and 5 Hz. The frequency base was 1 Hz.

2.3.2. SEM-EDX Tests

The surface of Q235 steel was gotten by observance the coins for 3 days dipping in 1 M HCl existence and lack of seamless dose of spiropyrazoles derivatives. Then, after this time dipping, the coins were lotion gently with water distilled. The surface of alloy was tested utilized an X-ray diffractometer Philips (pw-1390) with Cu-tube (CuKα, l = 1.54051 Å), (SEM, JOEL, JSM-T20, Tokyo, Japan).

2.3.3. Theoretical Study

Accelrys (Material Studio Version 4.4) software for quantum chemical measurements has been utilized.

3. Results and Discussion

3.1. TP Tests

TP tests were conducted to obtain information regarding the kinetics of the anodic and cathodic reactions. Figure 1 demonstrations the TP performance of Q235 steel electrode in corrosive solution nonexistence and attendance unlike dose of spiropyrazoles derivatives (1). Figure 1 shows that the %IE$_p$ rise as the spiropyrazoles dose rise, while the cathodic reaction is efficient protective, i.e., the adding of spiropyrazoles decrease the anodic liquefaction of alloyand also hindrance the cathodic reactions. Therefore, spiropyrazoles are acts as mixed kind inhibitors.

The (θ) and %IE were measured from relation (1):

$$\%IE_p = \theta \times 100 = [1 - (i^0{}_{corr}/i_{corr})] \times 100 \tag{1}$$

where $i^0{}_{corr}$ and i_{corr} are the current lack and attendance of solution inhibitor, consecutively.

It is evident from Table 2 that the adsorbed inhibitors lessened the surface area for corrosion without effect on the mechanism of alloy corrosion in acidic solution [34,35]. The orders of IE% were: (1) > (2) > (3).

Table 2. Impact of spiropyrazoles derivatives for Q235 steel in in corrosive environments attendance and lack of unlike dose of spiropyrazoles.

Cpd. No.	Conc., M.	$-E_{corr}$ (mV vs. SCE)	$i_{corr} \times 10^{-5}$ (μA cm^{-2})	$\beta_a \times 10^{-3}$ (mV dec^{-1})	$\beta_c \times 10^{-3}$ (mV dec^{-1})	θ	%IE
–	Blank	489	5.02	106	145	–	–
(1)	1×10^{-6}	459	1.3	60	132	0.741	74.1
	3×10^{-6}	469	1.28	91	198	0.745	74.5
	5×10^{-6}	493	1.26	99	152	0.749	74.9
	7×10^{-6}	479	1.24	77	119	0.753	75.3
	9×10^{-6}	488	1.19	79	159	0.7629	76.29
	11×10^{-6}	467	1.05	104	146	0.7908	79.08
(2)	1×10^{-6}	457	1.51	34	56	0.6992	69.92
	3×10^{-6}	491	1.48	87	123	0.7052	70.52
	5×10^{-6}	466	1.45	53	135	0.7112	71.12
	7×10^{-6}	487	1.37	83	121	0.7271	72.71
	9×10^{-6}	458	1.35	62	115	0.7311	73.11
	11×10^{-6}	489	1.25	107	156	0.751	75.1
(3)	1×10^{-6}	439	2.4	52	127	0.5219	52.19
	3×10^{-6}	481	2.05	79	143	0.5916	59.16
	5×10^{-6}	483	1.92	84	129	0.6175	61.75
	7×10^{-6}	462	1.73	67	143	0.6554	65.54
	9×10^{-6}	461	1.64	58	117	0.6733	67.33
	11×10^{-6}	480	1.48	69	123	0.7052	70.52
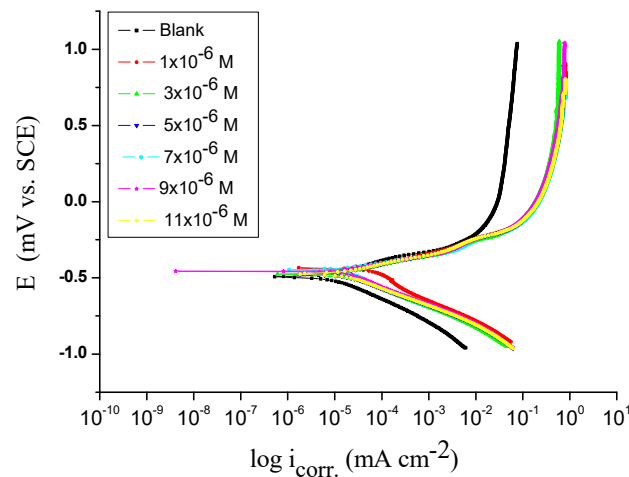
Figure 1. TP diagrams for the corrosion of Q235 steel in corrosive environments in the presence and lack of unlike dose of spiropyrazoles (1) at 25 ± 0.1 °C.

3.2. EIS Tests

One of the most effective tests in corrosion study is EIS. The properties of mechanical materials for surface and electrode motility can be obtained using impedance diagrams [36–40]. Figure 2 illustrated Nyquist (a) and Bode (b) bends given at OCP both in lack and attendance of improving dose of spiropyrazole derivatives. The values from EIS tests for a Q235 steel electrode were given utilizing the equivalent circuit demonstrated in Figure 3.The improvement in the size of the capacitive loop with the attachment of spiropyrazole derivatives demonstrate that a barrier gradually forms on the surface of metal [41,42]. The higher in the size of capacitive loop Figure 2 aimproves, at a fixed inhibitor dose, conformed the order: (1) > (2) > (3). The C_{dl} is measured from Equation (2):

$$C_{dl} = Y_o\ \omega^{n-1}/\sin[n(\pi/2)] \tag{2}$$

where $\omega = 2\pi f_{max}$, f_{max} = the maximum frequency.

After EIS exam the figure of the Nyquist bends, the corrosion procedure was measured principally charged-transfer [43–46]. From Table 3 for the EIS data, we distinguished that the results of Rct improve with increasing the dose of spiropyrazoles and this result in improving in %IE. Data of Cdl are also minor to the maximum spiropyrazole inhibitor range [47,48]. The main merits of EIS are to monitor the corrosion performance of the metal with constant time. The %IEEIS was gotten from the EIS data from Equation (3) [49]:

$$\%IE_{EIS} = [1 - (R^{\circ}_{ct}/R_{ct})] \times 100 \tag{3}$$

where R°_{ct} and R_{ct} are the resistance values existence and lack of spiropyrazole, consecutively.
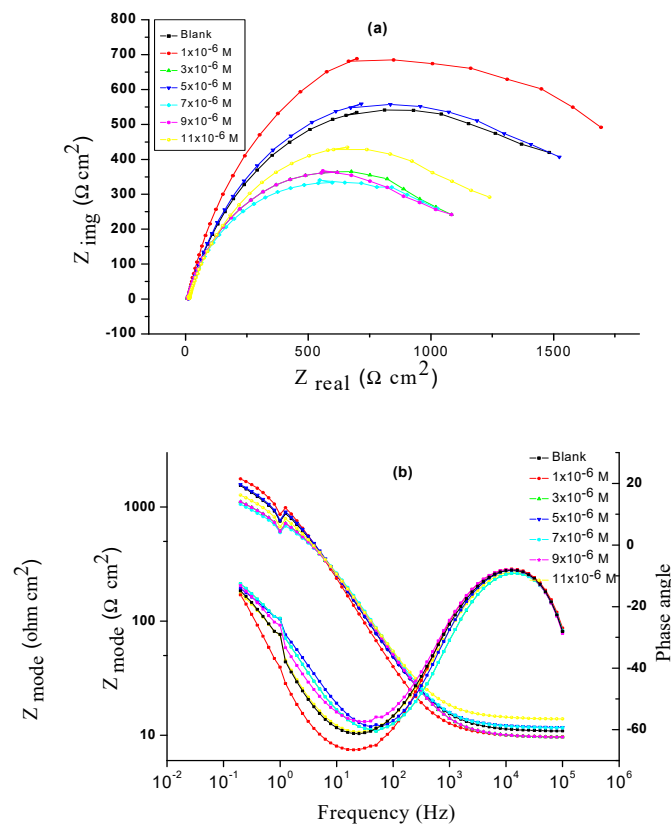
Figure 2. EIS Nyquist (**a**) and Bode diagrams (**b**) for the corrosion of Q235 steel inattendance and lack of unlike dose of compound (1) at 25 ± 0.1 °C.
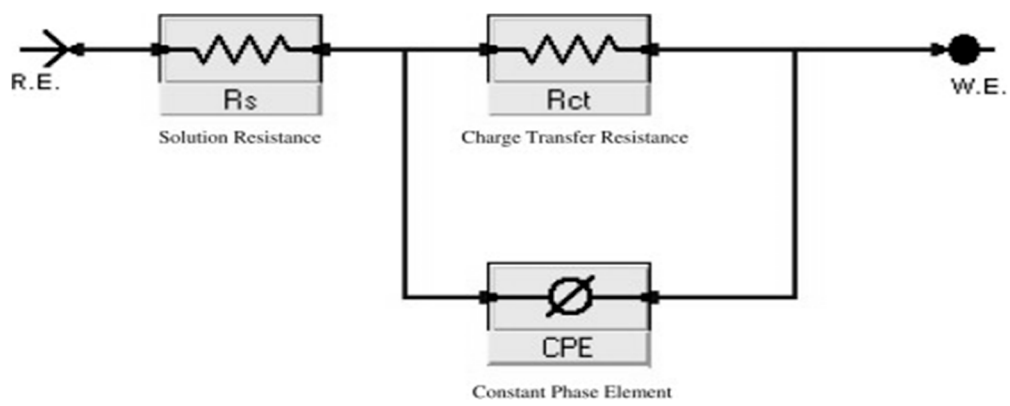
Figure 3. Equivalent circuit utilized to fit EIS data.

Table 3. Parameters given by EIS test for Q235 steel in corrosive environments attendance and lack of unlike dose of spiropyrazoles derivatives.

Cpd. No.	Conc., M.	$R_S \times 10^{-3}$ (Ω cm^2)	$Y_o \times 10^{-6}$	$n \times 10^{-3}$	$R_{ct} \times 10^{-3}$ (Ω cm^2)	$C_{dl} \times 10^{-5}$ (μFcm^{-2})	θ	IE
–	Blank	11.1	18.2	1.01	36.9	8.93	–	–
(1)	1×10^{-6}	9.7	12.6	1.03	178	1.24	0.793	79.3
	3×10^{-6}	9.7	12.2	1.04	179	1.23	0.794	79.4
	5×10^{-6}	10.8	12.7	1.12	194.7	1.22	0.81	81
	7×10^{-6}	10.6	16.8	1.05	220.1	1.29	0.832	83.2
	9×10^{-6}	9.6	16.3	1.07	361.7	1.2	0.898	89.8
	11×10^{-6}	9.7	12.3	1.06	428.1	1.19	0.914	91.4
(2)	1×10^{-6}	9.6	9	1.05	78.61	1.67	0.531	53.1
	3×10^{-6}	11.4	18.3	1.03	105.3	1.31	0.65	65
	5×10^{-6}	13.9	13	1.05	112.3	1.3	0.671	67.1
	7×10^{-6}	15.9	19.8	1.12	119.5	1.29	0.691	69.1
	9×10^{-6}	9.7	12.6	1.04	123.2	1.26	0.7	70
	11×10^{-6}	11.1	19	1.06	134.2	1.25	0.725	72.5
(3)	1×10^{-6}	10	27.6	1.01	42.13	6.24	0.124	12.4
	3×10^{-6}	9.5	13.7	1.02	49.85	2.75	0.26	26
	5×10^{-6}	11.89	18.15	1.05	55.28	1.98	0.332	33.2
	7×10^{-6}	13.37	11.98	1.03	66.76	1.9	0.447	44.7
	9×10^{-6}	9.5	12.99	1.02	67.12	1.83	0.45	45
	11×10^{-6}	13.81	12.98	1.06	77.56	1.7	0.524	52.4

3.3. The Method of EFM

The advantages of EFM test gotten it a perfect for online monitoring of corrosion [50]. The data of EFM in corrosive environments existance and lack of unlike dose of spiropyrazoles was obtain in Figure 4. The results of EFM-tests were applied two unlike models: diffusion complete control of the cathodic reaction was quantified by and the "activation" model [51]. The (i_{corr}), (CF-2 and CF-3), and (βc and βa) were quantified by the higher peaks. The preferable data of CF-2 and CF-3 in Table 4 are parallel to their theoretical numbers of 2.0 and 3.0, individually result in excellent quality of the measured data.

The %IE$_{EFM}$ raising by improvement the inhibitor dose and was calculated from Equation (4):

$$\%IE_{EFM} = [1 - (i_{corr}i^o{}_{corr})] \times 100 \qquad (4)$$

where $i^o{}_{corr}$ and i_{corr} are current attendance and lack of spiropyrazoles, consecutively.

The order of %IE$_{EFM}$: (1) > (2) > (3).
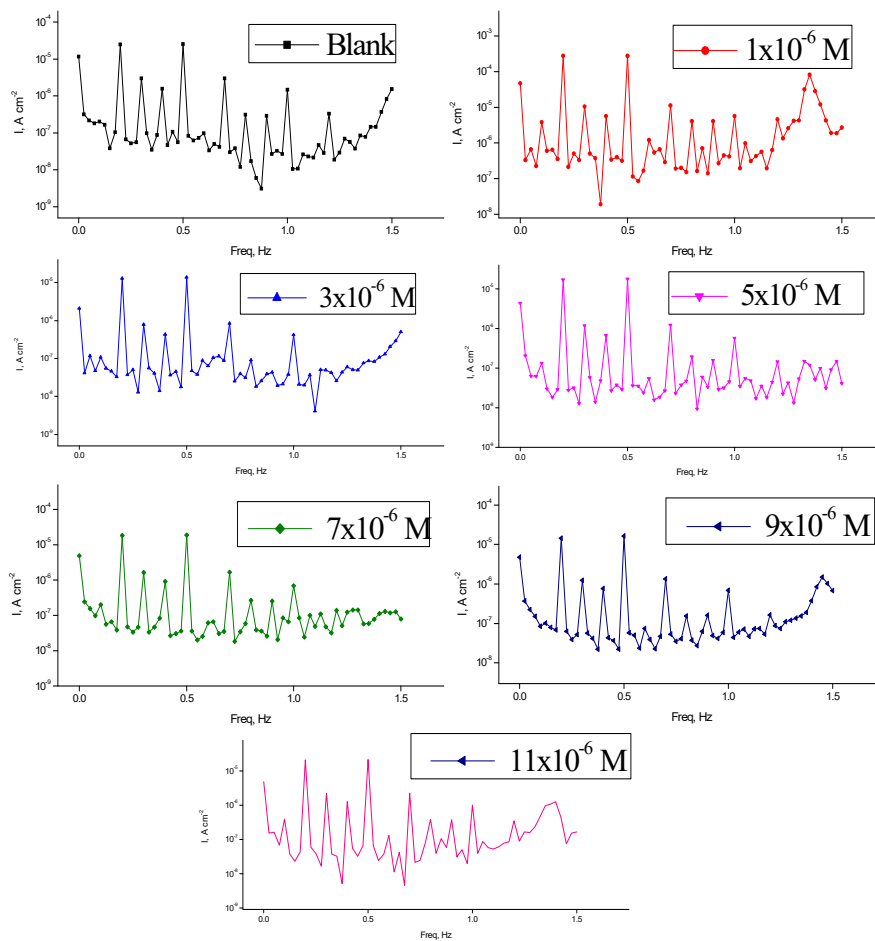
Figure 4. EFM bends for the corrosion of Q235 steel in corrosive environments attendance and lack of unlike dose of spiropyrazoles (1).

Table 4. EFM parameters for Q235 steel in corrosive environments attendance and lack of unlike dose of spiropyrazoles derivatives at 25 ± 1 °C.

| Cpd. No.	Conc., M.	i_{corr} $(\mu A\ cm^{-2})$	$\beta_a \times 10^{-3}$ $(mV\ dec^{-1})$	$\beta_c \times 10^{-3}$ $(mV\ dec^{-1})$	CF-2	CF-3	θ	%IE
–	Blank	58.04	98	331	2.02	2.87	–	–
(1)	1×10^{-6}	21.99	88	350	1.94	2.95	0.6211	62.11
	3×10^{-6}	19.09	82	129	1.89	2.9	0.6711	67.11
	5×10^{-6}	15.29	87	146	1.85	3.02	0.7366	73.66
	7×10^{-6}	14.91	74	105	1.87	3.12	0.7431	74.31
	9×10^{-6}	11.48	46	49	1.89	3.01	0.8022	80.22
	11×10^{-6}	9.33	55	71	2.01	2.74	0.8392	83.92
(2)	1×10^{-6}	32.5	97	193	1.99	2.89	0.44	44
	3×10^{-6}	31.02	121	227	2.02	2.87	0.4655	46.55
	5×10^{-6}	28.8	79	90	2.02	2.91	0.5038	50.38
	7×10^{-6}	28.03	91	195	1.97	3	0.5171	51.71
	9×10^{-6}	27.04	92	165	1.87	2.91	0.5341	53.41
	11×10^{-6}	25.36	84	162	1.93	3.05	0.5631	56.31
(3)	1×10^{-6}	38.22	86	108	1.97	3.08	0.3415	34.15
	3×10^{-6}	37.55	141	298	1.92	2.87	0.353	35.3
	5×10^{-6}	36.32	106	190	1.89	3.14	0.3742	37.42
	7×10^{-6}	35.12	93	189	2.08	3.04	0.3949	39.49
	9×10^{-6}	33.04	105	227	1.83	3.02	0.4307	43.07
	11×10^{-6}	30.34	76	148	1.76	2.78	0.4773	47.73

3.4. Molecular Docking

The docking study presented a favorable contact among spiropyrazoles derivatives and the receptor of 3tt8-hormone of crystal structure analysis of Cu human insulin derivative. The energy calculated is recorded in Table 5 and Figure 5. According to the outcome data in this study, HB diagrams specified that the spiropyrazoles derivatives bind to the proteins via hydrogen bond and disintegrated interactions energies in kcal/mol existed among the spiropyrazoles derivatives with 3tt8 receptor as exposed in Figure 6. Also, based on this value, it can propose that interaction among the 3tt8 receptor and the spiropyrazoles is possible [52]. Further, 2D plot bends of docking with spiropyrazole products are displayed in Figure 7.

Table 5. Energy data gotten in docking measurements of spiropyrazoles derivatives with 3tt8 receptor.

Cpd. No.	Est. Free Energy of Binding (kcal/mol)	Est. Inhibition Constant (K_i) (µM)	vdW+ bond+ Desolve Energy (kcal/mol)	Electrostatic Energy (kcal/mol)	Total Intercooled Energy (kcal/mol)	Interact Surface
(1)	−5.06	193.78	−6.45	−0.03	−6.48	640.460
(2)	−4.92	247.10	−6.57	+0.01	−6.56	594.819
(3)	−6.36	21.62	−7.32	−0.01	−7.33	611.749

Cpd. No.	(A)	(B)
(1)		
(2)		

Figure 5. *Cont.*

(3)
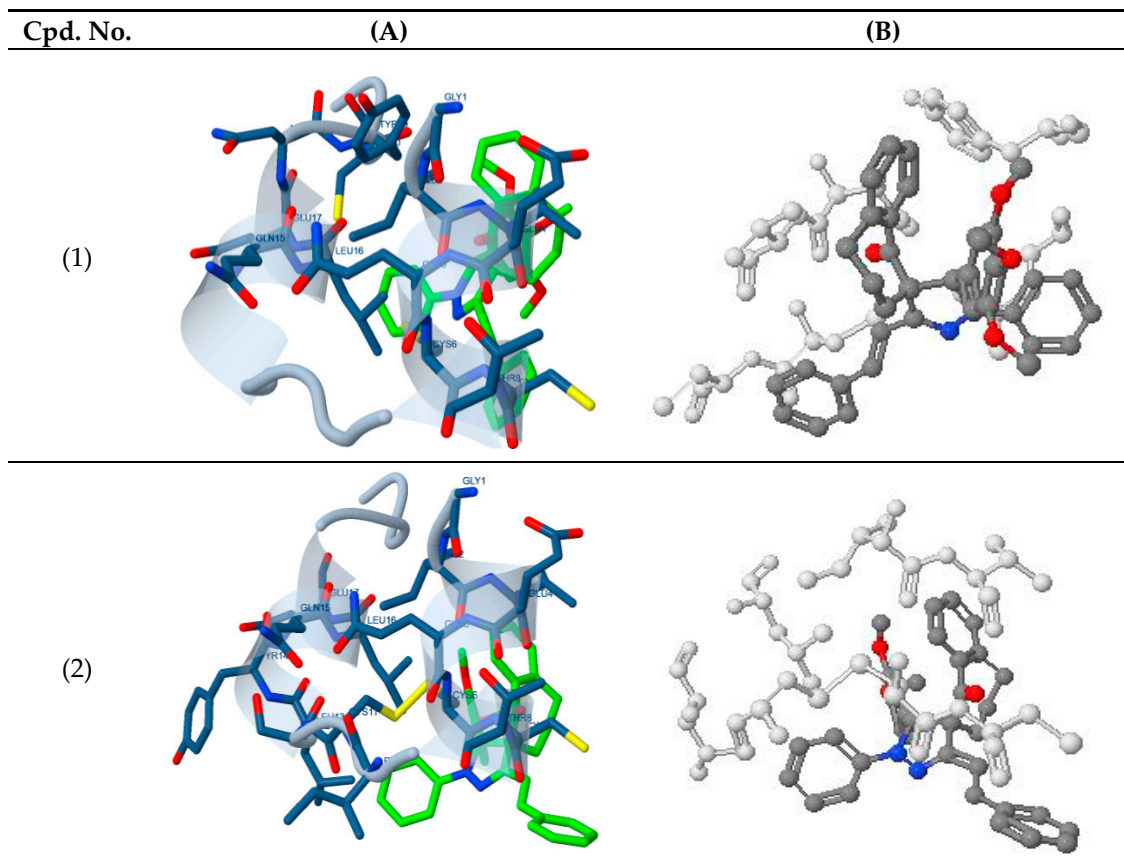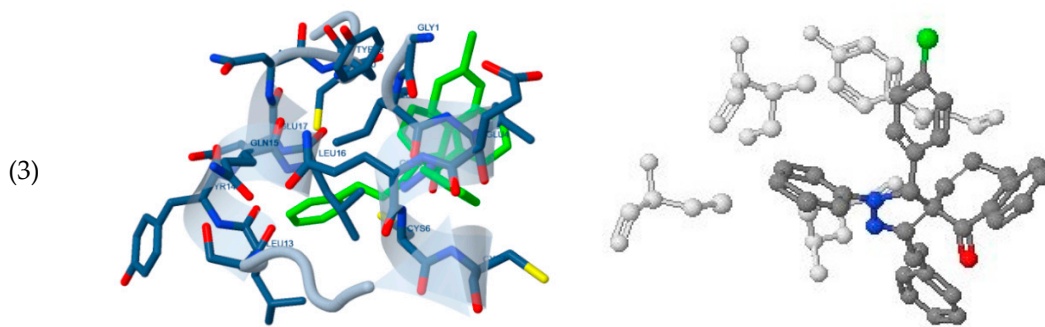
Figure 5. Spiropyrazoles derivatives (green in (**A**) and gray in (**B**)) in interaction with 3tt8 receptor. (For interpretation of the references to color in this figure legend, the reader is referred to the web version of this article).

Compound (1)

Compound (2)

Figure 6. *Cont.*

Compound (3)
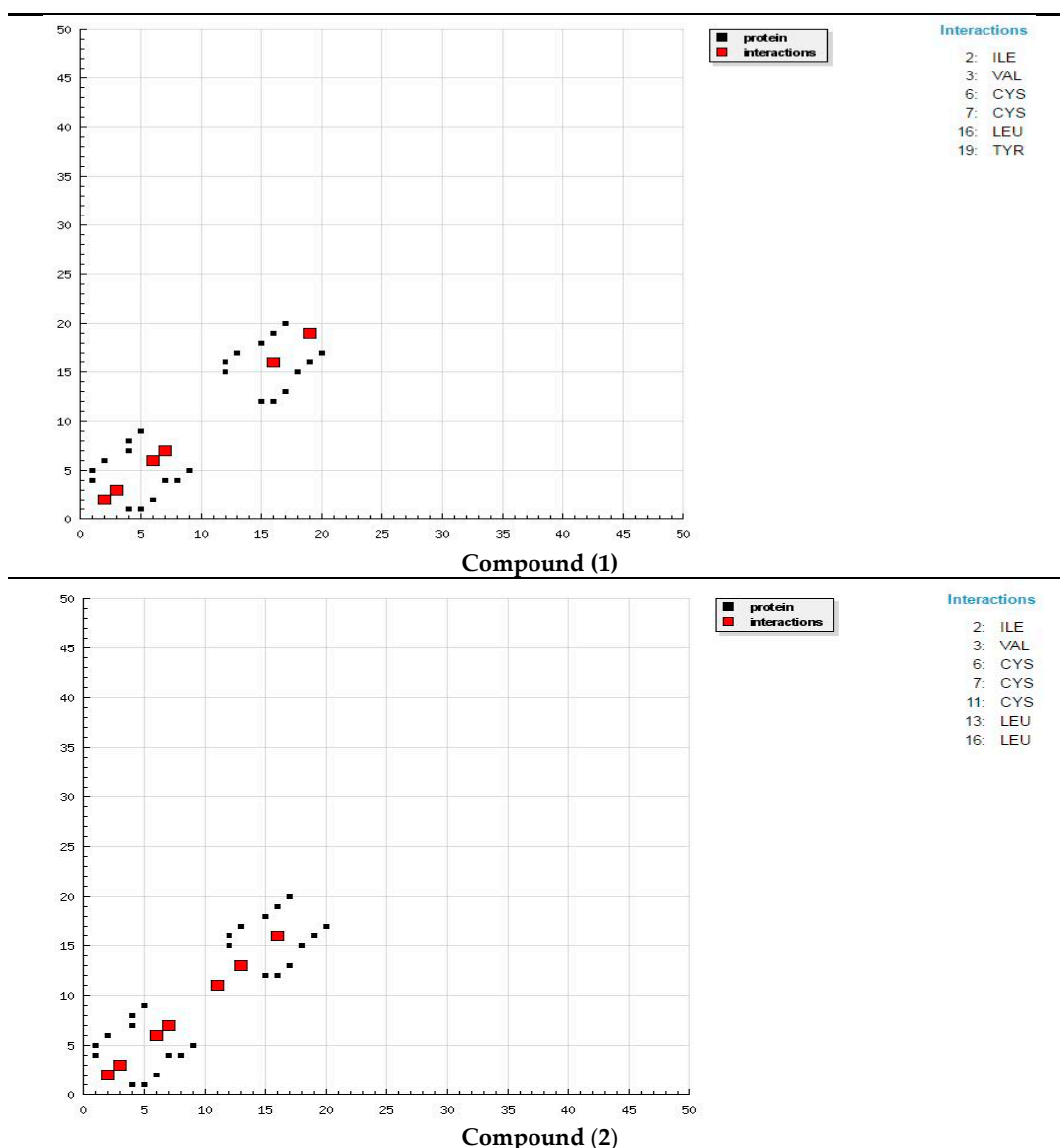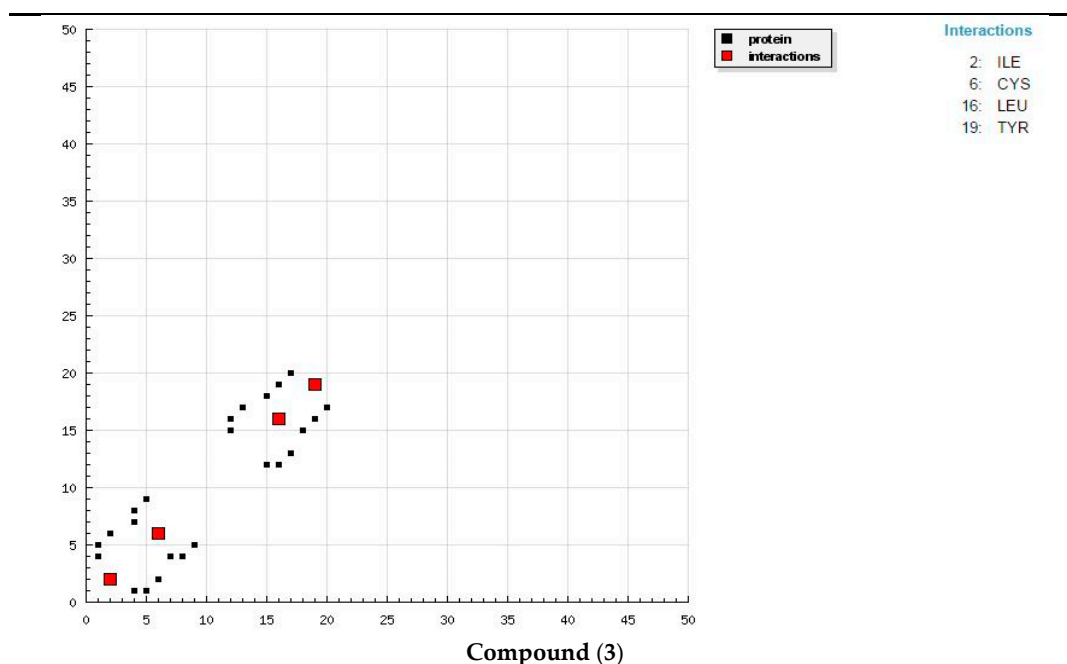
Figure 6. HB plot of interaction between spiropyrazoles products with receptor of breast cancer mutant 3tt8.
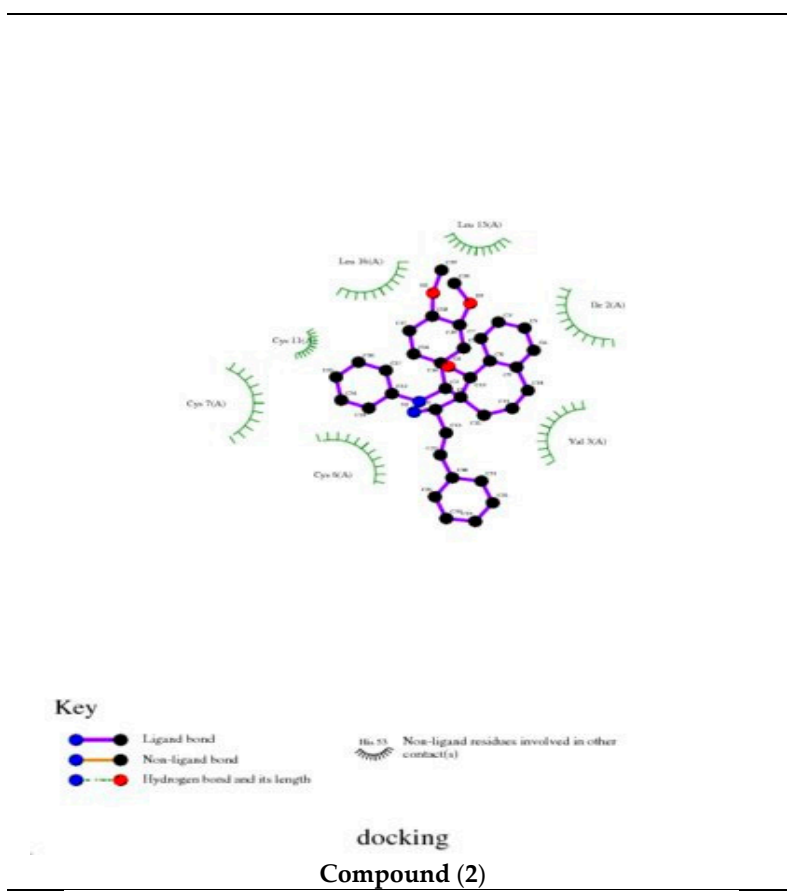

docking

Compound (1)

Figure 7. *Cont.*

docking
Compound (2)

docking
Compound (3)
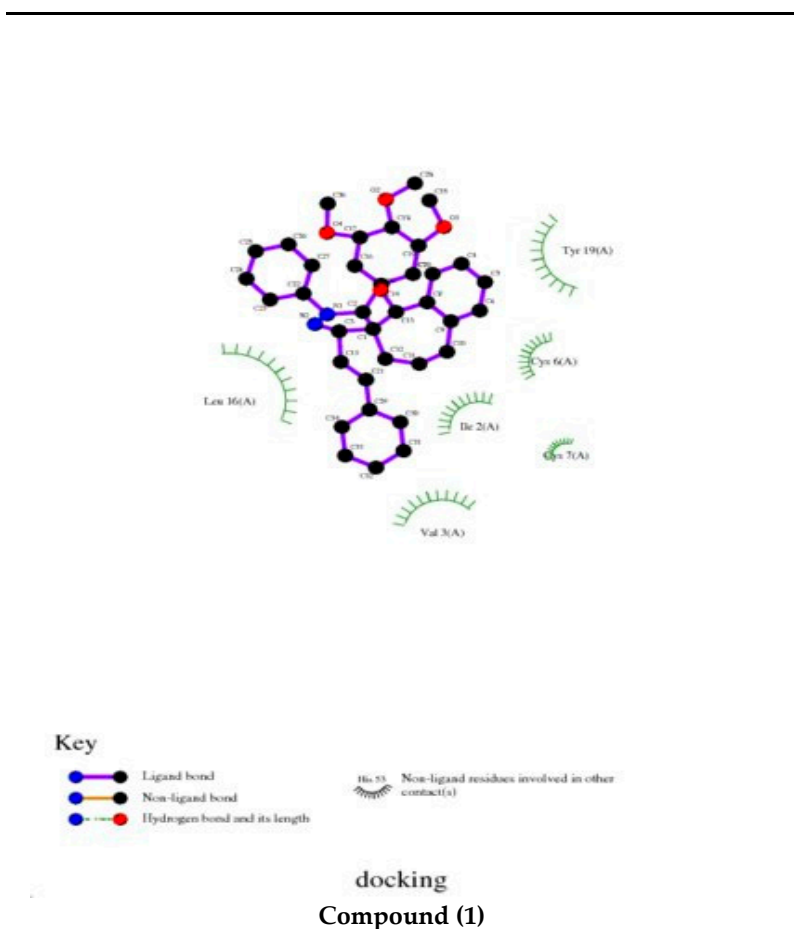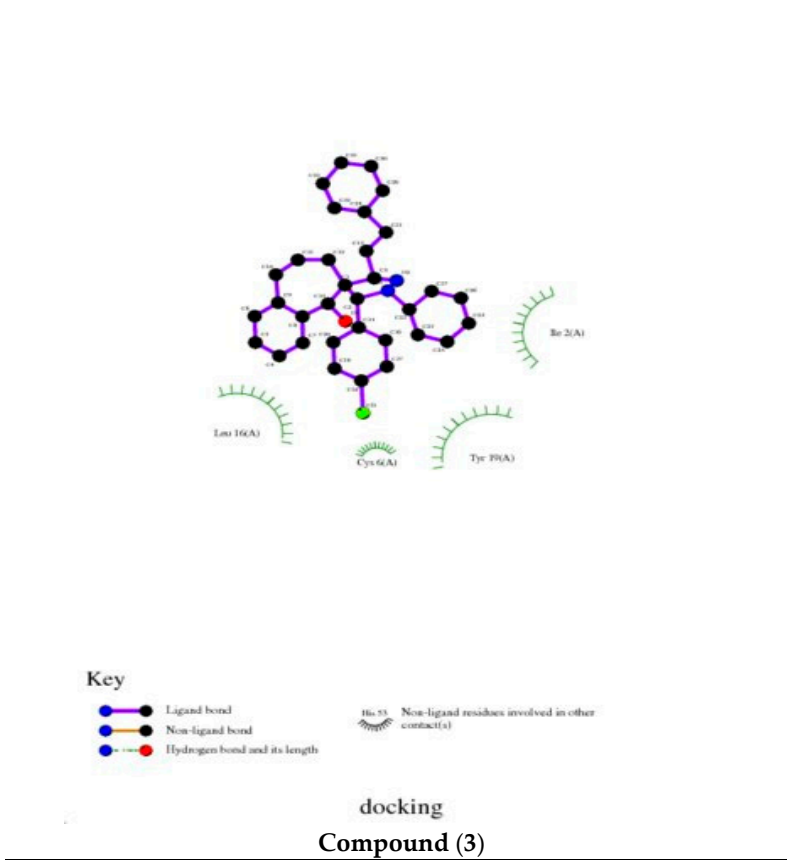
Figure 7. 2D plot of interaction among spiropyrazoles products with 3tt8 receptor.

3.5. SEM Tests

The SEM test gotten from coins of Q235 steel existence and lack of 11×10^{-6} M spiropyrazoles products after dipping for three days obtain in Figure 8. The surfaces suffer from damaged corrosion attack in the blank. Due to the stress out when the composite appending in the solution, the morphology of the tests free surfaces was smoother. We observed a film creation which distributed in a random way on the whole surface of Q235 steel. This may be understood as being due to the spiropyrazole products adsorbed of the on Q235 steel which block the active center on alloy. This causes less contact among alloys and the aggressive enlivenments, and sequentially gives best protection effect [53,54].
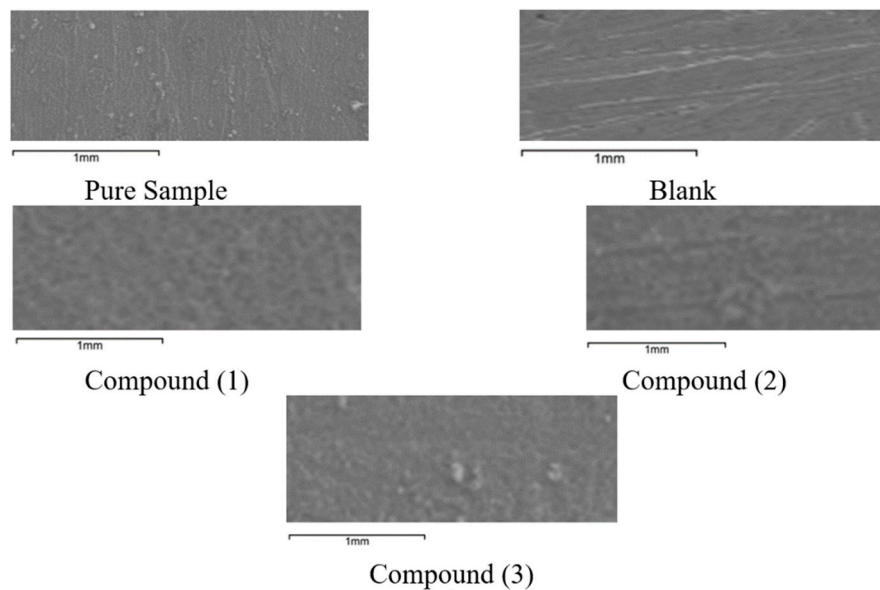
Figure 8. SEM images of Q235 steel in corrosive environments attendance and lack of unlike dose of 11×10^{-6} M spiropyrazoles.

3.6. EDS Test

The EDS tests were applied to measure the elements obtain on the surface of Q235 steel and after 3 days of coated in the lack and attendance of corrosive solution. Figure 9 gives the EDS data from the composition of Q235 steel only without the acid and presence spiropyrazoles. The EDS show that only oxygen and iron were detected, and the film passive was obtained with only Fe_2O_3.

The spectra give added lines, lead to the existence of C (C atoms of spiropyrazoles products). These data provide that the O and C atoms enclosed surface. The elemental detected is listed in Table 6.
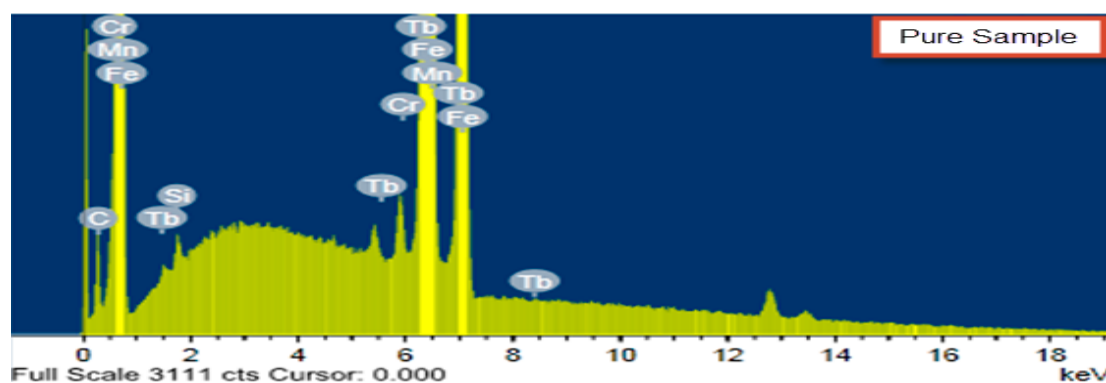
Figure 9. *Cont.*
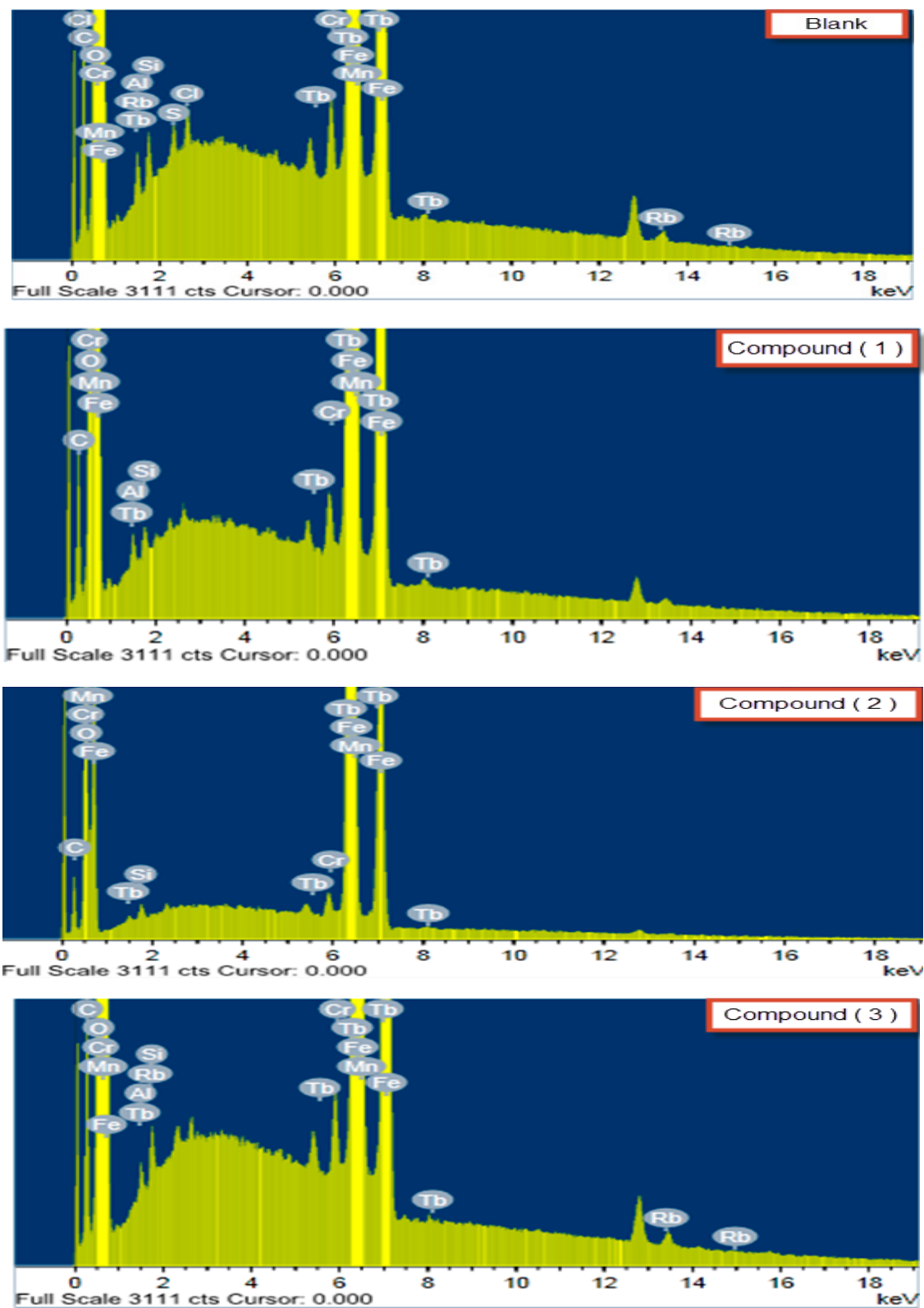
Figure 9. EDS study of Q235 steel after 3 days in corrosive environments attendance and lack of unlike dose of 11×10^{-6} M spiropyrazoles.

Table 6. Mass % of Q235 steel after 3 days in corrosive environments attendance and lack of unlike dose of 11×10^{-6} M spiropyrazoles.

(Mass %)	C	O	Al	Si	S	Cl	Cr	Mn	Fe	Rb	Tb
Pure Sample	7.08	–	0.28	0.27	–	–	0.24	0.46	87.14	–	4.53
Blank	11.98	17.64	0.29	0.30	0.14	0.18	0.19	0.39	65.54	0.46	2.89
Compound (1)	13.05	14.03	0.31	0.23	–	–	0.20	o.43	67.56	–	4.19
Compound (2)	12.68	16.99	0.01	0.26	–	–	0.19	0.41	65.70	–	3.76
Compound (3)	12.53	16.07	0.23	0.28	–	0.03	0.18	0.40	65.68	0.73	3.87

3.7. Quantum Chemical Calculations

The Mulliken charges and molecular orbital bends of spiropyrazole products given in Figure 10. Theoretical tests were obtained for only the forms of neutral, in order to gotten further insight into the experimental results. Data of quantum chemical chief to ΔE and E_{HOMO} and E_{LUMO} are measured and listed in Table 7. The improved or lesser negative E_{HOMO} is inhibitor related, the higher the trend of offering electrons to unoccupied d orbital of Q235 steel, and the progress of the corrosion hindrance. The lesser E_{LUMO}, the greater the acceptance of plain electrons from surface of Q235 steel [55,56]. ΔE assumed by the tests in case of spiropyrazole (1) is less than (3) (Table 7) given spiropyrazole (1) molecule will absorb more highest on alloy surface than others, due to electron easy transfer between HOMO and LUMO occurred among its adsorption on the surface of Q235 steel and the maximum of hindrance productivity [57]. It can be seen that all tests of quantum checking these results from experimental.

Inhibitors	HOMO	LUMO	Molecular Structure
(1)			
(2)			
(3)			
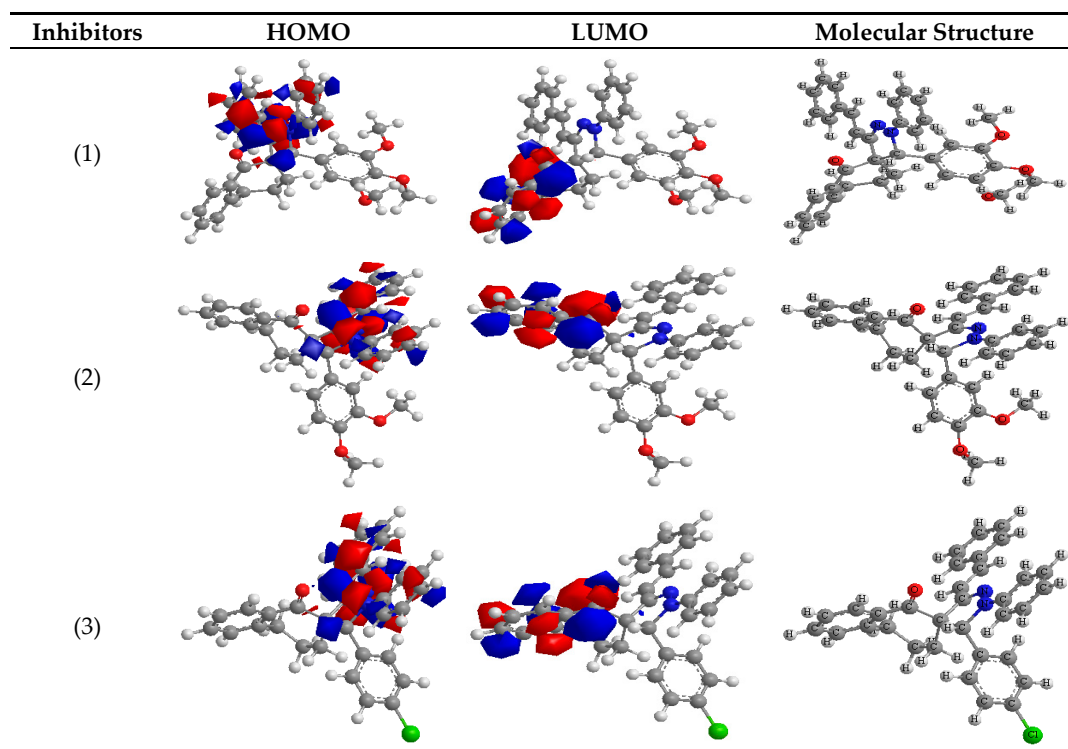
Figure 10. Molecular orbital bends of study spiropyrazoles.

Table 7. The measured quantum chemical propertiesfor spiropyrazoles products.

Quantum Chemical Properties	(1)	(2)	(3)
$-E_{HOMO}$ (eV)	8.006	8.007	8.021
$-E_{LUMO}$ (eV)	4.318	4.317	4.309
ΔE (eV)	3.688	3.690	3.712
η (eV)	1.844	1.845	1.856
σ (eV)$^{-1}$	0.542	0.542	6.165
$-Pi$ (a.u)	6.162	6.162	0.538
χ (eV)	6.162	6.162	6.165
S (eV)$^{-1}$	0.271	0.271	0.269
ω (a.u)	3.081	3.081	3.0825
ΔN_{max}	3.341	3.339	3.321

3.8. Mechanism of Protection

From the results of electrochemical tests, the IE% relies on metal nature, dose, surface conditions, and the kind of spiropyrazole derivatives adsorption on Q235-steel.

The outcome data of corrosion data attendance of these inhibitors:

- With an increase in the dose of the inhibitor, the corrosion rate becomes lower
- The exchange in Tafel lines to extreme regions of potential.
- The %IE relies on excharge density and their equipment of adsorption centers in the molecule.

Metals such as iron, which are highly attractive to aromatic rings, were gotten to adsorb benzene rings in a flat direction. The order of breakdown of the %IE of the spiropyrazoles in the corrosion solution was in the following order: (1) > (2) > (3).

Spiropyrazoles (1) demonstrations best hindrance power because: (i) it has greater molecular size (558.25) that may enable best surface coated and bigger molecular area and (ii) its adsorption among 6 active sites (2-N and 4-O atoms). Spiropyrazoles (2) comes after (1) in %IE because it has fewer molecular size (528.24) and minus active site (1-O and 2-N atoms). Spiropyrazoles (3) is the smallest one in %IE, this is due to it having a minor molecular size (502.18), the appending of p-Cl group is electron withdrawing group with (σ Cl = +0.23), and its order of protection relies on the magnitude of their withdrawing character.

Concentration of the inhibitor is an important factor in adsorption. As illustrated in Figure 11, at the adsorption density less than monolayer (Figure 11a), most of the nucleus sites are still likely to be exposed to hydrochloric acid, as the inhibitor absorbs them less. When the adsorption intensity reaches monolayer adsorption (Figure 11b), some nucleus sites begin to cover with the barrier particles. At the maximum absorption density (Figure 11c), the inhibitor particles cover the entire surface, including the sites of the nucleus, and then complete inhibition occurs.
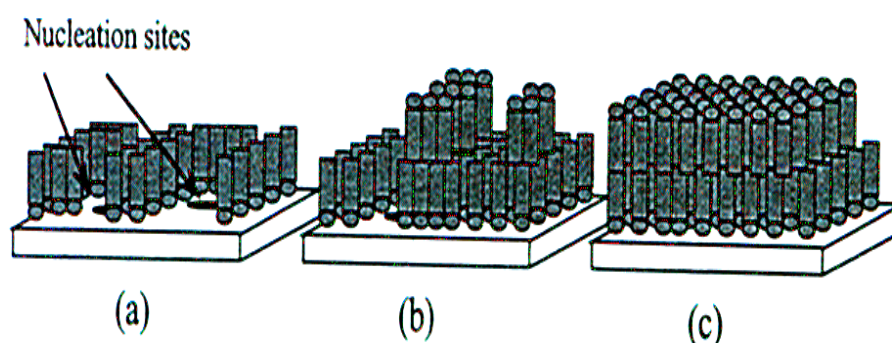
Figure 11. Adsorption diagrams for spiropyrazoles additives as inhibitors at: (**a**) Low concentration, (**b**) intermediate concentration, (**c**) high concentration on Q235 steel.

3.9. Conclusions

- All the spiropyrazole products are potentially brilliant corrosion inhibitors for Q235 steel. The structures of these spiropyrazole inhibtors as well as the presence of certain substituents play a vital role on their effectiveness anticorrosive agents.

- The results of EIS display enhancement in the charge transfer resistance and a decline in double layer capacitances. When adding an inhibitor and thus an increase in% IE due to an increase in the electrical double layer the thickness.

- The outcome values from electrochemical tests were in good agreement. The % IE of these spiropyrazoles is: (1)>(2)>(3).

- Molecular docking and binding energy calculations of spiropyrazolederivatives (1)–(3) with the receptor of 3tt8-hormone of crystal structure analysis of Cu human insulin derivative indicated that the spiropyrazoles are %IE of receptor of 3tt8-hormone.

- The morphology of protected and no protected Q235 steel was tested by SEM and EDX.

- Quantum calculation results demonstrated that the heteroatoms of N and O are the active sites ofthe spiropyrazole derivatives.

Conflicts of Interest: The authors declare no conflict of interest.

Data Availability Statement: The authors declare the data availability to share researchers to verify the results of an article, replicate the analysis, and conduct secondary analyses.

References

1. Hou, X.; Gao, L.; Cui, Z.; Yin, J. Corrosion and Protection of Metal in the Seawater Desalination. In *IOP Conference Series: Earth and Environmental Science*; IOP Publishing: Bristol, UK, 2018; Volume 108, p. 022037.

2. Świetlik, J.; Raczyk-Stanisławiak, U.; Piszora, P.; Nawrocki, J. Corrosion in drinking water pipes: The importance of green rusts. *Water Res.* **2012**, *46*, 1–10. [CrossRef]

3. Nawrocki, J.; Raczyk-Stanisławiak, U.; Świetlik, J.; Olejnik, A.; Sroka, M.J. Corrosion in a distribution system: Steady water and its composition. *Water Res.* **2010**, *44*, 1863–1872. [CrossRef]

4. Alamineh, E.A. Study of iron pipe corrosion in municipal water distribution system and its effect. *Am. J. Chem. Eng.* **2018**, *6*, 19–24. [CrossRef]

5. Revie, R.W. *Corrosion and Corrosion Control: An Introduction to Corrosion Science and Engineering*, 4th ed.; John Wiley & Sons: hoboken, NJ, USA, 2008.

6. Wahdan, M.; Hermas, A.; Morad, M. Corrosion inhibition of carbon-steels by propargyltriphenylphosphonium bromide in H_2SO_4 solution. *Mater. Chem. Phys.* **2002**, *76*, 111–118. [CrossRef]

7. Bentiss, F.; Lebrini, M.; Vezin, H.; Lagrenée, M. Experimental and theoretical study of 3-pyridyl-substituted 1, 2, 4-thiadiazole and 1, 3, 4-thiadiazole as corrosion inhibitors of mild steel in acidic media. *Mater. Chem. Phys.* **2004**, *87*, 18–23. [CrossRef]

8. Liu, X.; Okafor, P.; Zheng, Y. The inhibition of CO_2 corrosion of N80 mild steel in single liquid phase and liquid/particle two-phase flow by aminoethyl imidazoline derivatives. *Corros. Sci.* **2009**, *51*, 744–751. [CrossRef]

9. Al Maofari, A.; Ezznaydy, G.; Idouli, Y.; Guédira, F.; Zaydoun, S.; Labjar, N.; El, S. Inhibitive action of 3, 4′-bi-1, 2, 4-Triazole on the corrosion of copper in NaCl 3% solution. *J. Mater. Environ. Sci.* **2014**, *5*, 2081–2085.

10. Barouni, K.; Kassale, A.; Albourine, A.; Jbara, O.; Hammouti, B.; Bazzi, L. Amino acids as corrosion inhibitors for copper in nitric acid medium: Experimental and theoretical study. *J. Mater. Environ. Sci.* **2014**, *5*, 456–463.

11. Fouda, A.; Shalabi, K.; Elmogazy, H. Corrosion inhibition of α-brass in HNO3 by indole and 2-oxyindole. *J. Mater. Environ. Sci.* **2014**, *5*, 1691.

12. Ostovari, A.; Hoseinieh, S.; Peikari, M.; Shadizadeh, S.; Hashemi, S. Corrosion inhibition of mild steel in 1 M HCl solution by henna extract:A comparative study of the inhibition by henna and its constituents (Lawsone, Gallic acid, α-d-Glucose and Tannic acid). *Corros. Sci.* **2009**, *51*, 1935–1949. [CrossRef]

13. Bahrami, M.; Hosseini, S.; Pilvar, P. Experimental and theoretical investigation of organic compounds as inhibitors for mild steel corrosion in sulfuric acid medium. *Corros. Sci.* **2010**, *52*, 2793–2803. [CrossRef]

14. Solomon, M.; Umoren, S.; Udosoro, I.; Udoh, A. Inhibitive and adsorption behaviour of carboxymethyl cellulose on mild steel corrosion in sulphuric acid solution. *Corros. Sci.* **2010**, *52*, 1317–1325. [CrossRef]

15. Wang, H.-L.; Liu, R.-B.; Xin, J. Inhibiting effects of some mercapto-triazole derivatives on the corrosion of mild steel in 1.0 M HCl medium. *Corros. Sci.* **2004**, *46*, 2455–2466. [CrossRef]

16. Solmaz, R.; Kardas, G.; Yazici, B.; Erbil, M. Inhibition effect of rhodanine for corrosion of mild steel in hydrochloric acid solution. *Prot. Met.* **2005**, *41*, 581–585. [CrossRef]

17. Emregül, K.C.; Kurtaran, R.; Atakol, O. An investigation of chloride-substituted Schiff bases as corrosion inhibitors for steel. *Corros. Sci.* **2003**, *45*, 2803–2817. [CrossRef]

18. Chebabe, D.; Chikh, Z.A.; Hajjaji, N.; Srhiri, A.; Zucchi, F. Corrosion inhibition of Armco iron in 1 M HCl solution by alkyltriazoles. *Corros. Sci.* **2003**, *45*, 309–320. [CrossRef]

19. Liu, F.; Du, M.; Zhang, J.; Qiu, M. Electrochemical behavior of Q235 steel in saltwater saturated with carbon dioxide based on new imidazoline derivative inhibitor. *Corros. Sci.* **2009**, *51*, 102–109. [CrossRef]

20. Musa, A.Y.; Kadhum, A.A.H.; Mohamad, A.B.; Takriff, M.S. Experimental and theoretical study on the inhibition performance of triazole compounds for mild steel corrosion. *Corros. Sci.* **2010**, *52*, 3331–3340. [CrossRef]

21. Khaled, K.; Amin, M.A. Corrosion monitoring of mild steel in sulphuric acid solutions in presence of some thiazole derivatives–molecular dynamics, chemical and electrochemical studies. *Corros. Sci.* **2009**, *51*, 1964–1975. [CrossRef]

22. Quraishi, M.; Rafiquee, M.; Khan, S.; Saxena, N. Corrosion inhibition of aluminium in acid solutions by some imidazoline derivatives. *J. Appl. Electrochem.* **2007**, *37*, 1153–1162. [CrossRef]

23. Zhang, X.; Wang, F.; He, Y.; Du, Y. Study of the inhibition mechanism of imidazoline amide on CO_2 corrosion of Armco iron. *Corros. Sci.* **2001**, *43*, 1417–1431. [CrossRef]

24. Knag, M.; Bilkova, K.; Gulbrandsen, E.; Carlsen, P.; Sjöblom, J. Langmuir–Blodgett films of dococyltriethylammonium bromide and octadecanol on iron. Deposition and corrosion inhibitor performance in CO_2 containing brine. *Corros. Sci.* **2006**, *48*, 2592–2613. [CrossRef]

25. Wang, L.; Yin, G.-J.; Yin, J.-G. 2-Mercaptothiazoline and cetyl pyridinium chloride as inhibitors for the corrosion of a low carbon steel in phosphoric acid. *Corros. Sci.* **2001**, *43*, 1197–1202. [CrossRef]

26. Okafor, P.; Liu, X.; Zheng, Y. Corrosion inhibition of mild steel by ethylamino imidazoline derivative in CO_2-saturated solution. *Corros. Sci.* **2009**, *51*, 761–768. [CrossRef]

27. Zhang, J.; Liu, J.; Yu, W.; Yan, Y.; You, L.; Liu, L. Molecular modeling of the inhibition mechanism of 1-(2-aminoethyl)-2-alkyl-imidazoline. *Corros. Sci.* **2010**, *52*, 2059–2065. [CrossRef]

28. Eldesoky, A.; El-Bindary, M.; El-Sonbati, A.; Morgan, S.M. New eco-friendly corrosion inhibitors based on azo rhodanine derivatives for protection copper corrosion. *J. Mat. Environ. Sci.* **2015**, *6*, 2260–2276.

29. Eldesoky, A.; Diab, M.; El-Bindary, A.; El-Sonbati, A.; Seyam, H. Some antipyrine derivatives as corrosion inhibitors for copper in acidic medium: Experimental and quantum chemical molecular dynamics approach. *J. Mat. Environ. Sci.* **2015**, *6*, 2148–2165.

30. Bikadi, Z.; Hazai, E. Application of the PM6 semi-empirical method to modeling proteins enhances docking accuracy of AutoDock. *J. Cheminform.* **2009**, *1*, 15. [CrossRef]

31. Halgren, T.A. Merck molecular force field. I. Basis, form, scope, parameterization, and performance of MMFF94. *J. Comput. Chem.* **1996**, *17*, 490–519. [CrossRef]

32. Morris, G.M.; Goodsell, D.S.; Halliday, R.S.; Huey, R.; Hart, W.E.; Belew, R.K.; Olson, A.J. Automated docking using a lamarckian genetic algorithm and empirical binding free energy function. *J. Comp. Chem.* **1998**, *19*, 1639–1662. [CrossRef]

33. Riyadh, S.M.; Farghaly, T.A. Effect of solvent on the regioselective synthesis of spiropyrazoles. *Tetrahedron* **2012**, *68*, 9056–9060. [CrossRef]

34. Al-Khaldi, M.; Al-qahtani, K. Corrosion inhibition of steel by Coriander extracts in hydrochloric acid solution. *J. Mater. Environ. Sci.* **2013**, *4*, 593–600.

35. Schultze, J.; Wippermann, K. Inhibition of electrode processes on copper by AHT in acid solutions. *Electrochim. Acta* **1987**, *32*, 823–831. [CrossRef]

36. Silverman, D.; Carrico, J. Electrochemical impedance technique—A practical tool for corrosion prediction. *Corrosion* **1988**, *44*, 280–287. [CrossRef]

37. Macdonald, D.D.; McKubre, M.C. Impedance measurements in electrochemical systems. In *Modern Aspects of Electrochemistry*; Springer: Boston, MA, USA, 1982; pp. 61–150.

38. Mansfeld, F. Recording and analysis of AC impedance data for corrosion studies. *Corrosion* **1981**, *37*, 301–307. [CrossRef]

39. Gabrielli, C. *Identification of Electrochemical Processes by Frequency Response Analysis*; Technical Report No. 004; Solartron Instrumentation Group, Morris Bros. Ltd.: London, UK, 1980.

40. El Achouri, M.; Kertit, S.; Gouttaya, H.; Nciri, B.; Bensouda, Y.; Perez, L.; Infante, M.; Elkacemi, K. Corrosion inhibition of iron in 1 M HCl by some gemini surfactants in the series of alkanediyl-α, ω-bis-(dimethyl tetradecyl ammonium bromide). *Prog. Org. Coat.* **2001**, *43*, 267–273. [CrossRef]

41. Anejjar, A.; Zarrouk, A.; Salghi, R.; Zarrok, H.; Hmamou, D.B.; Hammouti, B.; Elmahi, B.; Al-Deyab, S. Studies on the inhibitive effect of the ammonium Iron (II) sulphate on the corrosion of carbon steel in HCl solution. *J. Mater. Environ. Sci.* **2013**, *4*, 583–592.

42. Mertens, S.; Xhoffer, C.; De Cooman, B.; Temmerman, E. Short-term deterioration of polymer-coated 55% Al-Zn—Part 1: Behavior of thin polymer films. *Corrosion* **1997**, *53*, 381–388. [CrossRef]

43. Trabanelli, G.; Monticelli, C.; Grassi, V.; Frignani, A. Electrochemical study on inhibitors of rebar corrosion in carbonated concrete. *Cem. Concr. Res.* **2005**, *35*, 1804–1813. [CrossRef]

44. Trowsdale, A.; Noble, B.; Harris, S.; Gibbins, I.; Thompson, G.; Wood, G. The influence of silicon carbide reinforcement on the pitting behaviour of aluminium. *Corros. Sci.* **1996**, *38*, 177–191. [CrossRef]

45. Reis, F.; De Melo, H.; Costa, I. EIS investigation on Al 5052 alloy surface preparation for self-assembling monolayer. *Electrochim. Acta* **2006**, *51*, 1780–1788. [CrossRef]

46. Lagrenee, M.; Mernari, B.; Bouanis, M.; Traisnel, M.; Bentiss, F. Study of the mechanism and inhibiting efficiency of 3, 5-bis (4-methylthiophenyl)-4H-1, 2, 4-triazole on mild steel corrosion in acidic media. *Corros. Sci.* **2002**, *44*, 573–588. [CrossRef]

47. McCafferty, E.; Hackerman, N. Kinetics of iron corrosion in concentrated acidic chloride solutions. *J. Electrochem. Soc.* **1972**, *119*, 999–1009. [CrossRef]

48. Ma, H.; Chen, S.; Niu, L.; Zhao, S.; Li, S.; Li, D. Inhibition of copper corrosion by several Schiff bases in aerated halide solutions. *J. Appl. Electrochem.* **2002**, *32*, 65–72. [CrossRef]

49. Kuş, E.; Mansfeld, F. An evaluation of the electrochemical frequency modulation (EFM) technique. *Corros. Sci.* **2006**, *48*, 965–979. [CrossRef]

50. Caignan, G.A.; Metcalf, S.K.; Holt, E.M. Thiophene substituted dihydropyridines. *J. Chem. Crystallogr.* **2000**, *30*, 415–422. [CrossRef]

51. Samie, F.; Tidblad, J.; Kucera, V.; Leygraf, C. Atmospheric corrosion effects of HNO_3—Method development and results on laboratory-exposed copper. *Atmos. Environ.* **2005**, *39*, 7362–7373. [CrossRef]

52. Refaat, H.M.; El-Badway, H.A.; Morgan, S.M. Molecular docking, geometrical structure, potentiometric and thermodynamic studies of moxifloxacin and its metal complexes. *J. Mol. Liq.* **2016**, *220*, 802–812. [CrossRef]

53. Prabhu, R.; Venkatesha, T.; Shanbhag, A.; Kulkarni, G.; Kalkhambkar, R. Inhibition effects of some Schiff's bases on the corrosion of mild steel in hydrochloric acid solution. *Corros. Sci.* **2008**, *50*, 3356–3362. [CrossRef]

54. Moretti, G.; Quartarone, G.; Tassan, A.; Zingales, A. Inhibition of mild steel corrosion in 1N sulphuric acid through indole. *Mater. Corros.* **1994**, *45*, 641–647. [CrossRef]

55. Samie, F.; Tidblad, J.; Kucera, V.; Leygraf, C. Atmospheric corrosion effects of HNO_3—Influence of concentration and air velocity on laboratory-exposed copper. *Atmos. Environ.* **2006**, *40*, 3631–3639. [CrossRef]

56. Lukovits, I.; Palfi, K.; Bako, I.; Kalman, E. LKP model of the inhibition mechanism of thiourea compounds. *Corrosion* **1997**, *53*, 915–919. [CrossRef]

57. Zhao, P.; Liang, Q.; Li, Y. Electrochemical, SEM/EDS and quantum chemical study of phthalocyanines as corrosion inhibitors for mild steel in 1 mol/l HCl. *Appl. Surf. Sci.* **2005**, *252*, 1596–1607. [CrossRef]

BOD Composite as a New Eco-Friendly Corrosion Inhibitor

A.M. Eldesoky[1,5], A. Attia[2,6], Omayma E. Ahmed[3] and M. Abo-Elsoud[4]

1. Engineering Chemistry Department, High Institute of Engineering & Technology, New Damietta 34517, Egypt

2. Chemistry Department, Mansoura University, Faculty of Science, Mansoura 35516, Egypt

3. Evaluation and Analytical Department Egyptian Petroleum Research Institute, Nasr City, Cairo 11717, Egypt

4. Physics Department, Umm Al-Qura University, Al-Qunfudhah University College, Al-Qunfudhah 21912, Saudi Arabia

5. Chemistry Department, Umm Al-Qura University, Al-Qunfudhah University College, Al-Qunfudhah 21912, Saudi Arabia

6. Chemistry Department, Najran University, Faculty of Science and Arts, Najran 21497, Saudi Arabia

Abstract: BOD composite, (E)-4-(2-(benzo[d]oxazol-2-yl) vinyl)-N,N-dimethylaniline is a new eco-friendly corrosion inhibitor versus P355 Carbon Steel (Cs). BOD was examined in 1.0 N HCl corrosive solution utilizing TP, EIS and EFM tests. EIS curves show that adsorption of BOD increases the transfer resistance and decrease the capacitance of interface metal/solution. Molecular docking was utilized to predict the binding between BOD composite with the receptor of 3tt8-hormone of crystal structure analysis of Cu Human Insulin Derivative. The morphology of inhibited P355 Cs was analyzed by checking electron magnifying instrument innovation with energy dispersive X-beam spectroscopy (SEM–EDX).

Keywords: BOD, eco-friendly, P355 Cs, SEM, EDX, molecular docking.

1. Introduction

Over the previous decades, the passivation and corrosion performance of the steel in existing have been studied [1, 2]. In the typical environment, numerous research has attentive on the electrochemical performance of traditional Cs, austenitic or duplex stainless steel (SS) kinds such as Q235 [3], 304 [4], 316 [5] or 2205 [6, 7] SS [8]. In the field of nuclear manufacturing, the steel strengthening is showing to concrete pore solution over the pH range 12 to 14 in the anoxic environs even for hundreds of years [9]. In these great alkaline environs, an inhibitive passive film will be designed spontaneously and maintained on the surface of the P355 Cs [10, 11]. The conformation of the existing pore solution has great influence on the protection of the Cs [12, 13]. However, till now, few preceding works have

Corresponding author: M. Abo-Elsoud, doctor, professor, research field: experimental physics.

attentive on the electrochemical performance of the P355 Cs in "high alkaline" and "super-anoxic" environment [14]. We trust that the analysis of the passive manner in saturated Ca(OH)$_2$ solution (SCS) with altered pH by appending of NaOH, which was utilized as simulated concrete pore solution (SCPS), will give to an enhanced understanding of the corrosion manner of the Cs in concrete.

Since the accepted rate of corrosion of the steel in focused is very low, very long time is wanted to estimate the corrosion manner which is impractical to attain based on research laboratory experiments [15]. Therefore, electrochemical test is often utilized for rapid estimation of steel corrosion [16, 17]. Till currently, the electrochemical and protected films of P355 Cs joining in alkaline high (pH > 12.5) and anoxic environs at more polarization had negative (-1.0 V-0 V) potential are scarcely examined [18-20]. So, it is very worth travelling the structure and goods of the hindrance film obtain on P355 Cs in this condition [21-23].

The main scope of our work is to show that, the electrochemical habit of BOD as a new eco-friendly corrosion protection for P355 Cs hold 1.0 N corrosive solution is obtain by tafel polarization (Tp), (EIS) AC impedance spectroscopy and (EFM) electrochemical frequency modulation method. A few quantum-chemistry measurements have been gotten in order to record the inhibition and hindrance to the molecular properties of the composite [24, 25]. Molecular docking was utilized to predict the binding between BOD composite with the receptor of 3tt8-hormone of crystal structure analysis of Cu Human Insulin Derivative. SEM and EDX investigations of the P355 Cs in 1.0 N corrosive solution surface were examined.

2. Experimental Section

2.1 Measurements

This paper mimics the real docking procedure in which the ligand–protein pair-wise interface energies are calculated utilizing Docking Server [26]. Docking measurements were carried out on BOD composite protein model. Essential hydrogen atoms, Koll- man united atom type charges, and solvation parameters were additional with the aid of Auto-Dock tools [27]. Affinity (grid) maps of 20 × 20 × 20 A° grid points and 0.375 A° area were produced utilizing the Auto grid program [28].

2.2 Material and Medium

P355 Cs was utilized for the measurement of corrosion. It's percent composition is given in Table 1, the rest iron. The corrosion dose (1.0 N corrosive solution) (37% analytical grade) was ready by hydrochloric acid dilution with water double distilled. BOD composite utilized for this paper, whose structure was given in Table 2 [29].

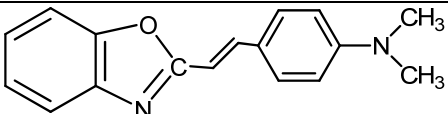### 2.3 Methods

2.3.1 Electrochemical Method

The electrochemical techniques have been performed utilizing 750 software for calculations. The utilized electrical circuit contains of three electrodes (SCE reference electrode, Pt auxiliary electrode and Cs electrode). 1 cm^2 of the Cs electrode is prepared. The pre-dipping oxide film was reduced by given a time period of about 20 minutes for open circuit potential (OCP). All electrochemical studies were performed at 25 ± 1 °C. *Tp* is a useful method because they give more information about the corrosion mechanism and the factors affecting the corrosion procedure and inhibition behavior of the BOD. This is done by measuring the potential-current characteristics of the metal/solution system. In *TP* measurements, electrode potential from −50 to 50 V was applied at scanning rate 1 mVs^{-1}.

(EFM) and (EIS) tests were gain by utilized the same tests as before with a Gamry framework system depend on ESA400. EIS tests were ready in a range of frequency of 100 kHz to 10 MHz with amplitude of 5 mV peak-to-peak. EFM had done utilized 2 frequencies 2 and 5 Hz. The frequency base was 1 Hz.

Table 1   Chemical conformation of the P355 Cs.

Mo	Cr	Ni	Cu	Si	S	P	Mn	C
0.009	0.082	0.05	0.043	0.324	0.0005	0.005	0.98	0.15
N	H	B	Co	Ti	V	Zr	Nb	Al
0.034	0.006	0.001	0.001	0.001	0.005	0.0001	1.95	0.034

Table 2   Chemical structure, name, molecular weight and molecular formula of inhibitor.

Structure	Name	Mol. Wt./M. formula
	BOD	264.32/C$_{17}$H$_{16}$N$_2$O

2.3.2 SEM-EDX Tests

The surface of P355 Cs was obtained by keeping the coins for 3 days putted in 1.0 N corrosive solution with and lack of perfect dose of BOD composite, after abraded mechanically utilized unlike papers emery up to grit size 1,200. Then, after this time dipping, the samples were lotion gently with distilled water, carefully dried and mounted into the spectrometer attendance of further treatment. The surface of P355 Cs was tested utilized an X-ray diffractometer Philips (pw-1390) with Cu-tube (CuK-α, λ = 1.54051 A°), (SEM, JOEL, JSM-T20, Japan).

2.3.3. Theoretical Study

Quantum chemical measurements have been utilized Accelrys (Material Studio Version 4.4).

3. Results and Discussion

3.1. Tp Tests

Tp curves without and with different BOD concentrations for P355 Cs dissolution in corrosive solution were illustrated in Fig. 1. The variation of corrosion potential E_{corr} and, i_{corr}, β_a, β_c, CR, θ and $\%IE_P$ with BOD concentration were given in Table 3 Experimental results indicate that i_{corr} is significantly decreases with increasing BOD concentration. Both the anodic and cathodic curves were affected by the presence of BOD, i.e. BOD limited both the anodic and cathodic reactions (mixed type inhibitor). The almost unchanged Tafel slopes indicate that BOD acts by just blocking the metal surface reaction sites without changing the mechanisms of the anodic and cathodic reaction.

The $\%IE_P$ and θ from *Tp* measurements, were determined by applying the following equation:

$$\%IE_P = \theta \times 100 = [1 - (i°_{corr}/i_{corr}] \times 100 \quad (1)$$

$i°_{corr}$ and i_{corr} are the current corrosion densities lack and attendance of solution inhibitor, sequentially.

The adding of BOD to 1.0 N HCl Makes E_{corr} slightly shifted, which suggests that BOD can be considered as a mixed type inhibitor [30, 31] and also,

this addition does not change the (β_a and β_c) remarkably, which designates that the liberated hydrogen mechanism and the dissolution process of *P*355 *Cs* are not affected.
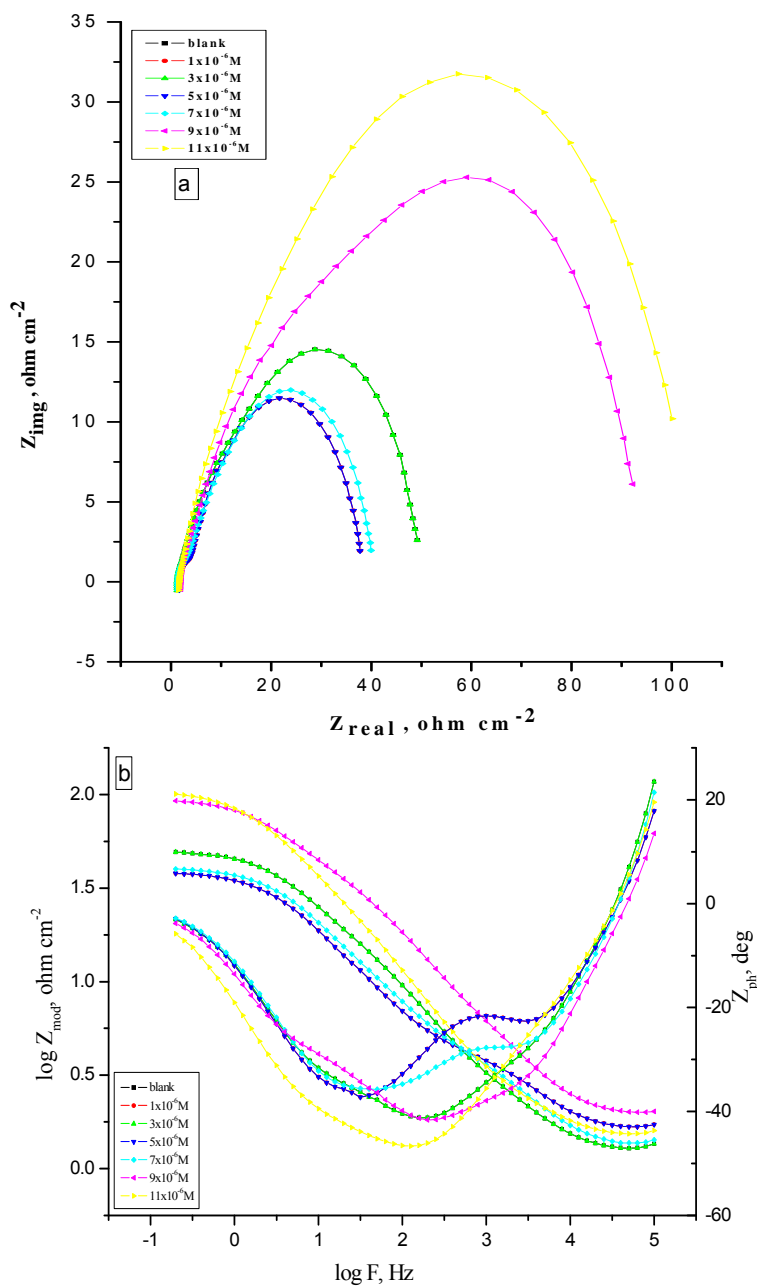
3.2. EIS Tests

Fig. 2 was given Nyquist (a) and Bode (b) curves for the corrosion behavior of P355 Cs in 1.0 M HCl with and without various doses of BOD after 30 min of immersion. Impedance spectra showed one time constant related to a single capacitive semi-circles, which indicated that the corrosion procedure was mostly controlled by charge transfer [32-39]. The
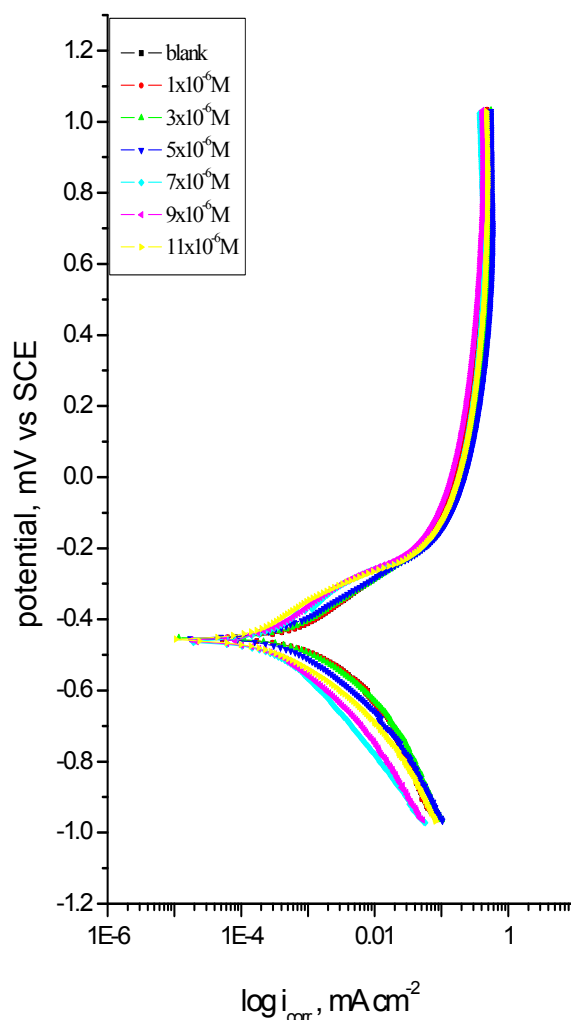
Fig. 1 *Tp* **curves without and with different BOD concentrations for P355 Cs dissolution in corrosive solution at 25 ± 0.1 °C.**

Table 3 Effect of BOD concentration on E_{corr}, i_{corr}, β_a, β_c, CR, θ, %IE_p.

Composite	Conc., M.	-E_{corr} (mV vs.SCE)	$i_{corr} \times 10^{-5}$ (μAcm^{-2})	$\beta_a \times 10^{-3}$ (mV dec^{-1})	$\beta_c \times 10^{-3}$ (mV dec^{-1})	θ	%IE_p
	Blank	456	78.2	138.9	162.4	----	----
BOD	1x10^{-6}	476	69.2	136.4	163.4	0.115	11.5
	3x10^{-6}	454	40.4	108.5	118.3	0.483	48.3
	5 x10^{-6}	456	39.2	131.7	126.9	0.498	49.8
	7x10^{-6}	455	33.1	201.2	173.7	0.576	57.6
	9x10^{-6}	476	26.5	168.3	162.4	0.661	66.1
	11x10^{-6}	461	17.9	109.1	151.8	0.771	77.1

Fig. 2 The Nyquist (a) and Bode (b) diagrams for P355 Cs in 1.0 N HCl before and after adding various doses of BOD at 25 ± 0.1 °C.
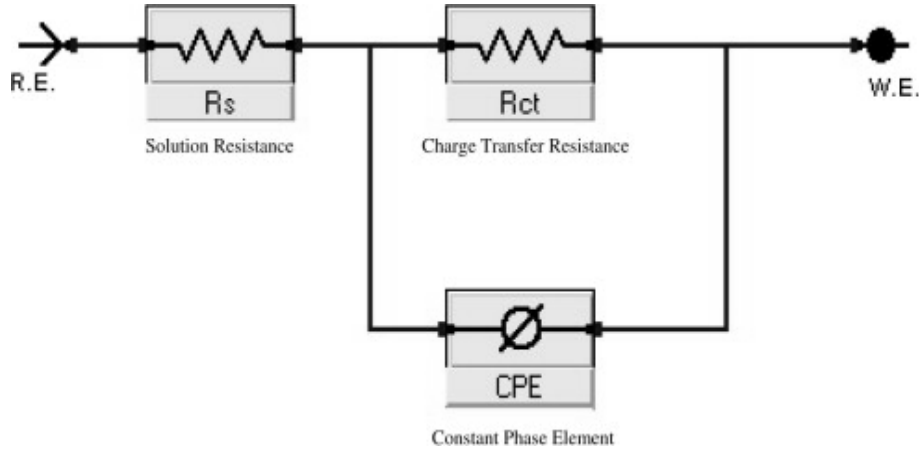
Fig. 3   Electrical equivalent circuit used to fit the EIS.

Table 4   EIS parameters for P355 Cs in 1.0 N HCl before and after adding different doses of BOD at 25 ± 0.1 °C.

Composite	Conc., M.	$R_S \times 10^{-3}$ $(\Omega\ cm^2)$	$Y_o \times 10^{-6}$	$n \times 10^{-3}$	R_{ct} $(\Omega\ cm^2)$	$C_{dl} \times 10^{-4}$ $(\mu F cm^{-2})$	θ	IE
	Blank	1.347	0.267	878.1	19.72	6.313	----	----
	1×10^{-6}	1.831	0.302	871.9	22.91	2.751	0.139	13.9
	3×10^{-6}	1.459	0.304	865.9	23.66	2.047	0.166	16.6
BOD	5×10^{-6}	1.793	0.213	874.7	28.92	1.986	0.318	31.8
	7×10^{-6}	1.247	3.521	551.2	46.11	1.856	0.572	57.2
	9×10^{-6}	1.705	1.211	590.1	97.01	1.858	0.796	79.6
	11×10^{-6}	1.451	1.489	642.1	111.04	1.394	0.822	82.2

obtained curves are very similar to each other, indicating that the mechanism of corrosion is not different after appending of BOD [40]. The diameter of Nyquist diagrams rises on rising of the BOD dose due to the creation of adsorbed layer of BOD on surface of P355 Cs. Fig. 3 showed the fitting equivalent circuit for EIS data, which is consisted of solution resistance (R_s), resistance charge-transfer (R_{ct}), and a CPE instead of a pure capacitor signifies the interfacial capacitance. The data of the capacitance double layer (C_{dl}) can be given   from equation 2 [41]:

$$C_{dl} = Y_o \omega^{n-1}/\sin [n(\pi/2) \qquad (2)$$

where $Y_o = CPE$ magnitude, $\omega = 2\pi f_{max}$, f_{max} is the imaginary frequency at which the component of the impedance is maximal.

Table 4 represents the data of R_s, R_{ct}, C_{dl}, and %IE. The R_{ct} is a diameter of great frequency loop, which enhancement with rising of BOD dose. While the values of C_{dl} decreases due to water replacement by extract molecules making a inhibitive layer at the P355 Cs [42-44].

The obtained (% IE) and (θ) of the ASE was elaborated from next (3) [45]:

$$\%IE_{EIS} = [1 - (R_{ct}^{\circ}/R_{ct}) \times 100 \qquad (3)$$

Where R_{ct}° and R_{ct} are the resistance data before and after adding ASE, respectively.

3.3. EFM Test

Electrochemical frequency modulation is AC technique, but it immediately gives corrosion current values without previous knowledge of Tafel constants. Fig. 4 shows the EFM spectra for P355 Cs in 1 N HCl without and with different concentrations of BOD at 25 °C.

The parameters from EFM measurements (i_{corr}, β_a, β_c, CF-2, CF-3, CR, θ and %IE) were listed in Table 5. It is observed from the data that, the value of i_{corr} decreases by increasing BOD concentration and %IE increases. If the causality factors are approximately equal to 2.0 and 3.0 for CF-2, CF-3, respectively, this indicates the presence of a causal relationship between the perturbation signal and the response signal, and
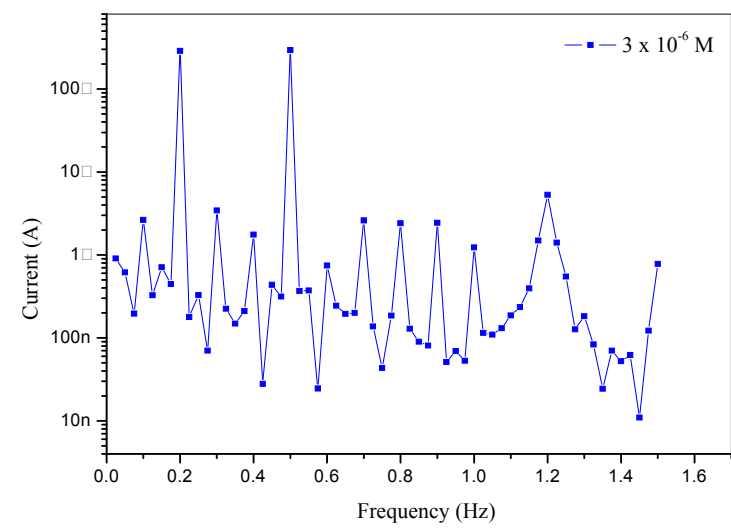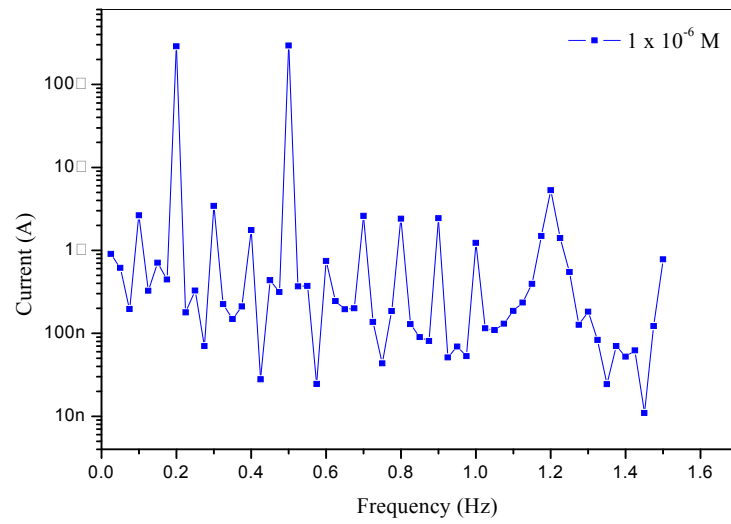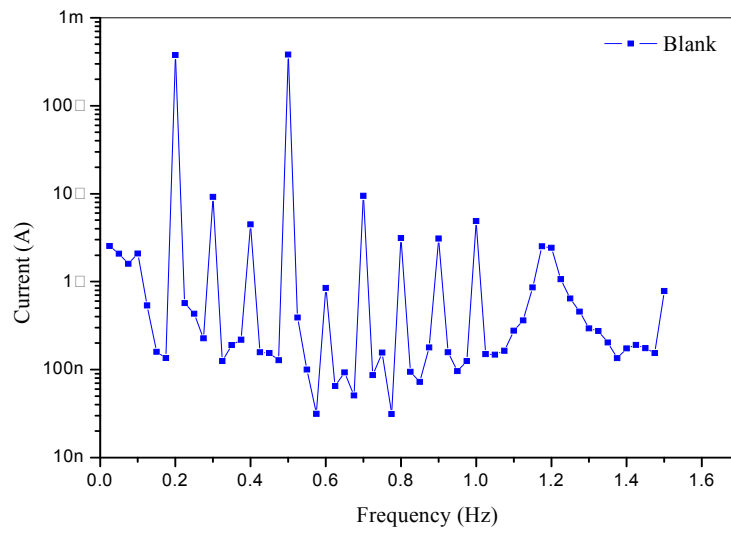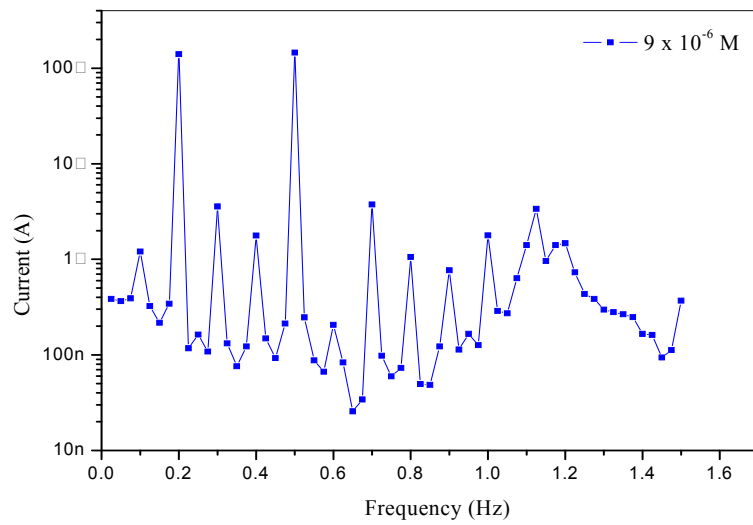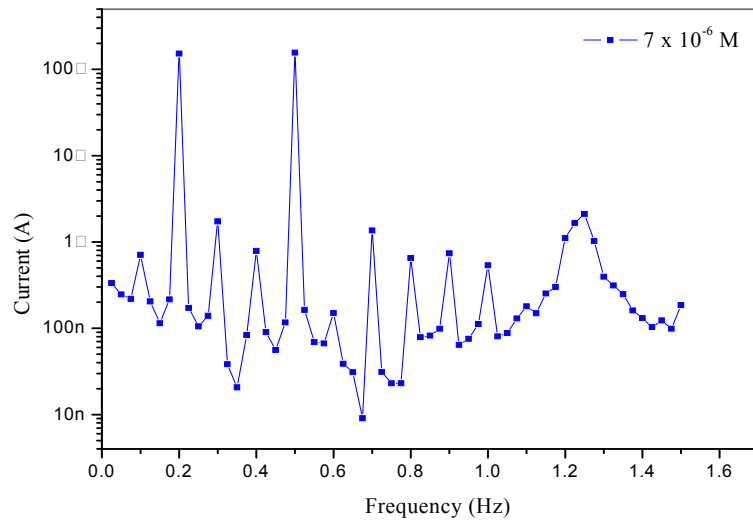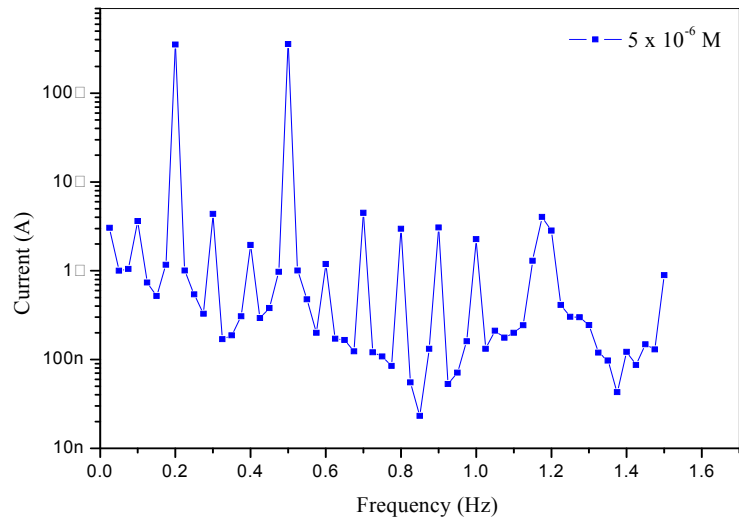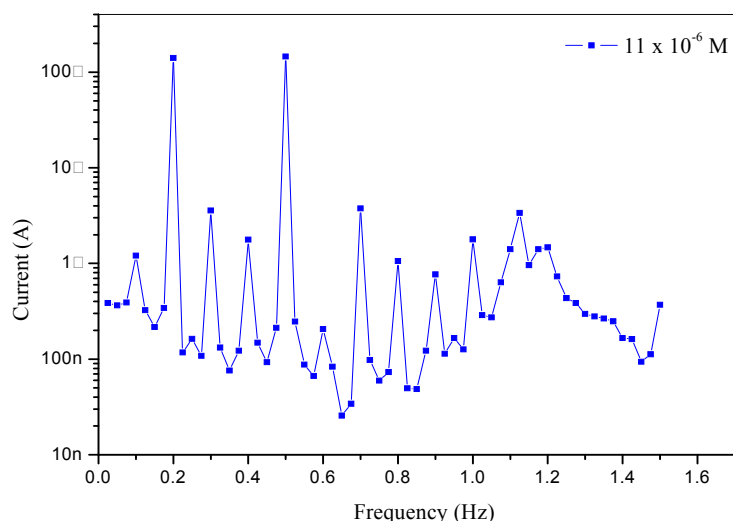
Fig. 4 EFM spectra for *P*355 CS in 1.0 N HCl before and after adding various.

Table 5 EFM parameters for P355 Cs before and after adding various doses of BOD in 1.0 N HCl at 25 ± 0.1 °C.

Composite	Conc., M.	i_{corr} (μAcm^{-2})	$\beta_a \times 10^{-3}$ (mV dec^{-1})	$\beta_c \times 10^{-3}$ (mV dec^{-1})	CF-2	CF-3	θ	%IE
	Blank	821.5	126.8	158.4	1.98	3.06	-----	------
	1×10^{-6}	666.3	118.9	130.4	2.02	3.01	0.188	18.8
	3×10^{-6}	488.2	107.5	123.2	2.03	3.07	0.405	40.5
	5×10^{-6}	471.6	107.9	113.6	2.01	3.02	0.425	42.5
BOD	7×10^{-6}	360.4	111.2	161.2	2.01	2.89	0.561	56.1
	9×10^{-6}	266.3	118.7	149.4	2.01	3.03	0.675	67.5
	11×10^{-6}	253.2	117.8	140.6	1.96	2.98	0.691	69.1

the results are considered to be trusted [46]. Deviation of CF-2 and CF-3 values from ideality may be because the perturbation amplitude was overly small, or the frequency spectrum resolution is not sufficiently high, or the inhibitor is not working very well [47].

The IE_{EFM} % improve by rising the BOD doses and was obtain as follows:

$$\%IE_{EFM} = [1 - (i_{corr}/i^{\circ}_{corr}) \times 100 \qquad (4)$$

where i°_{corr} and i_{corr} are current densities before and after adding BOD, correspondingly.

3.4. SEM Tests

Fig. 5 demonstrates the morphology of the surface of P355 *CS* coins polished before exposure to the corrosive solution, SEM image of the CS after dipping in HCl for 3 day. The micrographs displayed an extended etching contain green and dark areas with

damaged highly [48, 49].

Fig. 5 (with 11×10^{-6} M of BOD) is clear that BOD provided best protection at the surface of the P355 Cs metal as it forms a inhibitive film on the P355 Cs surface.

3.5 EDS Test

The EDS spectra were utilized to measure the elements found on the surface of P355 Cs after 3 days of covered in the lack and attendance of 1.0 N corrosive solution. Fig. 6 gives the EDS result measured on the composition of P355 Cs only without the acid and inhibitor modified. The EDS record that only oxygen and iron were observed, which given that the passive film found with only Fe_2O_3.

The EDS tests of P355 Cs in 1.0 N corrosive solution only and with of 11×10^{-6} M of BOD composite portrays in Fig. 6. The spectra give additional lines,
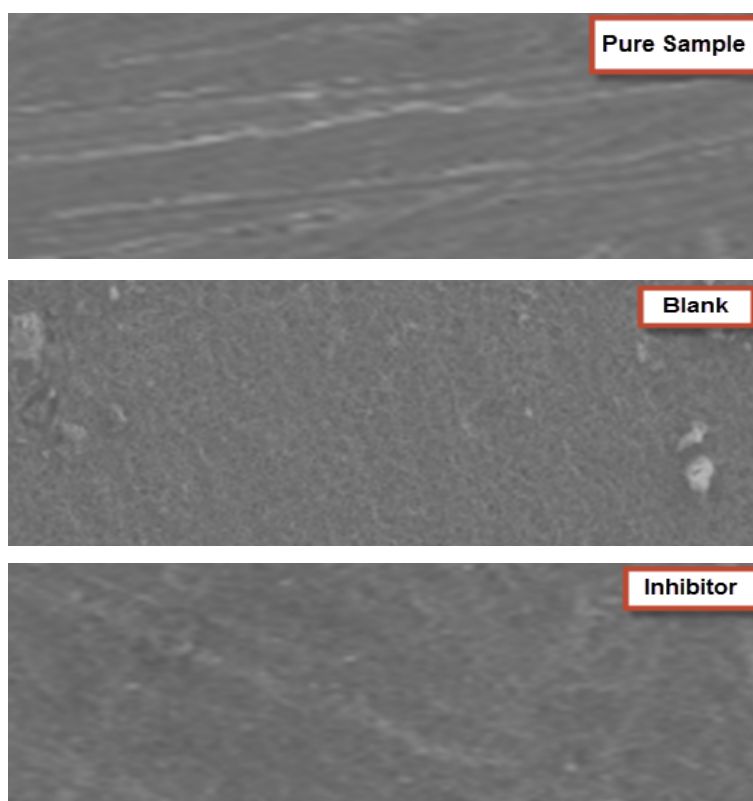
Fig. 5   SEM of P355 Cs in 1.0N corrosive solution after dipping for 3 days nonexistence inhibitor and existence of 11×10^{-6} M of BOD.

lead to the presence of C (the carbon atoms of BOD compound). These values give that the O and C atoms covered surface. The elemental observed is record in Table 6.

3.6. Quantum Chemical Measurements

The Mulliken charge and molecular orbital curve of BOD composite are given in Fig. 7. Theoretical measurements were found for only the forms of neutral, in order to obtain further insight into the results of experimental. Data of quantum chemical lead to energies of energy gap (ΔE) and (E_{HOMO}) energy of highest occupied molecular orbitals and (E_{LUMO}) are measured and record in Table 7. The increase or lower negative E_{HOMO} is inhibitor associated, the higher the trend of offering electrons to unoccupied d orbital of P355 Cs, and the improvement the corrosion protection. Due to the decrease of E_{LUMO}, the acceptance of electrons is plain from P355 Cs surface [50, 51].

Apparently, good corrosion protection is usually those BOD composites who are not only offer electrons to unoccupied orbital of the alloy, but also free electrons established from the metal [52]. It can be seen that all measurement of quantum parameters checking these results from experimental.

3.7 Molecular Docking

The docking research displayed a favorable interface among BOD composite and the receptor of 3tt8-hormone of crystal structure investigation of Cu Human Insulin Derivative. "The calculated energy is listed in Table 8 and Fig. 8. According to the results obtained in this study, HB plot curve indicated that, the BOD composite binds to the proteins hydrogen bond and decomposed interactions energies in kcal/mol were existed between the BOD composite with 3tt8 receptor as shown in Fig. 9. The calculated efficiency is favorable where K_i values estimated by Auto Dock were compared with experimental K_i
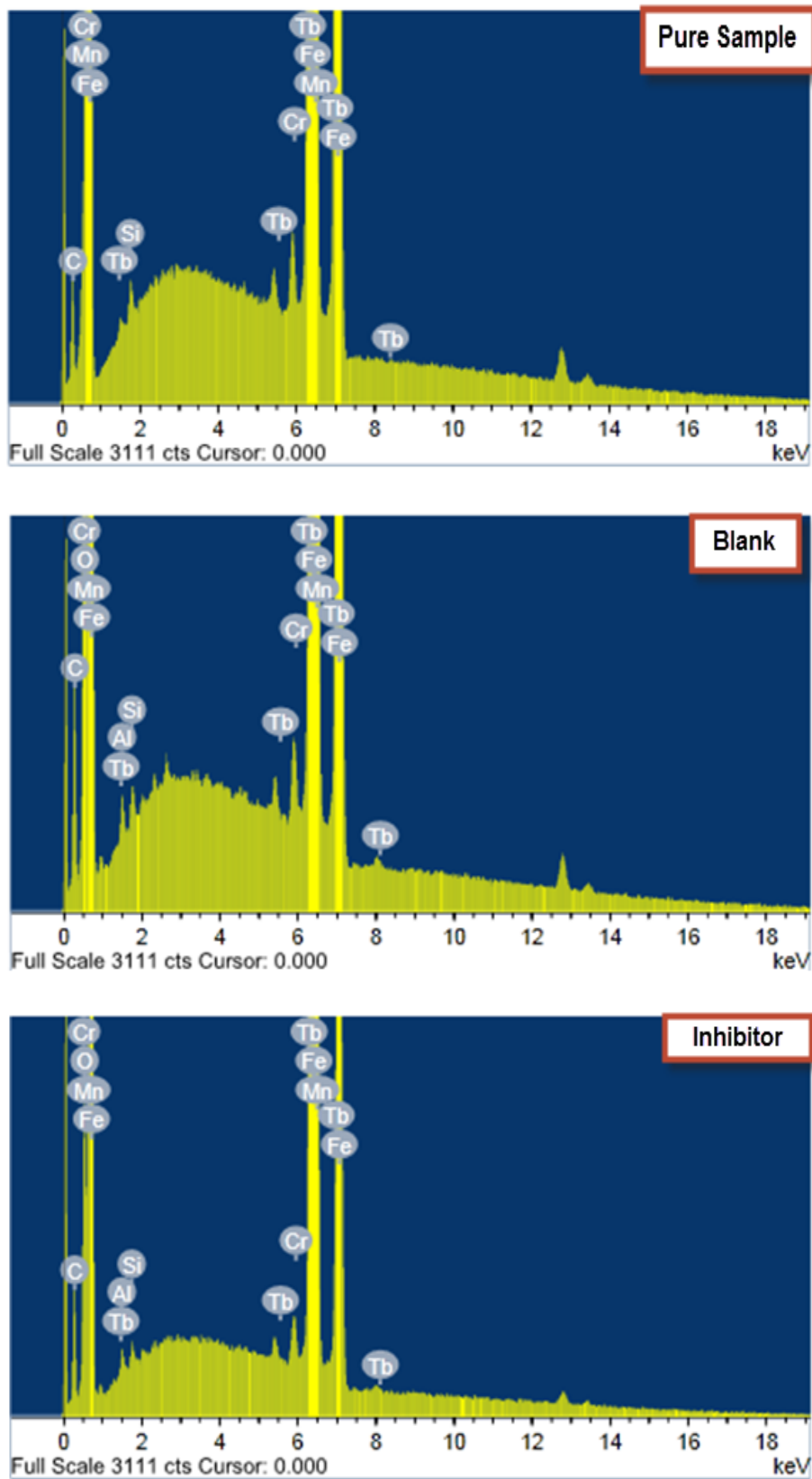
Fig. 6 *EDS* study of P355 Cs in 1.0 N corrosive solution after dipping for 3 days nonexistence inhibitor and existence of 11 × 10⁻⁶ *M* of BOD compound.
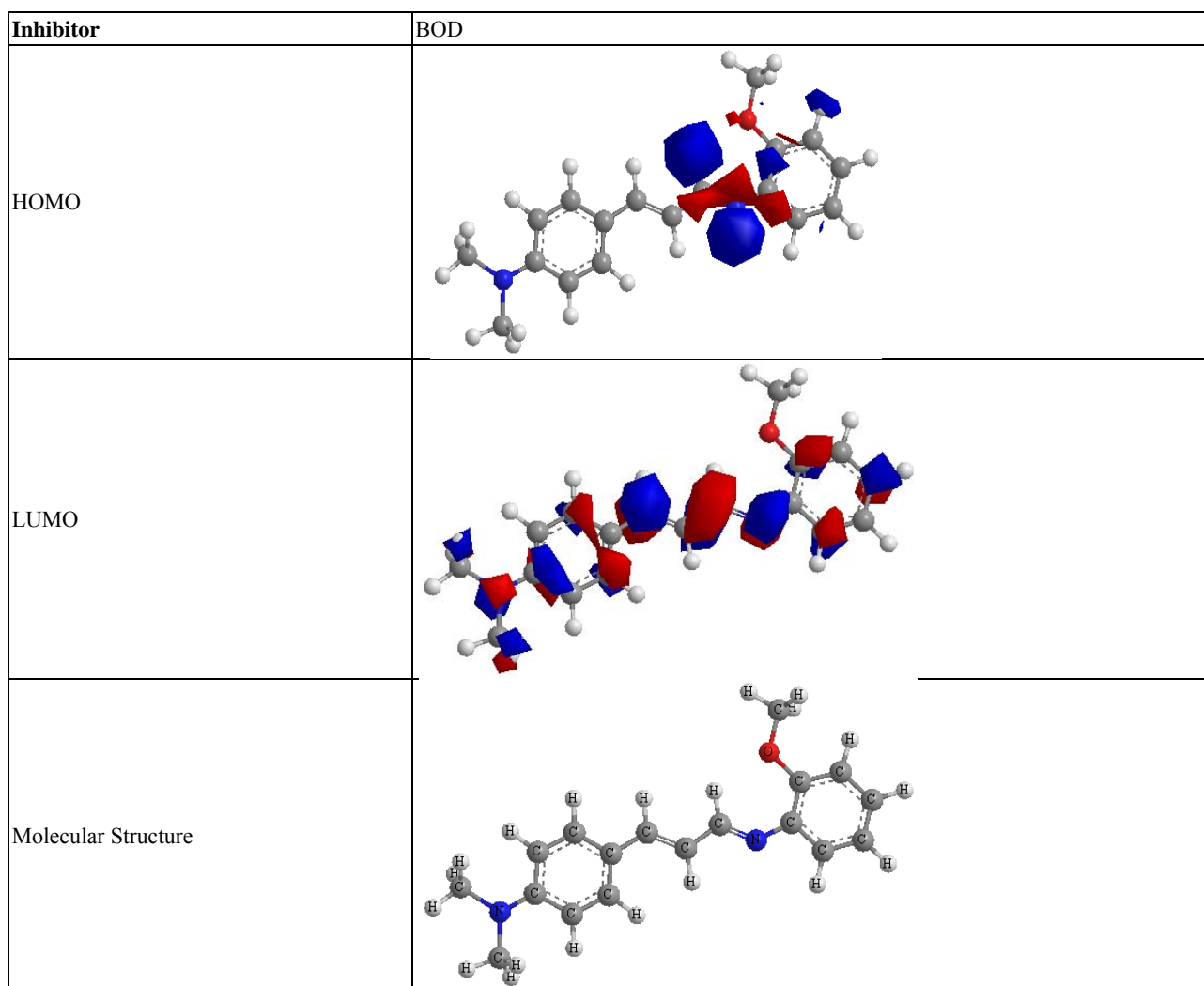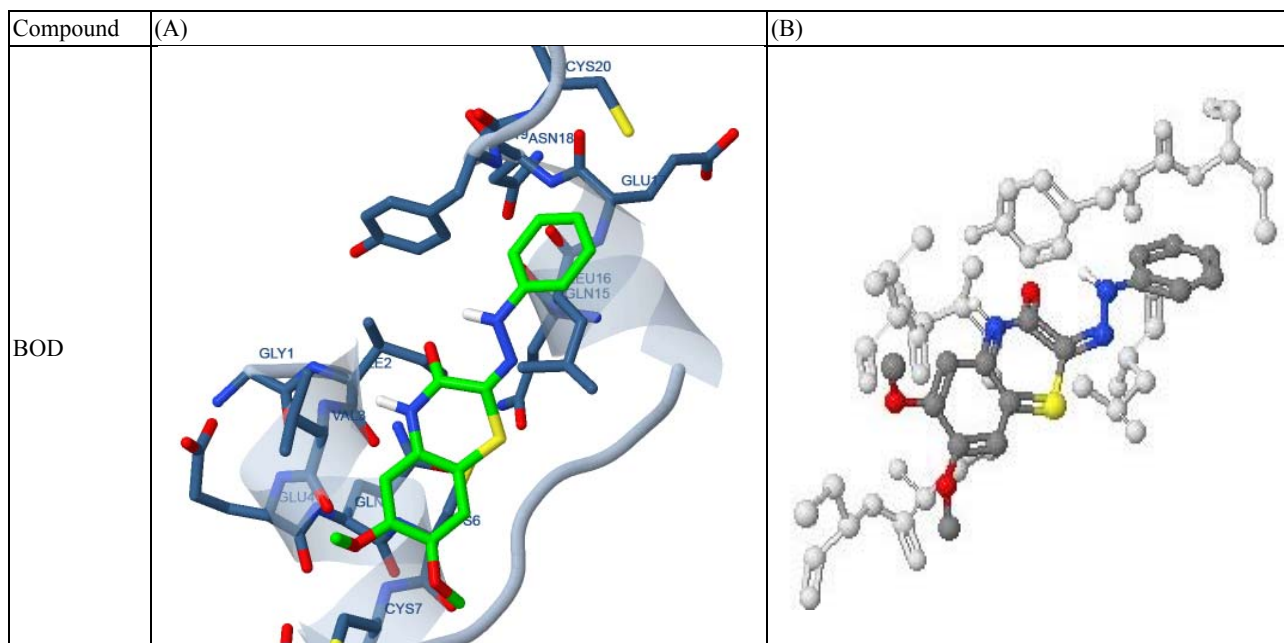
Table 6   Mass % of P355 Cs after 3 days in HCl lack and attendance of the optimum dose of the studied BOD compound.

(Mass %)	C	O	Al	Si	Cr	Mn	Fe	Tb
Pure Sample	6.79	---	0.28	0.25	0.26	0.49	89.60	2.33
Blank	8.51	14.99	0.26	0.24	0.13	0.41	73.37	2.09
Inhibitor	13.23	6.77	0.27	0.23	0.19	0.42	76.58	2.31

Table 7   The quantum chemical properties for examined BOD compound.

Properties	Inhibitor
$-E_{HOMO}$ (eV)	0.2767
$-E_{LUMO}$ (eV)	0.1555
ΔE (eV)	0.1211
η (eV)	0.0605
σ (eV)$^{-1}$	16.5111
$-Pi$ (a.u)	0.2161
X (eV)	0.2161
S (eV)$^{-1}$	8.2555
ω (a.u)	0.3857
ΔN_{max}	3.5689

Inhibitor	BOD
HOMO	
LUMO	
Molecular Structure	

Fig. 7   Molecular orbital plots of investigated BOD compound.

Compound	(A)	(B)
BOD		

Fig. 8   BOD composite (green in (A) and gray in (B)) in interaction with 3tt8 receptor. (For interpretation of the references to color in this figure legend, the reader is referred to the web version of this article).

Table 8   Energy data gotten in docking tests of BOD composite with 3tt8 receptor.

Compound	Est. free energy of binding (kcal/mol)	Est. inhibition constant (K_i) (μM)	vdW+ bond+ desolve energy (kcal/mol)	Electrostatic energy (kcal/mol)	Total intercooled energy (kcal/mol)	Interact surface
BOD	-4.66	383.22	-5.41	-0.01	-5.41	533.617
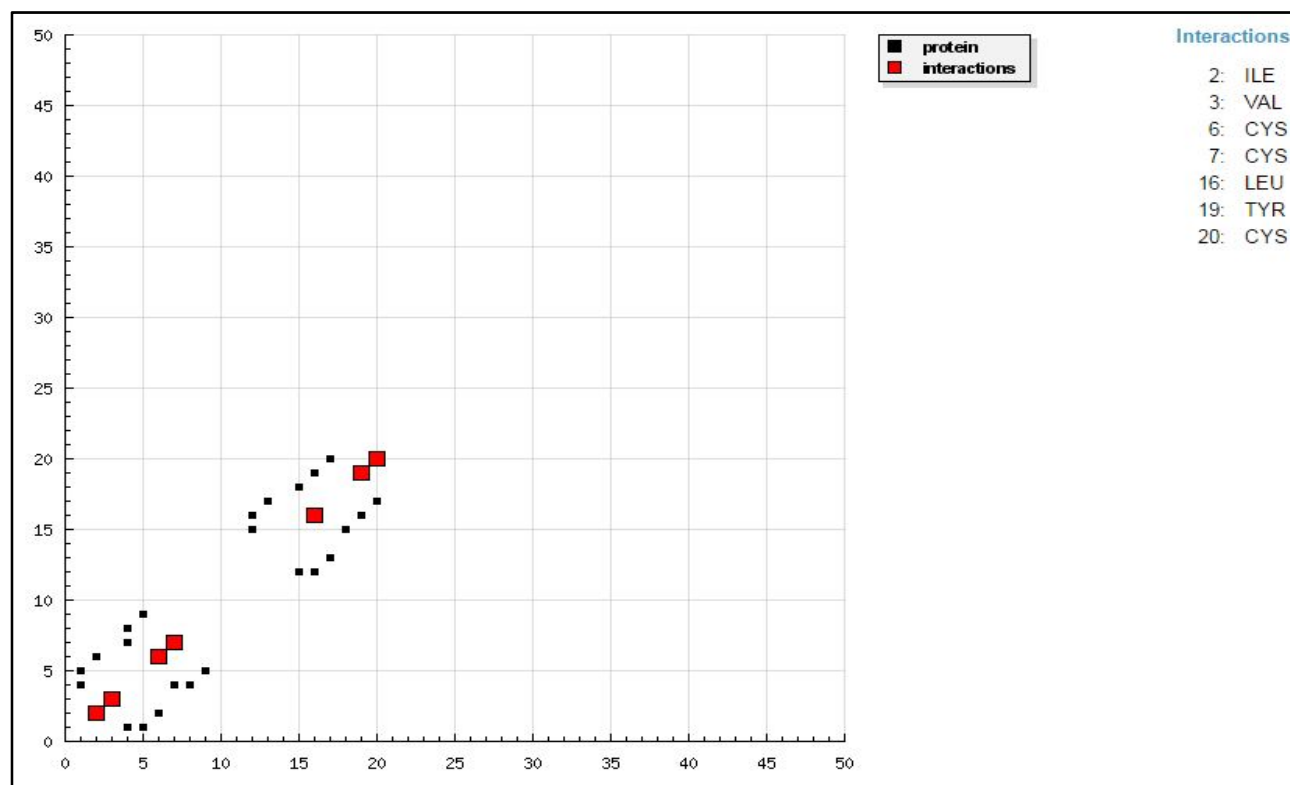
Fig. 9   HB bends of interface among BOD composite with receptor of breast cancer mutant 3tt8.

values, when available, and the Gibbs free energy is negative [53-55]. Also, based on this data, it can propose that interaction between the 3tt8 receptor and the BOD composite is possible". 2D diagrams of docking with BOD composite are revealed in Fig. 10.
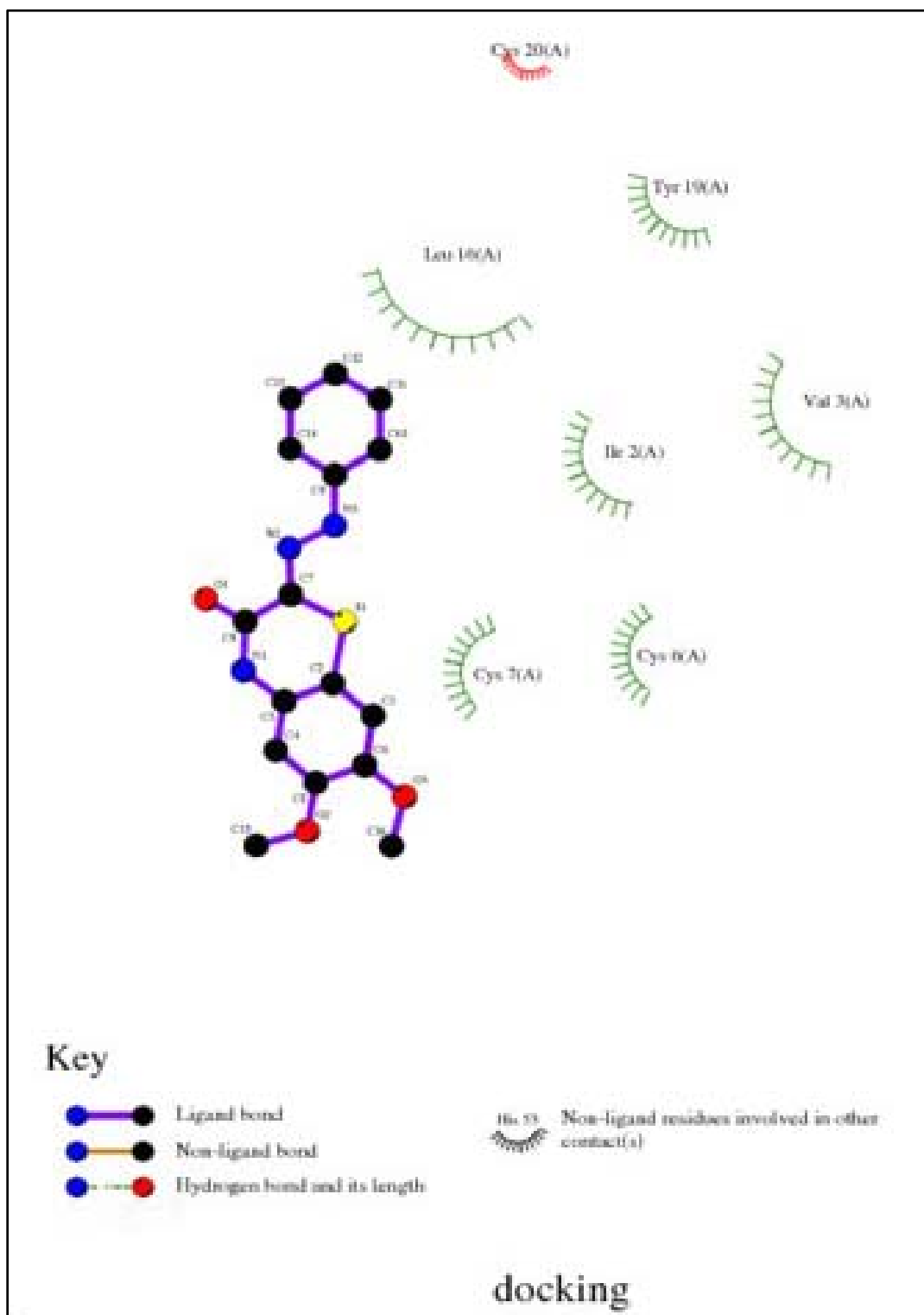

Fig. 10   2D bends of interface among BOD composite with 3tt8 receptor.

3.8. Mechanism of Corrosion Protection

From the electrochemical tests the *IE* % count on dose, nature of metal, surface conditions and the kind of adsorbed inhibitor on P355 Cs.

The outcome data of corrosion data presence of this inhibitor:

1. The minor of *CR* with increase in dose of the inhibitor.

2. The exchange in Tafel lines to higher regions of potential.

3. The %*IE* is dependent on charge density and their apparatus of adsorption centers in the BOD.

It was detected that the kind of adsorption relies on the affinity of P355 Cs and the against clouds of π-electron of the ring. Metals such as iron, which has a higher attract against aromatic moieties, was gotten to adsorb benzene rings in orientation flat.

BOD composite exhibits excellent inhibition power due to: (i) the existence of two methyl groups which are an electron donating groups, also these groups will improve the electron charge density on the molecule, (ii) its greater molecular size (264.32) that may facilitate excellent surface coverage, and (iii) its adsorption through three active centers $(1 - O$ and $2 - N$ atoms).

4. Conclusions

1. BOD is excellent corrosion inhibitor for P355 Cs in 1.0 N corrosive solution.

2. C_{dl} lower with respect to blank solution when the added BOD inhibitor. This fact may suggested by inhibitor BOD molecule adsorbed of the on the P355 Cs surface.

3. Molecular docking and binding energy measurements of BOD composite with the receptor of $3tt8 -$ hormone of crystal structure analysis of Cu Human Insulin Derivative indicated that the composite is efficient inhibitor of receptor of $3tt8 -$ hormone.

4. The morphology of protected and unprotected P355 Cs was examined by SEM and EDX.

5. Quantum chemistry measurement results showed that the heteroatoms of N and O are the active sites of the BOD compound. It can absorb on *Fe* surface firmly by donating electrons to Fe atoms and accepting electrons from 3d orbital of Fe atoms.

References

[1] Shahryari, A., Omanovic, S., Fan, B. M. 2018. "Understanding the Inhibition Mechanism of a Supramolecular Complex as the Corrosion Inhibitor for Mild Steel in the Condensate Water." *J. Materials Science Forum* 913: 424-38.

[2] Luo, H., Su, H., Dong, C., and Li, X. 2017. "Passivation and Electrochemical Behavior of 316L Stainless Steel in Chlorinated Simulated Concrete Pore Solution." *J. Appl. Surf. Sci.* 400: 38-48.

[3] Luo, H., Dong, C., and Xiao, K. 2017. "Passive Film Properties and Electrochemical Behavior of Co-Cr-Mo Stainless Steel in Chloride Solution." *J. Materials Engineering and Performance* 26: 2237-43.

[4] Olivio, P. H. P., and Correia, L. A. 2018. "Exploring Electrochemical Reactivity toward Ametryn of Hybrid Silicate Films with Phosphomolybdic Acid." *J. Materials Science and Engineering: B.* 229: 13-9.

[5] Shahryari, A., Omanovic, S., and Szpunar., J. A. 2016. "Enhancement of biocompatibility of 316LVM Stainless Steel by Cyclic Potentiodynamic Passivation." *J. Biomedical Materials Research* 676: 414-23.

[6] Wan, H., Song, D., Zhang, D., and Du., C. 2018. "Corrosion Effect of Bacillus Cereus on X80 Pipeline Steel in a Beijing Soil Environment." *J. Bioelectrochemistry* 121: 18-26.

[7] Zhang, S., Jiang, Z., and Zhang, B. 2017. "Detection of Susceptibility to Intergranular Corrosion of Aged Super Austenitic Stainless Steel S32654 by a Modified Electrochemical Potentiokinetic Reactivation Method." *J. Alloys and Compounds* 695: 3083-93.

[8] Juan, L., Rong, G., Lan, G., and Liy, F. 2016. "Mechanical characterization of Waste-Rubber-Modified Recycled-Aggregate Concrete." *J. Cleaner Production* 124: 325-38.

[9] Liu, C. 2007. "Corrosion Resistance of Titanium Ion Implanted AZ91 Magnesium Alloy." *J. Vacuum Science & Technology A: Vacuum, Surfaces and Films* 25: 334-45.

[10] Fan, L., Tang, F., and Singo, T. 2017. "Corrosion Resistances of Steel Pipes Internally Coated with Enamel." *J. Corrosion* 73: 1335-45.

[11] Tavares, S. S. M., Pardal, J. M., and Pardal, J. P. 2016. "Investigation of the Failure in a Pipe of Produced Water

from an Oil Separator due to Internal Localized Corrosion." *J. Engineering Failure Analysis* 61: 100-7.

[12] S. M., Abd El Haleem, Abd, S., and Bahgat, A. 2013. "Environmental Factors Affecting the Corrosion Behaviour of Reinforcing Steel. V. Role of Chloride and Sulphate Ions in the Corrosion of Reinforcing Steel in Saturated $Ca(OH)_2$ Solutions." *J. Corros. Sci.* 75: 1-17.

[13] Videm, K., and Kavrekval, J. 1995. "Corrosion of Cs in Carbon Dioxide-Saturated Solutions Containing Small Amounts of Hydrogen Sulfide." *J. Corrosion* 52 (4): 260-9.

[14] Pan, Y., Dong, C., and Xiao, K. 2018. "In-situ Investigation of the Semiconductive Properties and Protective Role of Cu_2O Layer Formed on Copper in a Borate Buffer Solution." *J. Electroanalytical Chemistry* 809: 52-8.

[15] Arjmand, F., and Zhang, L. 2015. "Electrochemical Corrosion Performance of Mechanically Polished Alloy 690TT at High-Temperature Water (200°C)." *J. Corrosion* 71: 1481-14898.

[16] Xun, W., Lulu, L., and Hui, L. 2018. "Effect of Strain Level on Corrosion of Stainless Steel Bar." *J. Construction and Building Materials* 163: 189-99.

[17] Wang, Z., Zhang, L., and Tang, X. 2017. "The Surface Characterization and Passive Behavior of Type 316L Stainless Steel in H_2S-Containing Conditions." *J. Appl. Surf. Sci.* 423: 457-64.

[18] Shangyi, S., and Zuo, Y. 2014. "The Improved Performance of Mg-rich Epoxy Primer on AZ91D Magnesium Alloy by Addition of ZnO." *J. Corrosion Science* 87: 167-78.

[19] Bensabra, H., and Azzouz, N. 2013. "Study of Rust Effect on the Corrosion Behavior of Reinforcement Steel Utilizing Impedance Spectroscopy." *J. Metallurgical and Materials Transactions A* 44: 5703-10.

[20] Zhang, P., Zhaolin, L., and Wang, Y. 2018. "3D Neutron Tomography of Steel Reinforcement Corrosion in Cement Based Composites." *J. Constr. Build. Mater.* 162: 561-5.

[21] Sung, H., Kumar, J., and Sun, W. 2017. "Effect of $LiNO_2$ Inhibitor on Corrosion Characteristics of Steel Rebar in Saturated $Ca(OH)_2$ Solution Containing NaCl: An Electrochemical Study." *J. Constr. Build. Mater.* 133: 387-96.

[22] Ming, J., Jinjie, S., and Sun, W. 2018. "Effect of Mill Scale on the Long-Term Corrosion Resistance of a Low Alloy Reinforcing Steel in Concrete Subjected to Chloride Solution." *J. Constr. Build. Mater.* 163: 508-5176.

[23] Casini, J., Saeki, M., and Takiishi, H. 2017. "Effect of Sn and Cu on Corrosion Resistance of La Mg Al Mn Co Ni Type Alloys." *J. Materials Science Forum* 889: 353-7.

[24] Eldesoky, A. M., El-Bindary, M. A., El-Sonbati, A. Z., and Morgan, Sh. M. 2015. "New Eco-Friendly Corrosion Inhibitors based on Azo Rhodanine Derivatives for Protection Copper Corrosion." *J. Mater. Environ. Sci.* 6: 2260-76.

[25] Eldesoky, A. M., Diab, M. A., El-Bindary, A. A., El-Sonbati, A. Z., and Seyam, H. A. 2015. "Some Antipyrine Derivatives as Corrosion Inhibitors for Copper in Acidic Medium: Experimental and Quantum Chemical Molecular Dynamics Approach." *J. Mater. Environ. Sci.* 6: 2148-65.

[26] Shoair, A. F., El-Bindary, A. A., El-Sonbati, A. Z., and Beshry, N. M. 2016. "Molecular Docking, Potentiometric and Thermodynamic Studies of Some Azo Quinoline." *J. Molecular Liquids* 215: 740-8.

[27] Halgren, T. A. 1996. "Merck Molecular Force Field. I. Basis, Form, Scope, Parameterization, and Performance of MMFF94." *J. Comput. Chem.* 17: 490-519.

[28] Morris, G. M., and Goodsell, D. S. 1998. "Automated Docking Utilizing a Lamarckian Genetic Algorithm and an Empirical Binding Free Energy Function." *J. Comput. Chem.* 19 (14): 1639-62.

[29] Sharma, N. K., Jha, K. K., and Vijaya Kumar, M. 2014. "Synthesis and Antimicrobial Evaluation of 2-(2-(Benzo [d] Oxazol-2-yl) Phenylamino)-n-(Substituted Phenyl) Acetamides." *J. Pharmaceutical Science and Research* 5 (8): 3260-6.

[30] Al-Khaldi, M. A., and Al-qahtani, K. Y. 2013. "Corrosion Inhibition of Steel by Coriander Extracts in Hydrochloric Acid Solution." *J. Mater. Environ. Sci.* 4 (5): 593-600.

[31] Khaled, K. F. 2008. "Adsorption and Inhibitive Properties of a New Synthesized Guanidine Derivative on Corrosion of Copper in 0.5 M H_2SO_4." *J. Applied Surface Science* 255(5): 1811-8.

[32] Rios, J. F., Calderon, J. A., and Nogueira, R. P. 2013. "Electrochemical Behavior of Metals Utilizied in Drinking Water Distribution Systems: A Rotating Cylinder Electrode's Study." *J. Corrosion* 69 (9): 875-85.

[33] Macdonald, D. D., and Mckubre, M. C. H. 1982. "Impedance Measurements in Electrochemical Systems." *Modern Aspects of Electrochemistry*, edited by Bockris, J. O'M., Conway, B. E., and White, R. E.: Plenum Press, New York 14: 61-150.

[34] Carbonini, P., Monetta, T., and Scatteia, B. 1979. "Degradation Behaviour of 6013-T6, 2024-T3 Alloys and Pure Aluminium in Different Aqueous Media." *J. Applied Electrochemistry* 27: 1135-43.

[35] Gabrielli, C. 1984. "Identification of Electrochemical Processes by Frequency Response Analysis." *Solarton Instrumentation Group*, 2-15.

[36] Sun, Y. M., and Chen, H. L. 2012. "Electrochemical Measurements of Corrosion Inhibition of Mild Steel in Sulfuric Acid by BIMGCS12-3." *J. Advanced Materials Research* 402: 800-3.

[37] Anejjar, A., Zarrouk, A., Salghi, R., Zarrok, H., Ben Hmamou, D., Hammouti, B., Elmahi, B., and Al-Deyab, S. S. 2013. "Studies on the Inhibitive Effect of the Ammonium Iron (II) Sulphate on the Corrosion of Cs in HCl Solution." *J. Mater. Environ. Sci.* 4 (5): 583-92.

[38] Mertens, S. F., Xhoffer, C., Decooman, B. C., and Temmerman, E. 1997. "Short-Term Deterioration of Polymer-Coated 55% Al-Zn Part 1: Behavior of Thin Polymer Films." *J. Corrosion* 53: 331-88.

[39] Murthy, H. C. 2015. "Electroanalytical Study on the Corrosion Behaviour of TiO_2 Particulate Reinforced Al 6061 Composites." *J. Material Science Research India* 12 (2): 112-26.

[40] Fouda, A. S., Ibrahim, H., and Atef, M. 2017. "Adsorption and Inhibitive Properties of Sildenafil (Viagra) for Zinc in Hydrochloric Acid Solution." *J. Results in Physics* 7: 3408-18.

[41] Abdulwahed, J. A. M., Younis, R. M., Hassan, H. M., Elsayad, M. R., and Eldesoky, A. M. 2016. "Electrochemical and Surface Characterization Studies on C38 Steel in 1 M Hydrochloric Acid Medium Utilizing Prop-2-en-1-one Derivatives as Corrosion Inhibitors." *Int. J. Adv. Res.* 4 (11): 1192-203.

[42] Lagrenée, M., Mernari, B., Bouanis, M., Traisnel, and M., Bentiss, F. 2002. "Study of the Mechanism and Inhibiting Efficiency of 3,5-bis(4-methylthiophenyl)-4H-1,2,4-triazole on Mild Steel Corrosion in Acidic Media." *J. Corros. Sci.* 44: 573-88.

[43] McCafferty, E. 2005. "Validation of Corrosion Rates Measured by the Tafel Extrapolation Method." *J. Corros. Sci.* 47 (12): 3202-15.

[44] Zhang, S. S., Xu, K., and Jow, T. R. 2003. "The Low Temperature Performance of Li-ion Batteries." *J. Power Sources* 115 (1): 137-40.

[45] Rauf, A., Bogaertsd, W. F., and Mahdi, E. 2012. "Implementation of Electrochemical Frequency Modulation to Analyze Stress Corrosion Cracking." *J. Corrosion* 68 (3): 1-9.

[46] Fouda, A. S., and Abdulwhed, H. A. 2016. "Corrosion Inhibition of Copper in HNO_3 Solution Utilizing Thiophene and its Derivatives." *Arabian, J. of Chemistry* 9: 519-99.

[47] Samie, F., and Tidblad J. 2008. "Influence of Nitric Acid on Atmospheric Corrosion of Copper, Zinc and Css." *J. Corrosion Engineering, Science and Technology* 43 (2): 117-22.

[48] Javadian, S., Yousefi, A., and Neshati, J. 2013. "Synergistic Effect of Mixed Cationic and Anionic Surfactants on the Corrosion Inhibitor Behavior of Mild Steel in 3.5% NaCl." *J. Applied Surface Science* 285: 674-81.

[49] Jafari, H., and Sayin, K. 2016. "Sulfur Containing Composites as Corrosion Inhibitors for Mild Steel in Hydrochloric Acid Solution." *J. Transactions of the Indian Institute of Metals* 69 (3): 805-15.

[50] Han, W., Pan, C., Wang, Z., and Guocai, Y. 2015. "Initial Atmospheric Corrosion of Cs in Industrial Environment." *J. Materials Engineering and Performance* 24 (2): 864-74.

[51] Lukovits, I., Palfi, K., Bako, I., and Kalman, E. 1997. "LKP Model of the Inhibition Mechanism of Thiourea Composites." *J. Corrosion* 53 (12): 915-9.

[52] Zhang, S., and Zhihua, T. 2009. "The Effect of Some Triazole Derivatives as Inhibitors for the Corrosion of Mild Steel in 1.0 N Corrosive Solution." *J. Appl. Surf. Sci.* 255 (15): 6757-63.

[53] Morgan, Sh. M., and Refaat, H. M. 2016. "Molecular Docking, Geometrical Structure, Potentiometric and Thermodynamic Studies of Moxifloxacin and its Metal Complexes." *J. Mol. Liq.* 220: 802-12.

[54] Sayin, K., and Karakas, D. 2018. "Computational Investigations of Trans-Platinum(II) Oxime Complexes Utilizied as Anticancer Drug." *J. Spectrochimica Acta Part A: Molecular and Biomolecular Spectroscopy* 188: 537-46.

[55] El-Bindary, A. A., El-Sonbati, A. Z., and Diab, M. A. 2016. "Molecular Docking, Potentiometric and Thermodynamic Studies of Some Azo Composites." *J. Solution Chemistry* 45 (7): 990-1008.